TOWARD THE DEVELOPMENT OF A BIOCATALYTIC PROCESS FOR THE PRODUCTION OF β-ARYL-β-AMINO ACIDS

By

Nishanka Dilini Ratnayake

A DISSERTATION

Submitted to
Michigan State University
in partial fulfillment of the requirements
for the degree of

Chemistry - Doctor of Philosophy

2015

ABSTRACT

TOWARD THE DEVELOPMENT OF A BIOCATALYTIC PROCESS FOR THE PRODUCTION OF β-ARYL-β-AMINO ACIDS

By

Nishanka Dilini Ratnayake

While not abundant in nature, aromatic β-amino acids are found occasionally in pharmacologically important natural products such as andrimid, bestatin, and Taxol. In addition, they are used as important precursors for the synthesis of β-peptides and pharmaceuticals. Given the importance of β-amino acids, several methods are explored for the stereoselective synthesis of β-amino acids. Phenylalanine aminomutases, which isomerize (2*S*)-α-phenylalanine to β-phenylalanine with >99.9% *ee*, are efficient biocatalysts to produce enantiopure β-aryl-β-amino acids. The ultimate goal of this work was to use the knowledge from mechanistic investigations to rationally design *Pantoea agglomerans* phenylalanine aminomutase (*Pa*PAM) as a biocatalyst to produce industrially relevant compounds on scale.

The 4-methylidene-1*H*-imidazol-5(4*H*)-one (MIO) cofactor is believed to serve as the electrophile in the isomerization reactions performed by phenylalanine aminomutases. Over several decades, debates have centered on whether π-electrons at the phenyl ring or the amino group of the substrate act as the nucleophile. The structure of *Pa*PAM determined at 1.7 Å resolution revealed that the substrate (α-phenylalanine) and the product (β-phenylalanine) covalently bind to the MIO via the amino group. This data confirmed a *Pa*PAM mechanism where the amino group of the substrate acts as the nucleophile.

*Pa*PAM was incubated with various isotopically labeled substrates to establish the stereochemistry and mechanism of the reaction. The reaction was found to proceed through removal, and interchange of the *pro*-(3*S*) hydrogen and the α-amino-group of the substrate,

followed by intramolecular reattachment of the migration partners on the vicinal carbon from the same stereo-face that they originated from. Thus, *Pa*PAM catalyzes its isomerization reaction with the inversion-of-configuration at both reaction termini.

Variously ring-substituted α-phenylalanine analogues (19) were used to probe the substituent effects on the intermediate steps of *Pa*PAM isomerization mechanism. Influence of the substituents on the catalytic rate (k_{cat}) of *Pa*PAM revealed concave-down correlations with Hammett substituent constants (σ). This trend suggested the rate-determining step changes from the step that eliminates hydrogen and amino group from the substrate to the 'hydroamination' step, based on the direction and magnitude of the electronic properties of the substituent. Theoretical calculations on analyzing enzyme-substrate interaction energies revealed that the steric effects in the protein-ligand adduct and within the ligand are dominant over electrostatic interactions when the substrate binds.

The *Pa*PAM *E. coli* whole-cell biocatalyst was shown to produce several non-natural (3*S*)-β-aryl-β-amino acids at >99.9% *ee*, with the highest turnover rate in M9 minimal medium at 16 °C. The whole-cell biocatalyst biosynthesized 18 β-arylalanines with moderate to excellent converted yield (4-96%) at production levels of 8.5 – 235 $mg \cdot L^{-1}$ over 6 h, respectively. More notably, *E. coli* cells are reusable over *at least* five reaction cycles without a noticeable loss in activity and cell viability. This biocatalyst offers notable advantages over conventional synthetic methods and other biocatalysts because of its excellent enantioselectivity, broad substrate scope, single-step conversion, and sustainability.

I dedicate this dissertation to my loving parents, siblings and my husband who made countless sacrifices to make me who I am today.....

ACKNOWLEDGEMENTS

I am yet to fully comprehend that I have come to the end of a long, challenging, but rewarding five-year journey through graduate school. I could never have come this far without the guidance, inspiration, and support of many wonderful people.

First, I sincerely thank my advisor Prof. Kevin D. Walker for his guidance, understanding, patience, and support all through my graduate studies at Michigan State University. I am forever grateful to him for his continuous motivation and encouragement, and for guiding me to grow as an independent scientist. Without his guidance and persistent help, this dissertation and all the publications would not have been possible.

To the members of my guidance committee, I am sincerely thankful to all of you. I thank Prof. Babak Borhan for being a great mentor, teacher, and for his tremendous advice on preparing my second year literature seminar. Many thanks to Prof. Leslie Kuhn for introducing me to computational docking and for providing excellent guidance while I was learning the SLIDE docking tool. I am really thankful for her suggestions on various other research questions, and most importantly for writing impactful recommendation letters on my behalf. I am thankful to Prof. Dana Spence for the suggestions on improving the *in vivo* biocatalytic investigations of *Pa*PAM. Also, I cannot forget late Prof. Gregory Baker, a former member of my guidance committee who was very supportive during my early years at Michigan State University.

I would like to thank Prof. Dr. J. H. Gieger and Dr. Susan Strom for collaborating with us to obtain the structure of *Pa*PAM, which provided a lot of insight into my research project. My gratitude extends to Prof. Leslie Kuhn and Ms. Nan Liu for their support on computational modeling investigations of phenylalanine analogues. Your findings added a significant value to our publication.

My sincere appreciation goes to Prof. Daniel Jones and members of the technical staff at the mass spectrometry and metabolomics core, Dr. Daniel Holmes at the NMR facility, Dr. Kaillathe (Pappan) Padmanabhan at the macromolecular computing facility, Dr. Kathy Severin, and many other faculty members in the Departments of Chemistry and Biochemistry who went above and beyond their ways to assist me. I would also like to thank Dr. Amy Pollock and Dr. Ardeshir Azadnia for being supportive while I was teaching undergraduate Chemistry courses. Further, many thanks to all the administrative personnel in the Department of Chemistry for your continuous support during my time at Michigan State University.

I am indebted to Department of Chemistry and College of Natural Sciences for supporting me with graduate teaching assistantships and fellowships, which greatly helped me financially over the past five years. I am also thankful to American Chemical Society local section, College of Natural Sciences, Graduate School, and Council of Graduate Students (COGS) at the Michigan State University for the travel funds to attend various scientific conferences.

All the people who I met in Walker lab were very resourceful in making my graduate school career a success. Many thanks to Dr. Mark Ondari for not only helping me to get started in the lab, but also continuing to help me until I graduate; I thank you for encouraging me to do my best in graduate school, and most importantly, for being a wonderful friend and a brother. I would like to thank Dr. Irosha Nawarathne, Dr. Danielle Nevarez Mcbride, Ms. Getrude Dibo, Mr. Sean Sullivan, Dr. Udayanga Wanninayake, and Dr. Washington Mutatu for your help to learn many techniques, and providing suggestions on improving my research presentations. My sincere appreciation goes to Chelsea, Ruth, Tyler, and Prakash for making a nice, friendly working environment in the lab. I would also like to thank Chelsea for being a great friend and

for being there with me during the hard times throughout all these years. I will miss you all so much. Many thanks to all the undergraduates who worked in Walker lab; Olivia, Chelsea T., Jenna, Yvonne, Manisha, Doug, and Aws: thank you very much for all your technical support. You all were great to work with and I would not forget that you helped me somewhere along the way.

I am thankful to all my college teachers and mentors who guided me towards a fruitful career in science. Many thanks to my pre-undergraduate research mentor, Prof. Lalith Jayasinghe at the Institute of Fundamental Studies, Sri Lanka, for identifying my potential in pursuing a career in Chemistry. I sincerely thank Prof. Veranja Karunaratne and Prof. B. M. R. Bandara for patiently guiding me while working on my undergraduate research project.

To my extended family in USA; words cannot convey how grateful I am for helping me and my husband to resettle in the USA, and for continuously maintaining a sense of home here in the USA. We never felt alone, although our home country is thousands of miles away. My appreciation extends to all the Sri Lankan friends in East Lansing for all your support, and making my years at the Michigan State University a great experience. I will miss you all!

None of the achievements I have made in my life would have been possible without the great support from my loving family. Appachchi (dad) and ammi (mom), I am truly grateful for recognizing my strengths, believing in me, and for giving me the support to chase after my career goals. Without you two, I would be nowhere near the person I am today. I cannot find words to appreciate enough for the sacrifices you both made to give us the best always; I owe you a lot and love you always. I sincerely thank my sister and brother for being there always whenever I needed help, and for looking out for me. Regardless how much we fought and argued, and where we are today; you two always hold a special place in my heart. Last, but not least, I thank my

husband Salinda for his immense support, love, and care throughout past five years. Words cannot express how thankful I am for selflessly sacrificing your own dreams and goals to support my career goals. Thank you very much for keeping me sane when the things were not going well. I truly appreciate everything you have done for me and I love you always!

TABLE OF CONTENTS

LIST OF TABLES

LIST OF FIGURES

KEY TO ABBREVIATIONS

ATP: Adenosine triphosphate

BME-vitamins: Eagle's basal medium vitamins

Bu_3N: Tributylamine

BzCl: Benzoyl chloride

$CaCl_2$: Calcium chloide

CD: Circular dichroism

CFU: Colony-forming units

CH_2N_2: Diazomethane

$CHCl_3$: Chloroform

$ClCO_2Et$: Ethyl chloroformate

D_2O: Deuterium oxide

DMSO: Dimethyl sulfoxide

DNA: Deoxyribonucleic acid

E. coli: *Escherichia coli*

EDTA: Ethylenediaminetetraacetic acid

EtOH: Ethanol

GC/EI-MS: Gas chromatography electron ionization mass spectrometry

HCl: Hydrochloric acid

IPTG: Isopropyl-β-d-thiogalactopyranoside

KCN: Potassium cyanide

KH_2PO_4: Monopotassium phosphate

KOH: Potassium hydroxide

MeOH: Methanol

$MgSO_4$: Magnesium sulfate

MIO: 4-methylidene-1*H*-imidazol-5(4*H*)-one

mRNA: Messenger ribonucleic acid

MTBE: Methyl tert-butyl ether

MWCO: Molecular weight cutoff

$Na_2HPO_4.7H_2O$: Sodium monohydrogen phosphate heptahydrate

$NaBH_4$: Sodium borohydrate

NaCl: Sodium chloride

NaCN: Sodium cyanide

NAD(P): Nicotinamide adenine dinucleotide phosphate

$NaHSO_3$: Sodium bisulfite

NaOH: Sodium hydroxide

NH_4Cl: Ammonium chloride

NH_4OH: Ammonium hydroxide

NMR: Nuclear magnetic resonance

n-PrOH: Propyl alcohol

OD: Optical density

PCR: Polymerase chain reaction

$Pd(OH)_2$: Palladium hydroxide

PLP: Pyridoxal 5'-phosphate

SAM: *S*-adenosyl methionine

SDS−PAGE: Sodium dodecyl sulfate Polyacrylamide gel electrophoresis

$SOCl_2$: Thionyl chloride

TCP: Total cell protein

THF: Tetrahydrofuran

$TMSCH_2N_2$: Trimethylsilyldiazomethane

UV: Ultraviolet

CHAPTER 1: Overview of Biocatalysis in Organic Chemistry and Biotechnology

Biocatalysis, the use of isolated enzymes or microbial whole-cells as catalysts, offers various unique advantages over conventional chemical catalysis.[1,2] The most important advantages of a biocatalyst include, excellent stereo-, regio- and chemo-selectivity. Additionally, protection/deprotection steps are can often be avoided, and therefore, the reactions are generally atom- and reaction-step economical. Other advantages, such as mild operational conditions and reduced hazardous waste generation are also very attractive in large scale applications.

Traditionally, the enzymes were directly isolated from their corresponding sources such as microbes, plants, insects, and mammalian species. Consequently, the main drawback in enzyme catalysis until the end of the 1970s was the enzyme production in large enough quantities for practical applications.[3] However, with advances in recombinant DNA technology, the DNA sequences could be manipulated and proteins overexpressed in non-native host organisms.[2] This provided a means to produce biocatalysts in large quantities in fast-growing organisms.

Nonetheless, narrow substrate scope, substrate or product inhibition and low stability of the biocatalysts limit the application of enzymes in industrial scale applications.[2] Developments in protein engineering methods using rational design or directed evolution (by error-prone PCR or gene shuffling) and advances in understanding protein structure-function relationships are enabling scientists to rapidly tailor the properties of biocatalysts for particular chemical processes.[1]

Generally, improvements in enzyme thermal stability often results in loss of the catalytic activity at lower temperatures.[4] However, the thermal stability of *Bacillus subtilis*, *p*-nitrobenzyl esterase was increased significantly without reducing the catalytic activity at lower temperature.[4] Six generations of random mutagenesis increased the melting temperature of the esterase by 14 °C.

Rational design based on site-specific mutagenesis has also been instrumental in enhancing the thermostability of enzymes. For example, a moderately stable protease from *Bacillus stearothermophilus* (TLP-ste) was made hyper-stable by rationally designed mutations.[5] By comparing the structure of TLP-ste with naturally occurring more thermostable homologues, eight point mutations and a disulfide bridge were introduced in TPL-ste. These modifications resulted in a 340-fold more stable protein compared to *wt*- TLP-ste at 100 °C.[5] Additionally, the 8-fold mutant retained its activity at high concentrations of denaturing agents.

Although it is more challenging, rational design of proteins has been used to improve their stereoselectivity.[3] For example, the enantioselectivity and catalytic activity of *Burkholderia cepacia* lipase toward poor substrates bearing bulky substituents was improved by site-specific mutagenesis.[6] Based on molecular docking, a double mutant (I290A/I287F) was designed to create more space for bulkier substrates and to improve the catalytic activity of the (*R*)-enantiomer of the racemic substrates. Consequently, the *E* value ($E = \ln[1-c(1+ee)]/\ln[1-c(1-ee)]$, where c = conversion; *ee* = enantiomeric excess) for bulkier substrates increased from five (wild-type) to 200 for the double mutant.[6]

Merck and Codexis researchers recently engineered an (*R*)-selective transaminase (ATA-117) to increase the efficiency of a large-scale manufacturing process of the antidiabetic

compound sitagliptin (Figure 1.1).[7] Starting from ATA-117, which was active only toward methyl- and small cyclic- ketones, a combination of computational modeling and site-saturation mutagenesis was used to create a biocatalyst with marginal activity for prositaglipin ketone (4% conversion). The ATA-117 variant with the highest activity was further engineered via 11 rounds of directed evolution to optimize the activity, tolerance for organic cosolvents and higher substrate concentrations, and stability at the elevated reaction temperatures.[7] The evolved transaminase contained 27 mutations in the active site and the dimer interface, which improved the substrate binding as well as protein stability. In the optimized process, 6 g/L of the best transaminase variant tolerates a 200 g/L concentration of prositagliptin ketone in 50% DMSO at 40 °C, and produces sitagliptin in 92% yield at >99.95% *ee*.[7] This biocatalytic route replaced the high pressure (250 psi), Rh-catalyzed enamine asymmetric hydrogenation for the large-scale manufacture of sitagliptin (Figure 1.1). The biocatalytic route not only reduced the total waste (19% reduction) and eliminated all transition metals, but also increased the overall yield (10-13% increase) and the productivity (53% increase) compared to the metal-catalyzed process.[7]

Biocatalysis became a mature technology through several protein engineering innovations, and currently several biocatalytic processes are operational in pharmaceutical, chemical, agricultural, and food industries.[8,9] Hydrolases[10] and ketoreductases[11] are the most frequently used biocatalysts in industrial organic synthesis. For example, *Candida antarctica* lipase B led to a more efficient and less expensive manufacturing process for the key intermediate L-fluoroleucine (**1**) (Table 1.1A) in the synthesis of antiresorptive agent odanacatib (Merck).[12] This process was demonstrated at 100 kg scale with >90% yield and 88% *ee*. Additionally, enzymatic kinetic resolution by *Thermomyces lanuginosus* lipase was used in preparative scale synthesis of (1*S*,3*S*)-3-aminocyclohexanol (**2**) (Table 1.1B) with >96% *ee*

(Novartis).[13] An engineered ketoreductase in combination with a glucose dehydrogenase for cofactor regeneration has been widely investigated for the manufacture of atorvastatin, the active ingredient of cholesterol lowering drug Lipitor (Codexis).[14] Biocatalytic reduction of ethyl-4-chloroacetoacetate by the ketoreductase produced ethyl-4-chloro-3-hydroxybutyrate (**3**) (Table 1.1C), a key intermediate of atorvastin, in 96% isolated yield and >99.5% *ee*.

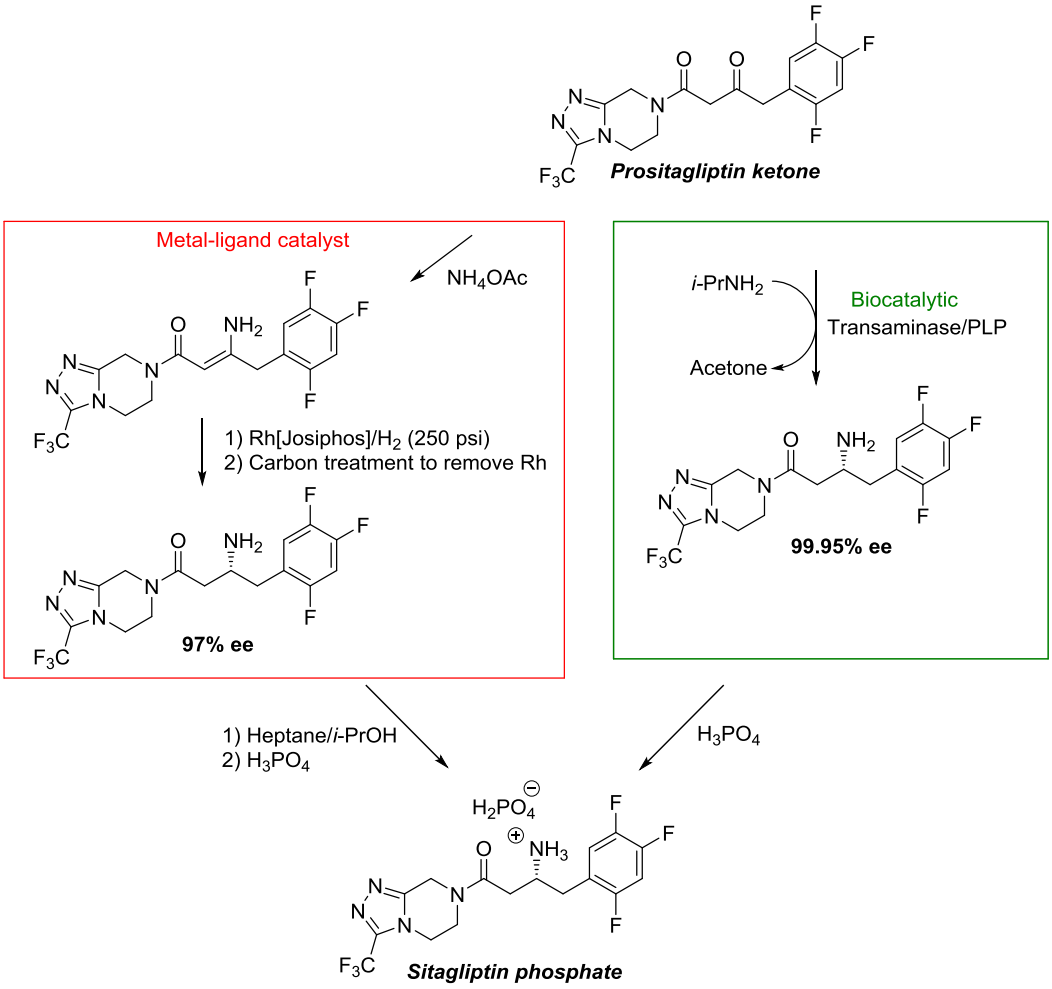

Figure 1.1. Comparison of the biocatalytic and chemical hydrogenation processes for sitagliptin synthesis. The enzymatic route using an engineered transaminase is superior (higher yield and enantioselectivity) to the metal-catalyzed asymmetric hydrogenation method.

In addition to lipases and ketoreductases, various other classes of enzymes are also emerging and expanding as industrially relevant biocatalysts. Examples include transaminases in the sitagliptin manufacture (Merck and Codexis) (cf. Figure 1.1),[7] aldolases in the production of the natural sweetener monatin (**4**) (CSIR Biosciences) (Table 1.1D),[15] an (*R*)-amino acid oxidase used in (*S*)-2-amino-3-(6-*o*-tolylpyridin-3-yl)propanoic acid (**5**) production (Bristol-Myers Squibb) (Table 1.1E),[16] and proteolytic enzyme thermolysin in the production of low-calorie sweetener aspartame (**6**) (DSM) (Table 1.1F).[8,17]

In view of increasing demand for renewable sources for energy and chemical feedstock, biocatalysis is becoming an attractive process.[18] Although many biocatalysts are implemented in the syntheses of various fine chemicals, there is still a growing need for more efficient or novel biocatalysts to supply the increasing demand of chiral compounds for industrial purposes. The impact of emerging technologies in bio-informatics, next generation sequencing, and high-throughput screening open up new avenues to discover novel biocatalysts and to create efficient enzyme variants.[19,20] *De novo* design of enzymes with pre-determined characteristics,[21] powerful microorganism screening methods such as metagenomics,[22] as well as the exploration of the catalytic flexibility and efficiency of existing biocatalysts offer new approaches for the exploration of enzyme catalysts.

Table 1.1. Biocatalytic processes in industrial applications

Enzyme	Product	Source	Reference
A. Lipase (*Candida antarctica)*	L-Fluoroleucine (**1**)	Merck	12
B. Lipase (*Thermomyces lanuginosus*)	(1*S*,3*S*)-3-aminocyclohexanol (**2**)	Novartis	13
C. Ketoreductase and glucose dehydrogenase	Ethyl (*S*)-4-chloro-3-hydroxybutanoate (**3**)	Codexis	14
D. Aldolase	(2*S*,4*S*)-monatin (**4**)	CSIR Biosciences	15
E. (*R*)-amino acid oxidase	(*S*)-amino acid (**5**)	Bristol-Myers Squibb	16
F. Protease thermolysin	Aspartame (**6**)	DSM	8, 17

Phenylalanine aminomutases (PAM) are responsible for the biosynthesis of enantiopure β-phenylalanines in structurally diverse bioactive natural products.[23,24] In *Taxus* plants, *Tc*PAM catalyzes the conversion of (2*S*)-α-phenylalanine to (3*R*)-β-phenylalanine, a proposed biosynthetic precursor of the phenylisoserine side chain of Taxol (Figure 1.2).[24] A homologous enzyme from *Pantoea agglomerans* (*Pa*PAM) produces the enantiomeric (3*S*)-β-phenylalanine in the biosynthetic pathway of the antibiotic andrimid (Figure 1.2).[23]

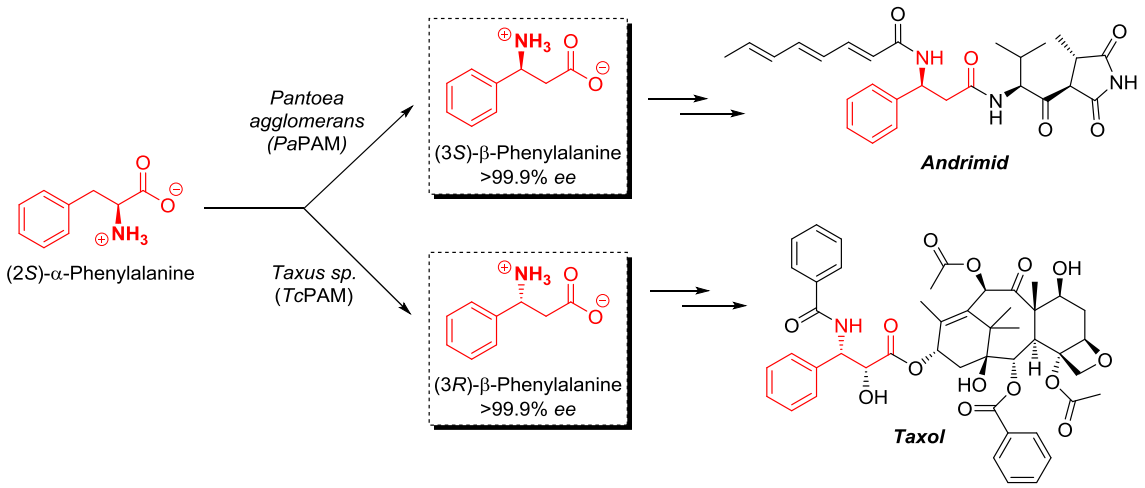

Figure 1.2. Reactions catalyzed by phenylalanine aminomutases *Pa*PAM and *Tc*PAM in their corresponding biosynthetic routes for andrimid and Taxol.

The excellent product enantioselectivity (99.9% *ee*) and non-reliance on external cofactors make PAMs attractive biocatalysts for producing β-amino acids, which are highly valuable building blocks of peptidomimetics and pharmaceutics.[25] While the potential of *Tc*PAM for the synthesis of β-amino acids has been demonstrated in various investigations in this area,[26-30] *Pa*PAM has not been evaluated for its biocatalytic potential and applications. The main objective of this work was to investigate the mechanistic, stereochemical, kinetic and whole-cell biocatalytic characteristics aimed at developing *Pa*PAM as a biocatalyst for producing β-arylalanines. Chapter 2, 3, and 4 of this dissertation will highlight the stereochemical, mechanistic, kinetic, and structural investigations that will guide the rational design of *Pa*PAM as a better biocatalyst. Further, the initial investigations on developing *Pa*PAM as a whole-cell biocatalyst will be described in chapter 5.

REFERENCES

REFERENCES

(1) de Carvalho, C. C. *Biotechnol. Adv.* **2011**, *29*, 75-83.

(2) Arnold, F. H. *Nature* **2001**, *409*, 253-257.

(3) Reetz, M. T. *J. Am. Chem. Soc.* **2013**, *135*, 12480-12496.

(4) Giver, L.; Gershenson, A.; Freskgard, P. O.; Arnold, F. H. *Proc. Natl. Acad. Sci. USA* **1998**, *95*, 12809-12813.

(5) Van den Burg, B.; Vriend, G.; Veltman, O. R.; Venema, G.; Eijsink, V. G. *Proc. Natl. Acad. Sci. USA* **1998**, *95*, 2056-2060.

(6) Ema, T.; Kamata, S.; Takeda, M.; Nakano, Y.; Sakai, T. *Chem. Commun.* **2010**, *46*, 5440-5442.

(7) Savile, C. K.; Janey, J. M.; Mundorff, E. C.; Moore, J. C.; Tam, S.; Jarvis, W. R.; Colbeck, J. C.; Krebber, A.; Fleitz, F. J.; Brands, J.; Devine, P. N.; Huisman, G. W.; Hughes, G. J. *Science* **2010**, *329*, 305-309.

(8) Schmid, A.; Dordick, J. S.; Hauer, B.; Kiener, A.; Wubbolts, M.; Witholt, B. *Nature* **2001**, *409*, 258-268.

(9) Breuer, M.; Ditrich, K.; Habicher, T.; Hauer, B.; Kesseler, M.; Sturmer, R.; Zelinski, T. *Angew. Chem. Int. Ed.* **2004**, *43*, 788-824.

(10) Gotor-Fernandez, V.; Brieva, R.; Gotor, V. *J. Mol. Catal. B: Enzym.* **2006**, *40*, 111-120.

(11) Moore, J. C.; Pollard, D. J.; Kosjek, B.; Devine, P. N. *Acc. Chem. Res.* **2007**, *40*, 1412-1419.

(12) Truppo, M. D.; Hughes, G. *Org. Process Res. Dev.* **2011**, *15*, 1033-1035.

(13) Brocklehurst, C. E.; Laumen, K.; La Vecchia, L.; Shaw, D.; Vogtle, M. *Org. Process Res. Dev.* **2011**, *15*, 294-300.

(14) Ma, S. K.; Gruber, J.; Davis, C.; Newman, L.; Gray, D.; Wang, A.; Grate, J.; Huisman, G. W.; Sheldon, R. A. *Green Chemistry* **2010**, *12*, 81-86.

(15) L., R. A.; Buddoo, S. R.; Gordon, G. E. R.; Beemadu, S.; Kupi, B. G.; Lepuru, M. J.; Maumela, M. C.; Parsoo, A.; Sibiya, D. M.; Brady, D. *Org. Process Res. Dev.* **2011**, *15*, 249–257.

(16) Chen, Y.; Goldberg, S. L.; Hanson, R. L.; Parker, W. L.; Gill, I.; Tully, T. P.; Montana, M. A.; Goswami, A.; Patel, R. N. *Org. Process Res. Dev.* **2011**, *15*, 241–248.

(17) Schulze, B.; Wubbolts, M. G. *Curr. Opin. Biotechnol.* **1999**, *10*, 609-615.

(18) Pollard, D. J.; Woodley, J. M. *Trends Biotechnol.* **2007**, *25*, 66-73.

(19) Turner, N. J.; Truppo, M. D. *Curr. Opin. Chem. Biol.* **2013**, *17*, 212-214.

(20) Davids, T.; Schmidt, M.; Bottcher, D.; Bornscheuer, U. T. *Curr. Opin. Chem. Biol.* **2013**, *17*, 215-220.

(21) Kries, H.; Blomberg, R.; Hilvert, D. *Curr. Opin. Chem. Biol.* **2013**, *17*, 221-228.

(22) Lorenz, P.; Eck, J. *Nat. Rev. Microbiol.* **2005**, *3*, 510-516.

(23) Magarvey, N. A.; Fortin, P. D.; Thomas, P. M.; Kelleher, N. L.; Walsh, C. T. *ACS Chem. Biol.* **2008**, *3*, 542-554.

(24) Walker, K. D.; Klettke, K.; Akiyama, T.; Croteau, R. *J. Biol. Chem.* **2004**, *279*, 53947-53954.

(25) Lelais, G.; Seebach, D. *Biopolymers* **2004**, *76*, 206-243.

(26) Klettke, K. L.; Sanyal, S.; Mutatu, W.; Walker, K. D. *J. Am. Chem. Soc.* **2007**, *129*, 6988-6989.

(27) Wanninayake, U.; DePorre, Y.; Ondari, M.; Walker, K. D. *Biochemistry* **2011**, *50*, 10082-10090.

(28) Szymanski, W.; Wu, B.; Weiner, B.; de Wildeman, S.; Feringa, B. L.; Janssen, D. B. *J. Org. Chem.* **2009**, *74*, 9152-9157.

(29) Wu, B.; Szymanski, W.; Wietzes, P.; de Wildeman, S.; Poelarends, G. J.; Feringa, B. L.; Janssen, D. B. *ChemBioChem* **2009**, *10*, 338-344.

(30) Wu, B.; Szymanski, W.; Wybenga, G. G.; Heberling, M. M.; Bartsch, S.; de Wildeman, S.; Poelarends, G. J.; Feringa, B. L.; Dijkstra, B. W.; Janssen, D. B. *Angew. Chem. Int. Ed.* **2012**, *51*, 482-486.

CHAPTER 2: Stereochemistry and Mechanism of Phenylalanine Aminomutase from *Pantoea Agglomerans*

2.1. Introduction

2.1.1. Aminomutases: Enzyme Class of 1,2-Amino Isomerases

Intramolecular transferase (EC 5.4) family contains enzymes that transfer acyl-, amino-, phospho- or other functional groups from one position of a molecule to another.[1] Aminomutases (EC 5.4.3) comprise a subclass of the intramolecular isomerase family and catalyze the chemically challenging exchange of an amino group and a proton present on the vicinal carbons of a substrate (Figure 2.1).[2]

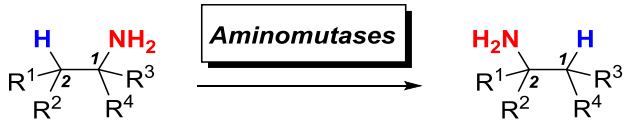

Figure 2.1. 1,2-Amino shift reaction catalyzed by aminomutases.

Aminomutases have gained much attention in recent years due to their potential application as biocatalysts in the production of pharmacologically significant molecules and intermediates.[3] The aminomutase family consists of lysine 2,3- (EC 5.4.3.2),[4,5] β-lysine 5,6- (EC 5.4.3.3),[6,7] D-lysine 5,6- (EC 5.4.3.4),[6,7] D-ornithine 4,5- (EC 5.4.3.5),[8] tyrosine 2,3- (EC 5.4.3.6),[9,10] leucine 2,3- (EC 5.4.3.7),[11] glutamate-1-semialdehyde 2,1- (EC 5.4.3.8),[12,13]

glutamate 2,3- (EC 5.4.3.9),[14] and phenylalanine- (EC 5.4.3.10[15] and EC 5.4.3.11[16]) aminomutase enzymes. Additionally, a very recently discovered 2-aza-L-tyrosine aminomutase catalyzes a 2,3-isomerization reaction.[17]

2.1.2. Mechanistic Diversity of Aminomutases

Aminomutases use various cofactors to catalyze the challenging vicinal exchange of the amino group and a proton. The aminomutase reaction bifurcate into homolytic and heterolytic mechanistic classes. The mechanisms of lysine 2,3-,[4,5] β-lysine 5,6-,[6,7] D-lysine 5,6-,[6,7] D-ornithine 4,5-,[8] leucine 2,3-,[11] and glutamate 2,3-aminomutases[14] involve radical intermediates. These enzymes use either *S*-adenosyl methionine (SAM), pyridoxal 5'-phosphate (PLP) and a $[4Fe\text{-}4S]^{+}$ cluster or adenosylcobalamin (vitamin B12) and PLP as cofactors. Tyrosine-[9,10] and phenylalanine-aminomutases[15,16] catalyze their reactions by a heterolytic isomerization mechanism that requires the 4-methylidene-1*H*-imidazol-5(4*H*)-one (MIO) prosthetic group.

2.1.3. Homolytic Mechanisms of Aminomutases

2.1.3.1. Adenosylcobalamin-dependent Mechanisms

Adenosylcobalamin-dependent aminomutases rely on coenzyme B_{12} and PLP cofactors are mainly involved in catabolic pathways of amino acids. For example, lysine 5,6-[6,7] and ornithine 4,5-aminomutase[8,18] isolated from *Clostridium sticklandii* participates in fermentation of DL-lysine and L-ornithine, respectively.

Lysine 5,6-aminomutases catalyze the migration of the ε-amino group of either D-lysine or L-β-lysine to the δ-carbon, respectively producing 2,5-diminohexanoate and (3*S*,5*S*)-diaminohexanoate.[7] Similarly, D-ornithine aminomutase catalyzes the conversion of D-ornithine to (2*R*,4*S*)-2,4-diaminopentanoic acid by exchanging the δ-amino group and a γ-proton.[8] These enzymes follow a radical-mediated mechanism using adenosylcobalamin as the source of radicals (Figure 2.2). Binding of the substrate to the enzyme induces the homolytic cleavage of the weak Co-C bond in adenosylcobalamin, generating cob(II)alamin and 5'-deoxyadenosyl radical (Ado-$^{\bullet}CH_2$) (Figure 2.2).[7,8]

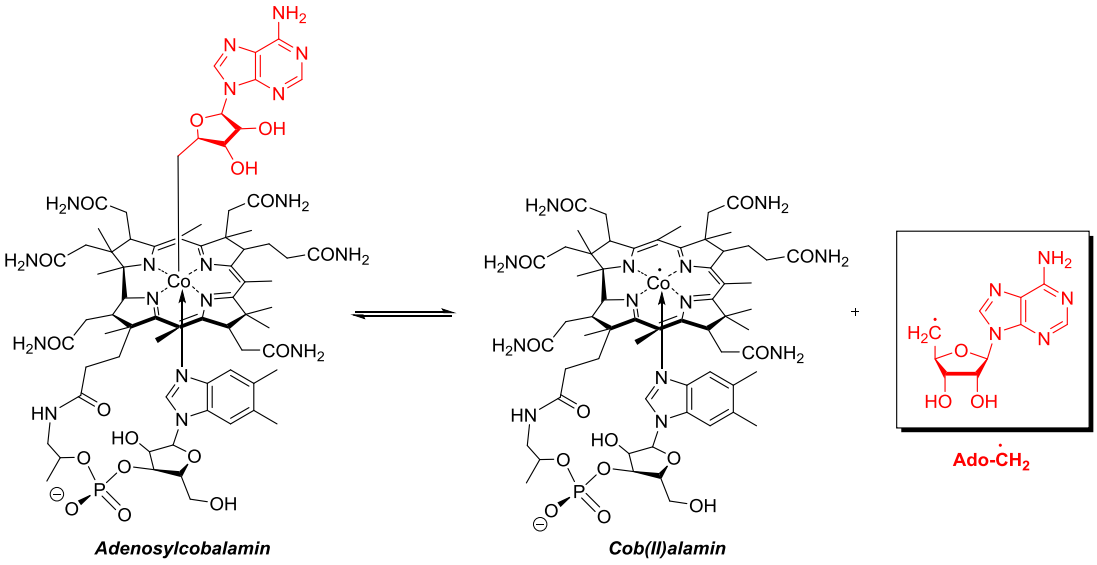

Figure 2.2. Generation of the 5'-deoxyadenosyl radical (Ado-$^{\bullet}CH_2$) species from the homolytic Co-C bond cleavage of adenosylcobalamin.

During the isomerization reactions (Figure 2.3), PLP cofactor covalently bound as a schiff base to an active site lysine residue (**1**) makes an imine (**2**) with the ε/δ-amino group of the substrate via a transaminase reaction. Then the highly reactive Ado-$^{\bullet}CH_2$ species abstracts a

hydrogen from the PLP-bound substrate producing 5'-deoxyadenosine (Ado-CH_3) and a carbon-centered substrate radical intermediate **3**. The PLP-bound substrate radical in turn rearranges to the product radical **5**, which regains a proton from Ado-CH_3 generating the PLP-bound product **6**. Finally, the isomerized amino acid **7** is released while PLP rebinds with the enzymatic lysine residue as a schiff base. Investigation of the steric course of β-lysine 5,6-aminomutase indicated that the overall substitution at δ-C occurs with inversion of configuration.[19,20] However, stereochemical control of other enzymes of this class has not been evaluated so far.

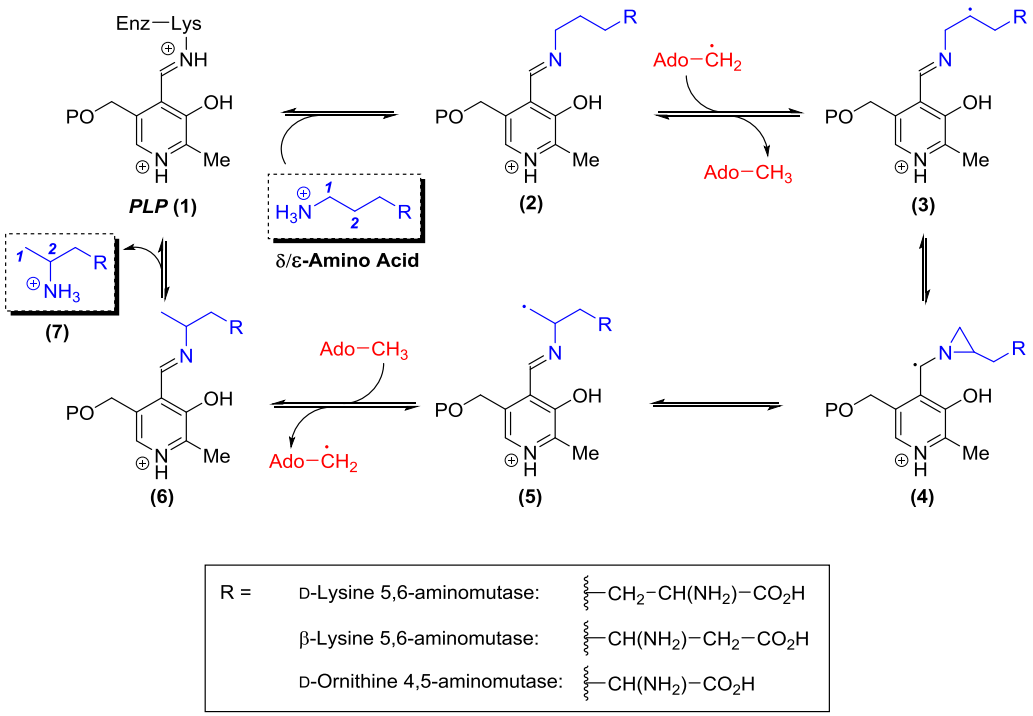

Figure 2.3. Mechanism of isomerization reaction catalyzed by adenosylcobalamin-dependent aminomutases. 5'-Deoxyadenosyl radical (Ado-$^{\bullet}CH_2$) formed from adenosylcobalamin and PLP cofactor assists the chemically challenging 1,2-amino shift.

2.1.3.2. *S*-Adenosyl Methionine-dependent Mechanisms

The reactions catalyzed by *S*-adenosyl methionine (SAM)-dependent isomerases are closely related to the coenzyme B_{12}-dependent rearrangements.[21] The $[4Fe\text{-}4S]^+$ cluster functions analogous to adenosylcobalamin and mediates the formation of highly reactive 5'-deoxyadenosyl radical from SAM (Figure 2.4A).[21] Furthermore, similar to adenosylcobalamin-dependent aminomutases, radical-stabilizing PLP serves as a cofactor in this class of enzyme catalysis. However, in contrast to adenosylcobalamin-dependent enzymes, these enzymes catalyze the α- to β-amino acid conversions. For example, lysine 2,3-, and glutamate 2,3-aminomutases isomerize (2*S*)-α-lysine and -glutamate, respectively, to their corresponding β-amino counterparts.[4,14] In anaerobic bacteria such as *Clostridium subterminale* and *Porphyromonas gingivalis*, which utilize L-lysine for growth as a carbon and nitrogen source, lysine 2,3-aminomutase plays a role in L-lysine metabolism.[4] Furthermore, the conversions catalyzed by lysine 2,3-aminomutases provide a pool of β-lysine for the biosynthesis of antibiotics such as streptothricin F, viomycin and Capreomycin IB.[5,22,23] A recently characterized glutamate 2,3-aminomutase found in *Clostridium difficile* is believed to participate in glutamate metabolism.[14] Additionally, the β-glutamate likely serves as an osmolyte in bacterial and archeal species.[24]

The mechanism of the 1,2-amine shift catalyzed be SAM-dependent aminomutases is similar to the adenosylcobalamin-dependent mechanism (Figure 2.4B).[21] PLP reacts initially with the α-amino group of the substrate (**7**) to form an external aldimine. In this mechanism, Ado-$^{\bullet}CH_2$ mediated abstraction of a prochiral proton from β-carbon of the PLP bound substrate followed by radical rearrangements produce the product-like radical intermediate **11**. A proton is

transferred to intermediate **11** from Ado-CH_3, and then the β-amino acid **13** is released from a transamination reaction.

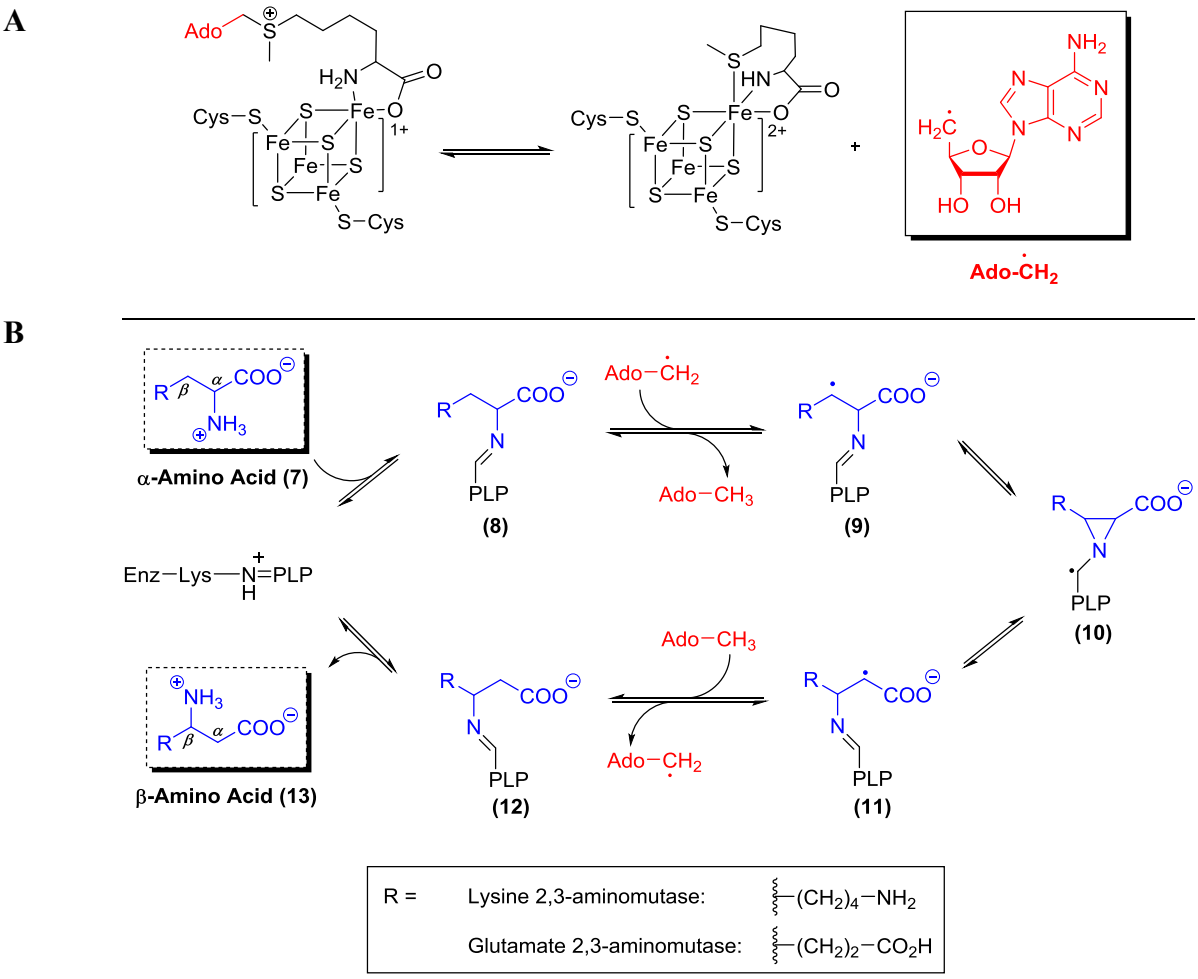

Figure 2.4. Mechanism of isomerization reaction catalyzed by SAM-dependent aminomutases. *A*) $[4Fe\text{-}4S]^+$ mediated formation of Ado-$^{\bullet}CH_2$ species from SAM. *B*) PLP-dependent mechanism of α- to β-amino acid isomerization.

Although the stereochemical control of recently discovered glutamate 2,3-aminomutase is still unknown,[14] the stereochemistry of lysine 2,3-aminomutase has been studied extensively.[24] In

Clostridium sp., the conversion of (2*S*)-α-lysine to (3*S*)-β-lysine proceeds with inversion of configuration at both C-2 and C-3 (Figure 2.5).[25] Ado-$^{\bullet}CH_2$ species abstracts the *pro*-(3*R*) hydrogen from the lysyl-side chain of the PLP bound substrate and transfers it to the *pro*-(2*R*)-position of β-lysine. Furthermore, amino group transfer occurs intramolecularly to the original position of *pro*-(3*S*)-proton in (2*S*)-α-lysine. In addition, the interconversion of α- to β-lysine was shown to occur with little or no exchange of substrate hydrogens with solvent hydrogens.[26]

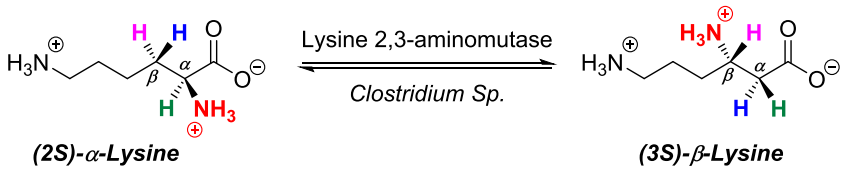

Figure 2.5. Stereochemical course of lysine 2,3-aminomutase from *Clostridium sp.*

Lysine 2,3-aminomutase (LAM) from *E. coli* produces (3*R*)-β-lysine which is the enantiomer produced by the analogous enzymes from *Clostridium* and *Bacillus sp*.[4] Most of the active site residues that make contacts with the substrate are conserved in both enzymes, except the Asp330 in the Clostridial lysine aminomutase.[4] The *E. coli* homologue has a glutamate residue in the corresponding position, and these residues make ionic contacts with the ε-amino group of the substrate. It was suggested that the steric bulk of the glutamate residue in the *E. coli* LAM forces the lysyl-side chain of the substrate to bind in a more restricted conformation. The variant configuration of the lysyl-side chain allows the abstraction of the *pro*-(3*R*) hydrogen from (2*S*)-α-lysine.[4] Furthermore, This configuration leads to an (*R*)-configuration in the azacyclopropylcarbinyl radical (**10**) and in the β-lysine product (Figure 2.4).

2.1.4. Heterolytic Mechanisms of Aminomutases: MIO-dependent Mechanisms

In contrast to other aminomutases, recently characterized MIO-dependent aminomutases catalyze a heterolytic isomerization mechanism.[9,15] In 1998, Walker and coworkers reported an unusual aminomutase from *Taxus brevifolia*, which was the first aminomutase found in a higher plant.[27] This enzyme is the first ever reported example of a phenylalanine aminomutase, and it was proposed to catalyze the production of (3*R*)-β-phenylalanine for the biosynthesis of anti-cancer drug Taxol.[27] Furthermore, the reaction was shown to proceed with intramolecular amino group migration with retention of configuration at the β-carbon. The retention-of-configuration observed for this enzyme was distinctly different from inversion-of-configuration of all other microbial aminomutases characterized at that time. However, the MIO-dependency of phenylalanine aminomutases was not established from the assays carried out with crude cell-free extracts of *T. brevifolia* bark.[27]

After a span of five years, in 2003, Christenson et. al. discovered the novel MIO-dependent class of aminomutases, which are principally homologous to a family of ammonia lyases.[9] They identified a tyrosine aminomutase (TAM) form *Streptomyces globisporos* (*Sg*TAM) that is homologous to MIO-dependent *Streptomyces griseus* histidine ammonia lyase[28] (39% identity and 56% similarity) and *Streptomyces maritimus* phenylalanine ammonia lyase[29] (38% identity and 56% similarity). The MIO cofactor in ammonia lyases was previously identified in the X-ray structure of a histidine ammonia lyase (EC 4.3.1.3).[30] This cofactor was proposed to form autocatalytically by cyclization three active-site residues (Ala-Ser-Gly) followed by dehydration (Figure 2.6). The *Taxus* phenylalanine aminomutase and tyrosine aminomutase consist of an MIO group formed from the signature Ala-Ser-Gly motif.[9,15] By

contrast, the MIO moiety of a recently characterized phenylalanine aminomutase from *Pantoea agglomerans* is formed from a *Thr*-Ser-Gly sequence.[16]

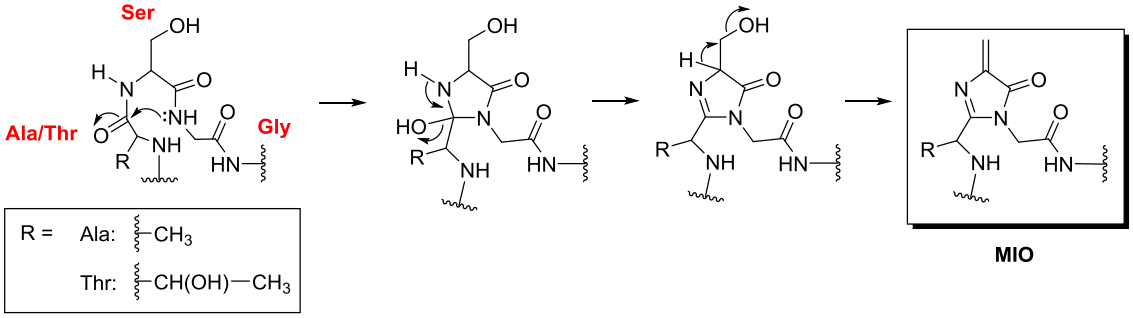

Figure 2.6. Mechanism of MIO cofactor formation from active site residues Ala/Thr-Ser-Gly.

Pre-incubation of *Sg*TAM with $NaBH_4$ and KCN abolished the activity by presumed nucleophilic inactivation of the MIO cofactor.[9] In addition, the Ser153Ala mutation of Ala-Ser-Gly catalytic triad decreased the activity of *Sg*TAM 340-fold compared to the wild-type enzyme.[9] Taken together, these results strongly suggested the dependency of *Sg*TAM catalysis on the MIO cofactor.

MIO-dependent aminomutases occur on various biosynthetic pathways and catalyze the 2,3-amino group migration to make non-proteinogenic β-amino acids from the corresponding (2*S*)-α-aromatic amino acid (Table 2.1). Phenylalanine 2,3-aminomutases from *Taxus sp.* (*Tc*PAM) and *Pantoea agglomerans* bacteria (*Pa*PAM) catalyze the production of β-phenylalanine in Taxol and antibiotic andrimid biosynthesis, respectively.[16,20] In addition to *Sg*TAM on the enediyne antitumor antibiotic C-1027 biosynthetic pathway, another TAM from *Chondromyces cracatu*s (*Cc*TAM) is involved in the production of β-tyrosine for cytotixic chondramides biosynthesis.[31] Furthermore, MdpC4 TAM from *Actinomadura madurae*, MfTAM

from *Myxococcus fulvus*, and MxTAM from *Myxococcus sp.* Mx-BO have also been characterized.[10,32] A recently discovered KedY4 aminomutase on the antitumor antibiotic kedarcidin biosynthetic pathway in *Streptoalloteichus sp.* now increases the breadth of MIO-dependent aminomutases.[17] The latter aminomutase stereospecifically catalyzes the conversion of 2-aza-L-tyrosine to (*R*)-2-aza-β-tyrosine and is the first MIO-dependant aminomutase found to accept a natural product heteroaromatic substrate.[17]

The MIO cofactor is believed to serve as the electrophile in the isomerization reactions performed by this class of enzymes.[30] However, an active debate for decades centers on whether the amino group or the aromatic ring of the substrate acts as the nucleophile. Two mechanisms have been proposed for MIO-catalyzed isomerization of α- to β-amino acids (Figure 2.1).[33]

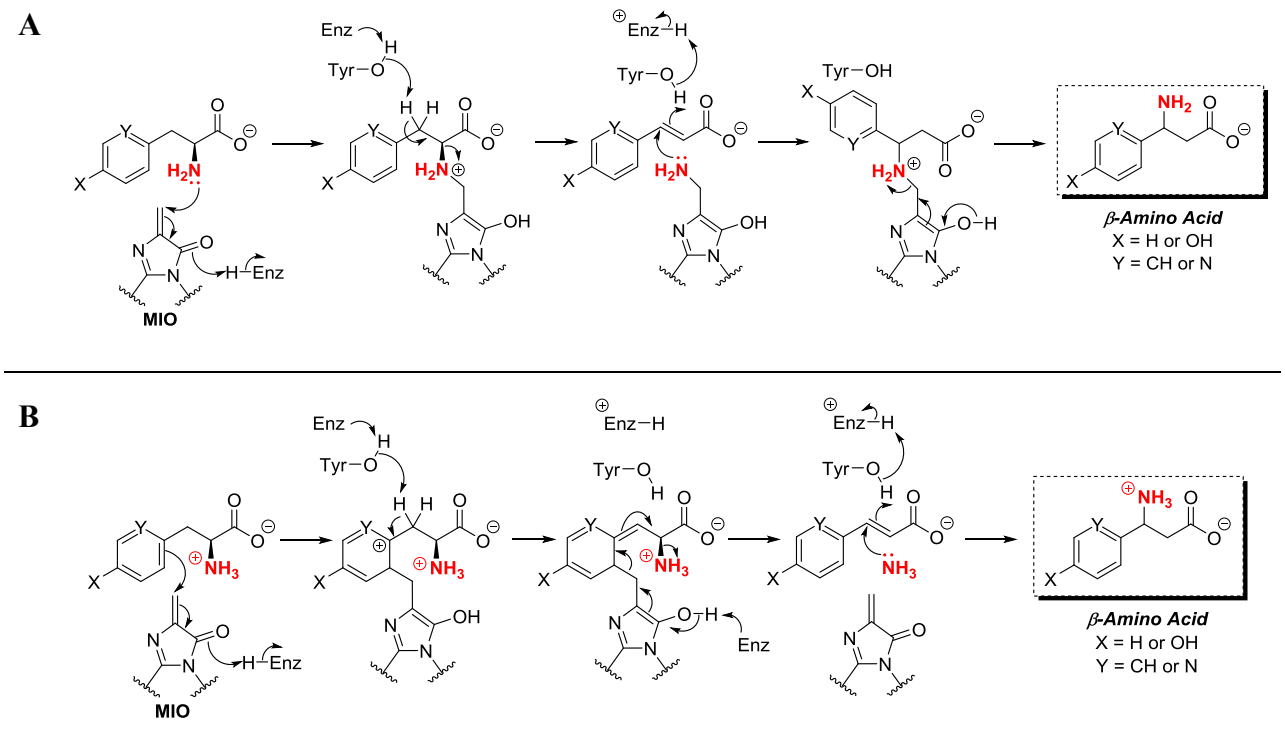

Figure 2.7. Mechanistic proposals for MIO-dependant aminomutases. *A*) Amino-alkylation and. *B*) Friedel-Crafts aryl-alkylation pathway.

In the amino-alkylation mechanism, the electrophilic methylidene of the MIO cofactor was postulated to react with the α-amino group of the substrate (Figure 2.7A). The second proposed mechanism suggests π-electrons of the aromatic ring act as the nucleophile in an Friedel-Crafts-type addition to attack the *ortho*-carbon to the MIO (Figure 2.7B). Both mechanisms are proposed to reduce the p*K*a of the β-hydrogens and facilitate their removal by an enzymatic base (Tyr).[33] Subsequent elimination of ammonia generates an aryl acrylate intermediate that is occasionally released, yet also serves as a scaffold for stereospecific amination at the β-carbon to produce the corresponding β-amino acid.

The stereochemical course of tyrosine- (TAMs) and phenylalanine-aminomutases (PAMs) are extensively studied (Table 2.1), and these enzymes can be categorized based on the enantioselectivity for the β-amino acid. *Sg*TAM[9] and *Pa*PAM[16] produce (3*S*)-β-arylalanines while *Tc*PAM[20] and *Cc*TAM[31] make (3*R*)- β-isomers. However, TAMs are less enantioselective compared to PAMs. Both TAMs produce one enantiomer under kinetic control, but the opposite stereoisomer is also produced upon prolonged incubation of the enzyme with the substrate.[10,33] For *Sg*TAM, (3*R*)-β-tyrosine is produced more slowly, but eventually reaches a 1:1 ratio with the (3*S*)-isomer due to the β-tyrosine racemase activity of TAMs.[33] By comparison, *Cc*TAM produces 85% of (3*R*)-β-tyrosine and 15% of (3*S*)-β-tyrosine at pH 8.5, and this ratio varies with the pH.[34] Consequently, TAMs catalyze the isomerization reaction with both inversion and retention of configuration at the α- and β-carbons.

Table 2.1. Stereochemistry of β-arylalanine products produced from MIO-dependent aminomutases and their corresponding biosynthetic products

Enzyme	Substrate	Product	Configuration at C-α & C-β	Biosynthetic product
Tyrosine Aminomutase (*Streptomyces globisporus*)	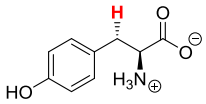 (2*S*)-α-Tyrosine	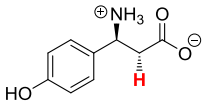 (3*S*)-β-Tyrosine	Inversion	Antitumor antibiotic C-1027
		1:1 (3*S*):(3*R*)-β-tyrosine at equilibrium conditions	Inversion and retention	
Tyrosine Aminomutase (*Chondromyces cracatus*)	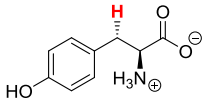 (2*S*)-α-Tyrosine	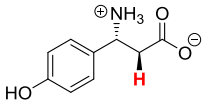 (3*R*)-β-Tyrosine	Retention	Cytotoxic chondramides
		6:1 (3*R*):(3*S*)-β-tyrosine at equilibrium conditions	Inversion and retention	
Tyrosine Aminomutase (*Actinomadura madurae*)	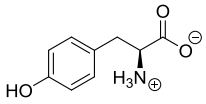 (2*S*)-α-Tyrosine	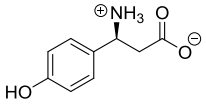 (3*S*)-β-Tyrosine	Unknown	Antitumor antibiotic maduropeptin
Tyrosine Aminomutase (*Myxococcus sp.*)				Bacterial protein biosynthesis inhibitor myxovalargin
Phenylalanine Aminomutase (*Taxus sp.*)	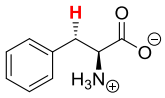 (2*S*)-α-Phenylalanine	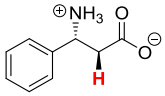 (3*R*)-β-Phenylalanine	Retention	Anti-cancer Taxol
Phenylalanine Aminomutase (*Pantoea agglomerans*)	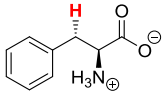 (2*S*)-α-Phenylalanine	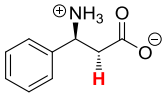 (3*S*)-β-Phenylalanine	Unknown	Antibiotic andrimid
2-Aza-tyrosine Aminomutase (*Streptoalloteichus sp.*)	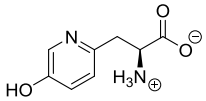 2-Aza-L-Tyrosine	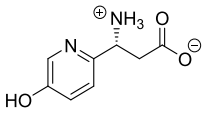 (*R*)-2-Aza-β-Tyrosine	Unknown	Antitumor antibiotic kedarcidin

Interestingly, isomerization reactions of PAMs are highly enantioselective (>99.9%) and preclude enantiomeric mixtures. Thus, PAMs are potential sources for the scalable biocatalytic production of enantiomerically pure β-arylalanines as synthetic building blocks of pharmaceuticals.[35] The formation of (3*R*)-β-phenylalanine catalyzed by *Tc*PAM occurs with intramolecular exchange of the *pro*-(3*S*)-proton and the α-amino group with the retention-of-configuration at both reaction termini.[15,20] Consequently, this process demands the removal and reattachment of the migrating partners from the opposite stereo-faces of the cinnamic acid intermediate. The homologous *Pa*PAM enzyme makes the opposite β-phenylalanine stereoisomer and its stereochemical course is described herein.

2.1.5. Other Aminomutases

Few initial reports were published about the occurrence of a coenzyme B_{12}-dependent leucine 2,3-aminomutase involved in leucine catabolism in various organisms including animals, plants, and microorganisms.[36-38] Freer and co-workers in 1981 reported on an *Andrographis panicdata* leucine 2,3-aminomutase that converted (2*S*)-α- to (3*R*)-β-leucine, yet coenzyme B_{12} was not required.[11] In addition, the existence of leucine 2,3-aminomutase in mammalian tissues has been questioned since β-leucine has not yet detected in rat liver or human blood.[39] Further, there are no detailed studies describing the mechanism and stereochemistry of the characterized leucine 2,3-aminomutase.

In 1980, Parry and coworkers suggested the occurrence of an ATP-dependent *Bacillus brevis* Vm4 tyrosine 2,3-aminomutase (*Bb*TAM) in biosynthetic pathway to the antibiotic

edeine-A and -B.[40] From a recent (2004) personal communication with Parry, this original obeservation was likely an error (K.D.W.). However, this investigation did substantiate that *Bb*TAM does not require PLP, *S*-adenosylmethionine, and adenosylcobalamin as a cofactor, and that the enzyme was inhibited with reagents that react with carbonyl groups.[40] While the exact carbonyl reacting reagents are not described, this data suggest the dependency of *Bb*TAM on an MIO, which bears an α,β-unsaturated carbonyl group that reacts with reducing agents ($NaBH_4$) and nucleophiles (KCN).[9,20] Detailed mechanistic analyses carried out with cultures of *B. brevis* suggested that (3*S*)-β-tyrosine was formed with the inversion-of-configuration at C_β after the *pro*-(3*S*) proton is removed.[40] However, the configuration of C_α was not analyzed in this study and no further investigations are reported.

The mechanism and stereochemistry of the (3*S*)-β-arginine made on the biosynthetic pathway of antibiotic blasticidin S biosynthesis was examined by feeding variously labeled α-arginines to whole-cell cultures of *Streptomyces griseochromogenes*.[41] The aminomutase reaction was observed to proceed with inversion-of-configuration at the reaction termini. The α-amino group was transferred intramolecularly to the β-carbon of the substrate. This arginine 2,3-aminomutase is 48% identical and 65% similar to *C. subterminale* lysine aminomutase, and includes the conserved lysine for PLP attachment;[42] however, the cofactor requirement of this enzyme could not assessed in this *in vivo* experiments. But based on sequence similarity alone, the arginine aminomutase likely catalyzes the isomerization reaction via a radical-dependent homolytic mechanism. Unfortunately, recent efforts on detecting the aminomutase activity of arginine 2,3-aminomutases from *E. coli* and *Streptomyces lividans* were not successful.[42]

Glutamate 1-semialdehyde 2,1-aminomutase uses only PLP as a cofactor for the amino group shift, without the involvement of free radical intermediates.[12] In cyanobacteria, green and purple sulphur bacteria, and higher plants, glutamate 1-semialdehyde 2,1-aminomutase catalyzes the conversion of glutamate 1-semialdehyde to δ-aminolevulinic acid (Figure 2.8), the universal precursor for the biosynthesis of heme, chlorophyll, and other tetrapyrroles.[12,13] However, these enzymes demonstrate a clear sequence similarity to aminotransferases of the α-family of B_6-dependent enzymes, and mechanistically act as an aminotransferase rather than an aminomutase.[43]

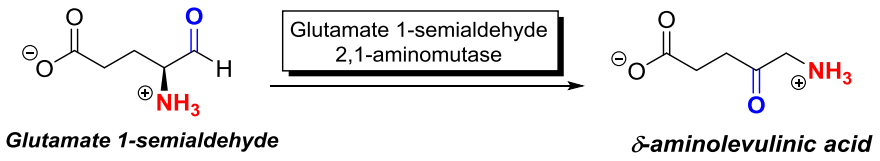

Figure 2.8. Reaction catalyzed by glutamate 1-semialdehyde 2,1-aminomutase.

2.2. Experimental

2.2.1. Chemicals and Reagents

Unlabeled (2*R*)- and (2*S*)-α-phenylalanines were obtained from Sigma-Aldrich; [3,3-$^{2}H_{2}$]-(2*S*)-α-phenylalanine, [U-^{13}C, 2-^{15}N]-(2*S*)-α-phenylalanine, [ring, β-C-$^{2}H_{6}$]-*trans*-cinnamate, and [2-^{15}N]-(2*S*)-α-phenylalanine were purchased from Cambridge Isotope Laboratories (Andover, MD). *ortho*-Methyl-(2*S*)-α-phenylalanine was obtained from Peptech (Burlington, MA). [2,3-$^{2}H_{2}$]-*N*- Acetyl (2*S*,3*R*)/(2*R*,3*S*)-β-phenylalanine methyl ester, [ring, 2,3-$^{2}H_{7}$]-(2*S*,3*S*)-α-phenylalanine (90% ee, 98+% enriched), and racemate [ring, 3-$^{2}H_{6}$]-(2*R*,3*S*)/(2*S*,3*R*)-α-phenylalanine (98+% enriched) were sample stocks from the Walker laboratory that had been synthesized according to reported literature[20,44] and were characterized as described below. All other chemicals and reagents were obtained from Sigma-Aldrich and utilized without further purification, unless noted otherwise.

2.2.2. Instrumentation

A gas chromatograph (model 6890N, Agilent) coupled to a mass selective detector (model 5973 *inert*®, Agilent) was used for the analysis of derivatized amino acids. Samples were loaded onto a 5HS GC column (0.25-mm inner diameter × 30 m, 0.25-μm film thickness) mounted in a GC oven. The GC oven conditions were as follows: column temperature was programmed from 70 °C to 250 °C or 300 °C at 10 °C/min (23 min and 18 min total runtime,

respectively), splitless injection was selected, and helium was used as the carrier gas (1.2 ml/min). The MS conditions were set with an ion scan mode from 100 - 400 atomic mass units at 70 eV ionization voltage. All ^{1}H- (500 MHz) and ^{2}H-NMR (76.7 MHz) spectra were obtained on a Varian superconducting NMR-Spectrometer using standard acquisition parameters.

2.2.3. Characterization of Racemate [ring, 3-$^{2}H_6$]-(2*R*,3*S*)/(2*S*,3*R*)-α-Phenylalanine and [ring, 2,3-$^{2}H_7$]-(2*S*,3*S*)-α-Phenylalanine

2.2.3.1. GC/EI-MS Analysis

The racemate and the enantiopure amino acid (~0.25 mg) were separately dissolved in 50 mM phosphate buffer (pH 8.5) and adjusted to pH > 10 (6 M NaOH). Camphanoyl chloride (0.5 mg) was added to derivatize the amino acids to their *N*-[(1'*S*)-camphanoyl] analogues. The solution was acidified to pH 2 (6 M HCl) and extracted with ethyl acetate, the organic fractions were combined (2 mL), to which methanol (700 μL) was added. A solution TMS-diazomethane was added dropwise to the ethyl acetate/methanol solution to convert the acids to their methyl esters. Each sample was separately analyzed by GC/EI-MS. (Figure A.1.1).

2.2.3.2. ^{1}H- and ^{2}H-NMR Analyses

The racemic mixture and the enantiopure amino acid (~0.5 mg of each, as their free amino acids) were separately dissolved in H_2O (600 μL) and D_2O (600 μL), and analyzed by ^{2}H-NMR (3,500 scans) and ^{1}H-NMR (200 scans), respectively (Figure A.1.2 and Figure A.1.3, respectively).

2.2.3.3. Analysis of Stereochemistry by the Phenylalanine Ammonia Lyase (PAL) Reaction Stereospecificity

Phenylalanine ammonia lyase (Sigma-Aldrich, St. Louis, MO; PAL) catalyzes the non-oxidative deamination of (2*S*)-α-phenylalanine to *trans*-cinnamic acid and ammonia. This deamination mechanism was shown to proceed stereospecifically with removal of the *pro*-(3*S*) proton and the ammonia from the substrate.[45] PAL was used to assess the stereochemistry at C_β of racemate [ring, 3-$^2H_6$]-(2*R*,3*S*)/(2*S*,3*R*)-α-phenylalanine and the enantiopure [ring, 2,3-$^2H_7$]-(2*S*,3*S*)-α-phenylalanine. Each compound at ~3 mM in 1 mL of 50 mM phosphate buffer (pH 7.5), were incubated with PAL (20 μg; from *Rhodotorula glutinis*; Sigma-Aldrich) for 1 h at 31 °C. The reactions were acidified to pH 2 (6 M HCl), extracted with ethyl acetate (2 × 1 mL), and the organic fractions were combined. Methanol (700 μL) was added to the ethyl acetate, and a TMS-diazomethane solution was added dropwise to methyl esterify the carboxylic acids. The cinnamic acid methyl esters were analyzed by GC/EI-MS (Figure A.1.4 and Figure A.1.5).

2.2.4. Protein Expression and Purification

E. coli (BL21) cells transformed to express the *papam* gene were grown in six 1-L cultures of Luria-Bertani medium. The media was supplemented with kanamycin (50 μg/mL) at 37 °C and grown until the cell density reached an optical density of A_{600} ~ 0.6, after which protein expression was induced with isopropyl-β-D-thiogalactopyranoside (100 μM) at 16 °C. After 16 h, the cells were harvested by centrifugation at 6,000*g* (15 min) and the cell pellet was resuspended in lysis buffer (50 mM sodium phosphate containing 5% (v/v) glycerol, 300 mM

NaCl and 10 mM imidazole, pH 8.0), and the suspension was lysed by sonication. The cellular debris and light membranes were removed by centrifugation at 9,700*g* (45 min), and 102,000*g* (1h), respectively, to provide soluble enzyme extract.

The resultant crude aminomutase in the soluble fraction was purified by Nickel-nitrilotriacetic acid (Ni-NTA) affinity chromatography according to the protocol described by the manufacturer (Qiagen, Valencia, CA). *Pa*PAM fractions eluted in 250 mM imidazole were combined and loaded into a size selective centrifugal filtration unit (Centriprep centrifugal filter units, 30,000 MWCO; Millipore). Then the protein solution was concentrated and the buffer was exchanged with 50 mM sodium phosphate containing 5% (v/v) glycerol (pH 8.0) using the same Centriprep centrifugal filter unit. The purity (>95%) of the concentrated enzyme was assessed by SDS−PAGE with Coomassie Blue staining, and the quantity was determined by the Bradford protein assay.

2.2.5. Assessment of Absolute Stereochemistry of the β-Phenylalanine Product Produced by *Pa*PAM

(2*S*)-α-Phenylalanine (500 μM) was incubated with *Pa*PAM (100 μg) in 1.0 mL of phosphate buffer (pH 8.0) at 31 °C. After 3 h, the reaction was terminated by basification to pH 10 (6 M NaOH). (1*S*)-(−)-camphanic chloride (0.5 mg) was then added and allowed to react for 30 min. After derivatization, the mixture was acidified to pH 2-3 (6 M HCl) and extracted with ethyl acetate (2 x 1 mL). Then the organic solvent was evaporated under vacuum, the residue was dissolved in ethyl acetate/methanol (3:1, v/v) (200 μL), and the solution was treated with

excess (trimethylsilyl)diazomethane until a persistent faint yellow color persisted. The derivatized β-amino acid was identified by GC/EI-MS analysis and compared against the retention time and mass spectral fragmentations of authentic *N*-[(1'*S*)-camphanoyl]-(3*S*)-β-phenylalanine methyl ester derivatized similarly.

2.2.6. Enzymatic assays

α-Phenylalanine isotopes (each at 500 μM) were incubated with *Pa*PAM (50 μg) in 1-mL assays for 1 h. When applicable, [ring, β-C-$^{2}H_{6}$]-(*E*)-cinnamic acid (500 μM) was added to the reaction in competitive assays. In each experiment, control experiments were run in parallel by incubating substrate without enzyme; enzyme without substrate; and a single substrate in competitive assays. After 1 h, the reaction was terminated by basification to pH 10 (6 M NaOH), and the resulting amino acids were derivatized for analysis by GC/EI-MS.

2.2.7. Derivatization and Analysis of Amino Acids

The amino acids in all assays were generally derivatized as follows: To each terminated assay at pH 10, benzoyl chloride (50 μl) was added, and the solution was thoroughly stirred. After 10 min, the solution was again basified to pH 10 (6 M NaOH) and a second batch of benzoyl chloride (50 μl) was added, stirred and allowed to react for 10 min. Then the mixture was acidified to pH 2-3 (6 M HCl) and extracted with ethyl acetate (2 x 1 mL). The organic solvent was evaporated under vacuum, and the resulting residue was dissolved in ethyl

acetate/methanol (3:1, v/v) (200 μL). The solution was treated with excess (trimethylsilyl)diazomethane until a faint yellow color persisted to convert the derivatized amino acids to their methyl esters. The derivatized β-amino acids were analyzed and identified by GC/EI-MS analysis.

2.2.8. Determining the Stereochemistry of Hydrogen Rebound

[3,3-$^2H_2$]-α-Phenylalanine (5 mM) was incubated with *Pa*PAM (2 mg) in 2.5 mL of phosphate buffer (pH 8.0) at 31 °C for 2 h. The amino acid isotopomers were derivatized as described before except the *N*-acetyl methyl esters were made using acetic anhydride instead of benzoyl chloride. The mixture of the derivatized deuterium-labeled α- and β-amino acids from the assay was dissolved in $CHCl_3$ (600 μL) and analyzed by ^{2}H-NMR (18,700 scans). Similarly, [3,3-$^2H_2$]-α-phenylalanine and a mixture of unlabeled (2*S*)-α- and (3*S*)-β-phenylalanine isolated from phosphate buffer (pH 8.0) were derivatized as their *N*-acetyl methyl esters and analyzed by ^{2}H-NMR (76.7 MHz, $CHCl_3$) and ^{1}H-NMR, respectively (500 MHz, $CDCl_3$). A ^{2}H-NMR spectrum of synthetically-derived authentic standard [2,3-$^2H_2$]-*N*-acetyl (2*S*,3*R*)/(2*R*,3*S*)-β-phenylalanine methyl ester was used for reference.

2.2.9. Kinetic Parameters of *Pa*PAM with *o*-Methyl-(2*S*)-α-Phenylalanine

*Pa*PAM (10 μg) was incubated with *o*-methyl-(2*S*)-α-phenylalanine (1 mM) to establish steady-state conditions with respect to a fixed protein concentration and time at 31°C. Under

steady-state conditions, the substrate at 10, 20, 40, 80, 150, 300, 500, 750 and 1000 μM were separately incubated with enzyme (10 μg) for 1 h in single stopped-time assays. Then the *o*-methylcinnamic acid product was derivatized as the methyl ester and the amino acids were derivatized as the *N*-(ethoxycarbonyl) methyl ester as described previously using ethyl chloroformate and (trimethylsilyl)diazomethane. Derivatized products were then quantified by GC/EI-MS analysis. The kinetic parameters (K_M and k_{cat}) were determined from the Hanes-Woolf plot (R^2 ~0.99).

2.3. Results and Discussion

2.3.1. Absolute Configuration of the Biosynthetic β-phenylalanine

Absolute configuration of biosynthetic β-phenylalanine derived from *Pa*PAM was assigned by incubating *Pa*PAM with (2*S*)-α-phenylalanine under standard assay conditions and converting the products to *N*-(1(*S*)-camphanoyl) methyl esters for subsequent GC/EI-MS analysis. The derivatized β-amino acid showed an identical retention time (16.02 min) and corresponding fragments ions to the authentic *N*-[(1'*S*)-camphanoyl]-(3*S*)-β-phenylalanine methyl ester (Figure 2.9). There was no detectable product at 15.86 min corresponding to the retention time of authentic *N*-[(1'*S*)-camphanoyl]-(3*R*)-β-phenylalanine methyl ester. Therefore the absolute configuration of the biosynthetic product was established as (3*S*)-β-phenylalanine.

2.3.2. Mechanism of Amino Transfer

Based on the reaction of the homologous PAM from *Taxus* plants, (*E*)-cinnamate is a proposed intermediate of the forward reaction during isomerization of α- to β-phenylalanine.[46] In addition, (*E*)-cinnamate is reported as a substrate used to make a mixture of α- and β-phenylalanines in presence of an amino source (6 M NH_3 and styrylalanine).[47,48] Thus, to evaluate whether *Pa*PAM could transfer the amino group from phenylalanine to an exogenous (*E*)-cinnamate, a mixture of [ring, β-C-$^2H_6$]-(*E*)-cinnamate (98+% ^{2}H-enriched, 500 μmol) and [^{15}N]-(2*S*)-α-phenylalanine (98+% ^{15}N-enriched, 500 μmol) were incubated with *Pa*PAM under

standard assay conditions. Resulting product mixtures were derivatized as *N*-benzoyl methyl esters and analyzed by GC/EI-MS. For quantitative analysis of isotopic enrichment and distribution, authentic standard (3*S*)-β-phenylalanine was also derivatized as *N*-benzoyl methyl ester and analyzed by GC/EI-MS. Authentic standard was comprised of low abundance molecular ion ($[M]^+$) of *m/z* = 283 and two diagnostic mass fragments ions at *m/z* = 210 $\{[M - CH_2C(O)OCH_3]^+\}$ and *m/z* = 178 $\{[M - PhC(O)]^+\}$ (Figure 2.10 and Table 2.2A).

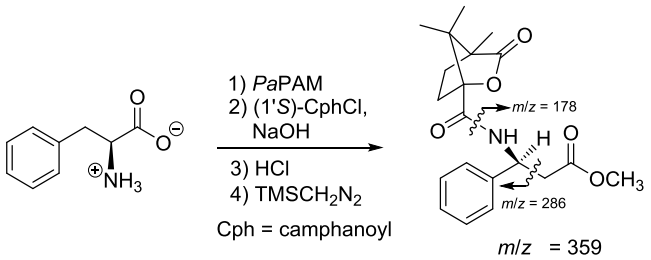

A **B**

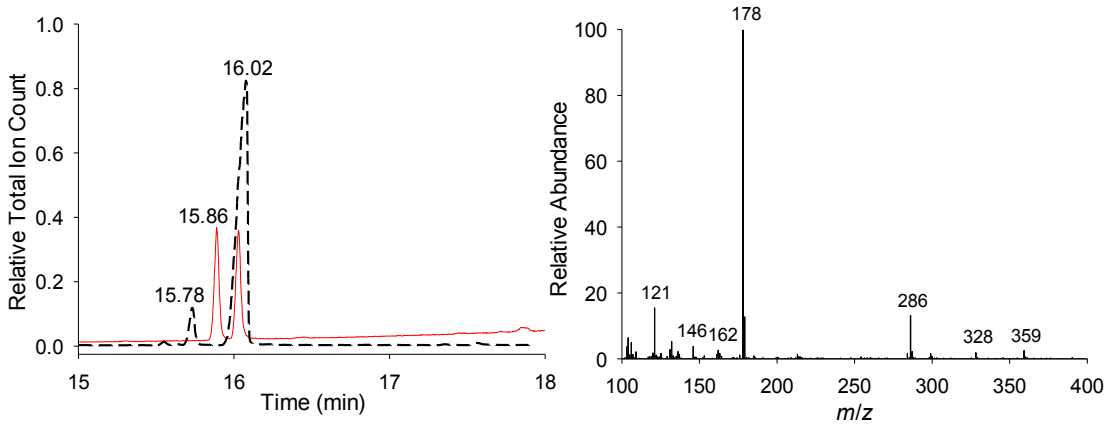

Figure 2.9 Stereochemical determination of biosynthetic β-phenylalanine. (*A*) Overlay of gas chromatography profiles of *N*-[(1'*S*)-camphanoyl] methyl esters of authentic racemic (3*R*)- (15.86 min) and (3*S*)-β-phenylalanine (16.02 min) (*solid red line*), and of the *N*-[(1'*S*)-camphanoyl] methyl ester of biosynthetic (3*S*)-β-phenylalanine (16.02 min) derived from *Pa*PAM catalysis (*dashed line*). The latter chromatogram shows the *N*-[(1'*S*)-camphanoyl] methyl ester of (2*S*)-α-phenylalanine (15.78 min) used as the substrate. (*B*) The mass spectrometry profile of the *N*-[(1'*S*)-camphanoyl] methyl ester of (3*S*)-β-phenylalanine (16.02 min) derived from *Pa*PAM catalysis.

Mass spectral analysis of products formed from the above assay with [ring, β-C-$^{2}H_{6}$]-(*E*)-cinnamate and [^{15}N]-(2*S*)-α-phenylalanine showed a molecular ion {[(3-^{15}N)-M]$^{+}$} of *m/z* = 284 and two diagnostic mass fragments ions at *m/z* = 211 {[(3-^{15}N) − $CH_2C(O)OCH_3$]$^{+}$} and *m/z* = 179 {[(3-^{15}N) − PhC(O)]$^{+}$} (Table 2.2B). No isotopic enrichment was observed for these mass fragments compared to the authentic standard, which suggests that the additional mass unit was derived from the ^{15}N-atom. Furthermore, there was no molecular ion at *m/z* = 290 nor a base peak at *m/z* = 185 with additional seven mass units, which indicates that no biosynthetically derived β-phenylalanine from [ring, β-C-$^{2}H_{6}$]-(*E*)-cinnamate is present in the product mixture. This shows that *Pa*PAM doesn't transfer the amino group to an exogenous (*E*)-cinnamate, a proposed intermediate of this isomerization reaction,[16] but it transfers the amino group intramolecularly to the same carbon skeleton to afford the isomerized amino acid.

Further proof for the intramolecular amino transfer from C_{α} to C_{β} was provided by incubating *Pa*PAM with a mixture of [U-$^{13}C_9$, 2-^{15}N]-(2*S*)-α-phenylalanine and unlabeled 2*S*-α-phenylalanine and analyzing the derivatized amino acids by GC/EI-MS. Mass spectral analysis of resulting β-phenylalanines showed molecular ions at *m/z* = 283 and 293 indicating the presence of unlabeled and [$^{13}C_9$, 3-^{15}N]-(3*S*)-β-phenylalanine (with ten additional mass units) respectively. This was further confirmed by the presence of diagnostic mass fragments at *m/z* = 210 {unlabeled, [M – $CH_2C(O)OCH_3$]$^{+}$}, *m/z* = 218 {[(U-$^{13}C_9$, 3-^{15}N)M – $CH_2C(O)OCH_3$]$^{+}$} and base peaks at *m/z* 178 {unlabeled, [M – PhC(O)]$^{+}$} and *m/z* 188 [(U-$^{13}C_9$, 3-^{15}N)M – PhC(O)]$^{+}$ (Table 2.2C). In addition, calculated ratios of ion abundance of *m/z* 178:*m/z* 179 (P+1) and *m/z* 188:187 (P−1) for derivatized biosynthetic amino acids were identical to that of authentic standard. The lack of enrichment for *m/z* 179 and *m/z* 187 in above mixed substrate assay

compared to authentic standards suggests that that intermolecular amino transfers did not occur, which further suggests an intramolecular amino transfer during *Pa*PAM aminomutase catalysis.

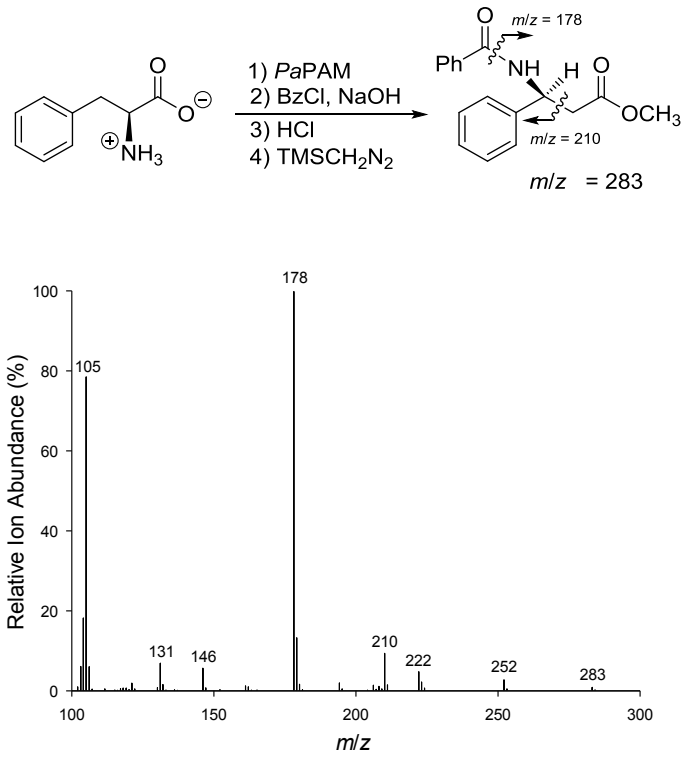

Figure 2.10. Diagnostic mass spectral fragments and mass spectrometric profile of authentic *N*-benzoyl-(3*S*)-β-phenylalanine methyl ester. Fragment ions *m/z* 178 $[M - PhC(O)]^+$ (base peak) and *m/z* 210 $[M - CH_2C(O)OCH_3]^+$ were diagnostic and present at 100% and 10% abundance, respectively.

2.3.3. Stereochemistry of Amino Transfer

Deuterium labeled α-amino acids, [ring, 2,3-$^2H_7$]-(2*S*,3*S*)-α-phenylalanine (90+% *ee*, 98+% ^{2}H-enriched) and racemate [ring, 3-$^2H_6$]-(2*R*,3*S*)/(2*S*,3*R*)-α-phenylalanine (98+% ^{2}H-enriched) were employed to assess the stereochemical course of this isomerization reaction. Stereospecifically deuterium labeled α-amino acids were separately incubated with *Pa*PAM under standard assay conditions and the resulting β-amino acids were converted to their *N*-

benzoyl methyl esters for subsequent GC/EI-MS analysis. The diagnostic mass fragments ions at *m/z* = 210 {$[M - CH_2C(O)OCH_3]^+$} and *m/z* = 178 {$[M - PhC(O)]^+$} obtained for the authentic unlabeled (2*S*)-α-phenylalanine was used to identify the fate of deuteriums during the isomerization reaction.

Mass spectral analysis of the derivatized biosynthetic β-phenylalanine obtained from [ring, 2,3-$^2H_7$]-(2*S*,3*S*)-α-phenylalanine showed diagnostic mass fragments (Table 2.2E) at *m/z* = 215 {$[(\text{ring-}^2H_5)M - CH_2C(O)OCH_3]^+$} with no *m/z* = 216 enrichment compared to authentic standard indicating that no deuterium retained on C_β. The base peak of the product with *m/z* = 185 (no *m/z* = 184 enrichment), consisted of seven additional mass units (seven deuteriums) compared to the unlabeled authentic standard, thus confirming that the deuterium removed from β-carbon migrated to C_α during the isomerization.

Incubation of *Pa*PAM with (2*S*)-α-phenylalanine and (2*R*)-α-phenylalanine separately indicated that only the 2*S*-isomer is a productive substrate for this aminomutase. Thus, the [ring, 3-$^2H_6$]-(2*S*,3*R*)/(2*R*,3*S*)-α-phenylalanine racemate contains only [ring, 3-$^2H_6$]-(2*S*,3*R*)-α-phenylalanine as a productive substrate. Derivatized β-phenylalanine obtained after incubation of [ring, 3-$^2H_6$]-(2*S*,3*R*)/(2*R*,3*S*)-α-phenylalanine racemate showed a mass fragment $[(^2H_1)M - CH_2C(O)OCH_3]^+$ at *m/z* 216 (no *m/z* 215 enrichment) and a base peak $[(^2H_1)M - PhC(O)]^+$ at *m/z* 184 (no *m/z* 183 enrichment) (Table 2.2D) indicating that the deuterium atom at β-position is retained during the enzymatic reaction.

These results confirm that *pro*-(3*S*) hydrogen is removed and transferred intramolecularly to the C_α during the isomerization reaction while the *pro*-(3*R*) Hydrogen is retained at the β-position. This observation coupled with the known 3*S* stereochemistry of the β-phenylalanine

product,[16] provides support for an inversion-of-configuration at C_β where the amino group reattaches after removal from the C_α. That is, after the *pro*-(3*S*) hydrogen is removed from β-position, amino group attaches to the position of *pro*-(3*R*) hydrogen and moves the latter to the position originally occupied by *pro*-(3*S*) hydrogen.

Table 2.2. Mass spectral fragment ions of isotopomers of *N*-benzoyl-β-phenylalanine methyl esters

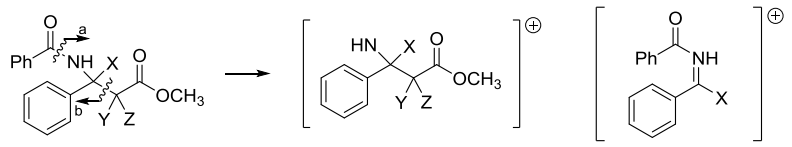

Derivatized biosynthetic β-phenylalanine

Substrate(s) incubated with *Pa*PAM	Biosynthetic products, and diagnostic mass fragments 'a' and 'b' in GC/EI-MS	
A 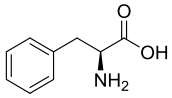	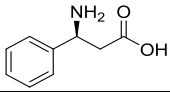	
	'a' *m/z* = 178 X, Y, Z = H	'b' *m/z* = 210 X = H
B 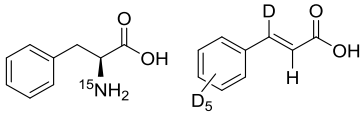	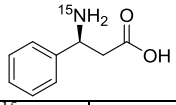	
	'a' *m/z* = 179 (^{15}N) X, Y, Z = H	'b' *m/z* = 211 (^{15}N) X = H
C 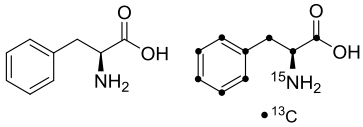	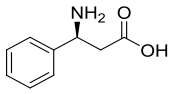	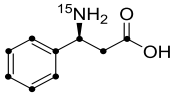
	'a' *m/z* = 178 X, Y, Z = H *m/z* = 188 ($^{13}C_9$, ^{15}N) X, Y, Z = H	'b' *m/z* = 210 X = H *m/z* = 218 ($^{13}C_7$, ^{15}N) X = H
D 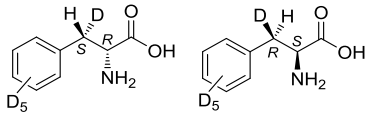	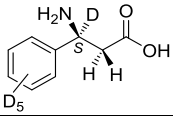	
	'a' *m/z* = 184 (D_6) X = D; Y, Z = H	'b' *m/z* = 216 X = D
E 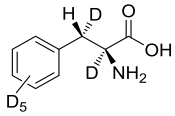	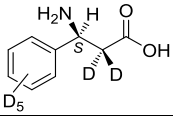	
	'a' *m/z* = 185 (D_7) X = H; Y, Z = D	'b' *m/z* = 215 X = H

2.3.4. Stereochemistry of Hydrogen Rebound

The stereochemistry of hydrogen rebound at C_α during the aminomutase reaction was assessed by incubating *Pa*PAM with [3,3-$^2H_2$]-α-phenylalanine under standard assay conditions. The biosynthetic product was converted to the *N*-acetyl methyl ester and analyzed using ^{2}H-NMR and GC/EI-MS. ^{2}H-NMR spectra of synthetic authentic racemate [2,3-$^2H_2$]-*N*-acetyl (2*S*,3*R*)/(2*R*,3*S*)-β-phenylalanine methyl ester and *N*-acetyl [3,3-$^2H_2$]-α-phenylalanine methyl ester, and ^{1}H-NMR spectra of a mixture of (2*S*)-α- and (3*S*)-β-phenylalanine *N*-acetyl methyl esters were also acquired for referencing the deuterium signals observed for the substrate/biosynthetic product mixture.

Proton-decoupled ^{2}H-NMR spectrum of synthetically-derived authentic racemate, [2,3-$^2H_2$]-*N*-acetyl (2*S*,3*R*)/(2*R*,3*S*)-β-phenylalanine methyl ester with spectroscopically equivalent deuteriums, showed two singlets at δ 2.83 and δ 5.40 for deuteriums at C_α and C_β, respectively (Figure 2.11C). The reason for observing singlets instead of doublets is due to the smaller deuterium-deuterium spin coupling compared to hydrogen-hydrogen spin couplings (about 40 times smaller).[49] Diagnostic ^{1}H-NMR chemical shifts of unlabeled *N*-acetyl (3*S*)-β-phenylalanine methyl ester were observed at δ 2.82 (dd) and δ 2.92 (dd) for the protons at C_α. By comparing the C_α deuterium chemical shift (δ 2.83) of authentic product standard, the chemical shifts δ 2.82 and δ 2.92 of *N*-acetyl (3*S*)-β-phenylalanine methyl ester were assigned for *pro*-(2*R*) and *pro*-(2*S*) hydrogens, respectively (Figure 2.11D). Similarly, *pro*-(3*S*) and *pro*-(3*R*) hydrogens of derivatized (2*S*)-α-phenylalanine showed chemical shifts at δ 3.13 and δ 3.07, respectively (Figure 2.11D). The chemical shift resonances observed for authentic *N*-acetyl [3,3-$^2H_2$]-α-phenylalanine methyl ester were at δ 3.10 and δ 3.08 (Figure 2.11A) and they were virtually

identical to the chemical shifts observed for the unlabeled *N*-acetyl (2*S*)-α-phenylalanine methyl ester. ^{2}H-NMR profile of the assay mixture obtained after incubating *Pa*PAM with [3,3-$^2H_2$]-α-phenylalanine (Figure 2.11B and inset) showed two unresolved singlets (δ 3.10, 3.08), which correspond to the unreacted substrate and two singlets [δ 2.83 ($HC_\alpha D$), 5.40 ($NC_\beta D$)], which correspond to biosynthetic (3*S*)-β-phenylalanine. The chemical shift resonance at δ 2.83 of the biosynthetic β-phenylalanine was identical to the chemical shift resonance observed for *pro*-(2*R*) hydrogen of the *N*-acetyl (3*S*)-β-phenylalanine methyl ester. Therefore this indicates that the *pro*-(3*S*) deuterium that was removed during the reaction rebinds at the α-carbon on the original spatial position of *pro*-(2*R*) hydrogen. These NMR data coupled with the known (3*S*)-stereochemistry[16] (also found herein) of the biosynthetically derived [^{2}H]-β-phenylalanine product established the biosynthetic product as the (2*R*,3*S*)-enantiomer.

Further analysis of the ^{2}H-NMR spectrum of the derivatized biosynthetic product obtained from the above assay showed that the integral of the peak area (set to 1.0 deuterium) for the resonance signal at δ 5.40 ($C_\beta D$) and for the signal at δ 2.83 ($C_\alpha D$) were equal. Furthermore, GC/EI-MS analysis of *N*-acetyl methyl ester of biosynthetic [^{2}H]-labeled β-phenylalanine showed a mass fragment ion at *m/z* = 180 {$[PhC_\beta D(NH)C_\alpha DHCO_2CH_3]^+$} without isotopic enrichment for the P−1 (monodeuterated product; $[PhC_\beta D(NH)C_\alpha H_2CO_2CH_3]^+$). The biosynthesized dideuterio-β-phenylalanine isotopomer was present at ~99% compared to the monodeuterio-β-isotopomer. These observations suggest that no hydrogen exchange occurs with the buffer protons during the isomerization catalyzed by this enzyme. In contrast, *Tc*PAM, which produces 3*R*-β-phenylalanine, has shown significant hydrogen exchange (~60%) over 1 h[20] and this suggests that the *Pa*PAM active site excludes water more effectively than the *Tc*PAM active site.

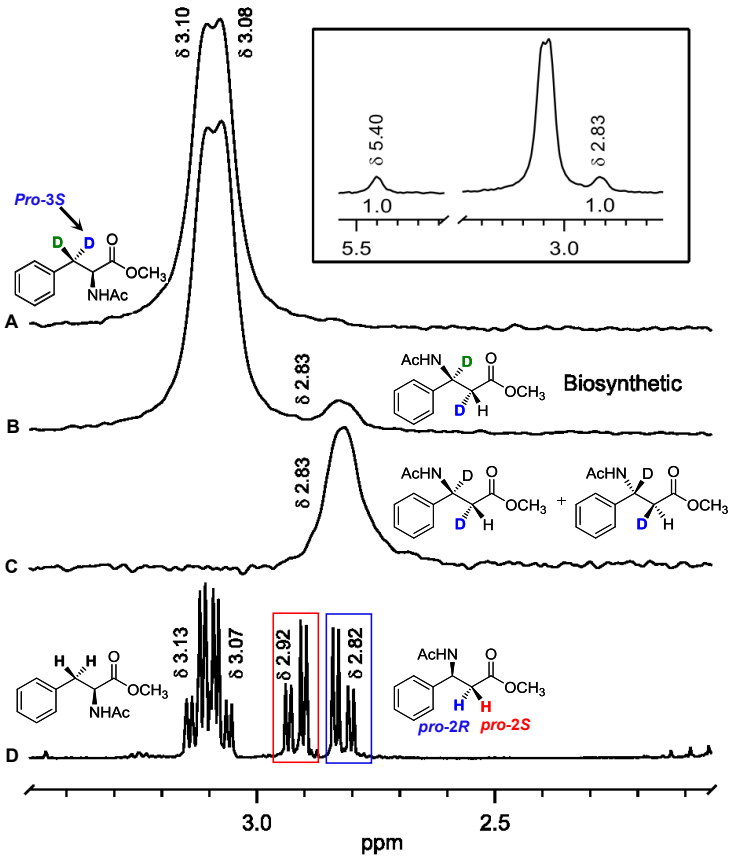

Figure 2.11. NMR spectra of *N*-acetyl methyl esters of various α- and β-phenylalanines. *A*) A partial ^{2}H-NMR (76.7 MHz, $CHCl_3$) spectrum of *N*-acetyl methyl ester of authentic [3,3-$^{2}H_2$]-(2*S*)-α-phenylalanine. *B*) A partial ^{2}H-NMR spectrum of *N*-acetyl methyl esters of unreacted [3,3-$^{2}H_2$]-(2*S*)-α-phenylalanine and biosynthetic [^{2}H]-labeled β-phenylalanine isotopomer. *C*) A partial ^{2}H-NMR (76.7 MHz, $CHCl_3$) spectrum of the authentic racemate [2,3-$^{2}H_2$]-*N*-acetyl (2*S*,3*R*)/(2*R*,3*S*)-β-phenylalanine methyl ester. *D*) A partial ^{1}H-NMR (500 MHz, $CDCl_3$) spectrum of a mixture of unlabeled (2*S*)-*N*-acetyl α- and (3*S*)-*N*-acetyl β-phenylalanine methyl esters.

2.3.5. Overall Mechanism and Stereochemistry of *Pa*PAM Isomerization

Taken together, these GC/EI-MS and ^{2}H-NMR data show that *Pa*PAM isomerization reaction occurs with inversion of configuration at both C_α and C_β (Figure 2.12). The hydrogen formerly at the *pro*-(2*R*) position is replaced by the *pro*-(3*S*) hydrogen, while the position formerly occupied by *pro*-(3*R*) hydrogen is replaced by the amino group (Figure 2.12).

According to the accepted mechanism of MIO-based aminomutases, both the amino group and hydrogen are removed heterolytically to form *trans*-cinnamic acid and then the amino group and hydrogen are rebound to afford the corresponding β-phenylalanine. The observations provided in the foregoing discussion suggest that the *Pa*PAM likely removes from and reattaches the amino and the hydrogen groups to the same stereo-face of the cinnamate intermediate from which they originated (Figure 2.12).

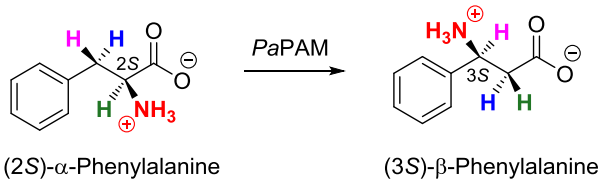

Figure 2.12. The stereochemistry of the isomerization reaction catalyzed by *Pa*PAM. During the α- to β-isomerization, *pro*-(3*S*) hydrogen (blue) and the amino group remove and reattach from the same stereo-face by inverting the stereochemistry at each reaction termini.

This observation is distinctly different than the retention-of-configuration at both reaction termini observed for *Tc*PAM from *Taxus* plants.[20] In this isomerization reaction catalyzed by *Tc*PAM, the amino group removed from the C_α must be reattached at C_β on the opposite face to produce (3*R*)-β-phenylalanine. Several hypotheses have been proposed to explain the stereochemical control of plant ortholog *Tc*PAM. The earliest hypothesis was that the phenyl ring and carboxylate group of (2*S*)-α-phenylalanine are arranged in a syn-periplanar orientation in which the amine group and the leaving *pro*-(3*S*) hydrogen atom positioned on the same side of the substrate, leading to the formation of *cis*-cinnamic acid.[20] However, it was shown later, only the *trans*-cinnamic is involved in PAM catalysis.[35,46] Accordingly, *Tc*PAM requires a reorientation of the *trans*-cinnamic to expose the C_α *re*- and C_β *si*-face respectively for the

amino- and proton-rebound. It has been proposed that the cinnamate intermediate undergoes a 180° rotation about the C_1-C_α and C_{ipso}-C_β bonds prior to the reattachment of the amino group from the MIO-NH_2 adduct (Figure 2.13 path *b*).[46] This bond rotation doesn't alter the salt bridge to Arg-325 of *Tc*PAM, but cause a minor displacement of the aromatic ring from its original position without resulting steric clashes in the active site. Alternatively, an internal rotation around the C_{ipso}-C_β bond to position the carboxylate group in two hydrogen bonds with neighboring active site residues (Asn355 and Asn231) is been proposed in a recent mutational investigation on *Taxus chinensis* PAM.[50] However, the latter proposal is energetically unfavorable since it requires the breakage of the high energy salt-bridge between the substrate carboxylate group and the active site Arg.

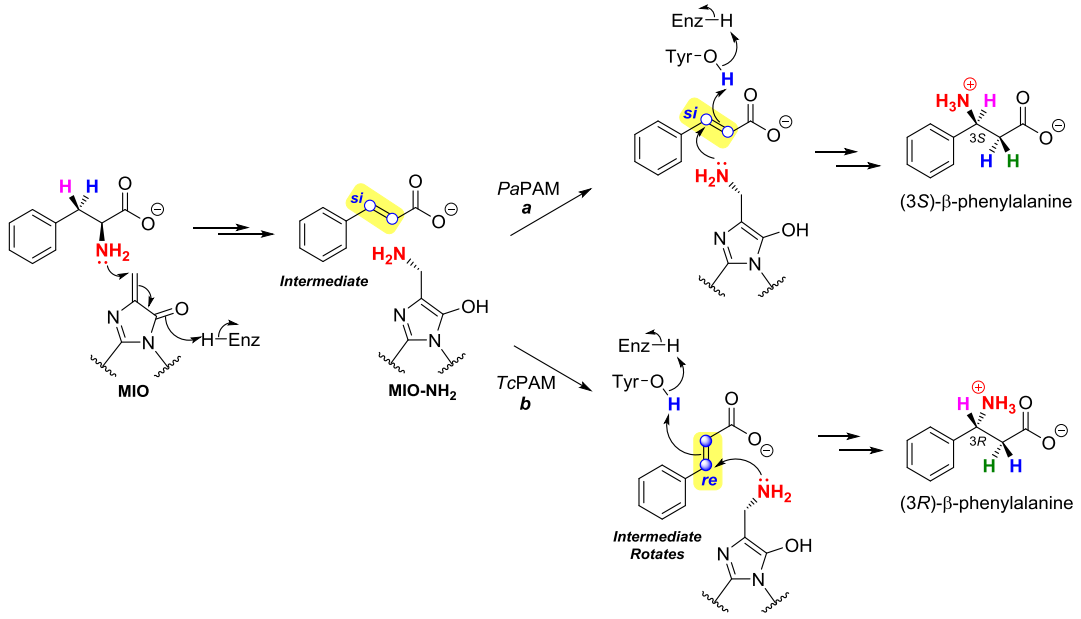

Figure 2.13. The stereochemistry and mechanism of isomerization reactions catalyzed by *Pa*PAM and *Tc*PAM. Isomerization mechanism begins with attack on the MIO by the amine at C_α of the substrate, followed by a concerted elimination of NH_3 to produce a cinnamate intermediate. *Pa*PAM (path *a*), remove and reattach the migrating proton and the amino group from the same face. In contrast, *Tc*PAM (path *b*) involves a rotation of the acrylate intermediate about the C_1-C_α and C_β-C_{ipso} bonds, prior to the reattachment of the migrating partners. The open circles (○) and the filled circles (●) on the cinnamate molecule are used to distinguish the *si*- and *re*-faces of the double bond, respectively, using C_β as the reference.

Incubation of *Pa*PAM and *Tc*PAM separately with *o*-methyl-(2*S*)-α-phenylalanine has provided some evidence for the proposed difference in the mechanistic pathways of these two enzymes that produce two enantiomeric forms of β-phenylalanine. When incubated with *o*-methyl-(2*S*)-α-phenylalanine, *Pa*PAM produces exclusively *o*-methyl-(3*S*)-β-phenylalanine, while *Tc*PAM produces 1% of *o*-methyl-(3*R*)-β-phenylalanine and 99% of *o*-methyl-(*E*)-cinnamate intermediate.[51] Steric barrier due to the methyl group on the aromatic ring likely prevents the proposed bond rotation in *Tc*PAM, and therefore the catalytic reaction cannot proceed beyond *o*-methyl-(*E*)-cinnamate intermediate to produce the corresponding β-phenylalanine enantiomer. In contrast, *Pa*PAM can produce *o*-methyl-(3*S*)-β-phenylalanine as it doesn't require any additional rotomeric forms of the intermediate. Furthermore, kinetic parameters of *Pa*PAM for *o*-methyl-(3*S*)-β-phenylalanine (k_{cat} = 0.061 s^{-1}; K_M = 0.05 mM) reveals that the catalytic efficiency (k_{cat}/K_M = 1.2 s^{-1}•mM^{-1}) of *Pa*PAM is 6-fold greater than the value reported for *Tc*PAM (0.2 s^{-1}•mM^{-1})[51] likely due to the use of a single rotamer instead of two rotamers as in *Tc*PAM catalysis.

2.4. Conclusion

*Pa*PAM catalytic mechanism likely proceeds through a stepwise mechanism where the migratory hydrogen and amino group are eliminated heterolytically from the substrate and held by the enzyme followed by an intramolecular transfer on to the same carbon skeleton. During the *Pa*PAM aminomutase catalysis, the *pro*-(3*S*) hydrogen and the α-amino group are eliminated from the substrate to produce cinnamic acid intermediate. Then, the migrating partners exchange their positions intramolecularly from the same stereo-face that they originated. For example, The amino group and the *pro*-(3*S*) hydrogen reattach respectively to original positions of *pro*-(3*R*)- and *pro*-(2*R*)-hydrogens of (2*S*)-α-phenylalanine. Consequently, the configuration of both α- and β-carbons are inverted during the isomerization. Thus, *Pa*PAM catalyzes the isomerization of (2*S*)-α-phenylalanine to (3*S*)-β-phenylalanine with inversion-of-configuration at both reaction termini.

The mechanism is clearly different from the retention of configuration observed for the plant ortholog *Tc*PAM, where the migrating partners exchange their positions in opposite stereo-faces. Thus, the mechanistic information obtained from this study revealed two classes of enzymes in MIO-family of PAMs. However, the exact mechanism responsible for the opposite stereocontrol origin in these homologous PAMs is not well understood from this study. Therefore, further future investigations are required to dissect the enantioselectivity origin of mechanistically similar MIO-dependant aminomutases.

APPENDIX

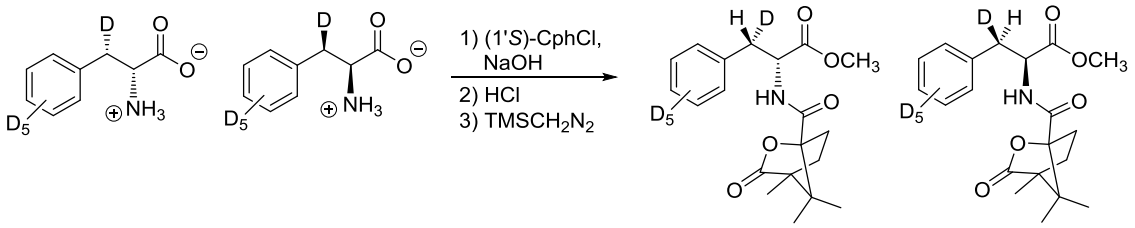

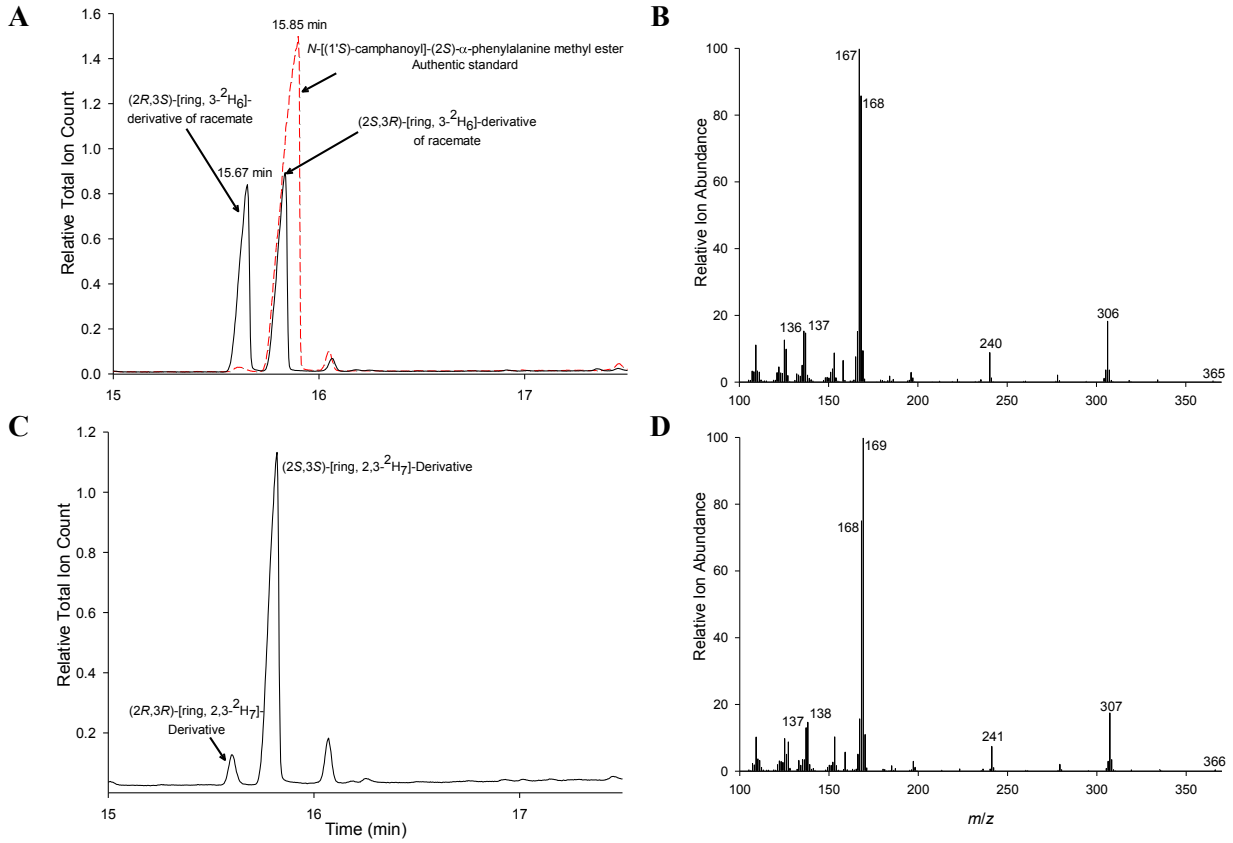

Figure A.1.1. GC and mass spectrometry profiles of various *N*-[(1'*S*)-camphanoyl]-phenylalanine methyl esters. *A*) GC profile of authentic *N*-[(1'*S*)-camphanoyl]-(2*S*)-α-phenylalanine methyl ester (15.85 min) (*dashed red line*); GC profile of *N*-[(1'*S*)-camphanoyl] methyl esters of racemate [ring, 3-$^2H_6$]-(2*R*,3*S*)/(2*S*,3*R*)-α-Phenylalanine, 15.67 and 15.85 min, respectively (*solid line*), *B*) and the corresponding mass spectrometry profile. *C*) GC profile of the *N*-[(1'*S*)-camphanoyl] methyl ester of [ring, 2,3-$^2H_7$]-(2*S*,3*S*)-α-Phenylalanine (90% ee.) [synthesized as shown above with the racemate], *D*) and its mass spectrometry profile.

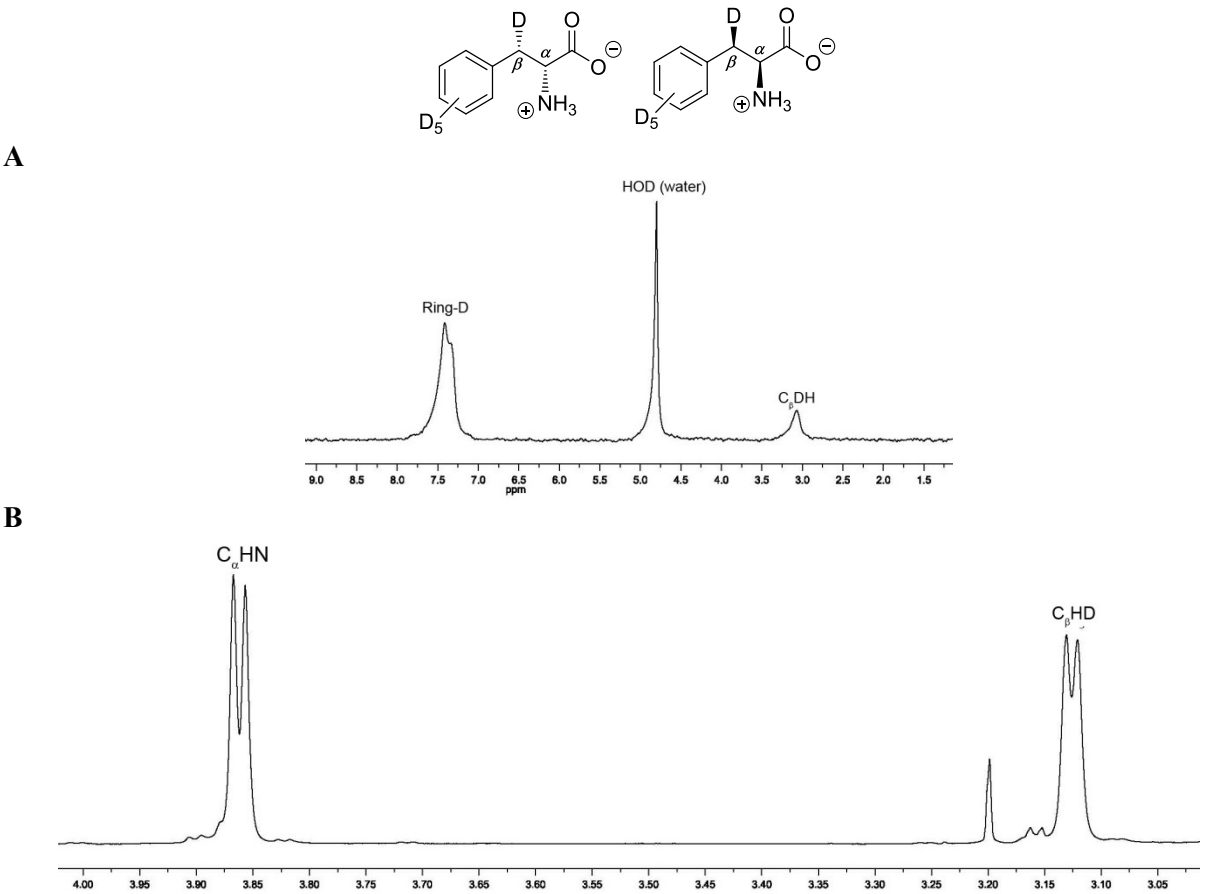

Figure A.1.2. NMR spectra of the racemate [ring, 3-$^2H_6$]-(2*R*,3*S*)/(2*S*,3*R*)-α-phenylalanine. *A*) ^{2}H-NMR spectrum (δ 3.08, br, C_βDH, D is *gauche* relative to amino group; 7.39, br, D_5 on phenyl). *B*) ^{1}H-NMR spectrum (δ 3.13, d, C_βHD, H is *anti* relative to amino group, J = 5.7 Hz; 3.87, d, C_α*H*NH_2, J = 5.7 Hz).

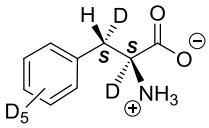

A

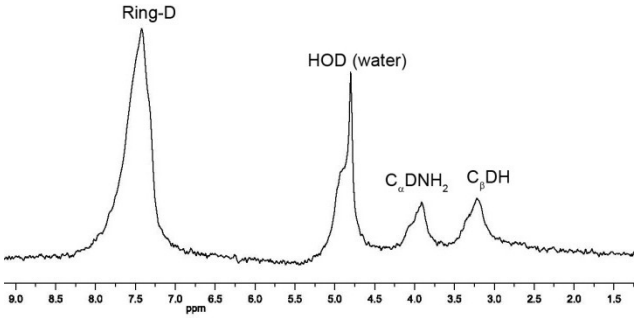

B

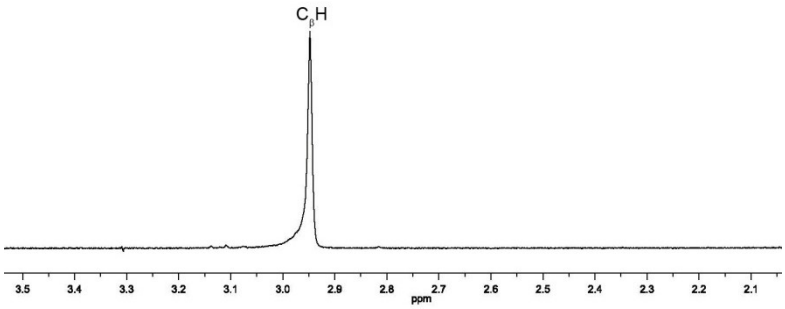

Figure A.1.3. NMR spectra of [ring, 2,3-$^2H_7$]-(2*S*,3*S*)-α-phenylalanine. *A*) ^{2}H-NMR spectrum (δ 3.19, br, C_βDH, D is *anti* relative to amino group; 3.25, br, $C_\alpha DNH_2$; 7.40, br, D_5 on phenyl). *B*) ^{1}H-NMR spectrum (δ 2.94, s, C_βH, H is *gauche* relative to amino group).

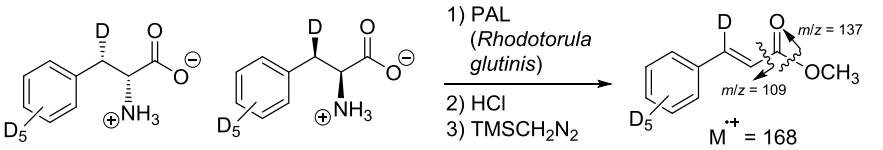

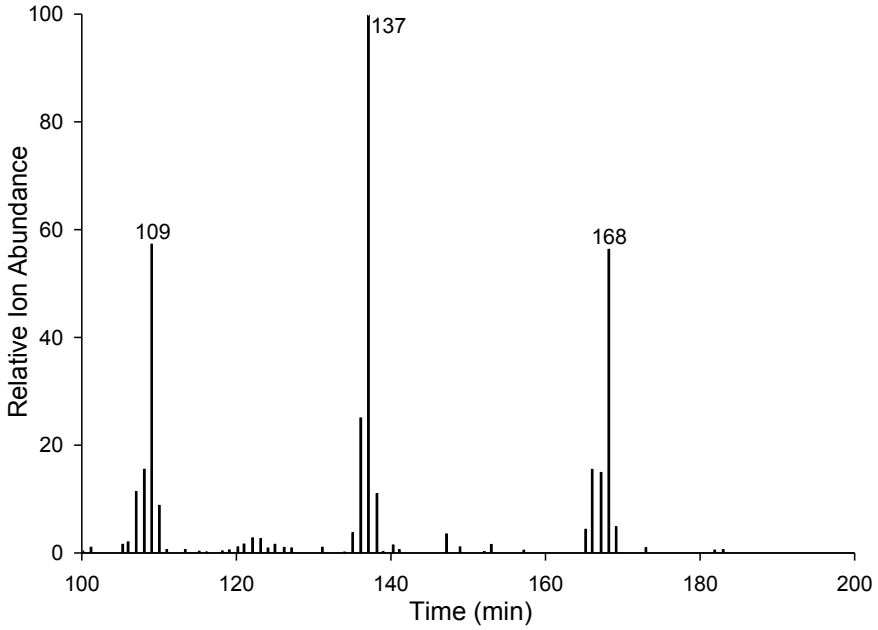

Figure A.1.4. Mass spectrometry profile of cinnamic acid methyl ester derived from the racemate [ring, 3-$^{2}H_{6}$]-(2*R*,3*S*)/(2*S*,3*R*)-α-phenylalanine by PAL catalysis. The source of the diagnostic fragment ions are depicted in the reaction scheme.

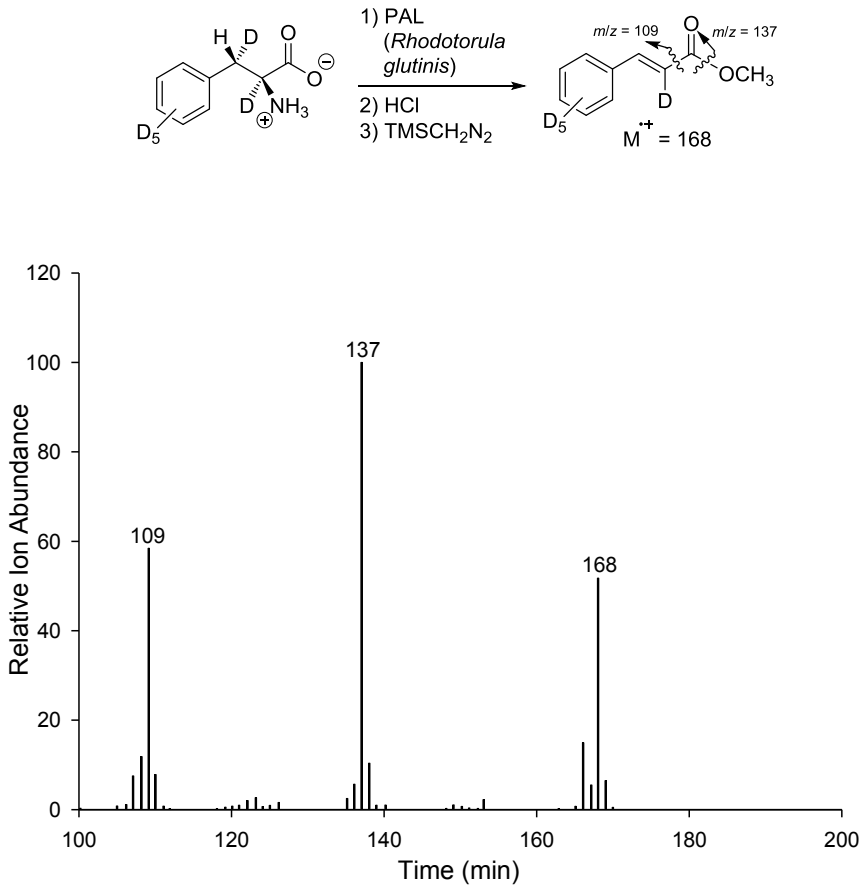

Figure A.1.5. Mass spectrometry profile of cinnamic acid methyl ester derived from [ring, 2,3-$^2H_7$]-(2*S*,3*S*)-α-phenylalanine by PAL catalysis. The source of the diagnostic fragment ions are depicted in the reaction scheme.

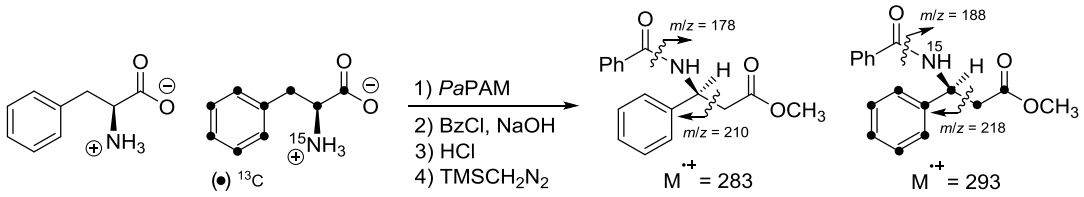

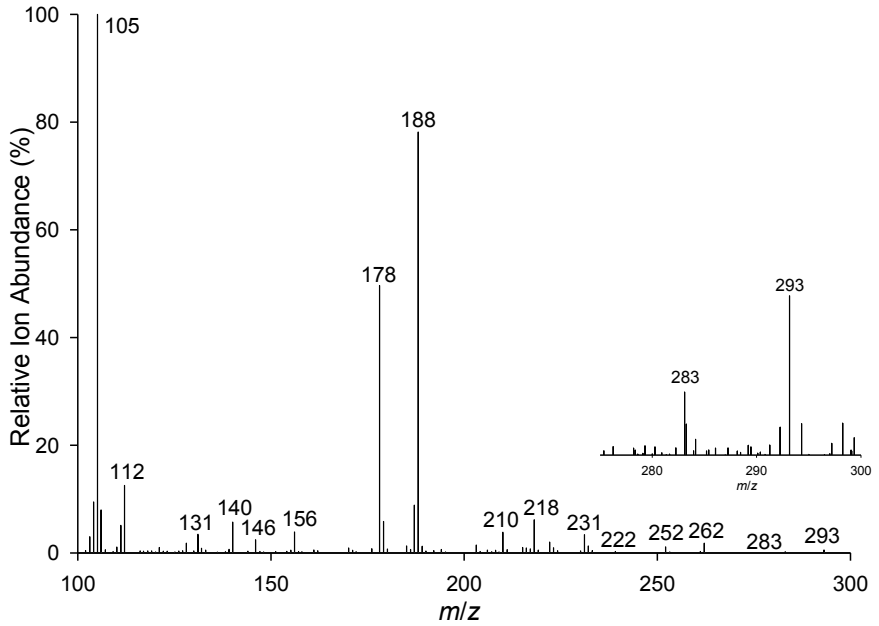

Figure A.1.6. Mass spectrometry profile of the derivatized biosynthetic β-phenylalanine product isolated after co-incubating *Pa*PAM with unlabeled and [U-$^{13}C_9$, ^{15}N]-α-phenylalanine (+98% enriched). Diagnostic ions at *m/z* 210 $[M–CH_2C(O)OCH_3]^+$and 218 $[\{U\text{-}^{13}C_9, 3\text{-}^{15}N\}M–CH_2C(O)OCH_3]^+$, and no *m/z* 211 $[\{3\text{-}^{15}N\}M–CH_2C(O)OCH_3]^+$ nor 217 $[(U\text{-}^{13}C_9, 2\text{-}^{14}N)M–CH_2C(O)OCH_3]^+$ were present, confirming that the nitrogen migrates completely intramolecularly during the isomerization. As further confirmation, the base peak ions at *m/z* 178 (no P + 1 present) and *m/z* 188 $[\{U\text{-}^{13}C_9, 3\text{-}^{15}N\}M – PhC(O)]^+$ (no P - 1 present) also indicated intramolecular nitrogen migration.

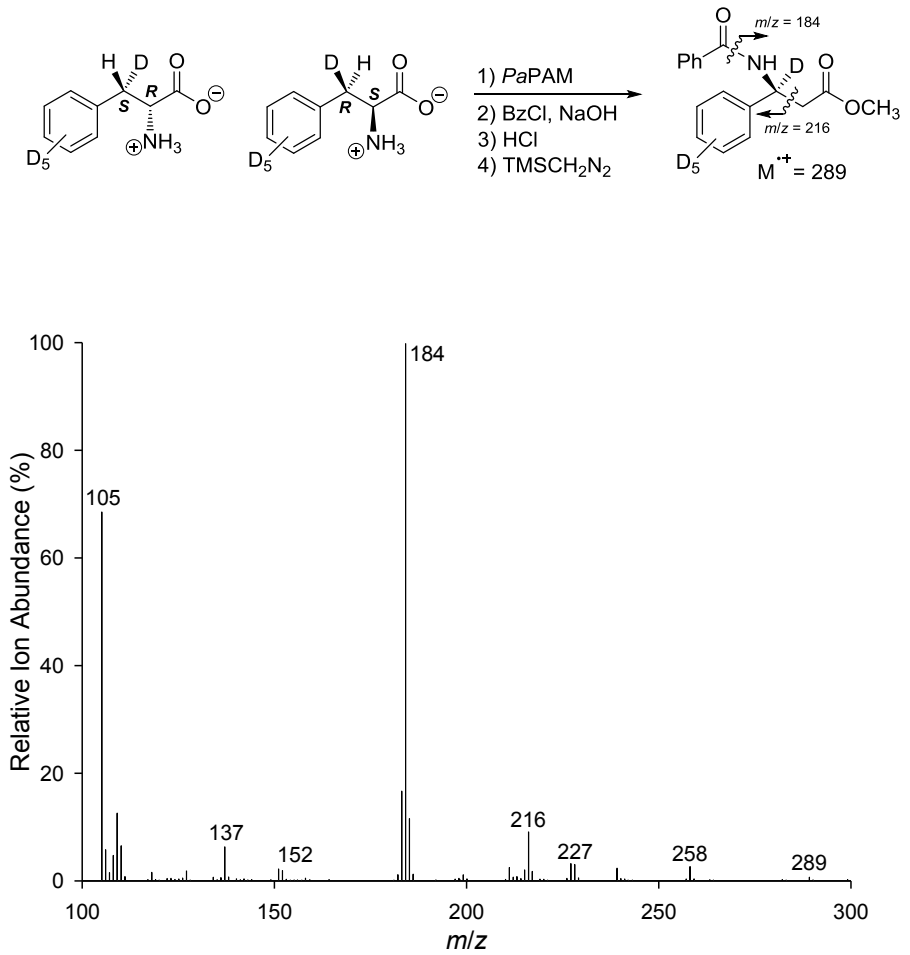

Figure A.1.7. Mass spectrometry profile of the derivatized biosynthetic β-phenylalanine product isolated after co-incubating *Pa*PAM with racemate [ring,3-$^2H_6$]-(2*R*,3*S*)/(2*S*,3*R*)-α-phenylalanine (98+% enriched). Diagnostic ions $[\{^2H_1\}M–PhC(O)]^+$ at *m/z* 184 (no *m/z* 183, P - 1) and $[\{^2H_1\}M–CH_2C(O)OCH_3]^+$ at *m/z* 216 (no *m/z* 215, P - 1), suggested that the deuterium and C3 of the productive (2*S*,3*R*)-α-phenylalanine was retained at C3 of the β-isomer.

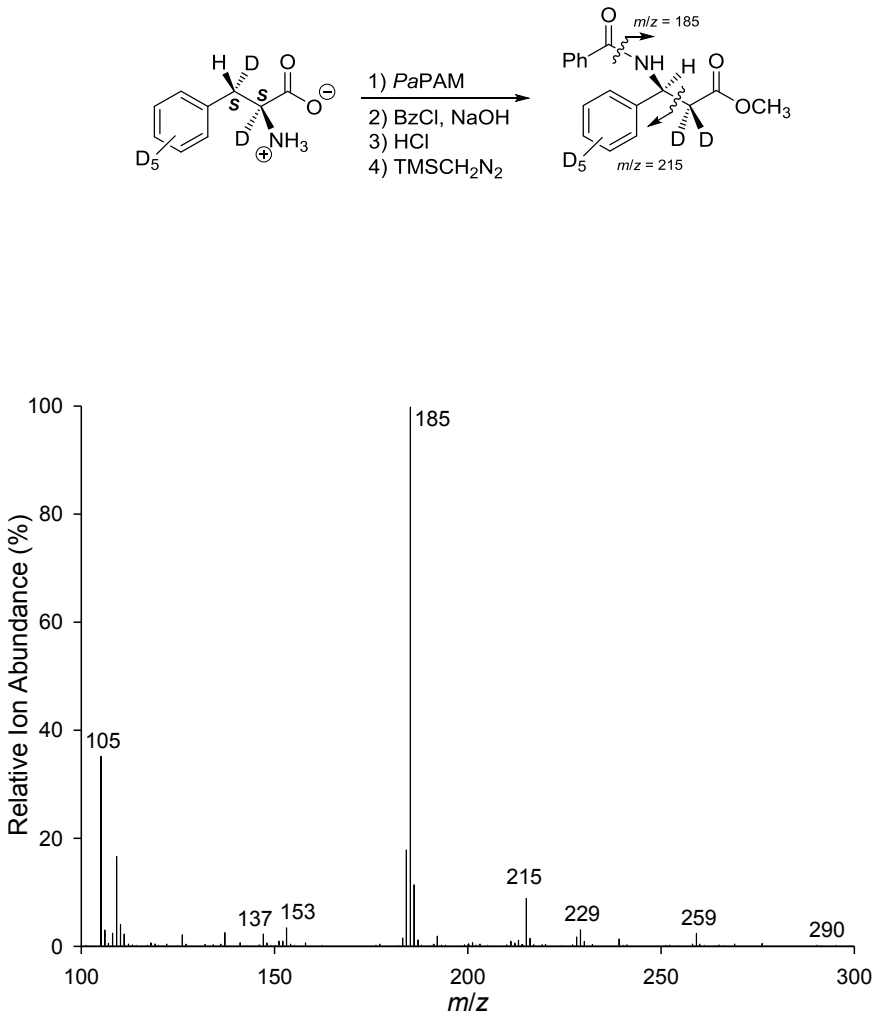

Figure A.1.8. Mass spectrometry profile of the derivatized biosynthetic β-phenylalanine product isolated after incubating *Pa*PAM with [ring, 2,3-$^2H_7$]-(2*S*,3*S*)-α-phenylalanine (90+% ee, 98+% ^{2}H-enriched). Fragment ion *m*/*z* 215 [{ring-$^2H_5$}M–$CH_2C(O)OCH_3$]$^+$ (no P+1 enrichment) indicated that all of the deuterium formerly at the C3 of the substrate was gone, while diagnostic ion *m*/*z* 185 [{ring, 2,2-$^2H_7$}vM–PhC(O)]$^+$ verified that it migrated to C2 (no P–1 observed).

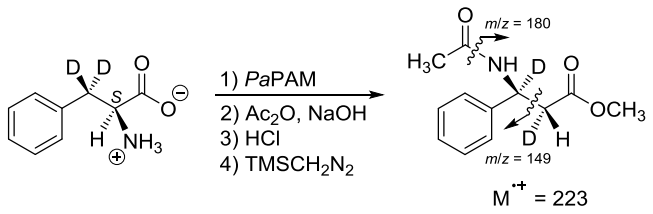

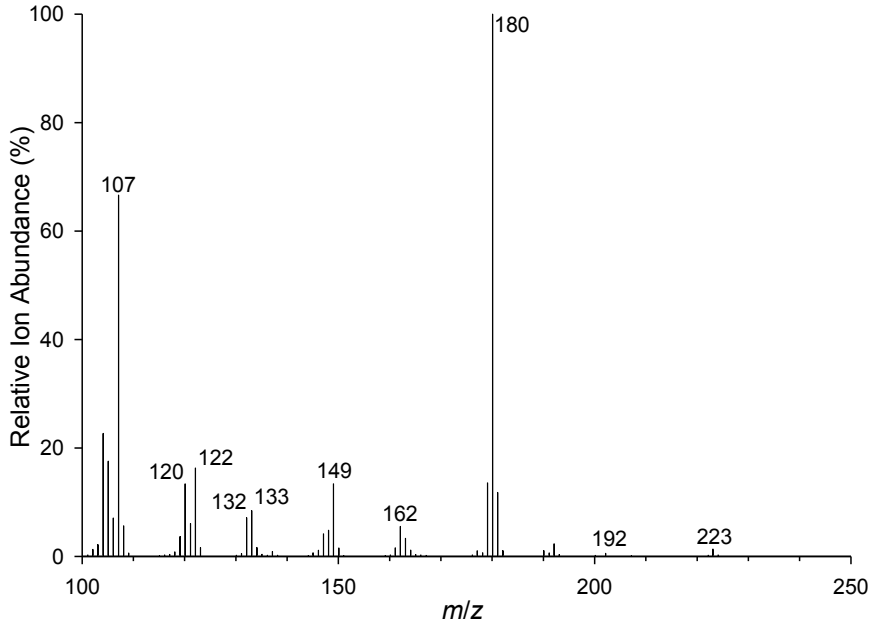

Figure A.1.9. Mass spectrometry profile of the *N*-acetyl methyl ester of dideuterio-β-phenylalanine isotopomer biosynthesized from [3,3-$^2H_2$]-(2*S*)-α-phenylalanine. A diagnostic fragment ion was found at *m/z* 180 $[PhC_\beta\underline{D}(NH)C_\alpha\underline{DH}CO_2CH_3]^+$ (~99%) virtually no P-1 corresponding to $[PhC_\beta\underline{D}(NH)C_\alpha\underline{H_2}CO_2CH_3]^+$ was observed (<1%). The relative abundance of these fragment ions was identical to the abundance of the counterpart ions derived from the unlabeled β-phenylalanine derivative.

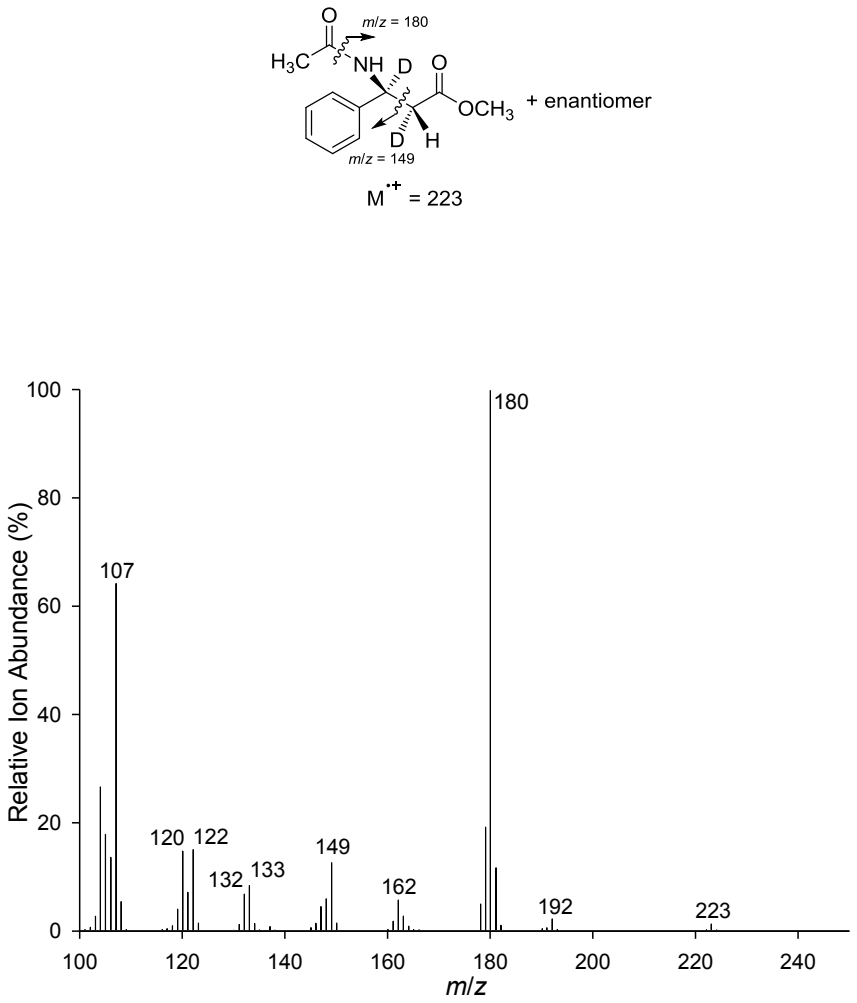

Figure A.1.10. Authentic racemate [2,3-$^2H_2$]-*N*-acetyl-(2*S*,3*R*)/(2*R*,3*S*)-β-phenylalanine methyl ester analyzed by GC/EI-MS. The mass spectrometry profile is shown.

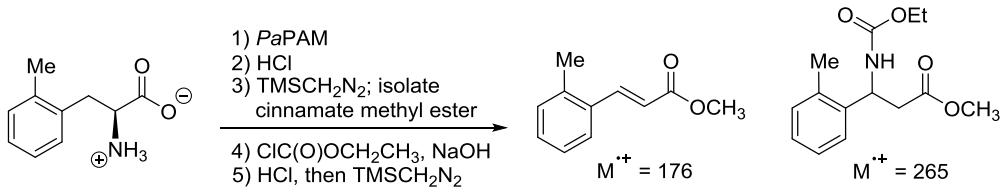

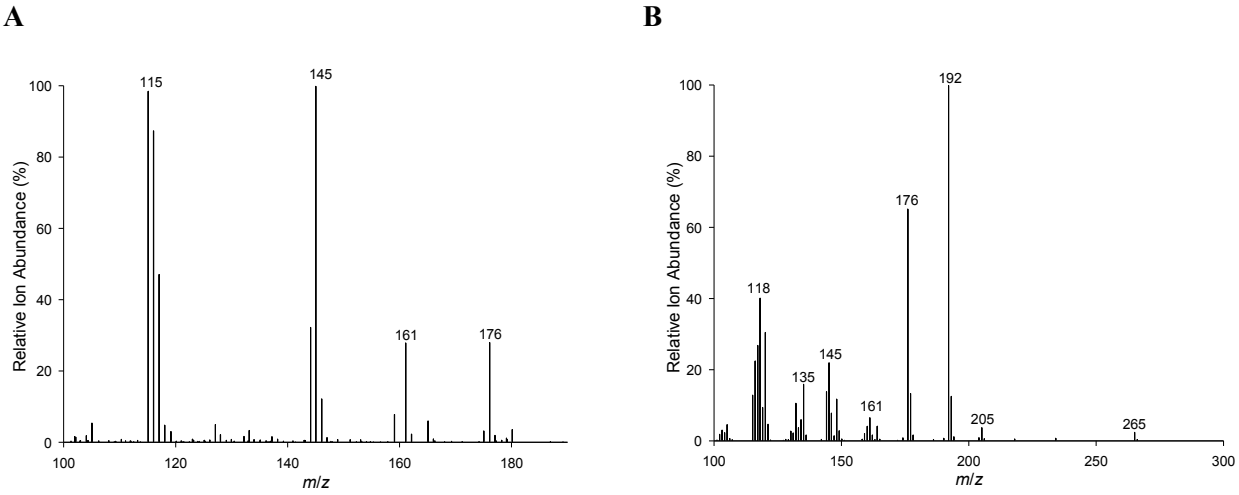

Figure A.1.11. Mass spectrometry profiles of *o*-methylcinnamate methyl ester (*A*) and *N*-(ethoxycarbonyl) *o*-methyl-β-phenylalanine methyl ester (*B*).

REFERENCES

REFERENCES

(1) Cai, C. Z.; Han, L. Y.; Ji, Z. L.; Chen, Y. Z. *Proteins* **2004**, *55*, 66-76.

(2) Wu, B.; Szymanski, W.; Heberling, M. M.; Feringa, B. L.; Janssen, D. B. *Trends Biotechnol.* **2011**, *29*, 352-362.

(3) Turner, N. J. *Curr. Opin. Chem. Biol.* **2011**, *15*, 234-240.

(4) Behshad, E.; Ruzicka, F. J.; Mansoorabadi, S. O.; Chen, D.; Reed, G. H.; Frey, P. A. *Biochemistry* **2006**, *45*, 12639-12646.

(5) Thiruvengadam, T. K.; Gould, S. J.; Aberhart, D. J.; Lin, H. J. *J. Am. Chem. Soc.* **1983**, *105*, 5470-5476.

(6) Morley, C. G.; Stadtman, T. C. *Biochemistry* **1970**, *9*, 4890-4900.

(7) Tang, K. H.; Casarez, A. D.; Wu, W.; Frey, P. A. *Arch. Biochem. Biophys.* **2003**, *418*, 49-54.

(8) Wolthers, K. R.; Rigby, S. E.; Scrutton, N. S. *J. Biol. Chem.* **2008**, *283*, 34615-34625.

(9) Christenson, S. D.; Liu, W.; Toney, M. D.; Shen, B. *J. Am. Chem. Soc.* **2003**, *125*, 6062-6063.

(10) Krug, D.; Muller, R. *Chembiochem* **2009**, *10*, 741-750.

(11) Freer, I.; Pedrocchifantoni, G.; Picken, D. J.; Overton, K. H. *J. Chem. Soc. Chem. Comm.* **1981**, 80-82.

(12) Grimm, B.; Bull, A.; Breu, V. *Mol. Gen. Genet.* **1991**, *225*, 1-10.

(13) Murakami, K.; Korbsrisate, S.; Asahara, N.; Hashimoto, Y.; Murooka, Y. *Appl. Microbiol. Biotechnol.* **1993**, *38*, 502-506.

(14) Ruzicka, F. J.; Frey, P. A. *Biochim. Biophys. Acta* **2007**, *1774*, 286-296.

(15) Walker, K. D.; Klettke, K.; Akiyama, T.; Croteau, R. *J. Biol. Chem.* **2004**, *279*, 53947-53954.

(16) Magarvey, N. A.; Fortin, P. D.; Thomas, P. M.; Kelleher, N. L.; Walsh, C. T. *ACS Chem. Biol.* **2008**, *3*, 542-554.

(17) Huang, S. X.; Lohman, J. R.; Huang, T.; Shen, B. *Proc. Natl. Acad. Sci. U. S. A.* **2013**, *110*, 8069-8074.

(18) Chen, H. P.; Wu, S. H.; Lin, Y. L.; Chen, C. M.; Tsay, S. S. *J. Biol. Chem.* **2001**, *276*, 44744-44750.

(19) Rétey, J.; Kunz, F.; Arigoni, A.; Stadtman, T. C. *Helv. Chim. Acta* **1978**, *61*, 2989−2998.

(20) Mutatu, W.; Klettke, K. L.; Foster, C.; Walker, K. D. *Biochemistry* **2007**, *46*, 9785-9794.

(21) Wang, S. C.; Frey, P. A. *Trends Biochem. Sci.* **2007**, *32*, 101-110.

(22) DeMong, D. E.; Williams, R. M. *J. Am. Chem. Soc.* **2003**, *125*, 8561-8565.

(23) Carter, J. H.; Dubus, R. H.; Dyer, J. R.; Floyd, J. C.; Rice, K. C.; Shaw, P. D. *Biochemistry* **1974**, *13*, 1227-1233.

(24) Robertson, D. E.; Noll, D.; Roberts, M. F. *J. Biol. Chem.* **1992**, *267*, 14893-14901.

(25) Aberhart, D. J.; Gould, S. J.; Lin, H. J.; Thiruvengadam, T. K.; Weiller, B. H. *J. Am. Chem. Soc.* **1983**, *105*, 5461-5470.

(26) Chirpich, T. P.; Zappia, V.; Costilow, R. N.; Barker, H. A. *J. Biol. Chem.* **1970**, *245*, 1778-1789.

(27) Walker, K. D.; Floss, H. G. *J. Am. Chem. Soc.* **1998**, *120*, 5333-5334.

(28) Wu, P. C.; Kroening, T. A.; White, P. J.; Kendrick, K. E. *Gene* **1992**, *115*, 19-25.

(29) Xiang, L.; Moore, B. S. *J. Bacteriol.* **2005**, *187*, 4286-4289.

(30) Schwede, T. F.; Retey, J.; Schulz, G. E. *Biochemistry* **1999**, *38*, 5355-5361.

(31) Rachid, S.; Krug, D.; Weissman, K. J.; Muller, R. *J. Biol. Chem.* **2007**, *282*, 21810-21817.

(32) Van Lanen, S. G.; Oh, T. J.; Liu, W.; Wendt-Pienkowski, E.; Shen, B. *J. Am. Chem. Soc.* **2007**, *129*, 13082-13094.

(33) Christenson, S. D.; Wu, W.; Spies, M. A.; Shen, B.; Toney, M. D. *Biochemistry* **2003**, *42*, 12708-12718.

(34) Wanninayake, U.; Walker, K. D. *J. Am. Chem. Soc.* **2013**, *135*, 11193-11204.

(35) Wu, B.; Szymanski, W.; Wietzes, P.; de Wildeman, S.; Poelarends, G. J.; Feringa, B. L.; Janssen, D. B. *ChemBioChem* **2009**, *10*, 338-344.

(36) Poston, J. M. *Science* **1977**, *195*, 301-302.

(37) Poston, J. M. *J. Biol. Chem.* **1976**, *251*, 1859-1863.

(38) Poston, J. M. *Biochem. Biophys. Res. Commun.* **1980**, *96*, 838-843.

(39) Stabler, S. P.; Lindenbaum, J.; Allen, R. H. *J. Biol. Chem.* **1988**, *263*, 5581-5588.

(40) Parry, R. J.; Kurlyo-Borowska, Z. *J. Am. Chem. Soc.* **1980**, *102*, 836-837.

(41) Prabhakaran, P. C.; Woo, N. T.; Yorgey, P. S.; Gould, S. J. *J. Am. Chem. Soc.* **1988**, *110*, 5785-5791.

(42) Cone, M. C.; Yin, X. H.; Grochowski, L. L.; Parker, M. R.; Zabriskie, T. M. *Chembiochem* **2003**, *4*, 821-828.

(43) Hennig, M.; Grimm, B.; Contestabile, R.; John, R. A.; Jansonius, J. N. *Proc. Natl. Acad. Sci. U. S. A.* **1997**, *94*, 4866-4871.

(44) Moore, B. S.; Walker, K.; Tornus, I.; Handa, S.; Poralla, K.; Floss, H. G. *J. Org. Chem.* **1997**, *62*, 2173-2185.

(45) Hanson, K. R.; Wightman, R. H.; Staunton, J.; Battersby, A. R. *J. Chem. Soc., Chem. Commun.* **1971**, 185-186.

(46) Feng, L.; Wanninayake, U.; Strom, S.; Geiger, J.; Walker, K. D. *Biochemistry* **2011**, *50*, 2919-2930.

(47) Szymanski, W.; Wu, B.; Weiner, B.; de Wildeman, S.; Feringa, B. L.; Janssen, D. B. *J. Org. Chem.* **2009**, *74*, 9152-9157.

(48) Wanninayake, U.; DePorre, Y.; Ondari, M.; Walker, K. D. *Biochemistry* **2011**, *50*, 10082-10090.

(49) Pines, A.; Vega, S.; M., M. *Phys. Rev. B* **1978**, *18*, 112-125.

(50) Wu, B.; Szymanski, W.; Wybenga, G. G.; Heberling, M. M.; Bartsch, S.; de Wildeman, S.; Poelarends, G. J.; Feringa, B. L.; Dijkstra, B. W.; Janssen, D. B. *Angewandte Chemie-International Edition* **2012**, *51*, 482-486.

(51) Ratnayake, N. D.; Wanninayake, U.; Geiger, J. H.; Walker, K. D. *J. Am. Chem. Soc.* **2011**, *133*, 8531-8533.

CHAPTER 3: Structural and Mutational Insights into *Pa*PAM Isomerization Reaction

The structural characterization investigations of PaPAM discussed in this chapter were carried out in collaboration with Prof. James H. Geiger and Ms. Susan Strom from the Department of Chemistry at Michigan State University.

3.1. Introduction

Phenylalanine aminomutase from *Pantoea agglomerans* (*Pa*PAM) is a member of the class I lyase-like family that includes phenylalanine[1,2] and tyrosine[3-5] aminomutases (PAM and TAM, respectively), and phenylalanine,[6,7] tyrosine[8] and histidine[9] ammonia lyases (PAL, TAL and HAL, respectively). Ammonia lyases produce aryl acrylates from the corresponding α-amino acid substrate by the elimination of ammonia, whereas aminomutases catalyze the isomerization of α- to β-amino acids. Isomerization and elimination reactions catalyzed by this family of enzymes depend on 4-methylidene-1*H*-imidazol-5(4*H*)-one (MIO) cofactor.[9] Most of the early structural and mechanistic discoveries on MIO-dependent enzymes are reported with histidine and phenylalanine ammonia lyases.[9-11]

3.1.1. Discovery of the Electrophilic MIO Group

3.1.1.1. Dehydroalanine as the Electrophile

The presence of a catalytically essential electrophilic group in MIO-dependent enzymes was first reported in 1967 by Abeles and coworkers.[12] Histidine ammonia lyase (*Pseudomonas*

sp.), which catalyze the transformation of L-histidine to urocanic acid was inactivated by $NaBH_4$, KCN, $NaHSO_3$, phenylhydrazine and NH_2OH.[12] However, tritium-labeled experiments employing NaB^3H_4 did not successfully identify the exact functional group. Since the enzyme was inactivated by reagents that reacted with carbonyl groups, it was believed that an enzyme bound carbonyl group was involved in the catalysis.[12] In the proposed mechanism, the amino group of the histidine substrate was hypothesized to add to an enzyme bound carbonyl group to form a protonated carbinolamine or a Schiff base. This amine activation step was envisioned to make a better leaving group and facilitate the elimination step (Figure 3.1).[12]

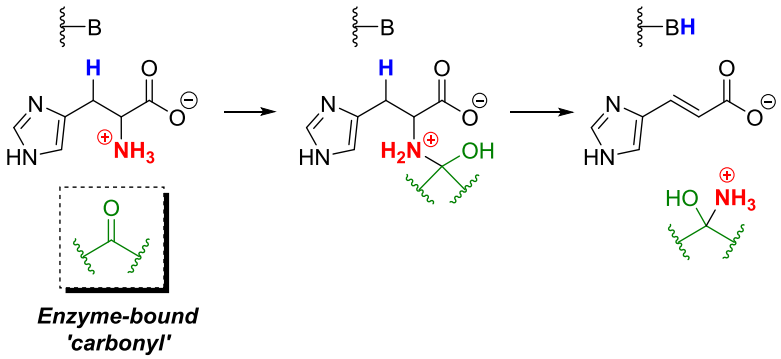

Figure 3.1. First reported mechanism for MIO-dependent enzymes suggesting the involvement of an enzyme bound carbonyl group as the electrophile.

Following their pioneering discovery, Abeles et. al. proposed a speculative structure of the electrophilic cofactor based on the investigations performed using ^{14}C-nitromethane.[13] Exposure of HAL to ^{14}C-nitromethane resulted in loss of the enzyme activity, and nitromethane was found to react at the active site. Catalytic reduction (H_2/Pt) and acid hydrolysis (6 N HCl) of the inactivated enzyme afforded 4-amino-2-hydroxybutyric acid (**2**) and 2,4-diaminobutyric acid (**3**) (Figure 3.2).[13] Based on the observation of these products, the electrophilic cofactor was

suggested to contain a dehydroalanine moiety, which is linked to the protein through an amide bond at C1 (Figure 3.2). Furthermore, the amino group of the dehydroalanine was suggested to form a Schiff base with a carbonyl compound. The nature of these linkages and the exact structure remained unknown. Nevertheless, the proposed structure **1** could account for all the reaction products identified from ^{14}C-nitromethane inactivation (Figure 3.2).[13]

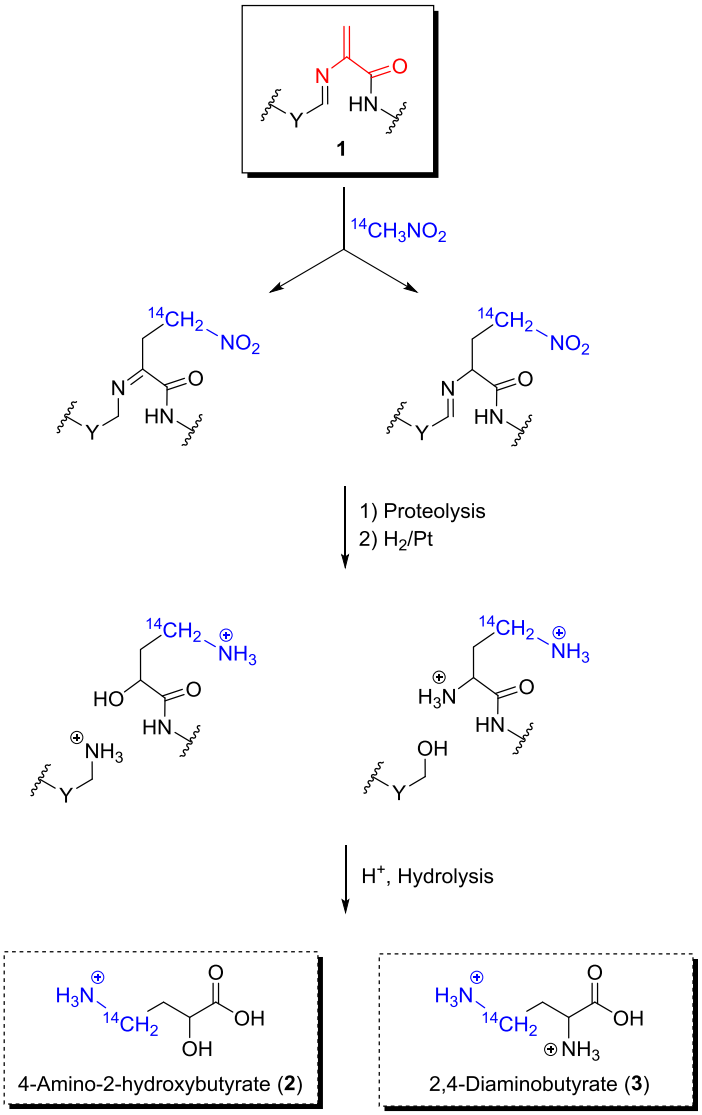

Figure 3.2. Formation of 4-amino-2-hydroxybutyric acid (2) and 2,4-diaminobutyric acid (3) from the proposed electrophilic cofactor (1) in HAL. Dehydroalanine moiety in the proposed structure of the cofactor is highlighted in red.

Surprisingly, the aforementioned investigation was not pursued in detail with HAL or other ammonia lyases. But more studies on the inactivation of ammonia lyases by $NaBH_4$ were reported, yet without successful identification of the moiety reduced by NaB^3H_4.[14,15] However, in 1969, Wickner identified the reduced tritiated moiety as [^{3}H]alanine.[16] When radioactively labeled inhibitor NaB^3H_4 was used with HAL from *Pseudomonas*, total hydrolysis of the inactivated protein afforded [^{3}H]alanine. From these results, it was concluded that the prosthetic electrophile was dehydroalanine. Furthermore, yeast phenylalanine ammonia-lyase treated with $Na^{14}CN$ resulted [^{14}C]aspartate following acid hydrolysis, presumably as a result of the intermediate formation of β-cyanoalanine from cyanide addition to a dehydroalanyl moiety.[17] Since then, a dehydroalanyl residue was generally accepted as the electrophilic cofactor of class I lyase-like family of enzymes.

3.1.1.2. Identification of the Precursor of Active Site Dehydroalanine

The proposed dehydroalanyl moiety as the electrophilic group in HAL and PAL active sites, prompted proposals of serine or cysteine as plausible precursors of the dehydroalanyl group.[16,18] Serine was identified as a precursor by mutating four serines of HAL (*Pseudomonas putida*), which are conserved in all known HALs and PALs.[19] The Ser143Ala mutation resulted a loss of 99.9% catalytic activity whereas the other Ser-Ala mutants were equally active compared to *wt-Pp*HAL. Thus, Ser143 was identified as the most likely precursor of dehydroalanine.[19] Similarly, site-directed mutagenesis investigations of PAL (*Petroselinum crispum*) suggested Ser202 as the precursor of dehydroalanine.[20] Ser143 in HAL was further defined by the Ser143Cys mutation which retained similar activity to wild type enzyme.[21]

3.1.1.3. Discovery of the 4-Methylidene-1*H*-imidazol-5(4*H*)-one (MIO) Group

Thirty years after the initial proposals on the origins of the electrophilic group, Rétey and coworkers, in 1999, solved the structure of *Pseudomonas putida* HAL (*Pp*HAL) at 2.1 Å, revealing a surprising structural moiety in the active site.[9] Observed electron density around Ser143, which was proposed as the precursor of electrophilic cofactor was inconsistent with a dehydroalanine or any of the standard amino acids. The catalytic electrophile in the active site was identified as a 4-methylidene-imidazol-5-one moiety, rather than a dehydroalanine residue (Figure 3.3A).[9] However, the MIO was deemed a modified dehydroalanine, and interestingly, the structure was highly consistent with the speculative structure proposed by Abeles et. al., who earlier investigated the electrophilic prosthesis with ^{14}C-nitromethane (cf. Figure 3.2).[13] As suggested before,[19] the MIO cofactor arose from Ser143 with the involvement of the adjacent Ala142 and Gly144 residues. An autocatalytic polypeptide modification of the ^{142}Ala–^{143}Ser–^{144}Gly tandem was proposed to produce the catalytic MIO group by the nucleophilic attack of the Gly144 nitrogen at the Ala142 carbonyl carbon followed by two dehydration steps (Figure 3.3B).[9]

3.1.2. Characteristics and Formation of the Electrophilic MIO Group

The MIO moiety found in class I lyase-like enzymes is the only catalytically important protein-derived cofactor with a heterocyclic imidazolone ring structure.[9] A similar post-translational modification that forms an imidazolone ring is found in the chromophore of green fluorescent protein (GFP) from the Pacific Northwest jellyfish *Aeqourea victoria* identified

earlier.[22,23] The *p*-hydroxybenzylidene-imidazolidinone fluorophore of GFP is generated by the Ser-Tyr-Gly sequence, which is different from Ala-Ser-Gly triad in *Pp*HAL.[22] While there is no evolutionary link or similarity in the tertiary structures of GFP and class I lyase-like family enzymes, they nonetheless make their prosthetic groups through analogous pathways (Figure 3.3B, C).[9,23]

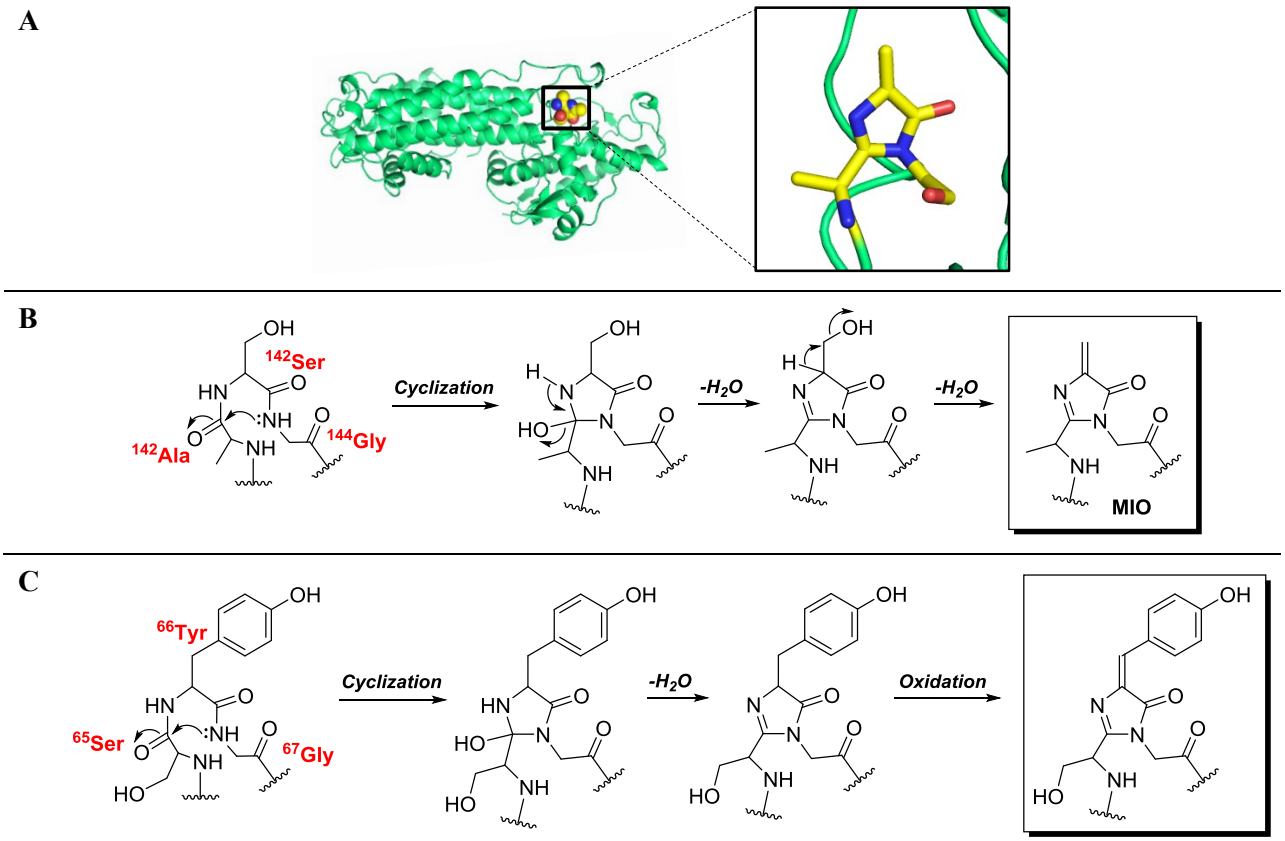

Figure 3.3. Discovery of the MIO group and autocatalytic peptide modifications involved in the MIO formation. *A*) The structure of HAL (PDB 1B8F) from *Pseudomonas putida* revealing the catalytic MIO group. Overall structure is shown in green color with the MIO group highlighted in spheres (atoms are color-coded as carbon: yellow; oxygen: red; nitrogen: blue). Expanded view: enzyme active site highlighting the MIO group. *B*) Proposed mechanism of autocatalytic formation of the MIO group from Ala-Ser-Gly triad in *Pp*HAL. *C*) Mechanism of chromophore formation in GFP from Ser-Tyr-Gly tripeptide.

Posttranslational modifications of both the GFP fluorophore and MIO in *Pp*HAL involve three major biosynthetic steps (cf. Figure 3.3B, C): 1) backbone cyclization via covalent bond formation between glycine nitrogen (Gly67 in GFP, Gly144 in *Pp*HAL) and Ala142 (in *Pp*HAL)/Ser65 (in GFP) carbonyl-carbon to from a carbinol intermediate; 2) dehydration of the same carbinol to form the imidazolin-5-one intermediate; and 3) oxidation of Tyr66 (GFP) or dehydration of Ser143 (*Pp*HAL) to generate an C_{α}-C_{β} exocyclic methylidene (cf. Figure 3.3B,C).

The tripeptide sequence used to form the MIO prosthesis is variable, in part, among class I lyase-like superfamily enzymes.[24-26] While Ala-Ser-Gly is the most common precursor,[7,9,24,27] Thr-Ser-Gly,[25] Ser-Ser-Gly[26] and Cys-Ser-Gly[28] sequences are also observed (Figure 3.4). MIO sequence variability is mostly observed in ammonia lyases, and *Pa*PAM with its Thr-Ser-Gly sequence is the only aminomutase that diverges from the Ala-Ser-Gly origin of MIO formation.[25] However, the basis for using variable residues for MIO formation has not been evaluated so far.

```
PpHAL     RRVVEALLALLNRGITPQVPSQGSVG ASG YLTHMAHISIALLGVGNVS---YRGQVVSAQ 176
PcPAL     FEILEAITKFLNQNITPCLPLRGTIT ASG DLVPLSYIAGLLTGRPNSKAVGPTGVILSPE 235
AoTAL     PELIERLALYLNLGIVPAIPEQGSLG ASG DLAPLSHIATTVIGEGYVL---RDGGKVATG 179
SgTAM     PIILERLAQYLNEGITPAIPEIGSLG ASG DLAPLSHVASTLIGEGYVL---RDGRPVETA 184
CcTAM     VETVKLLAEFINRGIHPVIPQQGSLG ASG DLSPLSHIALALIGEGTVS---FKGQVRKTG 170
SspTAM    VEVLEQLATYLNRGITPAIPELGSLG ASG DLAPLSHIASALIGEGYVL---RDGQPVPTG 181
TcPAM     WEVMEALEKLLNSNVSPKVPLRGSVS ASG DLIPLAYIAGLLIGKPSVIARIGDDVEVPAP 208
PaPAM     IVNFKKLIEIYNQGIVPCIPEKGSLG TSG DLGPLAAIALVCTGQWKAR---YQGEQMSGA 197
FnHAL     RIVVEKLVELLNKEVTPWIPEKGSVG SSG DLSPLAHMSLVLIGLGKAY---YKGELLEAK 177
SgHAL     PEVAQTMADVLNAGITPVVHEYGSLG CSG DLAPLSHCALTLMGEGEAEG--PDGTVRPAG 176
              : :    *  : * :   *::   **  *  ::  :    *          .
```

Figure 3.4. Partial CustalW2 multiple sequence alignment of class I lyase-like family enzymes showing the divergence in MIO forming residues (highlighted). *Pp*HAL, *Fn*HAL, and *Sg*HAL: Histidine ammonia lyases from *Pseudomonas putida*, *Fusobacterium nucleatum*, and *Streptomyces griseus*, respectively. *Pc*PAL: Phenylalanine ammonia lyase from *Petroselinum Crispum*. *Ao*TAL: Tyrosine ammonia lyase from *Actinomadura oligospora*. *Sg*TAM, *Cc*TAM, and *Ssp*TAM: Tyrosine aminomutase from *Streptomyces globisporus*, *Chondromyces crocatus*, and *Streptoalloteichus sp.*, respectively. *Tc*PAM and *Pa*PAM: Phenylalanine aminomutase from *Taxus canadensis* and *Pantoea agglomerans*. ***** (asterisk) indicates positions which have a fully conserved residue. **:** (colon) indicates conservation between groups of strongly similar properties. **·** (period) indicates conservation between groups of weakly similar properties.

3.1.2.1. Mutants of *Pp*HAL

Cyclization of the amino acids forming the MIO is difficult to detect, since MIO is not a strong chromophore.[9] Nevertheless, characteristics of autocatalytic MIO formation was elucidated by structure determination of various *Pp*HAL mutants.[29,30] Mutation of the highly conserved Asp145, which is strongly fixed in a hydrogen bonding network to an alanine inactivated the enzyme presumably by preventing MIO formation (Figure 3.5A).[29] MIO-forming loop ^{142}Ala-^{143}Ser-^{144}Gly was continuous without significant conformational changes outside the loop, but the MIO group was not formed. The distance between Gly144 amide-nitrogen (nucleophile) and Ala142 carbonyl-carbon (electrophile) was 3.7 Å, and thus, the cyclization precluded. Furthermore, the hydroxyl group of Ser143 was clearly visible indicating that the dehydration step was abolished.[29]

A similar mutant structure that lacked the MIO was observed for the Phe329Gly mutation in *Pp*HAL (Figure 3.5B).[29] Phe329 is in short distance contacts from MIO and is highly conserved in class I lyase-like superfamily. Asp145 retained its hydrogen bonding network and tight turn at Ser143 resulted a Gly144-N and Ala142-C distance of 3.0 Å. In contrast to Asp142Ala and Phe329Gly mutants, Phe329Ala mutant showed an intact MIO group.[29]

According to the mutant structures, the MIO was not formed if the strong interaction of the MIO triad with the bordering residue Asp145 was loosened, or steric constraints from Phe 329-C_β atom were removed.[29] Except the MIO forming tripeptide, there were no changes in overall structures compared to *wt-Pp*HAL. Thus, Asp145 and Phe 329-C_β function as anchor points that assist the compression of the ^{142}Ala-^{144}Gly loop.[29] In addition to the conformational pressure, hydrogen bonding interactions of the Gly144 amide-nitrogen and Ala142 carbonyl-

oxygen through an active site water molecule was also proposed to activate the late-stage MIO formation.[29] Furthermore, Ser143 dehydration was not affected by the environment of Ser143, and thus, the cyclization of the tripeptide was suggested to occur before the dehydration of Ser143.[29] During the dehydration step, Tyr280 and Glu414 likely facilitate the elimination of Ser143 C_α-proton and the hydroxyl group. Tyr280 can deprotonate Ser143-C_αH while Glu414 protonates the hydroxyl as it eliminated.

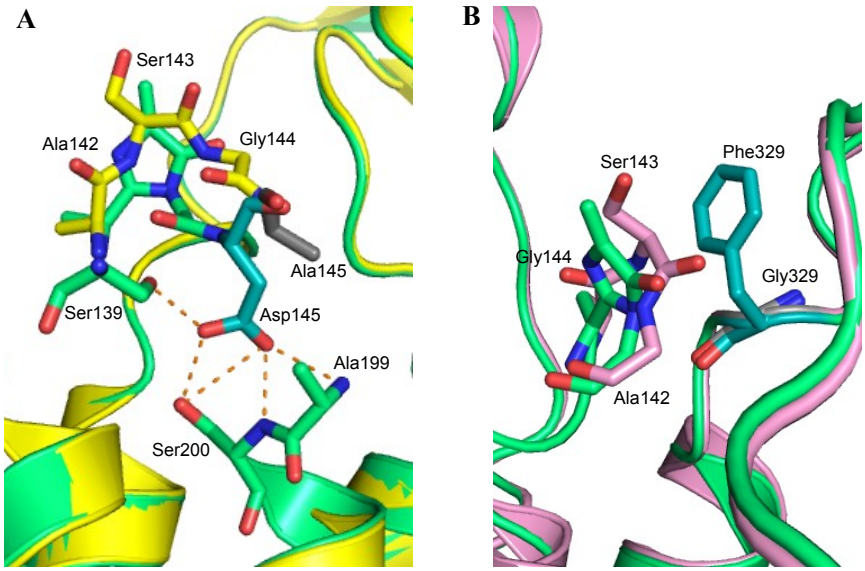

Figure 3.5. Comparison of *wt-Pp*HAL and *Pp*HAL mutants lacking an MIO. *A*) Overlay of *wt-Pp*HAL (PDB 1B8F; green) and Asp145Ala mutant structure (PDB 1GK3; yellow). Hydrogen bonding network of Asp145 is also shown. *B*) Overlay of *wt-Pp*HAL (green) and Phe329Gly mutant structure (PDB 1GK2; pink). Asp145/Phe329 in *wt-Pp*HAL and Ala145/Gly329 in mutants are shown in cyan and gray, respectively. Atoms are color-coded as carbon: green/yellow/pink; oxygen: red; nitrogen: blue.

Additional site-directed mutations of *Pp*HAL showed that modest substitutions in the ^{142}Ala-^{144}Gly tripeptide are tolerated, and the MIO was still formed (Table 3.1).[30] Ala142 and Gly144 were replaced by an Ala without much loss of activity. By contrast, changing the residues immediately adjacent to the MIO-forming loop prevented MIO formation, and no or

very low activity was seen.[30] The Gly141Ala mutant was only 1.1% active while Asp145Ala was totally inactive. These data indicate that the structure and conformation of the immediate environment of the MIO-forming loop affect the ability of *Pp*HAL to form the MIO group.[30]

Table 3.1. Mutations in ^{141}Gly-^{142}Ala-^{143}Ser -^{144}Gly-^{145}Asp sequence in *Pp*HAL and relative catalytic activity of corresponding mutants.

Mutation	Relative Activity (%)	MIO Formation	Reference
None (*wt-Pp*HAL)	100	Yes	31
Gly141Ala	1.1	ND*	31
Ala142Gly	93	Yes	31
Ser143Cys	100	Yes	22
Gly144Ala	37	Yes	31
Asp145Ala	0	No	30

* Crystal structure was not obtained. ND: Not Determined

3.1.2.2. Mutants of *Tc*PAM

Recently, the biosynthesis of the MIO in *Taxus chinensis* PAM (*Tch*PAM) was investigated using site-directed mutagenesis.[31] In a previous study, highly conserved, Tyr322 and Asn231 were identified as essential residues for *Tch*PAM activity; both Tyr322Ala and Asn231Ala mutants were inactive.[32] Recently, Janssen and coworkers determined Tyr322Ala and Asn231Ala mutant crystal structures revealing the intact ^{175}Ala-^{176}Ser-^{177}Gly tripeptide.[31] Enzyme containing Tyr322Ala and Asn231Ala mutants lacked a mature MIO and Ser176 was not dehydrated (Figure 3.6). In the structure of Asn231Ala mutant, the Gly177 amide-nitrogen and Ala175 carbonyl-carbon are in a proper position (2.8 Å) for the cyclization reaction, but seemingly the amide-nitrogen was not activated to initiate the nucleophilic attack when the Asn231 is removed (Figure 3.6A).[31] Thus, a hydrogen bonding interaction between Ser176

carbonyl-oxygen and Asn231 N_δ, likely increases the nucleophilicity of the Gly177 amide-nitrogen, thus MIO formation is prompted. Similarly, Arg96 in GFP was suggested to activate the amide-nitrogen of Gly67 to increase its nucleophilicity and facilitate the cyclization of ^{65}Ser-^{66}Tyr-^{67}Gly tripeptide.[33] Hydrogen bonding of the carbonyl-oxygens of Arg96 and Tyr66 increases the acidity of the Gly67 amide-nitrogen, and Arg96 stabilizes the peptide bond resonance form.[33,34]

In contrast to Asn231Ala mutant, the MIO-forming loop of the Tyr322Ala mutant was deviated from the normal spatial orientation of MIO group atoms in *wt-Tch*PAM (Figure 3.6B).[31] The Gly177 amide-nitrogen atom and the Ala175 carbonyl-carbon atom were not in a favorable orientation for MIO-formation. Tyr322 presumably positions Ala175 in a proper location for the nucleophilic attack by Gly177.[31] In addition, the carbonyl-oxygen atom of Ser176 was too far from the N_δ atom of the Asn231 side chain for a hydrogen bonding interaction. Thus, the Gly177 nitrogen atom is likely not activated to initiate the cyclization.[31]

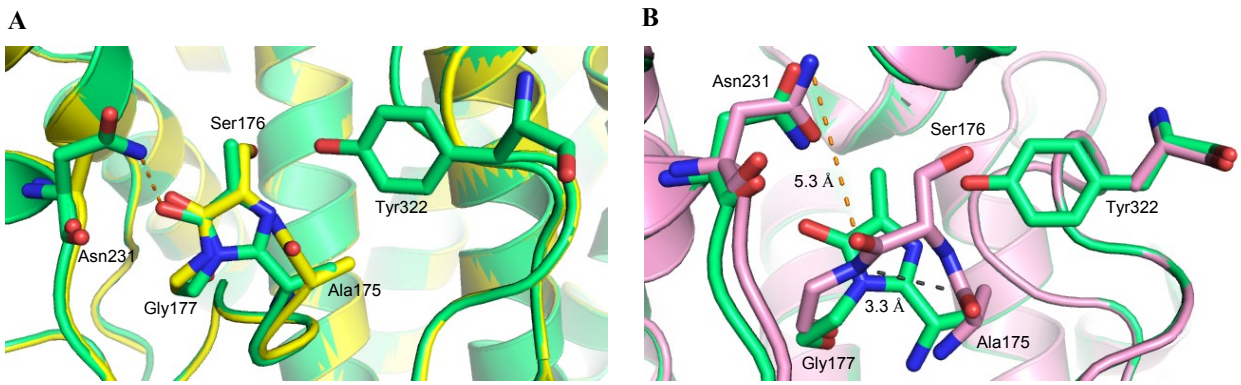

Figure 3.6. Comparison of *wt-Tch*PAM and *Tch*PAM mutants lacking an MIO. *A*) Overlay of *wt-Tch*PAM (PDB 2YII; green) and Asn231Ala mutant structure (PDB 4C6G; yellow). Hydrogen bonding interaction between Asn231 in *wt-Tch*PAM and Ser176 carbonyl-oxygen is shown. *B*) Overlay of *wt-Tch*PAM (green) and Tyr322Ala mutant structure (PDB 4C5U; pink). Shown are distance between Ala175 carbonyl-carbon and the Gly177 amide-nitrogen, and hydrogen bonding interaction between Asn231 and Ser176 carbonyl oxygen. Atoms are color-coded as carbon: green/yellow/pink; oxygen: red; nitrogen: blue.

3.1.3. Mechanism of MIO-dependent Enzymes

3.1.3.1. Mechanistic Proposals on Ammonia Lyase Elimination Reaction

After clarifying that the electrophilic cofactor as dehydroalanine, various mechanistic investigations were carried out on PALs and HALs.[11,35] First mechanistic proposal from Hanson and Havir (1970) described a mechanism, where the amino group of phenylalanine is added to the β-position of dehydroalanine.[18] Subsequent investigations by Hermes et. al. carried out on PAL also proposed a Michael addition of α-amino group of the substrate (Figure 3.7, path a).[35] According to this mechanism, nucleophilic addition of the α-amino group on the prosthetic electrophile produce a covalently bound enzyme intermediate. The addition of the amino group to the electrophile was suggested to enhance its leaving group ability.[35] However, this mechanism did not explain how the non-acidic β-proton ($pK_a \sim 40$)[36] of the substrate is abstracted by an enzymatic base.

In 1995, Rétey and coworkers found contradictory results to this mechanism that has been accepted widely for about 30 years.[10,11] Both a PAL Ser202Ala mutant and *wt*-PAL inactivated with $NaBH_4$ reacted much faster with *p*-nirophenylalanine than with the natural substrate.[11] These observations were thought to disagree with a mechanism involving nucleophilic attack of α-amino group at dehydroalanine cofactor. Thus, the function of dehydroalanine was proposed to be similar to that of the nitro substituent on a phenyl ring to increase the acidity of β-hydrogens of the substrate and promote the elimination reaction.[11] Analogous results were obtained for HAL when 5-nitrohistidine was reacted with the mutants lacking the dehydroalanine electrophile.[10] These observations lead to the proposal of an alternative mechanism, where the aromatic ring of the substrate reacted with the dehydroalanine

via Friedel-Crafts-like addition (Figure 3.7, path b).[10,11] The positive charge created at C_{ipso} enhances the acidity of β-hydrogens and thus facilitated the abstraction by an enzymatic base.[11] Further support for this mechanism was provided by the finding that *m*-hydroxyphenylalanine was a slightly better substrate for PAL than phenylalanine.[11] In contrast, *p*-hydroxyphenylalanine was a poor substrate, because unlike *m*-hydroxy, *p*-hydroxy group does not facilitate an electrophilic attack at *ortho*-position.

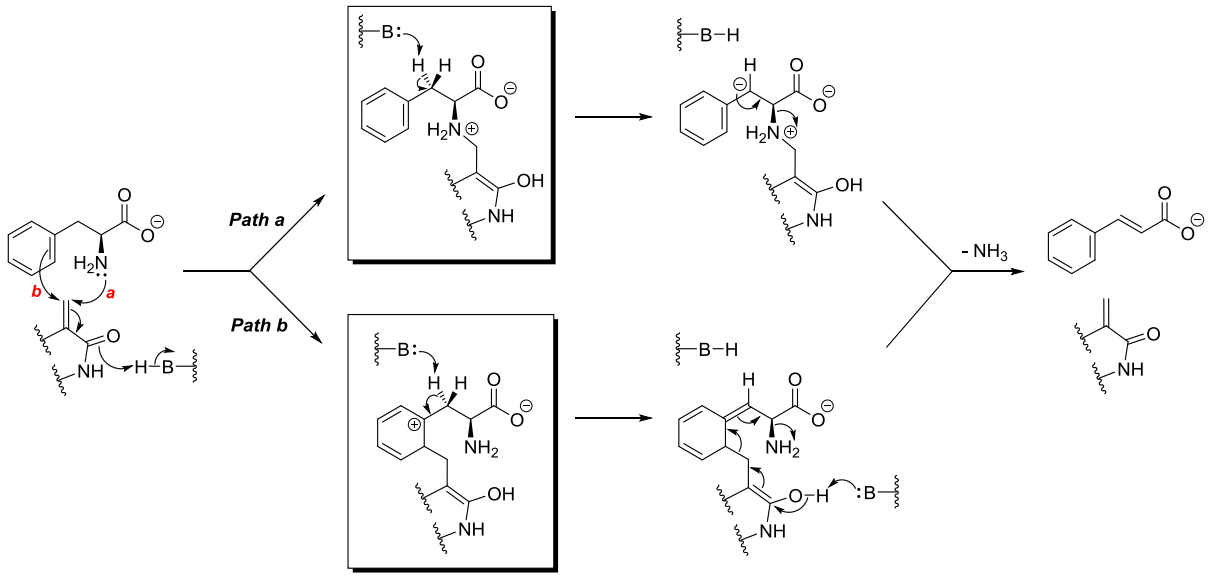

Figure 3.7. Proposed mechanisms of PAL reaction. *Path a*) Amino alkylation-mechanism proposed by Hanson and Havir[18] and modified by Hermes et.al.[35] *Path b*) Alternative Friedel-Crafts-like addition mechanism proposed by Rétey and coworkers.[11]

The Friedel-Crafts-like addition mechanism however did not explain the energy demands for losing aromaticity of the substrate phenyl ring, and why an exocyclic double bond was created when the ring could have been rearomatized by deprotonation of the σ-complex.[37] Described earlier, as the field advanced, crystallographic analysis revealed the dehydroalanine

was an MIO group and this electrophile is more electrophilic than the dehydroalanyl moiety and, thus, more opt to react with the aromatic ring.[9] The planar geometry of the MIO heterocyclic ring, which is maintained by the fold of the polypeptide chain, prevents delocalization of Gly144 nitrogen lone pairs into the α,β-unsaturated carbonyl system (cf. Figure 3.3A, B). Furthermore, addition of a nucleophile at the methylidene carbon renders the MIO imidazole ring aromatic, thus the transient loss of aromaticity in the phenyl ring of the substrate is compensated.[9] In addition, it was proposed that PAL and HAL prevent rearomatization of the phenyl ring by eliminating basic side chains in the aromatic ring binding pocket, while a basic group is properly positioned to remove a benzylic proton of the substrate.[38]

3.1.3.2. Mechanism of MIO-dependent Aminomutases

The dependency of aminomutases on an MIO-cofactor was identified when *Streptomyces globisporus* tyrosine aminomutase (*Sg*TAM), homologous to ammonia lyases, was characterized.[3] As with HALs[14,16] and PALs[15,17], *Sg*TAM was inactivated upon $NaBH_4$ and KCN treatment.[3] Furthermore, analogous Ser153Ala mutation on the precursor of exocyclic double bond of the MIO group resulted a 340-fold decrease in the catalytic efficiency compared to *wt*-*Sg*TAM. The mutase activity of a phenylalanine aminomutase from *Taxus cuspidata* (*Tc*PAM), which is homologous to *Sg*TAM (56% similarity) and ammonia lyases (50-70% similarity) was also abolished upon the pretreatment with KCN or $NaBH_4$.[1] Taken together with the conserved Ala-Ser-Gly motif, these results suggested the existence of the MIO cofactor in TAMs and PAMs.[1,3]

Analysis of the product pool catalyzed by *Sg*TAM and *Tc*PAM indicated that the corresponding *trans*-acrylic acid is produced as a minor product during catalysis, providing the

evidence for an initial elimination reaction during α- to β-amino acid conversion.[1,3] Based on the homology to ammonia lyases, it was envisioned that either an amino-MIO adduct (Figure 3.8A) or a Friedel-Crafts-like (Figure 3.8B) mechanism leads to an α,β-elimination reaction resulting *trans*-acrylate intermediate. Unlike ammonia lyases, which release ammonia and an α,β-unsaturated propenoate, aminomutases catalyze a subsequent conjugate addition reaction of ammonia to the β-position of *trans*-acrylate (Figure 3.8).[1,3]

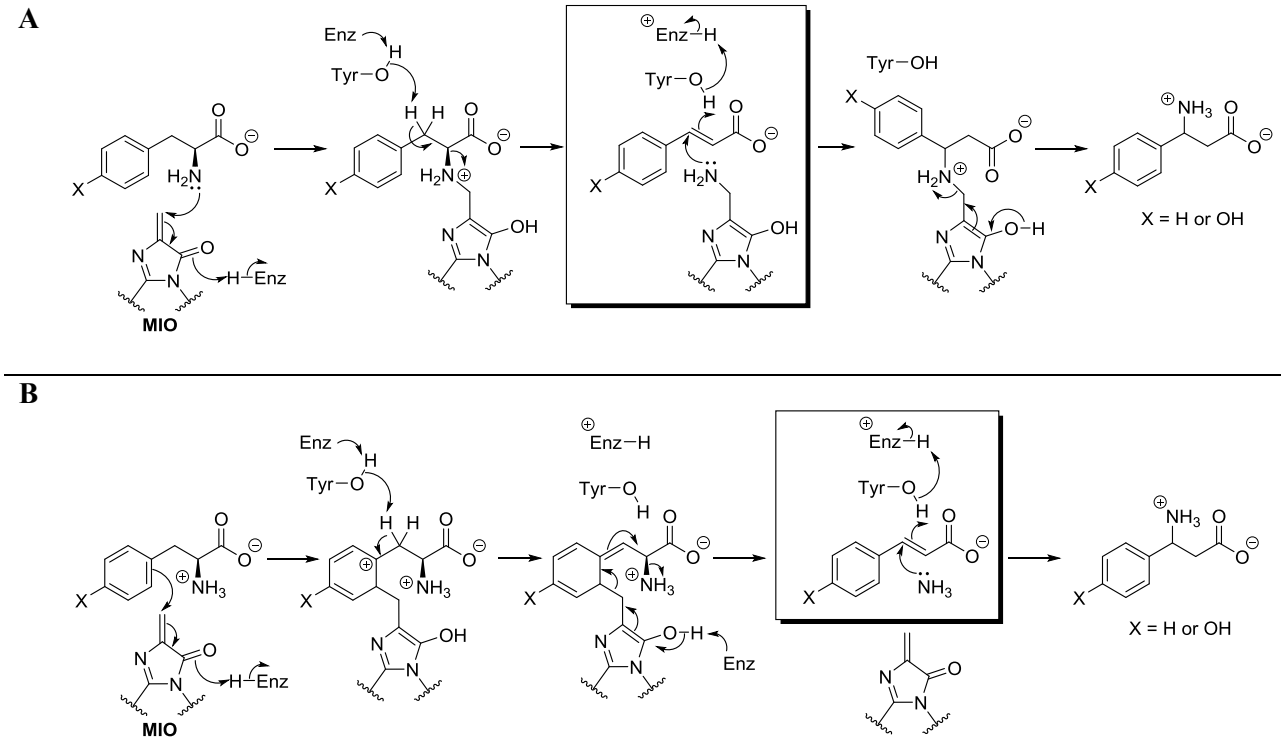

Figure 3.8. Amino-MIO adduct (*A*) and Friedel-Crafts-like (*B*) isomerization mechanisms of MIO-dependent aminomutases based on the proposed mechanistic proposals for MIO-based ammonia lyases.

Subsequent structure determination of *Sg*TAM[27] and *Taxus* phenylalanine aminomutases,[24,32] confirmed the presence of the MIO group in their active sites. The structures revealed that the overall architecture of aminomutases and that of their active sites are very similar to MIO-dependent ammonia lyases.[9,24,27] However, based on the mechanism, aminomutases are expected to retain ammonia in the active site to achieve the isomerization reaction. Bruner and co-workers compared the structures of *Rs*TAL[39] and *Sg*TAM, to investigate the structural basis for aminomutase activity of the latter.[27,40] It was proposed that the more solvent accessible *Rs*TAL active site lacks the ability to maintain ammonia and *p*-hydroxy cinnamate.[39] In contrast, the hydrogen bonding interaction of Tyr303 and Glu71 of *Sg*TAM (Figure 3.9), an interaction not present in *Rs*TAL or other ammonia lyases, blocks the solvent accessibility of *Sg*TAM and prevents ammonia from leaving the active site.[27] Tyr303Ala and Glu71Ala single mutants, and the double mutant probed the hypothesis of the varied solvent accessibility between the aminomutase and the lyase activities.[40] Although the mutations resulted in open tunnel, the activity of *Sg*TAM was not altered to a lyase. The mutants still catalyzed the ammonia rebound albeit with lower activity compared to *wt*-*Sg*TAM.[40]

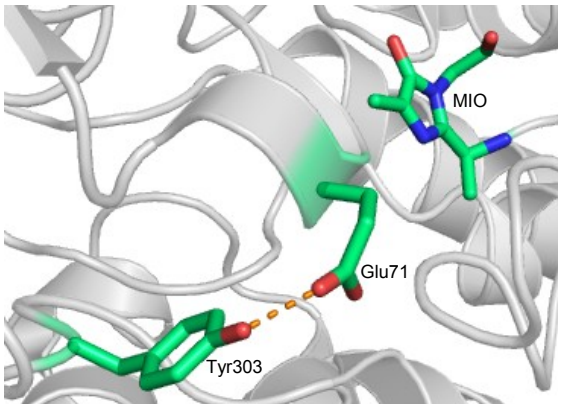

Figure 3.9. *wt-Sg*TAM active site (PDB 2OHY) showing the closed active site due to the hydrogen bonding between Glu71 and Tyr303. MIO is also shown. Atoms are color-coded as carbon: green; oxygen: red; nitrogen: blue

Structural characterization of *Sg*TAM bound to mechanism-based inhibitors provided significant insights into the mechanism of MIO-dependent aminomutases.[41,42] In their cocrystal complexes, product-like inhibitors, α,α-difluoro-β-tyrosine (Figure 3.10A) and -β-*p*-methoxyphenylalanine (Figure 3.10B) were covalently-bound to the MIO methylidene via the α-amino group.[41] The observed electron density of the active sites did not match an MIO-phenyl ring adduct consistent with the Friedel-Crafts-like mechanism suggesting the occurrence of an NH_2-MIO adduct mechanism. Additional cinnamate epoxide inhibitors were also designed to mimic the *p*-hydroxycinnamate intermediate in *Sg*TAM reaction.[42] The structure of the *p*-fluorocinnamate epoxide bound to *Sg*TAM confirmed the mechanism of catalysis via an NH_2-MIO adduct.

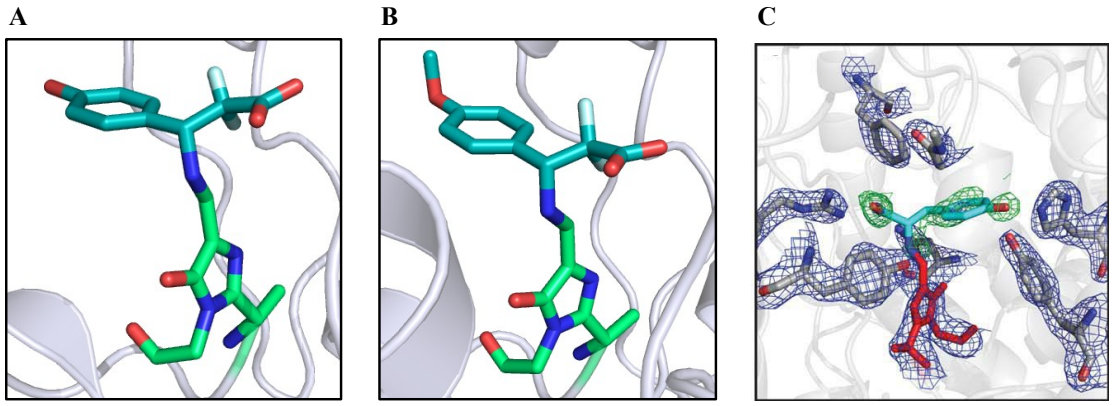

Figure 3.10. Structure of *Sg*TAM solved with various mechanism-based inhibitors and ligands. *wt-Sg*TAM bound to α,α-difluoro-β-tyrosine (*A*; PDB 2QVE) and α,α-difluoro-β-*p*-methoxyphenylalanine (*B*; PDB 2RJS) showing the NH_2-MIO adducts. Inhibitors are shown in cyan. *C*) Structure of Tyr63Phe mutant *Sg*TAM with L-tyrosine modeled into partially occupied electron density (PDB 3KDZ). L-Tyrosine and MIO are shown in cyan and red respectively. Atoms are color-coded as carbon: green/cyan/gray; oxygen: red; nitrogen: blue; fluorine: light blue.

Although the crystallization of mechanism-based inhibitors were successful, the attempts to obtain an enzyme-bound L-tyrosine (substrate) were not successful with *Sg*TAM.[40] The X-ray cocrystal structure of the *Sg*TAM mutant of the catalytic base (Tyr63Phe) with L-tyrosine revealed only a partial occupancy of the substrate. The electron density of the α- and β-carbons of L-tyrosine and their covalent bonding to the MIO via the amino group were very weak (cf. Figure 3.10C).[40] Currently, there are no reports in literature on the identification of naturally occurring mechanism-based intermediates. The work described herein involved the identification of naturally occurring reaction pathway intermediates using structural determination of *Pa*PAM.

In addition, as described before (see section 3.1.2), Thr167 in the MIO forming motif (^{167}Thr-^{168}Ser-^{169}Gly) of *Pa*PAM is different from other aminomutases,[24,27] and the basis for using variable residues for MIO formation is yet to be determined. The investigations on determining the catalytic and structural role of Thr167 during *Pa*PAM catalysis is described herein.

3.2. Experimental

3.2.1. Mutagenesis of *Pa*PAM cDNA

Point mutations of *Pa*PAM were performed using *PfuUltra* HF DNA polymerase provided with the QuikChange II XL site-directed mutagenesis kit or *PfuTurbo* polymerase (Stratagene, La Jolla, CA). The forward oligonucleotide primers used to exchange residue F455 to alanine (A) or asparagine (N); T167 to alanine (A), serine (S), glycine (G), valine (V) or cystine (C); and S168 to alanine (A) in the mutagenesis reactions were as follows (mutations are bold and underlined). The corresponding reverse-complement primer was paired with each forward primer.

F455A: 5′–GC ACC ACC GGA GAC **GC**T CAG GAT ATC GTC TC–3′

F455N: 5′–GC ACC ACC GGA GAC **AA**T CAG GAT ATC GTC TC–3′

T167A: 5′–GAA AAA GGT TCG CTG GGA **G**C**T** AGT GGC GAT–3′

T167S: 5′–GAA AAA GGT TCG CTG GGA A**G**C AGT GGC GAT–3′

T167G: 5′–GAA AAA GGT TCG CTG GGA **GG**C AGT GGC GAT–3′

T167V: 5′–GAA AAA GGT TCG CTG GGA **GTG** AGT GGC GAT–3′

T167C: 5′–GAA AAA GGT TCG CTG GGA **TG**C AGT GGC GAT–3′

S168A: 5′–GC CTG GGA ACC **GC**T GGC GAT CTG GGG C–3′

Expression vector pET24b(+) containing the wild-type *Pa*PAM cDNA was used as the DNA template in the PCR reactions. A typical PCR reaction mixture was consisited of wild-type

*Pa*PAM DNA template (10 ng), corresponding forward and reverse primers (150 ng each), dNTP mix (1 μL), 10X reaction buffer (5 μL), *PfuUltra* HF or *PfuTurbo* DNA polymerase (1 μL at 2.5 U/μL), and ddH_2O to bring the volume to 50 μL. QuickSolution reagent (3 μL) was added for PCR reactions performed with QuikChange II XL site-directed mutagenesis kit.

The PCR program conditions for *PfuUltra* HF DNA polymerase were as follows: initial denaturing at 95 °C for 2 min followed by 30 cycles at 95 °C for 50 s, 55 °C for 50 s, and 68 °C for 7 min, and finally, the reactions were held at 68 °C for 7 min. For *PfuTurbo* DNA polymerase, initial denaturation with similar conditions was followed by 30 cycles at 95 °C for 30 s, 60 °C for 30 s, and 72 °C for 7 min, and the temprature was held at 72 °C for 10 min. After temperature cycling, the reactions were place on ice, to each was added restriction enzyme *Dpn*I (1 μL at 10 U/μL), and the reactions were incubated at 37 °C for 1 h to digest the template DNA. An aliquot (2 μL) of the plasmid solution from each PCR reaction was used to transform XL10-Gold ultracompetent cells (provided in the QuikChange II XL site-directed mutagenesis kit) or DH5α competent *E. coli* cells. The resultant plasmids encoding mutations in the *papam* cDNA were confirmed by sequencing the each corresponding mutant cDNA.

3.2.2. Expression and Purification of *Pa*PAM Mutants

Plasmids of each mutant were used separately to transform BL21(DE3) *E. coli* cells. The transformants were grown on Luria-Bertani agarose medium supplemented with kanamycin (50 μg/mL) and grown overnight at 37 °C. Resistant cells harboring *Pa*PAM mutants were grown in liquid Luria-Bertani medium (5 mL) supplemented with kanamycin (50 μg/mL) at 37 °C for 16

h. The entire 5-mL inoculum of *E. coli* BL21(DE3) was added to Luria-Bertani medium (1 L) and incubated at 37 °C until the optical density (A_{600}) was ~0.6. The culture was cooled to 16 °C, and to the cell suspension was added isopropyl-β-D-thiogalactopyranoside (100 μM) to induce protein expression. The cells were incubated at 16 °C for 16 h. The subsequent steps were performed at 4 °C, unless otherwise indicated. The cells were harvested by centrifugation at 6,000*g* (15 min) and the cell pellet was resuspended in lysis buffer (50 mM sodium phosphate buffer containing 5% (v/v) glycerol, 300 mM NaCl, 10 mM imidazole, pH 8.0). The cells were lysed by sonication (Misonix sonicator, Farmingdale, NY), the lysate was centrifuged at 9,700*g* (45 min) to remove cell debris, and the supernatant was decanted and centrifuged at 102,000*g* (1 h) to remove light membranes. The resultant crude mutant proteins in the soluble fraction was separately purified by Nickel-nitrilotriacetic acid (Ni-NTA) affinity chromatography according to the protocol described by the manufacturer (Qiagen, Valencia, CA). Fractions containing the mutant enzyme that eluted in 250 mM imidazole were combined and concentrated. The buffer was exchanged with 50 mM sodium phosphate buffer containing 5% (v/v) glycerol (pH 8.0) using a size selective centrifugal filtration unit (Centriprep centrifugal filter units, 30,000 MWCO, Millipore). The purity of the concentrated enzyme was assessed by SDS−PAGE with Coomassie Blue staining, and the quantity was determined by the Bradford protein assay. The overexpressed *Pa*PAM mutants (~59 kDa) were at ~90% purity (~50 mg/L).

3.2.3. Assessing the Absolute Stereochemistry of the β-Phenylalanine Product Catalyzed by *Pa*PAM Mutants

(2*S*)-α-Phenylalanine (1 mM) was incubated separately with F455A and F455N (4 mg) in phosphate buffer (10 mL, pH 8.0) at 31 °C. Each reaction was quenched after 24 h by basifying to pH 10 (6 M NaOH). (1*S*)-(–)-Camphanic chloride (~2 mg) was added to each reaction mixture. The solution was stirred (45 min), acidified to pH 2-3 (6 M HCl), and extracted with diethyl ether (2 × 2 mL). The organic solvent was evaporated under vacuum, and the resulting residue was dissolved in ethyl acetate/methanol (3:1, v/v) (200 μL). The solution was treated with excess (trimethylsilyl)diazomethane until a faint yellow color persisted. The derivatized β-amino acid was identified by GC/EI-MS analysis and compared against the retention time and mass spectrometry fragmentation of authentic *N*-[(1'*S*)-camphanoyl]-(3*S*)-β-phenylalanine methyl ester

3.2.4. Total Cell Protein (TCP) Fraction Analysis

BL21(DE3) *E. coli* cells transformed to express *wt*- and mutant-*Pa*PAM were grown in liquid Luria-Bertani medium (10 mL) supplemented with kanamycin (50 μg/mL) at 37 °C. When the optical density (A_{600}) reached ~0.6, a 1-mL well-mixed culture sample was obtained from each transformant. The cultures were cooled to 16 °C, and isopropyl-β-D-thiogalactopyranoside (100 μM) was added to induce the protein expression. The cells were incubated at 16 °C for 16 h and a 1-mL induced cell sample was obtained from each culture. Uninduced and induced cell

samples were harvested by centrifugation (13,000 *g* for 5 min) and the TCP fractions were analyzed by SDS-polyacrylamide gel followed by Coomassie blue staining.

3.2.5. Circular Dichroism (CD) Spectroscopic Analysis

CD spectra of each protein were recorded in a CD spectrometer (Chirascan, Applied Photophysics, Surrey,United Kingdom) using a quartz cell of 1 mm path length. Spectra in far- (180-250 nm) and near-UV (260-310 nm) regions were obtained with 0.25 mg/mL and 8 mg/mL protein concentrations, respectively. The wavelength interval was set to 0.5 nm with 2.5 s signal average per point and each sample was scanned for five times. All CD spectra were obtained in phosphate buffer at pH 8. Reference spectra were obtained for all samples containing only the buffer components, and the final spectra are the difference of the protein sample spectra after subtraction of the reference spectra. For each sample, three separate samples were analyzed at each wave-length region. The fractional helicity (f_H) of *wt*- and mutant-*Pa*PAM was calculated using the following equation (θ: negative molar ellipticity).[43]

$$f_H = \frac{([\theta]_{208} - 4000)}{(-33000 - 4000)}$$

3.3. Results and Discussion

3.3.1. Structural Insights into Mechanism of *Pa*PAM Isomerization

3.3.1.1. Characteristics of the Overall Structure and the Active Site

The crystal structure of *Pa*PAM determined at 1.7 Å resolution displays structural homology to other MIO-dependent aminomutases (*Tc*PAM[24,31] and *Sg*TAM[27]) and homologous ammonia lyases.[6-9,44] The overall structure of the *Pa*PAM monomer (541 amino acids) was predominantly α-helical with most helices running along the long axis of the monomer structure (Figure 3.11A). There are nine short β-strands (the longest strand consists of four amino acids) that form three antiparallel and one parallel β-sheet. Also notable are two monomers per asymmetric unit, and the active unit exists as a tetramer (a head-to-tail dimer of dimers related by 222 point symmetry) (Figure 3.11B, C).

Each subunit of the catalytically functional tetramer consists of an active site located close to one end of the monomer at the termini of several α-helices (Figure 3.11A, C). Amino acid side chains from three monomers contribute to generate a composite active site (Figure 3.11D). The carboxylate group of the bound propanoate moiety forms a mono dentate salt-bridge interaction with the δ-guanido group of the active site Arg323. The non-polar side chains of Leu104, Val108, Leu171, Leu216, Leu421, Met424 and Phe455, and the hydrophilic side chain of Gln456 surround the aromatic ring of the bound phenyl propenoate moiety (Figure 3.11D). The Arg323−carboxylate salt-bridge interaction and the hydrophobic contacts between the aromatic ring likely anchor the aromatic amino acids in the *Pa*PAM active site.

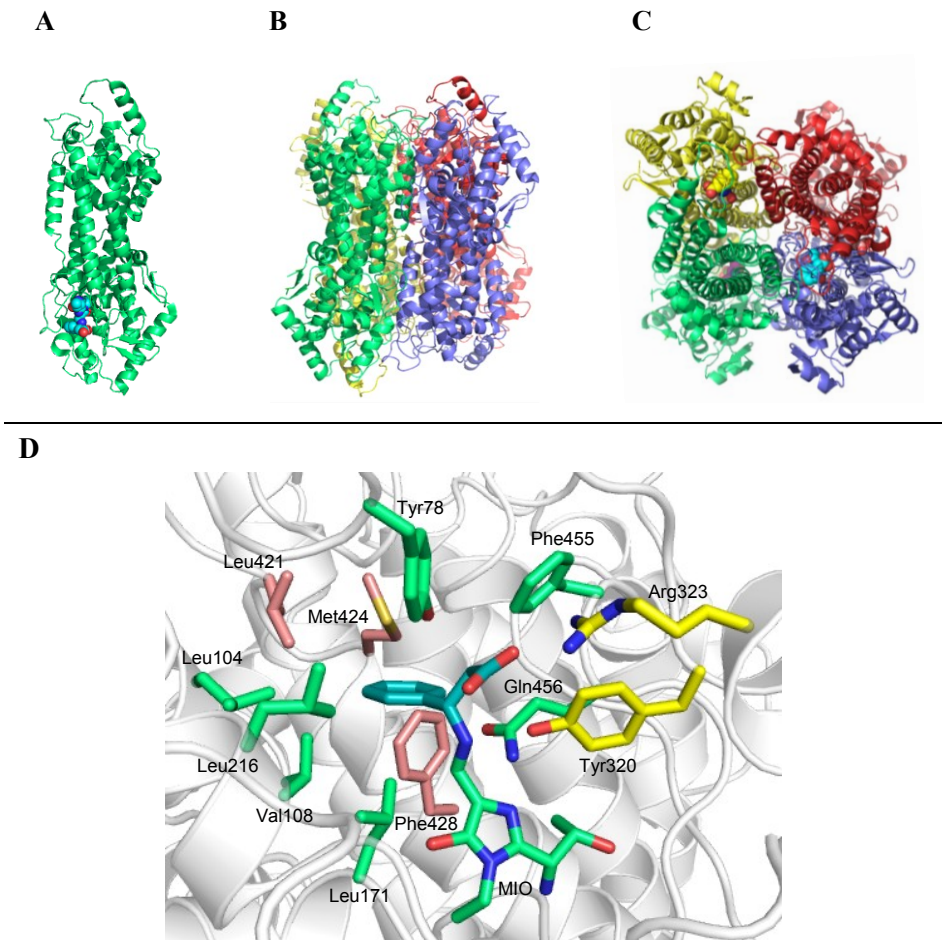

Figure 3.11. Overall structure and the active site characteristics of *Pa*PAM. *A*) Structure of *Pa*PAM monomer showing the active site positioned at the end of the four helix bundle. The MIO and the phenyl propenoate moiety are shown in spheres. The side- (*B*) and top- (*C*) view of the *Pa*PAM tetramer. Each monomer is distinctly colored. *D*) Active site of *Pa*PAM showing residues which are in 4 Å distance from the MIO-bound phenyl propenoate moiety (atoms are color-coded as carbon: teal; oxygen: red; nitrogen: blue). The active site residues are color-coded (carbon atoms in green, yellow, and wheat) to differentiate the involvement from each sub unit.

The MIO cofactor of *Pa*PAM, formed by the self-condensation of a Thr^{167}-Ser^{168}-Gly^{169} triad, was covalently bound to a phenyl propanoate substrate in each active site. In addition to the MIO cofactor, the *Pa*PAM active site contains key catalytic residues that are found in other structurally characterized enzymes[6,9,24,27] of class I lyase-like family (cf. Figure 3.11D). The enzymatic base Tyr78, required for the de- and re-protonation, is positioned ~3.5 Å above both

the α- and β-carbon atoms of the phenyl propanoate adducts. Further, Tyr320 is 2.6 Å from the amino group of the α-phenylalanine intermediate, and thus believed to facilitate C_β to C_α proton transfer when the amino group migrates reciprocally.[25]

3.3.1.2. Identification of Mechanism-based Intermediates

Active sites of the *Pa*PAM dimer revealed two different types of ligands bound to the methylidene of the MIO cofactor. The electron density observed in monomer "A" revealed a β-phenylalanine molecule covalently attached by its amino group to the methylidene of the MIO (Figure 3.12A). The electron density of monomer "B" (Figure 3.12B, C), however, suggested partial occupancy of two ligand types. The electron density for a β-phenylalanine-type adduct was evident, as seen in monomer "A", but there was also electron density that is consistent with a molecule indistinguishable from α-phenylalanine that was covalently attached by its amino group to the methylidene carbon atom of MIO (Figure 3.12B, C).

Observation of α/β-phenylalanine-type MIO-bound ligands in the *Pa*PAM active site was surprising, particularly, since the crystallization buffer for *Pa*PAM included cinnamate as a ligand. It should be mentioned that *Pa*PAM and homologous *Tc*PAM were shown to function as aminotranferases capable of transferring the amino group from an external amino source to an arylacrylate intermediate.[45-47] Both α- and β-phenylalanine (1:1) were produced by the addition of ammonia across the double bond of cinnamic acid.[46,47] With this data, the source of the α- and β-amino acids evidenced in this crystallographic study, described herein, could be reconciled. The LB media (pH 7.3) used to grow the bacteria, in which protein was overexpressed and used in the crystallographic study was estimated to contain ammonia at a concentration of 2.4 mM, as assessed in an earlier study.[48] It was imagined that this source of ammonia could bind to the MIO

(NH_2-MIO) of *Pa*PAM overexpressed in *E. coli*. Therefore, the α- and β-phenylalanines were likely formed by the reaction between cinnamate and NH_2-MIO adduct remained after protein purification.

The enzyme-bound ligands in *Pa*PAM active sites are consistent with a mechanism that proceeds *via* amino-alkylation pathway (Figure 3.12D) and not through a Friedel–Crafts-like pathway, as recently proposed.[49] This suggests that the nucleophilic amino group of the substrate and not the π-electrons of the aryl ring attacks the MIO of *Pa*PAM during the isomerization reaction. Further evaluation of the α- and β-phenylalanine complexes of monomer "B" (Figure 3.12B, C) suggested that during the amino group isomerization, the phenylpropanoid carbon backbone remains mostly stationary above NH_2-MIO adduct. Previous mechanistic studies on *Pa*PAM supported that the amino group of the substrate is removed from C_α and reattached at C_β of the cinnamate intermediate on the same stereoface.[25] These configurations are consistent with the mechanism of stereoselectivity for this enzyme that proceeds with inversion-of-configuration at each migration terminus.[25]

The MIO-adducts observed with *Pa*PAM are, in part, similar to the complexes of mechanism-based inhibitors in the *Sg*TAM structures.[41,42] The *Sg*TAM structural data confirmed that a covalent intermediate forms between the substrate or product and the MIO. The C_α of *p*-fluorocinnamate epoxide and C_β of α,α-difluoro-*p*-methoxy-β-phenylalanine (product mimic) were covalently bound to the MIO methylidene carbon by the epoxide-oxygen and the β-amino group, respectively (cf. Figure 3.10).[42] Nonetheless, the structure of *Pa*PAM was the first of the MIO-dependent enzyme to be crystallized with naturally occurring pathway intermediates.

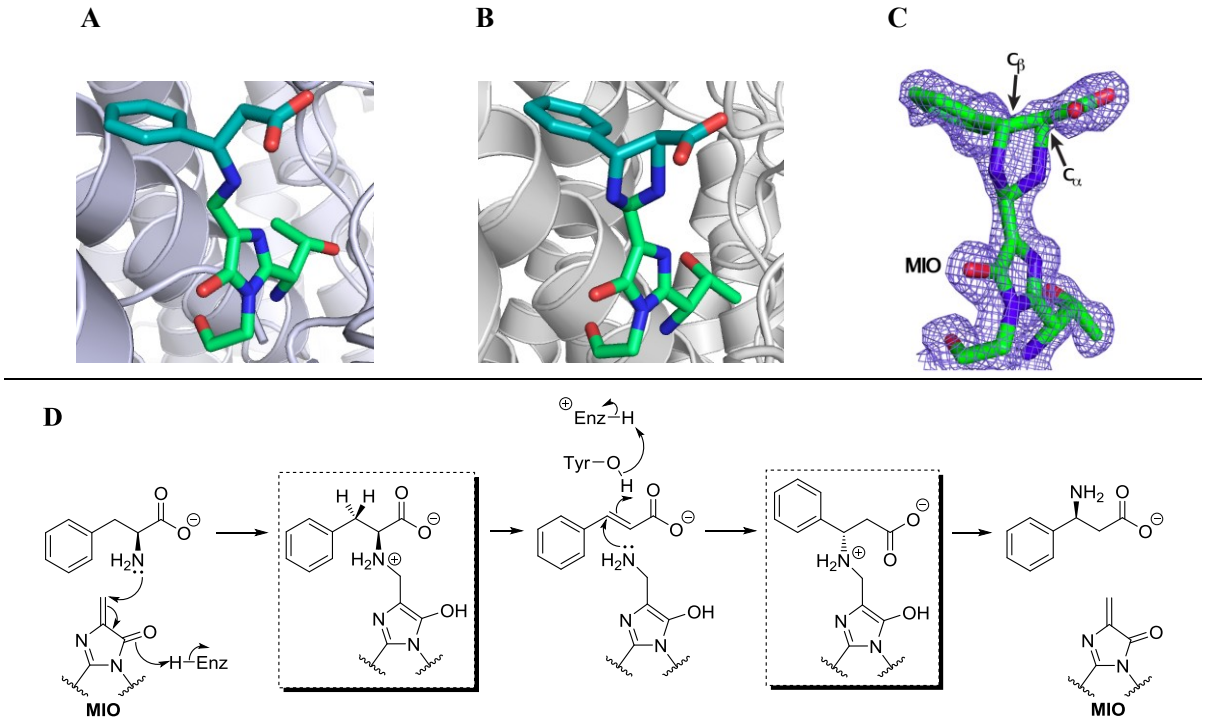

Figure 3.12. MIO-bound intermediates identified in *Pa*PAM active sites. β-Phenylalanine-type (*A*) and α/β-phenylalanine-type (*B*) molecules bound to the MIO cofactor. *C*) Electron density ($2F_o$-F_c map, blue mesh) calculated at 1.0 σ around the α- and β-phenylpropanoid that is covalently bound to the MIO found in monomer "B". Atoms are color-coded as carbon: green/teal; oxygen: red; nitrogen: blue. *D*) Amino-alkylation mechanism of *Pa*PAM isomerization. MIO-bond intermediates highlighted in dashed-squares resemble the enzyme-bound ligands seen in *Pa*PAM active site.

3.3.2. Mutational Insights into Mechanism and Stereochemistry of *Pa*PAM Isomerization

3.3.2.1 Comparison of the *Pa*PAM Active Site with other MIO-dependent Aminomutases

*Pa*PAM is homologous to *Taxus* phenylalanine aminomutase *Tc*PAM[1] (31% identity and 47% similarity), L-tyrosine 2,3-aminomutase *Sg*TAM from *Streptomyces globisporus*[3] (37% identity and 56% similarity) and *Cc*TAM from *Chondromyces crocatus*[4] (38% identity and 55% similarity). Structures of *Sg*TAM bound to different inhibitors (PDB 2QVE, 2RJS and 2RJR)[42]

and *Tc*PAM bound to cinnamate intermediate (PDB 3KDZ and 2YII)[24,31] have been solved previously. Overall, the active sites of the MIO aminomutases exhibit very similar architecture, and the amino acid side chains lining the active sites are largely conserved. *Sg*TAM, however, contains a non-conserved His93 (Val108 in *Pa*PAM and Leu108 in *Tc*PAM) (Figure 3.13B) and Tyr415 (Phe428 in *Pa*PAM and Ile431 in *Tc*PAM) to orient to the hydroxy group of the tyrosine substrate.[27,41] In addition to Phe428 in *Pa*PAM, two other residues of chain "B" contribute to *Pa*PAM active site are also not conserved among the aminomutases (cf. Figure 3.11D). Met424 in *Pa*PAM is a charged Lys427 in *Tc*PAM and a smaller, hydrophobic Ala411 in *Sg*TAM. Further, Leu421 in *Pa*PAM is a more polar Tyr424 in *Tc*PAM and Ser408 in *Sg*TAM. Although the side chain chemistry of these residues are variable among the members of aminomutase family, given their >5 Å distance from the bound ligand, they are less likely function catalytically in the isomerization reaction.

Two prominent differences were seen in the active sites of MIO-dependent enzymes. First, the trajectory of ligands in *Pa*PAM, *Sg*TAM and *Tc*PAM active sites was significantly different. Compared to the bi-dentate salt bridge in *Tc*PAM between the carboxylate of the cinnamate intermediate and the conserved Arg325 side chain,[24] ligands in *Pa*PAM form a presumably weaker mono-dentate salt bridge with Arg323 (Figure 3.13A). A similar alignment with a mono-dentate salt bridge was seen in *Sg*TAM structures containing α,α-difluoro-β-tyrosine (Figure 3.13B), α,α-difluoro-*p*-methoxy-β-phenylalanine and *p*-fluoro cinnamate epoxide intermediate.[41,42] The trajectory of MIO-bound ligands was almost identical in the *Pa*PAM and *Sg*TAM active sites, which catalyze an equivalent stereochemistry in the isomerization reaction.[3,25] A difference in residues near the carboxylate binding site of *Pa*PAM was notable when compared with those of other MIO-dependent enzymes. Phe455 in *Pa*PAM is

Asn458 in *Tc*PAM (Figure 3.13A), Asn442 in *Sg*TAM (Figure 3.13B)] or glutamine[6,9] in almost all other enzymes in the lyase family. Presumably, steric clash from Phe455 alters the trajectory of the covalently bound α- and β-phenylalanine ligands and forces a weaker mono-dentate salt bridge in *Pa*PAM. A ligand trajectory consisted with a bi-dentate salt bridge, as seen in *Tc*PAM,[24] causes steric overlap between the carboxylate group and Phe455. Interestingly, *Sg*TAM which has Asn442 (similar to Asn458 in *Tc*PAM) at a position equivalent to Phe455 also engaged in a mono-dentate salt bridge between the ligands and conserved Arg311 (Figure 3.13B). The *p*-hydroxy group of L-tyrosine in *Sg*TAM, however, makes a hydrogen bond with the non-conserved His93 (Figure 3.13B).[27] The hydrogen bonding interaction, absent in *Pa*PAM, can therefore enforce the altered trajectory of ligands in the *Sg*TAM active site. Thus, *Sg*TAM and *Pa*PAM catalyze equivalent stereochemistries, presumably by orienting their substrates identically in their active sites using a distinct set of enzyme–substrate interactions.

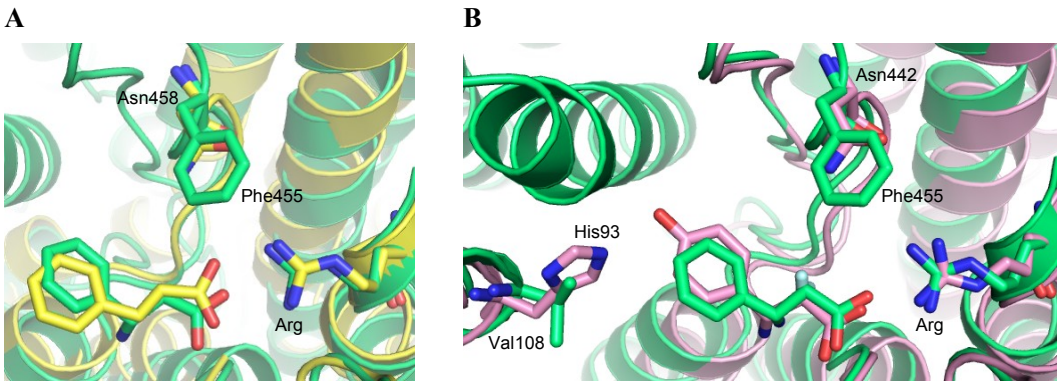

Figure 3.13. Comparison of *Pa*PAM (green) with *Tc*PAM (yellow) and *Sg*TAM (pink) active sites. Atoms are color-coded as carbon: green/yellow/pink; oxygen: red; nitrogen: blue *A*) Overlay of the *Tc*PAM active site (PDB 3NZ4; showing the cinnamate, Arg 325, and Asn458) and the *Pa*PAM active site (showing the (*S*)-β-phenylalanine/MIO adduct, Arg 323, and Phe455). *B*) Overlay of the *Sg*TAM active site (PDB 2QVE; showing the α-difluoro-β-tyrosine, Arg 311, Asn442, and His93) and *Pa*PAM active site.

A second prominent difference in the *Pa*PAM active site was the residues used to form the MIO. Generally, the catalytic MIO cofactor in aminomutases forms autocatalytically by cyclization and dehydration of the Ala-Ser-Gly triad (in *Tc*PAM, *Sg*TAM, and *Cc*TAM) (cf. Figure 3.4).[9,24,27] However, the *Pa*PAM MIO is made from a *Thr*-Ser-Gly tandem instead of the common Ala-Ser-Gly sequence (Figure 3.14).

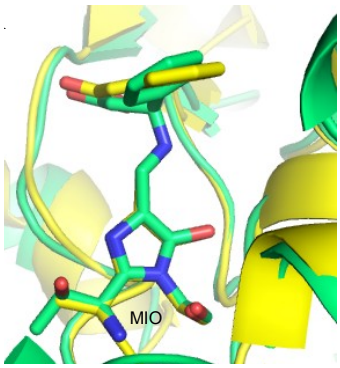

Figure 3.14. Overlay of the *Tc*PAM (yellow; showing the cinnamate and MIO) and the *Pa*PAM (green; showing the (*S*)-β-phenylalanine/MIO adduct) MIO groups. Atoms are color-coded as carbon: green/yellow; oxygen: red; nitrogen: blue.

3.3.1.2. Mutational Analysis to Assess the Role of Phe455 in the Isomerization Reaction

*Tc*PAM is a homologue of *Pa*PAM and makes the enantiomer of the (3*S*)-product made by *Pa*PAM.[50] Recent studies on these enzymes suggest that they follow a similar mechanism.[25] In both enzymes, the *pro*-(3*S*) proton and α-amino group exchange their positions intramolecularly.[25,50] *Tc*PAM, however, is proposed to rotate the cinnamate intermediate on the reaction pathway to obtain the observed product stereochemistry, while this intermediate remains stationary in the *Pa*PAM reaction.[24,25] Therefore, point mutations within the *Pa*PAM active site

were used to investigate the structural differences between these isozymes that may be responsible for the origin of their enantioselectivities.

As described before, the sterically bulkier Phe455 side chain likely orients the substrate/intermediates in *Pa*PAM active site towards a mono-dentate salt bridge interaction with active site Arg323. In contrast, Asn458 in *Tc*PAM is void of unfavorable steric interactions with the substrates/intermediates. Consequently, *Tc*PAM has more flexibility that enables the proposed bond rotation of the cinnamate intermediate.[24,25] It was hypothesized that mutating Phe455 in *Pa*PAM to a smaller side chain would allow for the rotation of the cinnamate intermediate in the active site, and thus change its enantioselectivity. Phe455 was mutated to Asn455, which is analogous to Asn458 in *Tc*PAM[24] and Ala455 with a smaller side chain. The activity and the enantioselectivity of each mutant were evaluated. At steady state, *wt-Pa*PAM converts (*S*)-α-phenylalanine to (*S*)-β-phenylalanine and *trans*-cinnamate in a 90:10 ratio.[25] By contrast, *Pa*PAM mutants Phe455Ala and Phe455Asn form (*S*)-β-phenylalanine and *trans*-cinnamate in a 40:60 ratio at approximately 2% of the rate of *wt-Pa*PAM. Therefore, in Phe455 mutants, the catalytic efficiency of the enzyme was dramatically eroded. Likely, the cinnamate intermediate aligns in an unfavorable orientation that impairs the transfer of the amino group from the MIO to the β-carbon. Consequently, compared to *wt-Pa*PAM, a higher ratio of cinnamate is produced from Phe455 mutants. These data are consistent with the hypothesis that Phe455 is important for the proper orientation of the substrate/intermediate in the *Pa*PAM active site.

The stereochemistry of the biosynthetic β-phenylalanine was not however affected as imagined. The *N*-(1(*S*)-camphanoyl) methyl esters of biosynthetic products from Phe445Ala and

Phe455Asn mutants (14.48 min and 14.49 min, respectively) eluted at retention times identical to that of authentic *N*-[(1*S*)-camphanoyl]-(3*S*)-β-phenylalanine (14.47 min) (Figure 3.15) suggesting that the enantioselectivity was unaffected.

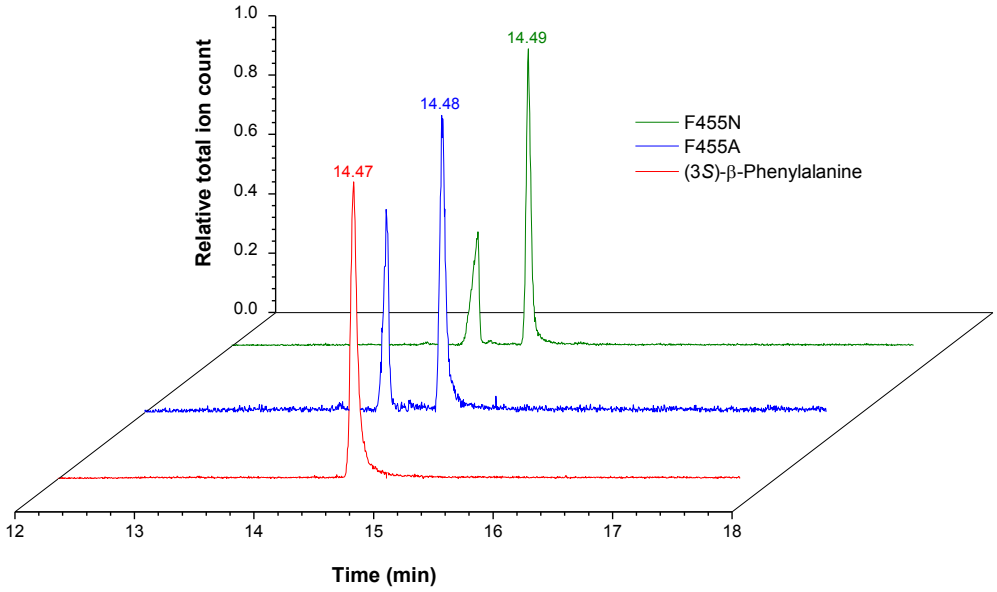

Figure 3.15. Overlay of gas chromatography profiles of *N*-[(1'*S*)-camphanoyl] methyl ester of authentic (*S*)-β-phenylalanine (14.47 min) (*red*), *N*-[(1'*S*)-camphanoyl] methyl ester of (*S*)-β-phenylalanine derived from Phe455Ala (14.48 min; *blue*), and Phe455Asn (14.49 min; *green*).The *N*-[(1'*S*)-camphanoyl] methyl ester of (*S*)-α-phenylalanine used as the substrate in assays is shown at 14.06 and 14.02 min.

These results demonstrate that the difference in stereospecificity of PAMs includes as yet unknown factors and is not exclusively based on Phe455 or Asn458 residues. Although *Pa*PAM and *Tc*PAM have an almost similar active site topology, a combination of subtle structural differences between them are likely of relevance with respect to the mechanism and stereospecificity of catalysis.

3.3.2.3. Mutational Analysis of Thr167 to Assess its Dependence on MIO Construction

Thr167 in the MIO forming motif (^{167}Thr-^{168}Ser-^{169}Gly) of *Pa*PAM is different from other aminomutases,[24,27] and therefore, the catalytic or structural role of Thr167 during *Pa*PAM catalysis was assessed. Thr167 of *Pa*PAM was systematically mutated to Ala, Cys, Ser, Val, and Gly167 to prevent significant alteration of the enzyme structure, and the activity of the resulting mutants was evaluated. The Ala167, Cys167 and Ser167 mutants were designed based on the occurrence in homologous structures.[24,26-28] As mentioned previously, in class I lyase-like family of enzymes, MIO cofactor is commonly made from an Ala-Ser-Gly sequence. By comparison, histidine ammonia lyase (HAL) from *Streptomyces griseus*[28] and *Fusbocterium sp.*[26] use <u>*Cys*</u>-Ser-Gly and <u>*Ser*</u>-Ser-Gly MIO sequences, respectively. In addition, Thr167Ser was prepared to assess the role of β-methyl of threonine, while maintaining the hydrogen bonding of the pendant hydroxyl group. Thr167Val was made to introduce an isosteric residue that lacked the hydrogen bonding capability. Thr167Gly was an exchange analogous to that of the Ala142Gly mutant of the HAL from *Pseudomonas putida*. The latter did not affect on MIO formation nor the activity.[30]

3.3.2.3.1. Expression of Mutant Genes

After sequence verification of the mutants, gene expression and Ni-NTA affinity purification of mutant enzymes were performed similar to those for *wt-Pa*PAM. While Thr167Gly, Thr167Val and Thr167Cys mutants expressed at similar levels (~50 mg/mL) to *wt-Pa*PAM, Thr167Ala and Thr167Ser mutants did not express in *E. coli*. Therefore, four other sequence verified colonies harboring Thr167Ala and Thr167Ser mutant *papam* genes were analyzed for the expression of *m-Pa*PAM. The total cell protein (TCP) fractions of uninduced

(U) and induced (I) cells were compared to assess the expression level of each *m-Pa*PAM (Figure 3.16). However, none of the Thr167Ala (Figure 3.16A) and Thr167Ser (Figure 3.16B) mutant clones produced detectable levels of protein from SDS-PAGE. In addition, there was no indication of truncated protein products, both uninduced and induced TCP fractions were similar for all the clones expressed in bacteria.

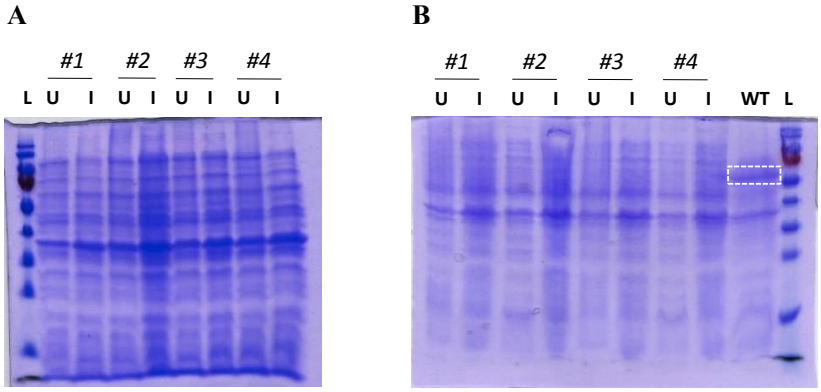

Figure 3.16. Total cell protein (TCP) fraction analysis of Thr167Ala (*A*) and Thr167Ser (*B*) mutants. SDS-PAGE gels of denatured proteins from uninduced (U) and induced (I) cells from each clone (#1 − #4) are shown. L: PageRuler™ prestained protein ladder; WT: Induced TCP fraction of *wt-Pa*PAM showing expressed *Pa*PAM (59 kDa, dashed square).

It is known that even after careful selection of the vector plasmid and host, recombinant proteins often express poorly due to various reasons such as toxicity to the host cell,[51,52] insolubility,[53,54] or codon bias.[55] The problem of protein toxicity arises when the recombinant protein performs detrimental functions in the host cell. Toxic heterologous proteins cause slow growth rates and death of host cells that ultimately affect the protein expression.[51] Nevertheless, three of the six Thr167 mutants were expressed successfully, suggesting that the recombinant *Pa*PAM proteins are not toxic to *E. coli* cells. The presence of codons in the target mRNA that are rare in *E. coli* genes is one of the most common reasons for poor heterologous protein

expression.[55,56] A high frequency of rare codons leads to amino acid misincorporation and/or truncation of the polypeptide, thus affecting the heterologous protein expression levels. However, the reading frame of the Thr167 mutants do not contain any rare codons that could stall the translation machinery in *E. coli*. In addition, analysis of TCP fractions of mutant clones indicated that the expressed proteins are not associated with the insoluble fraction, and none of the clones evaluated indicated that the protein was truncated (cf. Figure 3.16).

Properties of the expression vector can also influence the level of recombinant protein expression; For example, promoters, regulatory sequences and transcriptional terminators can affect the expression levels.[57] Three of the six mutants were expressed successfully in pET-24b(+) vector. Therefore, Thr167Ala mutant *papam* gene was sub-cloned into a fresh pET-24b(+) vector, which also gave no observable expression as assessed by TCP analysis (data not shown).

The presence of recombinant plasmid DNA and the expression of a recombinant protein generally impose a metabolic consumption of cellular energy resources.[58,59] This added metabolic burden often causes metabolic, genetic and physiological changes in the host cell. As a result, conditions such as temperature, growth medium, inducer concentration, and duration of the induction phase may affect expression levels of target proteins.[60-63] To assess the effect of duration of the induction-phase, protein production of three sequence verified clones from Thr167Ala and Thr167Ser mutants were analyzed at different times after induction of gene expression with IPTG. Similar to the aforementioned colony screening, TCP fractions of cells collected at 1, 2, 3, 5, 7 and 20 h after induction of expression of each clone with IPTG were compared with those of uninduced cells. Cells harboring *wt-Pa*PAM were used as a positive

control for this investigation. Analysis of TCP fractions containing *wt-Pa*PAM showed, as expected, that the *Pa*PAM production increased with longer induction periods (Figure 3.17A). The highest *Pa*PAM expression was observed 20 h after induction. However, there was no protein production seen either with Thr167Ser (Figure 3.17B) or Thr167Ala (Figure 3.17C) over the duration of the time course, suggesting that no mutant protein was produced or prematurely degraded. In addition, there was no effect on mutant gene expression with varying temperature. Thr167Ala and Thr167Ser mutants of *Pa*PAM were not expressed at 20 or 25 °C which are different from the original induction temperature (16 °C) for *wt-Pa*PAM.

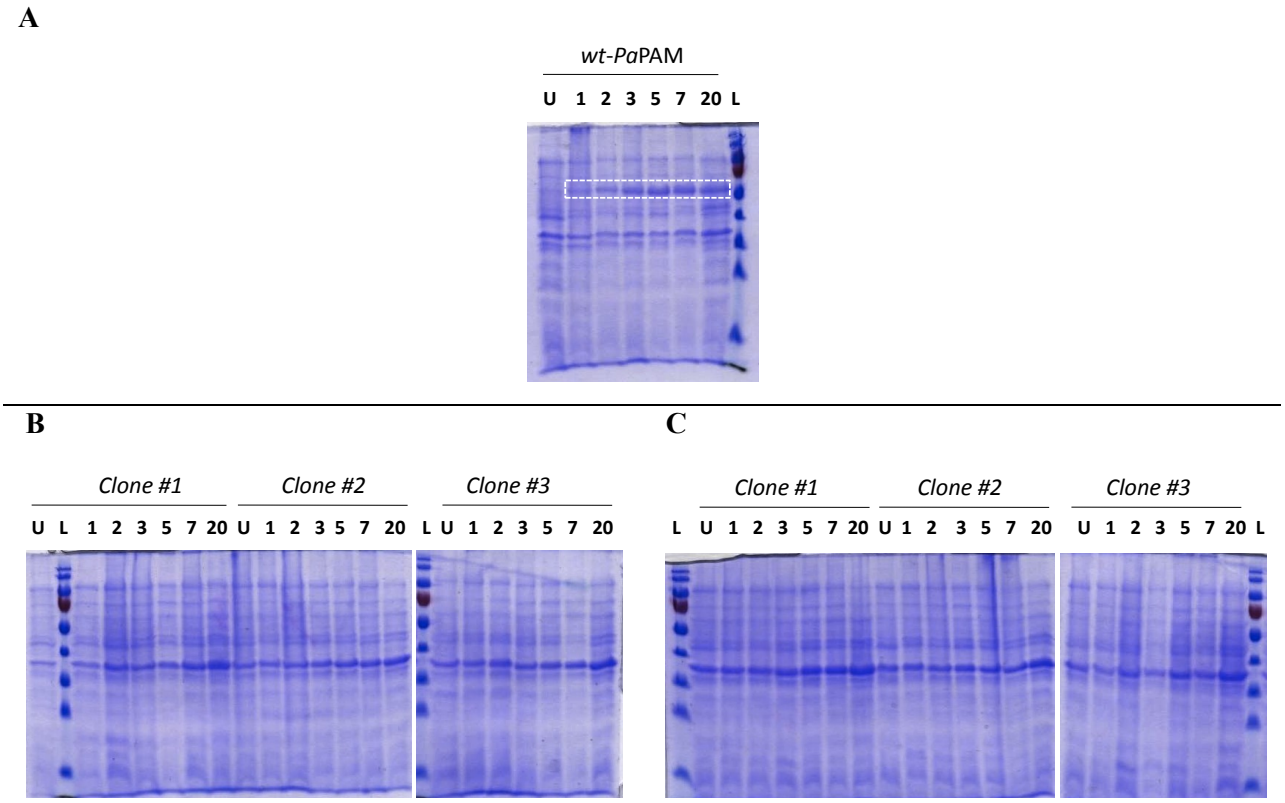

Figure 3.17. Protein production levels of *wt-Pa*PAM (*A*), Thr167Ser (*B*), and Thr167Ala (*C*) mutants. Expressed *Pa*PAM (59 kDa) of induced *wt-Pa*PAM TCP fractions are shown in a dashed square. SDS-PAGE gels of TCP fractions from uninduced (U) and induced cells from each clone (#1 − #3) at 1, 2, 3, 5, 7 and 20 h induction periods are shown for mutants. L: PageRuler™ prestained protein ladder.

3.3.2.3.2.Activity and Stability of Expressible Thr167 Mutants

The purified *Pa*PAM mutant enzymes Thr167Val, Thr167Cys, and Thr167Gly were operationally expressed in soluble form but were shown to be functionally inactive after incubating each protein separately with (*S*)-α-phenylalanine. β-Phenylalanine and *trans*-cinnamic acid were not detected. The inactivity of the three mutants was likely caused by a non-functional MIO resulting from mutation of the key Thr167 residue that participate in the formation of this prosthesis. In addition, the loss of activity could also be attributed to conformational changes in

the protein structure upon Thr167 mutation. Since single point-mutations can significantly change the stability and conformation of a protein,[64,65] circular dichroism (CD) spectroscopy[66-68] was used to assess the effect of Thr167 mutations on protein conformation and stability. Both far- (180-250 nm) and near- (260-310 nm) UV CD spectra of mutant proteins were compared with those of *wt-Pa*PAM (Figure 3.18A, B). The far-UV spectra showed a significant decrease in negative molar ellipticity at 208 and 222 nm upon replacement of Thr167 by Val and Cys (Figure 3.18A). According to the molar ellipticity, the fractional helicity of *wt-Pa*PAM, Thr167Val, and Thr167Cys were 44%, 34%, and 17%, respectively. Similarly, near-UV spectra indicated a significant change in tertiary structure of *Pa*PAM due to the Thr167 to Val and Cys mutations (Figure 3.18B). The shape and magnitude of the near-UV CD spectrum of a protein is a fingerprint of the number of aromatic amino acids and their mobility, interactions with other residues and the local environment.[67] Thus, the Thr167 to Val and Cys mutations likely altered both secondary and tertiary structural features of *Pa*PAM. However, the Thr167Gly mutation displayed a fractional helicity (41%) similar to that of *wt-Pa*PAM (44%). Furthermore, the near-UV CD spectrum for this mutant was of similar shape and magnitude as the spectrum for *wt-Pa*PAM (Figure 3.18B).

Melting temperature (T_m) curves of all three mutants were also compared with that of *wt-Pa*PAM to investigate the relative stability of the mutants (Figure 3.18C). Compared to *wt-Pa*PAM (T_m = 57 °C), both Thr167Val and Thr167Cys mutants (T_m = 35 °C) displayed a 22 °C decrease in their T_m that supported a change in their tertiary structures. The T_m change for Thr167Gly (T_m = 52 °C) was only slight (5 °C) suggesting a retention of the native tertiary conformation. Taken together, these results indicate that the Thr167Val and Thr167Cys

mutations significantly affect the secondary and tertiary conformations of *Pa*PAM, while Thr167Gly mutation had less of an effect.

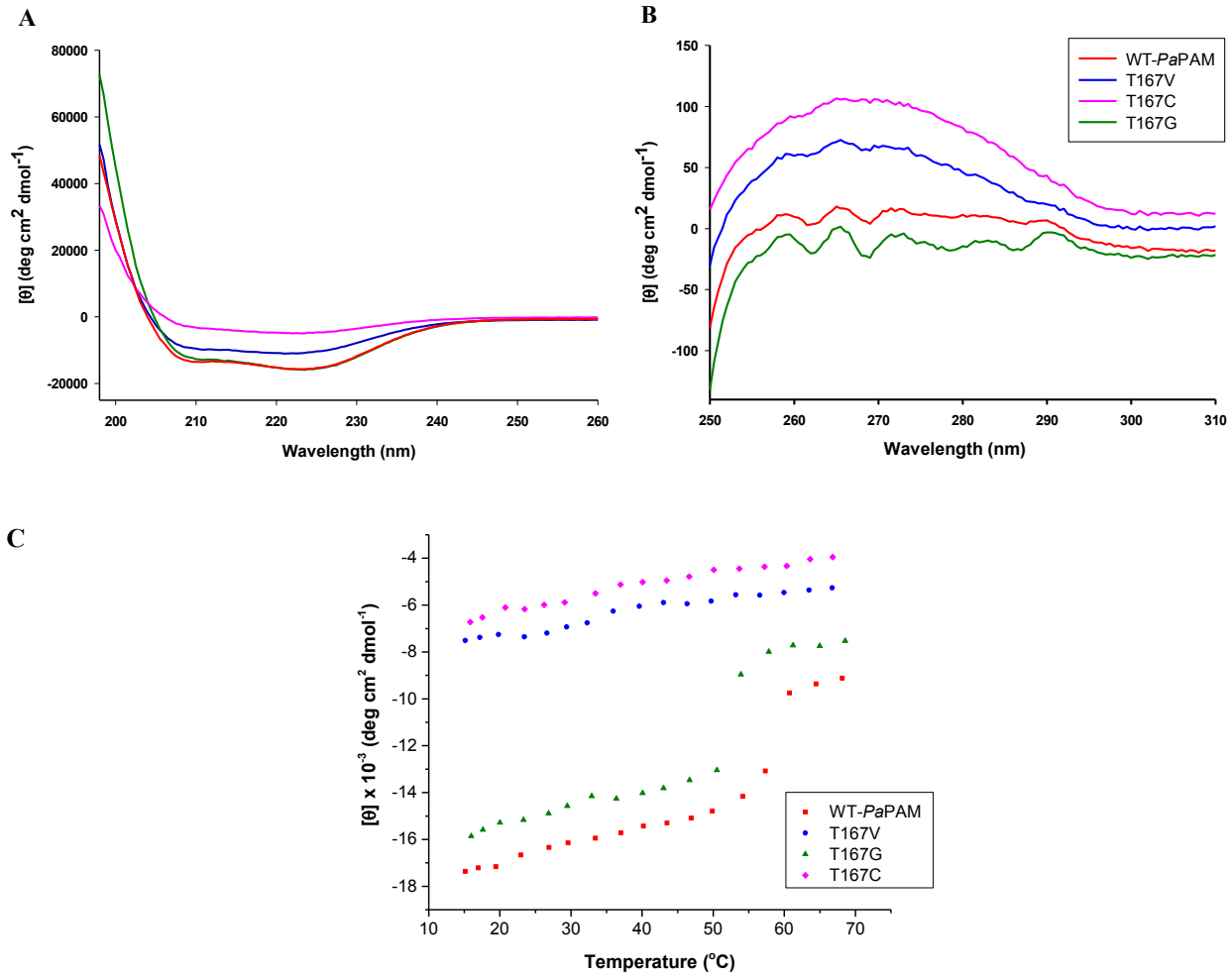

Figure 3.18. Far- (*A*) and near- (*B*) UV CD spectra of *wt-Pa*PAM and Thr167 mutants. Each spectrum represents the average of three plots, which were scanned five times in corresponding wavelength window. *C*) Thermal denaturation profiles of *wt-Pa*PAM and Thr167 mutants acquired in far UV region.

The local environment around of Thr167 was examined to identify the local interactions of its β-hydroxy and β-methyl groups. The β-hydroxy group is strongly fixed in an extended hydrogen-bonding network with Gln456, Tyr320, Leu165, Leu171, Gly172, Gly169 and active

site water molecules (Figure 3.19). The β-methyl group makes hydrophobic interactions with Val459 side chain (Figure 3.19). It was therefore hypothesized that removal of the Thr167 side chain may locally alter the binding of water molecules and disrupt the hydrogen-bonding network. In addition, the hydrophobic contacts will also be disordered. In turn, this is imagined to possibly affect the conformation and stability of the protein. Thr167Val mutation, which significantly altered the protein conformation and stability, would likely retain the hydrophobic contacts, but disrupt the hydrogen bonding network in *Pa*PAM. Although Thr167Cys mutant could still make hydrogen-bonding, interactions of the Cys167 are weaker than that of the Thr167. Sulfhydryl group of Cys167 is a moderately good hydrogen-bond donor and a very poor hydrogen-bond acceptor,[69,70] and, thus, likely alter the conformation and stability of the protein. Theoretically, Thr167Gly mutation should also disrupt the local interactions similar to aforementioned mutants. Surprisingly, according to CD spectroscopic investigations, the latter mutant did not affect the conformation and the stability of *Pa*PAM as much as Thr167Val and Thr167Cys mutations. Conceivably, binding of water molecules in the void left by Thr167Gly mutation could maintain the hydrogen-bonding network and maintain the conformational and stability of *Pa*PAM mutant.

In addition to the effects on the stability and conformation, Thr167 mutants likely affect the MIO formation. As mentioned before, Thr167 is highly involved in hydrogen-bonding in *Pa*PAM (Figure 3.19). β-Hydroxy group of Thr167 is hydrogen-bonded to Gly169 of the MIO-forming loop via a bound water molecule (HOH242; PDB: 3UNV) in the local vicinity. Thus, the β-hydroxy group of Thr167 likely fixes the MIO-forming tandem ^{167}Thr-^{168}Ser-^{169}Gly in a proper orientation for cyclization and dehydration. It was suggested for GFP,[33] *Pp*HAL[29,30] and *Tc*PAM,[31] that the MIO-forming loop needs to orient favorably for the intramolecular

rearrangement to happen. Furthermore, Gln456, which is hydrogen-bonded to Thr167, makes hydrogen bonding interactions with the ζ-hydroxy group of Tyr320 (Figure 3.19). Analogous residue Tyr322 in *Tc*PAM was suggested to position Ala175 (Thr167 in *Pa*PAM) in a proper location for the nucleophilic attack from Gly177 (cf. Figure 3.6).[31] Similarly, in *Pa*PAM, an extended hydrogen bonding interaction between the side chain of Thr167 and the hydroxyl group Tyr320 likely positions the latter residue to facilitate the development of the MIO. Presumably, mutating Thr167 affected the favorable interactions required to from the MIO in *Pa*PAM.

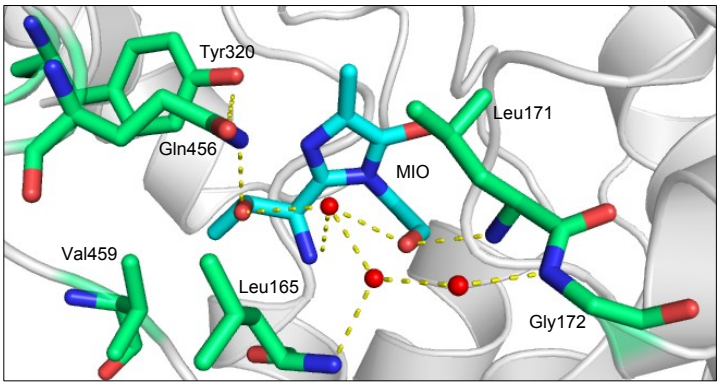

Figure 3.19. Local environment of *Pa*PAM MIO group. Extended hydrogen-bonding network of Thr167 side chain. MIO is shown in cyan. Atoms are color-coded as carbon: green/yellow; oxygen: red; nitrogen: blue

3.4. Conclusion

The structure of *Pa*PAM was solved in complex with α- and β-phenylpropanoid adducts with (S)-α- *and* (S)-β-phenylalanine bound to the active site MIO. These intermediates provide strong evidence that *Pa*PAM reacts by an alkylamine elimination pathway, which involves covalent attachment between the α-amino group of the substrate and the MIO cofactor. These results also indicate that the carbon skeleton of the (*S*)-α-phenylalanine substrate remains in one rotameric conformation, while the exocyclic C–N bond of the NH_2–MIO adduct initially positioned below the α-carbon rotates to a position below the β-carbon to complete the isomerization reaction. The *Pa*PAM structure also confirms an inversion-of-configuration mechanism to account for the inverted stereochemistry at each migration terminus.

Residue Phe455 in *Pa*PAM is required for catalysis and likely positions the substrate and cinnamate intermediate in the active site. However, Phe455 alone does not account for the stereochemical outcome, since mutation of this residue to the analogously positioned Asn in *Tc*PAM (that makes the antipode β-isomer) did not change the product stereochemistry of *Pa*PAM. Future investigations are planned to substitute residues that putatively bind the substrate and reaction intermediate in *Pa*PAM with those found at the corresponding positions in *Tc*PAM. This would potentially unravel the phenomenon that causes these similar enzymes to catalyze reactions of opposite enantioselectivity.

The construction of the MIO prosthesis in *Pa*PAM is highly dependent on the local hydrophobic and hydrogen bonding interactions, and Thr167 of *Pa*PAM likely orients MIO-forming loop in a proper orientation for the autocatalytic post translational modification.

REFERENCES

REFERENCES

(1) Walker, K. D.; Klettke, K.; Akiyama, T.; Croteau, R. *J. Biol. Chem.* **2004**, *279*, 53947-53954.

(2) Magarvey, N. A.; Fortin, P. D.; Thomas, P. M.; Kelleher, N. L.; Walsh, C. T. *ACS Chem. Biol.* **2008**, *3*, 542-554.

(3) Christenson, S. D.; Liu, W.; Toney, M. D.; Shen, B. *J. Am. Chem. Soc.* **2003**, *125*, 6062-6063.

(4) Krug, D.; Muller, R. *Chembiochem* **2009**, *10*, 741-750.

(5) Huang, S. X.; Lohman, J. R.; Huang, T.; Shen, B. *Proc. Natl. Acad. Sci. U. S. A.* **2013**, *110*, 8069-8074.

(6) Moffitt, M. C.; Louie, G. V.; Bowman, M. E.; Pence, J.; Noel, J. P.; Moore, B. S. *Biochemistry* **2007**, *46*, 1004-1012.

(7) Calabrese, J. C.; Jordan, D. B.; Boodhoo, A.; Sariaslani, S.; Vannelli, T. *Biochemistry* **2004**, *43*, 11403-11416.

(8) Louie, G. V.; Bowman, M. E.; Moffitt, M. C.; Baiga, T. J.; Moore, B. S.; Noel, J. P. *Chem. Biol.* **2006**, *13*, 1327-1338.

(9) Schwede, T. F.; Retey, J.; Schulz, G. E. *Biochemistry* **1999**, *38*, 5355-5361.

(10) Langer, M.; Pauling, A.; Rétey, J. *Angew. Chem. Int. Ed.* **1995**, *34*, 1464–1465.

(11) Schuster, B.; Retey, J. *Proc. Natl. Acad. Sci. U. S. A.* **1995**, *92*, 8433-8437.

(12) Smith, T. A.; Cordelle, F. H.; Abeles, R. H. *Arch. Biochem. Biophys.* **1967**, *120*, 724–725.

(13) Givot, I. L.; Smith, T. A.; Abeles, R. H. *J. Biol. Chem.* **1969**, *244*, 6341-6353.

(14) Rechler, M. M. *J. Biol. Chem.* **1969**, *244*, 551-559.

(15) Havir, E. A.; Hanson, K. R. *Biochemistry* **1968**, *7*, 1904-1914.

(16) Wickner, R. B. *J. Biol. Chem.* **1969**, *244*, 6550-6552.

(17) Hodgins, D. S. *J. Biol. Chem.* **1971**, *246*, 2977-2985.

(18) Hanson, K. R.; Havir, E. A. *Arch. Biochem. Biophys.* **1970**, *141*, 1-17.

(19) Langer, M.; Reck, G.; Reed, J.; Retey, J. *Biochemistry* **1994**, *33*, 6462-6467.

(20) Schuster, B.; Retey, J. *FEBS Lett.* **1994**, *349*, 252-254.

(21) Langer, M.; Lieber, A.; Retey, J. *Biochemistry* **1994**, *33*, 14034-14038.

(22) Cody, C. W.; Prasher, D. C.; Westler, W. M.; Prendergast, F. G.; Ward, W. W. *Biochemistry* **1993**, *32*, 1212-1218.

(23) Barondeau, D. P.; Kassmann, C. J.; Tainer, J. A.; Getzoff, E. D. *J. Am. Chem. Soc.* **2006**, *128*, 4685-4693.

(24) Feng, L.; Wanninayake, U.; Strom, S.; Geiger, J.; Walker, K. D. *Biochemistry* **2011**, *50*, 2919-2930.

(25) Ratnayake, N. D.; Wanninayake, U.; Geiger, J. H.; Walker, K. D. *J. Am. Chem. Soc.* **2011**, *133*, 8531-8533.

(26) Kapatral, V.; Anderson, I.; Ivanova, N.; Reznik, G.; Los, T.; Lykidis, A.; Bhattacharyya, A.; Bartman, A.; Gardner, W.; Grechkin, G.; Zhu, L. H.; Vasieva, O.; Chu, L.; Kogan, Y.; Chaga, O.; Goltsman, E.; Bernal, A.; Larsen, N.; D'Souza, M.; Walunas, T.; Pusch, G.; Haselkorn, R.; Fonstein, M.; Kyrpides, N.; Overbeek, R. *J. Bacteriol.* **2002**, *184*, 2005-2018.

(27) Christianson, C. V.; Montavon, T. J.; Van Lanen, S. G.; Shen, B.; Bruner, S. D. *Biochemistry* **2007**, *46*, 7205-7214.

(28) Wu, P. C.; Kroening, T. A.; White, P. J.; Kendrick, K. E. *Gene* **1992**, *115*, 19-25.

(29) Baedeker, M.; Schulz, G. E. *Structure* **2002**, *10*, 61-67.

(30) Baedeker, M.; Schulz, G. E. *Eur. J. Biochem.* **2002**, *269*, 1790-1797.

(31) Wybenga, G. G.; Szymanski, W.; Wu, B.; Feringa, B. L.; Janssen, D. B.; Dijkstra, B. W. *Biochemistry* **2014**, *53*, 3187-3198.

(32) Wu, B.; Szymanski, W.; Wybenga, G. G.; Heberling, M. M.; Bartsch, S.; de Wildeman, S.; Poelarends, G. J.; Feringa, B. L.; Dijkstra, B. W.; Janssen, D. B. *Angewandte Chemie-International Edition* **2012**, *51*, 482-486.

(33) Barondeau, D. P.; Putnam, C. D.; Kassmann, C. J.; Tainer, J. A.; Getzoff, E. D. *Proc. Natl. Acad. Sci. U. S. A.* **2003**, *100*, 12111-12116.

(34) Sniegowski, J. A.; Lappe, J. W.; Patel, H. N.; Huffman, H. A.; Wachter, R. M. *J. Biol. Chem.* **2005**, *280*, 26248-26255.

(35) Hermes, J. D.; Weiss, P. M.; Cleland, W. W. *Biochemistry* **1985**, *24*, 2959-2967.

(36) Bordwell, F. G.; Zhao, Y. Y. *J. Org. Chem.* **1995**, *60*, 6348-6352.

(37) Hess, B. A.; Schaad, L. J. *J. Am. Chem. Soc.* **1983**, *105*, 7500-7505.

(38) Gloge, A.; Zon, J.; Kovari, A.; Poppe, L.; Retey, J. *Chem-Eur. J.* **2000**, *6*, 3386-3390.

(39) Louie, G. V.; Bowman, M. E.; Moffitt, M. C.; Baiga, T. J.; Moore, B. S.; Noel, J. P. *Chem. Biol.* **2006**, *13*, 1327-1338.

(40) Cooke, H. A.; Bruner, S. D. *Biopolymers* **2010**, *93*, 802-810.

(41) Christianson, C. V.; Montavon, T. J.; Festin, G. M.; Cooke, H. A.; Shen, B.; Bruner, S. D. *J. Am. Chem. Soc.* **2007**, *129*, 15744-15745.

(42) Montavon, T. J.; Christianson, C. V.; Festin, G. M.; Shen, B.; Bruner, S. D. *Bioorg. Med. Chem. Lett.* **2008**, *18*, 3099-3102.

(43) Greenfield, N. J.; Fasman, G. D. *Biopolymers* **1969**, *7*, 595-610.

(44) Ritter, H.; Schulz, G. E. *Plant Cell* **2004**, *16*, 3426-3436.

(45) Strom, S.; Wanninayake, U.; Ratnayake, N. D.; Walker, K. D.; Geiger, J. H. *Angew. Chem. Int. Ed.* **2012**, *51*, 2898-2902.

(46) Szymanski, W.; Wu, B.; Weiner, B.; de Wildeman, S.; Feringa, B. L.; Janssen, D. B. *J. Org. Chem.* **2009**, *74*, 9152-9157.

(47) Wu, B.; Szymanski, W.; Wietzes, P.; de Wildeman, S.; Poelarends, G. J.; Feringa, B. L.; Janssen, D. B. *ChemBioChem* **2009**, *10*, 338-344.

(48) Dunkley, K. D.; Callaway, T. R.; Chalova, V. I.; Anderson, R. C.; Kundinger, M. M.; Dunkley, C. S.; Nisbet, D. J.; Ricke, S. C. *Anaerobe* **2008**, *14*, 35-42.

(49) Bartsch, S.; Bornscheuer, U. T. *Angew. Chem. Int. Ed.* **2009**, *48*, 3362-3365.

(50) Mutatu, W.; Klettke, K. L.; Foster, C.; Walker, K. D. *Biochemistry* **2007**, *46*, 9785-9794.

(51) Dong, H. J.; Nilsson, L.; Kurland, C. G. *J. Bacteriol.* **1995**, *177*, 1497-1504.

(52) Doherty, A. J.; Connolly, B. A.; Worrall, A. F. *Gene* **1993**, *136*, 337-340.

(53) Hartley, D. L.; Kane, J. F. *Biochem. Soc. Trans.* **1988**, *16*, 101-102.

(54) Carrio, M. M.; Villaverde, A. *J. Biotechnol.* **2002**, *96*, 3-12.

(55) Robinson, M.; Lilley, R.; Little, S.; Emtage, J. S.; Yarranton, G.; Stephens, P.; Millican, A.; Eaton, M.; Humphreys, G. *Nucleic Acids Res.* **1984**, *12*, 6663-6671.

(56) Gustafsson, C.; Govindarajan, S.; Minshull, J. *Trends Biotechnol.* **2004**, *22*, 346-353.

(57) Francis, D. M.; Page, R. *Curr. Prot. Protein Sci.* **2010**, *Chapter 5*, 1-29.

(58) Glick, B. R. *Biotechnol. Adv.* **1995**, *13*, 247-261.

(59) Bentley, W. E.; Mirjalili, N.; Andersen, D. C.; Davis, R. H.; Kompala, D. S. *Biotechnol. Bioeng.* **1990**, *35*, 668-681.

(60) Wood, T. K.; Peretti, S. W. *Biotechnol. Bioeng.* **1991**, *38*, 397-412.

(61) Chalmers, J. J.; Kim, E.; Telford, J. N.; Wong, E. Y.; Tacon, W. C.; Shuler, M. L.; Wilson, D. B. *Appl. Environ. Microbiol.* **1990**, *56*, 104-111.

(62) Whitney, G. K.; Glick, B. R.; Robinson, C. W. *Biotechnol. Bioeng.* **1989**, *33*, 991-998.

(63) Neubauer, P.; Hofmann, K.; Holst, O.; Mattiasson, B.; Kruschke, P. *Appl. Microbiol. Biotechnol.* **1992**, *36*, 739-744.

(64) Cheng, J.; Randall, A.; Baldi, P. *Proteins* **2006**, *62*, 1125-1132.

(65) Parthiban, V.; Gromiha, M. M.; Schomburg, D. *Nucleic Acids Res.* **2006**, *34*, 239-242.

(66) Greenfield, N. J. *Nat. Protoc.* **2006**, *1*, 2876-2890.

(67) Kelly, S. M.; Price, N. C. *Curr. Protein Pept. Sc.* **2000**, *1*, 349-384.

(68) Greenfield, N. J. *Nat. Protoc.* **2006**, *1*, 2527-2535.

(69) Pal, D.; Chakrabarti, P. *J. Biomol. Struct. Dyn.* **1998**, *15*, 1059-1072.

(70) Gregoret, L. M.; Rader, S. D.; Fletterick, R. J.; Cohen, F. E. *Proteins* **1991**, *9*, 99-107.

CHAPTER 4: Substrate Scope of *Pa*PAM and Effect of Ring Substituents on the Isomerization Mechanism

The computational modeling investigations related to this study were carried out in collaboration with Prof. Leslie Kuhn and Ms. Nan Liu from the Departments of Biochemistry and Molecular Biology, and Computer Science and Engineering at Michigan State University.

4.1. Introduction

4.1.1. Biocatalytic Production of Novel β-Aryl-β-Amino Acids

β-Amino acids, including β-aryl-β-amino acids are widely used in numerous applications.[1,2] Novel thiazolone compounds containing *p*-fluoro, *p*-bromo, *p*-methyl, and *o*,*p*-dichloro-β-phenylalanine as key components were recently developed as highly potent hepatitis C virus (HCV) NS5B polymerase inhibitors (Figure 4.1A).[3] Inhibition of NS5B controls the replication of HCV and, thus represents a valid target for antiviral therapy. Additionally, *o*-methyl-(*S*)-β-phenylalanine derivative **2** was identified as a potent inhibitor for Cathepsin A (Figure 4.1B), which is a serine carboxypeptidase with potential beneficial applications in cardiovascular diseases.[4]

Strategic placement of fluorines in drug molecules is known to enhance pharmacodynamic and pharmacokinetic properties because of the strong electronegativity, small size, lipophilicity, and electrostatic interactions of the fluorine. The adventitious effects dramatically influence the chemical reactivity of pharmaceuticals.[5] In addition, metabolic stability of drug candidates can be increased by replacing aromatic hydrogens with fluorine.[6] *m*-

Fluoro-β-phenylalanine containing dipeptidyl boronic acid **3** (Figure 4.1C) inhibits the 20S human proteasome at <2 nM level and showed comparable activity to the commercial counterpart bortezomib.[7] *m*-Fluoro-β-phenylalanine has also been used as an intermediate in the synthesis of potent chemokine receptor CCR5 antagonist.[8]

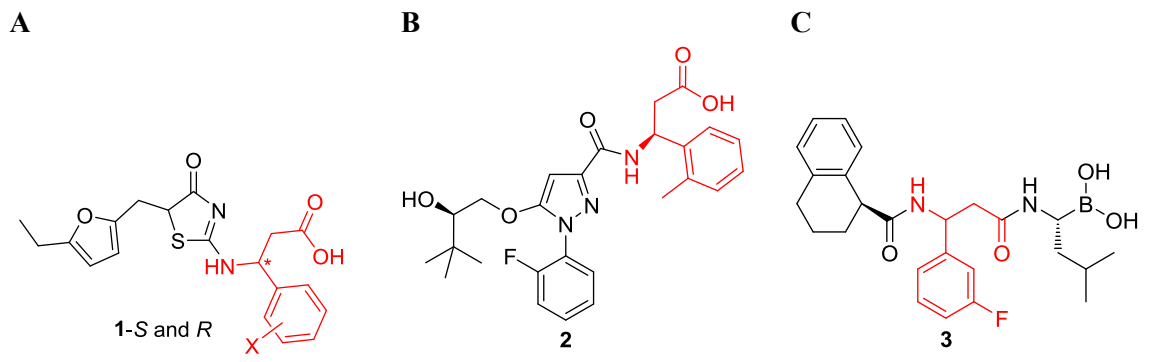

Figure 4.1. β-Aryl-β-amino acids as key components of pharmaceutically important molecules.

Class I lyase-like family aminomutases produce β-aryl-β-amino acids by isomerizing readily available natural and non-natural α-amino acids.[9-11] Phenylalanine aminomutases from *Pantoea agglomerans* (*Pa*PAM) and *Taxus sp.* (*Tc*PAM) isomerize (*S*)-α-phenylalanine to (*S*)- and (*R*)-β- phenylalanine, respectively.[9,11] *Tc*PAM was shown convert various aryl-substituted and heteroaromatic α-alanines to corresponding β-amino acids.[10] However, tyrosine aminomutases *Sg*TAM (from *Streptomyces globisporus*)[12] and CmdF (from *Chondromyces crocatus*)[13] that isomerize (*S*)-α- to β-tyrosine has a limited substrate scope. Substrate specificity of *Sg*TAM has been limited only to *m*-chloro- and *m*-hydroxytyrosine in addition to its natural substrate (*S*)-α-tyrosine.[14] A recently discovered aminomutase on the biosynthetic pathway to the enediyne kedarcidin increased the scope of aminomutases and now includes a catalyst for making of (*R*)-2-aza-β-tyrosine from 2-aza-α-tyrosine.[15]

4.1.2. MIO-dependent Isomerization Mechanism of *Pa*PAM

Aminomutases of the class I lyase-like family require the 4-methylidene-1*H*-imidazol-5(4*H*)-one (MIO) cofactor to carry out the chemically challenging exchange of NH_2/H pair.[16] The role of MIO cofactor has been long-debated and the highly electrophilic MIO was postulated to react either with the aromatic ring or the amino group of the substrate.[17] However, recent structural characterization of *Pa*PAM supports the formation of an NH_2-MIO adduct, where the amino group of the substrate is covalently attached to the enzyme during the α/β-isomerization (Figure 4.2).[18] The *pro*-(3*S*) proton and the NH_2-MIO group are eliminated from the substrate to form a cinnamate intermediate (released occasionally as a minor by-product), followed by the hydroamination of the intermediate from NH_2-MIO to form the β-amino acid (Figure 4.2).

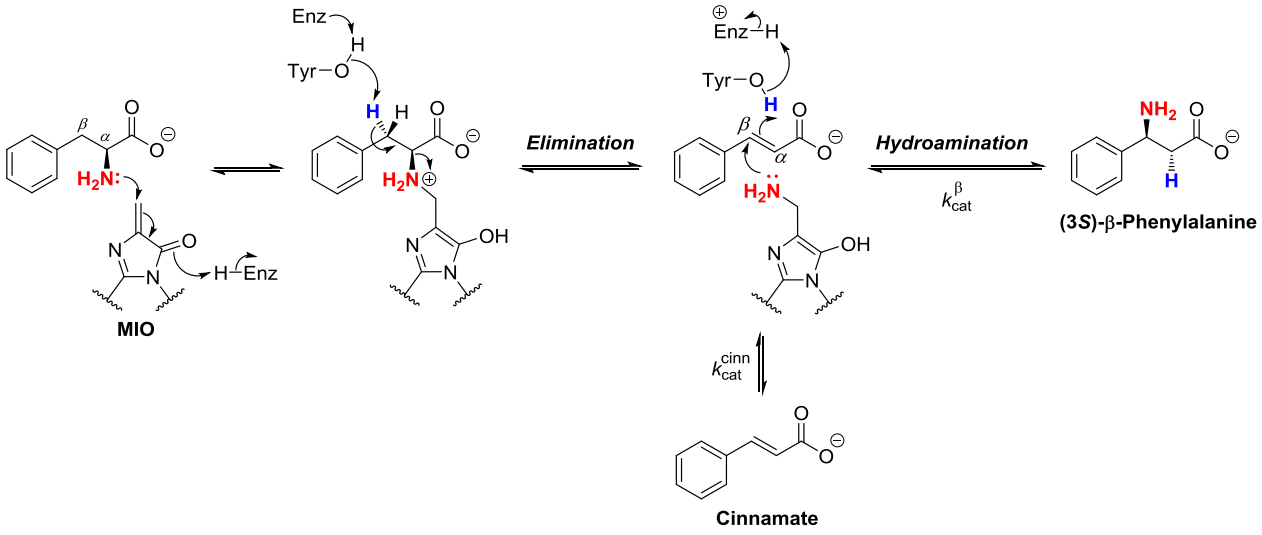

Figure 4.2. Mechanism of the MIO-dependent isomerization catalyzed by *Pa*PAM. $k_{\mathrm{cat}}^{\mathrm{cinn}}$: the rate at which the cinnamate by-product is released; k_{cat}^{β}: the rate at which the β-amino acid product is released.

4.1.2.1. Elimination of NH_2/H from α-Arylalanine Substrate

Phenylalanine aminomutases are mechanistically and structurally closely related to MIO-dependent ammonia lyases, which include tyrosine,[19] phenylalanine,[20,21] and histidine[16] ammonia lyases (TAL, PAL and HAL, respectively). Ammonia lyases catalyze the ammonia elimination from L-arylalanines (L-tyrosne, L-phenylalanine, and L-histidine) to produce corresponding (*E*)-aryl acrylates (coumaric acid from TAL, cinnamic acid from PAL and urocanic acid from HAL). Similar to the reactions catalyzed by homologous ammonia lyases, the *Pa*PAM reaction produces a cinnamate intermediate after elimination of the amino group and *pro*-(3*S*) benzylic hydrogen from the α-amino acid substrate.[22]

The nucleophilic addition of the α-amine group of the substrate to the MIO is proposed to make a good alkyl ammonium leaving group.[23] Thereafter, α,β-elimination of the *pro*-(3*S*) β-hydrogen and α-alkyl ammonium can occur via a stepwise or concerted processes. The concerted, one-step E2 (bimolecular elimination) mechanism leads to the cinnamate intermediate without involving high-energy charged intermediates. In the two-step E1cB (unimolecular conjugate-base elimination) mechanism, abstraction of the *pro*-(3*S*) proton leads to a benzylic carbanion intermediate, whereas for the E1 (unimolecular elimination) mechanism, cleavage of the C_α-N bond results a C_α-carbocation (Figure 4.3). However, the two-step E1 (unimolecular elimination) reaction is not likely for MIO-dependent reactions. The attached electron-withdrawing carboxylate of the substrate would destabilize the C_α-carbocation formed after displacement of the NH_2-MIO adduct (Figure 4.3).

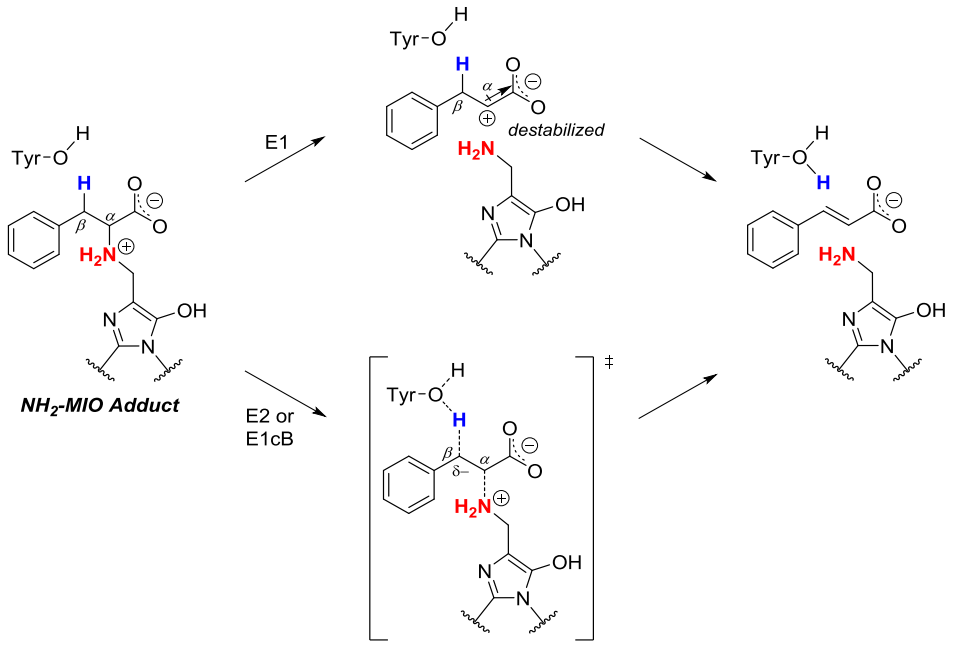

Figure 4.3. Proposed elimination mechanisms for displacement of the NH_2-MIO adduct. E1: unimolecular, E2: bimolecular and E1cB: conjugate-base eliminations

MIO-dependent aminomutase reactions likely follow an E2 or E1cB mechanism, which require the abstraction of the non-acidic (p*K*a = 40)[24] β-proton by an enzymatic base. The p*K*a of the C_β methylene protons would need to drop ~30 pH units to match the p*K*a of an unactivated general base such as a tyrosine residue. The E1cB mechanism has also been accepted for decades for ammonia lyases.[23] However, there are no experimental results that explain how the non-acidic benzylic proton is extracted by an enzymatic base. Molecular modeling studies in combination with structural analysis of PAL from *Rhodosporidium toruloides* (*Rt*PAL) suggested that the influence of α-helix dipole moments favor the development of a carbanion intermediate and assist the abstraction of the β-protons.[25] Most of the active site residues of *Rt*PAL are associated with α-helices and the positive poles of six of the seven α-helices of the PAL structure are directed toward the active site.[25] Therefore, the helix dipoles of the PAL active

site were proposed to likely support the formation of carbanion intermediate produced in the E1cB mechanism. In addition, electron-withdrawing active site residues that interact with the phenyl ring of the substrate were suggested to direct electron density away from the phenyl ring and thus lower the p*K*a of the β-protons.[25] MIO cofactor also resides atop the positive poles of three helices, and therefore, its electrophilicity was also suggested to increase.

Earlier deuterium isotope studies ($k_H/k_D > 2$) on *Tc*PAM suggested that the deprotonation step of the elimination reaction is rate-determining.[26] Electron-withdrawing substituents on the aryl ring of the substrate that stabilize a δ^- charge on C_β should therefore increase the rate of the elimination step. Klee and coworkers reported that in a HAL from *Pseudomonas sp.*, 4-nitro histidine with a K_M similar to that of the natural substrate deaminates eight times faster than the natural substrate L-histidine.[27] Furthermore, no deuterium isotope effect was found for the β-dideuterated 4-nitro histidine; the β-proton abstraction is no longer the rate determining step. It was suggested that the nitro group decreased the electron density of the imadazole ring and therefore increased the acidity of β-hydrogens. By contrast, the β-dideuterated histidine showed a kinetic isotope effect of 1.5-2.0 with HAL.[28] In other ammonia lyase studies, *para*-nitro phenylalanine was found to react faster than the un-substituted substrate with PAL from *Petroselinum crispum* (*Pc*PAL).[29] The *wt-Pc*PAL was inactivated with $NaBH_4$ and, *Pc*PAL mutant (Ser202Ala that ablated MIO formation) were reported to react 70-fold faster with *para*-nitro phenylalanine than the natural (2*S*)-α-phenylalanine substrate.[29] The highly electron withdrawing nitro group was posited to increase the acidity of the β-hydrogens and make the electrophilic MIO cofactor unnecessary for the elimination reaction.

A recent molecular mechanics calculations on TAL suggested that the ligand alignment in the active site caused a strain in C_α–N and C_β–*pro*-(3*S*)–H bonds and therefore an E2

elimination is favored over other mechanisms.[30] According to this study, both E1 and E1cB intermediates or transition states were not feasible in the TAL deamination reaction.

4.1.2.2. Hydroamination of the Cinnamate Intermediate

The final reaction sequence of the MIO-dependent aminomutases involves an α,β-addition reaction, where the NH_2-MIO and a proton (H^+) add across the double bond of the acrylate intermediate. To obtain the β-amino acid from the hydroamination, the polarity of the C_β (δ^+) needs to be opposite of that in the earlier elimination sequence. Here, the nucleophilic NH_2-MIO binds to C_β and the electrophilic H^+ attaches to C_α (Figure 4.4).

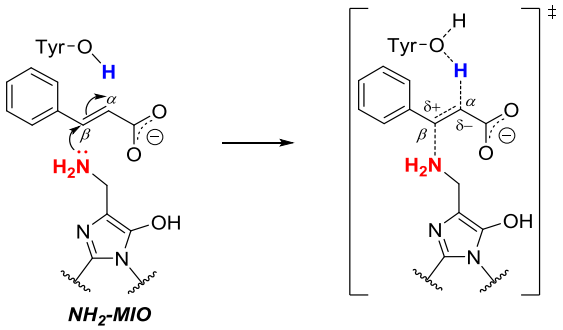

Figure 4.4. Hydroamination of the acrylate intermediate. Shown is a transition state intermediate highlighting the polarization of the π-bond in which the nucleophilic NH_2-MIO and the electrophilic H^+ approach C_β and C_α, respectively.

Similar to the ammonia elimination, hydroamination reaction of *Pa*PAM can follow either concerted or stepwise addition mechanisms (Figure 4.5). In the concerted mechanism, the NH_2-MIO and the *pro*-(3*S*) proton abstracted from the catalytic base add simultaneously onto the β- and α-carbons, respectively (Figure 4.5, path a). Alternatively, *Pa*PAM could use a stepwise addition sequence where the nucleophile (NH_2−MIO) or the electrophile (TyrO···H) first add at

the respective carbons of the arylacrylate double bond. In the nucleophilic addition mechanism, NH_2–MIO couples to form a 1,4-Michael adduct (Figure 4.5, path b). However, a presumed resonance structure has two repelling oxyanions on the carboxylate of the reactant that normally forms a monodentate salt bridge (Figure 4.5, path b), as evidenced in the *Pa*PAM crystal structure.[18] This conjugate addition route benefits from an electropositive (δ^+) C_β by delocalizing the π-electrons towards the carboxylate of the substrate. Theoretically, a substituent that places negative charge inductively within the ring or mesomerically on C_{ipso} of the β-arylacrylate intermediate should also strengthen the formation of a δ^+ on C_β.

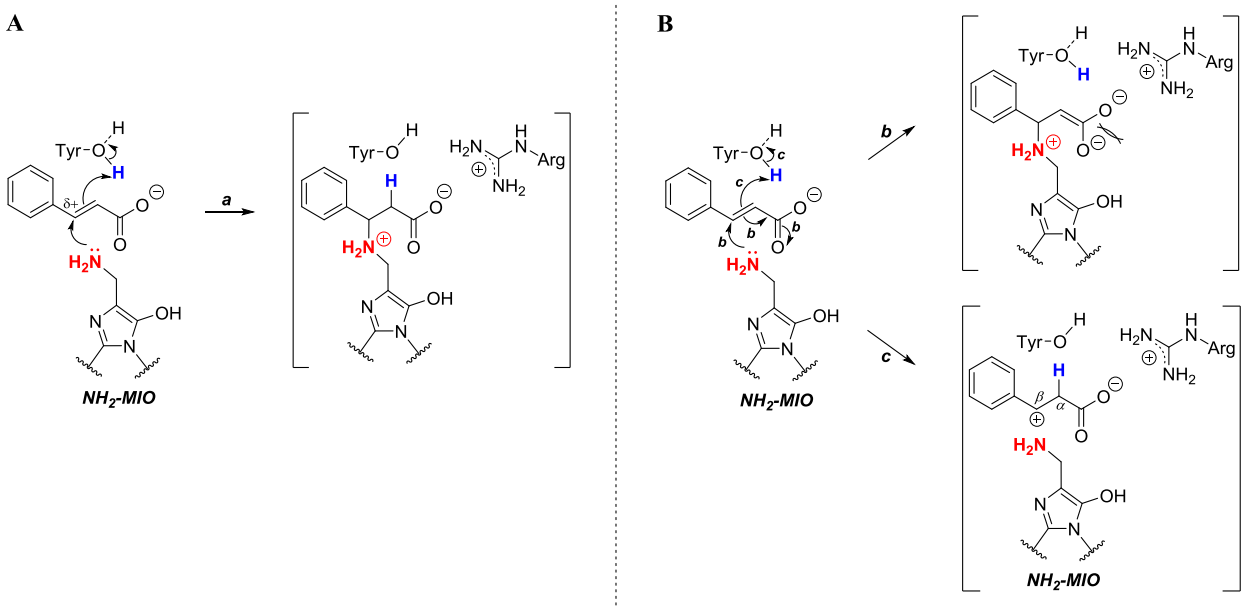

Figure 4.5. Concerted (*A*) and stepwise (*B*) hydroamination mechanisms of *Pa*PAM. *Route a*) Concerted hydroamination of the acrylate π-bond. Shown is an intermediate with maximal charge separation between repelling negative charges in the carboxylate group and the cation and anion. *Route b*) A stepwise Michael-addition pathway. Shown is an intermediate adduct with the π-electrons delocalized into the carboxylate group forming a repelling dianion prior to C_α-protonation. *Route c*) A stepwise hydroamination sequence. Shown is a proposed intermediate resulting from C_α-protonation as the first step, which places a positive charge at C_β, and C_β is now primed for nucleophilic attack by the NH_2-MIO adduct.

An electrophilic addition pathway is envisioned to first add the *pro*-(3*S*) proton at C_α of the acrylate intermediate (cf. Figure 4.5, path c). The resulting intermediate has a positive charge (δ^+) on the benzylic C_β, which is resonance stabilized by the aryl ring and further stabilized by electron-releasing substituents (cf. Figure 4.5, path c). Rapid, nucleophilic attack by the NH_2-MIO on the carbocation would ensue to complete the β-amino acid catalysis.

The second half of the aminomutase reaction has been employed to synthesize α- and β-amino acids from arylacrylates.[31,32] Phenylalanine aminomutase from *Taxus chinensis* (*Tch*PAM) catalyzes the highly enantioselective amination of variously substituted cinnamic acids from NH_4OH.[31] It has been reported that the regioselectivity of ammonia addition on the acrylate double bond is dependent on the substituents on the phenyl ring.[32] Electron rich aromatic rings with the electron donating substituents showed higher β-selectivity due to the lowered ability of the aromatic ring to accept electrons.[32] The carboxylate group is suggested to act as the electron sink in this reaction, whereas, electron deficient aromatic rings favor the α-addition and accepts electron delocalization into the aromatic ring.[32]

While this study above provided information about the partitioning of cinnamate to α- and β-phenylalanine it did not assess the substituent effects on the forward reaction of PAMs. The current study evaluated the substituent effects on α- to β-phenylalanine conversion by *Pa*PAM that involves both elimination and hydroamination steps.

4.2. Experimental

4.2.1. Substrates, Authentic Standards and Reagents

(*S*)-α-, *p*-Methoxy-(*S*)-α-, *p*-nitro-(*S*)-α-, and *p*-chloro-(*R*/*S*)-β-phenylalanine and (*E*)-*o*-methyl-, (*E*)-*p*-methyl-, (*E*)-*p*-methoxy- and (*E*)-*p*-nitro-cinnamic acid, (*E*)-*o*-furyl-acrylate and (trimethylsilyl)diazomethane (2.0 M in diethyl ether) were purchased from Sigma-Aldrich-Fluka (St. Louis, MO). Racemic *p*-nitro-β-phenylalanine was purchased from Oakwood Products, Inc. (West Columbia, SC), and *o*-methoxy-(*S*)-α-, *m*-methoxy-(*S*)-α-, *o*-nitro-(*S*)-α-, *m*-nitro-(*S*)-α-, *o*-methoxy-(*S*)-β-, *m*-methoxy-(*S*)-β-, *o*-nitro-(*S*)-β-, and *m*-nitro-(*S*)-β-phenylalanine were purchased from Chem-Impex International, Inc. (Wood Dale, IL). 2-Amino-5-phenylpentanoic acid was purchased from Acros Organics (New Jersey). All other (*S*)-α- and β-amino acids were purchased from PepTech Corporation (Burlington, MA) and the other (*E*)-cinnamic acids were purchased from Alfa Aesar (Ward, Hill, MA). All chemicals were used without further purification, unless noted.

4.2.2. General Instrumentation

GC-MS analysis was performed with an Agilent 6890N gas chromatograph equipped with a capillary GC column (30 m × 0.25 mm × 0.25 μM; HP-5MS; J&W Scientific) with helium as the carrier gas (flow rate, 1 mL/min). The injector port (at 250 °C) was set to splitless injection mode. A 1-μL aliquot of each sample was injected using an Agilent 7683 auto-sampler (Agilent,

Atlanta; GA). The column temperature was increased from 50 – 110 °C at 30 °C/min, then increased by 10 °C/min to 250 °C (total run time of 16 min), and returned to 50 °C over 5 min, with a 5 min hold. The gas chromatograph was coupled to a mass selective detector (Agilent, 5973 *inert*) operated in electron impact mode (70 eV ionization voltage). All spectra were recorded in the mass range of 50 – 400 *m*/*z*.

4.2.3. Expression and Purification of *Pa*PAM

Luria-Bertani medium (1 L) supplemented with kanamycin (50 µg/mL) was inoculated with 5 mL of an overnight culture of *E. coli* BL21(DE3) cells engineered to express the *papam* cDNA from the pET-24b(+) vector as a C-terminal His_6-tagged *Pa*PAM. These cultures were grown at 37 °C to an optical density of A_{600} ~ 0.6. *Pa*PAM expression was induced with isopropyl-β-D-thiogalactopyranoside (100 µM) at 16 °C and the cultures were grown for 16 h. The subsequent steps were performed at 4 °C, unless indicated otherwise. Cells were harvested by centrifugation at 6,000*g* (15 min) and the cell pellet was resuspended in lysis buffer (50 mM sodium phosphate buffer containing 5% (v/v) glycerol, 300 mM NaCl and 10 mM imidazole, pH 8.0). The cells were lysed by sonication (Misonix sonicator, Farmingdale, NY), and the lysate was centrifuged at 9,700*g* (45 min) and then at 102,000*g* (1 h) to remove cell debris and light membranes. The resultant crude, C-terminal His_6-tagged aminomutase in the soluble fraction was purified by Nickel-nitrilotriacetic acid (Ni-NTA) affinity chromatography according to the protocol described by the manufacturer (Qiagen, Valencia, CA). *Pa*PAM fractions, eluting in 250 mM imidazole, were concentrated by size-selective centrifugal filtration (Centriprep centrifugal filter units, 30,000 MWCO; Millipore), the buffer was exchanged with 50 mM sodium phosphate

buffer containing 5% (v/v) glycerol (pH 8.0). The purity of the concentrated enzyme was assessed by SDS−PAGE with Coomassie Blue staining, and the quantity was determined by the Bradford protein assay. The overexpressed *Pa*PAM (~59 kDa) was obtained at 95% purity (~25 mg/L).

4.2.4. Assessing the Substrate Specificity of *Pa*PAM for (2*S*)-α-Phenylalanine Analogues

(*S*)-α-Phenylalanine and each of its analogues (1 mM) were incubated for 2 h with *Pa*PAM (50 μg) in 1-mL assays of 50 mM phosphate buffer (pH 8.0) containing 5% glycerol. Control assays contained all ingredients except either the substrate or enzyme was omitted. Each reaction was quenched by acidifying to pH 2-3 (6 M HCl). Three internal standards (*m*-fluoro-β-phenylalanine, *p*-methyl-β-phenylalanine and β-phenylalanine at 20 μM) were used, respectively, to quantify three sets of biosynthetic β-amino acids products–Set 1: β-phenylalanine; *o*-, *m*-, and *p*-methyl-; *o*-, *m*-, and *p*-methoxy-; *m*- and *p*-nitro-; *m*- and *p*-chloro-β-phenylalanine; and (2-furyl)-β-alanine; Set 2: *o*- and *p*-fluoro; *m*-, and *p*-bromo-β-phenylalanine; and (2-thienyl)- and (3-thienyl)-β-alanine; and Set 3: *m*-fluoro-β-phenylalanine. Two internal standards (*p*-methylcinnamic acid and cinnamic acid at 20 μM) were used, respectively, to quantify two sets of biosynthetic aryl acrylic acid products: Set 1, cinnamic acid, *o*-, *m*-, and *p*-fluorocinnamic acid, and (2-thienyl)- and (3-thienyl)-acrylic acid; Set 2, *o*-, *m*-, and *p*-methyl-; *o*-, *m*-, and *p*-methoxy-; *m*- and *p*-nitro-; *m*- and *p*-chloro-; *m*- and *p*-bromo-cinnamic acid and (2-furyl)-acrylic acid. After acidifying the reactions solution, the aryl acrylates were extracted with diethyl ether (2 × 2 mL). The remaining aqueous fractions were basified to pH 10 (6 M NaOH) and treated with ethylchloroformate (50 μL) for 10 min. Each reaction was basified again to pH 10, a second

batch of ethylchloroformate (50 μL) was added, and each was stirred for 10 min. The solutions were separately acidified to pH 2-3 (6 M HCl), extracted with diethyl ether (2 × 2 mL). For each sample, the diethyl ether fractions were separately combined. The organic fraction was removed under vacuum, and the resulting residue was dissolved in ethyl acetate:methanol (3:1, v/v) (200 μL). The solution was treated with excess (trimethylsilyl)diazomethane until the yellow color persisted. The derivatized aromatic amino acids and aryl acrylates were quantified by GC/EI-MS. The peak area was converted to concentration by solving the linear equation obtained from the standard curves constructed with the corresponding authentic standards quantified by GC/EI-MS (Figure A.2.1-A.2.19).

4.2.5. Kinetic Parameters of *Pa*PAM for (2*S*)-α-Phenylalanine Analogues

*Pa*PAM (10, 25, 50 or 100 μg/mL) was incubated with each productive substrate (1000, 2000 or 2250 μM) in 12-mL assays to establish linearity with respect to time at a fixed protein concentration at 31 °C. Aliquots (1 mL) were withdrawn from each assay at 0.5 h intervals over 5 h and the reactions were quenched by adding 6 M HCl (100 μL). The products were derivatized and quantified as described above, and steady state conditions for each substrate were determined. To calculate the kinetic constants, each substrate was varied (10 – 2250 μM) in separate assays under the predetermined steady state conditions. Resultant products were quantified after terminating the reaction as described previously. Kinetic parameters (K_M and k_{cat}) were determined from Hanes-Woolf plots by plotting [S]/v against [S] (R^2 = 0.97 – 0.99) (Figure A.2.20-A.2.38).

4.2.6. Inhibition Assays for Non-productive Substrates

(2*S*)-α-Phenylalanine (at 10, 20, 40, 80, 100, 200, 300, 500, 750, 1000 μM) and *Pa*PAM (10 μg, 0.17 nmol) were mixed and incubated separately for 40 min with non-productive substrates *o*-chloro-, *o*-bromo-, or *o*-nitro-(*S*)-α-phenylalanine (at 50, 100 and 200 μM). The products were derivatized and quantified as described earlier. Inhibition constants (K_I) were calculated by non-linear regression analysis using GraphPad Prism 6 Software (La Jolla, CA).

4.3. Results and Discussion

4.3.1. Substrate Scope of *Pa*PAM and Kinetic Parameters of α-Phenylalanine Analogues

To gain further insights into the mechanism of *Pa*PAM, the substrate specificity was queried with 18 α-phenylalanine analogues and three heteroaromatic compounds. The substituents on the phenyl ring varied in position, size, inductive and mesomeric effects, polarizability, hydrophobicity, and the ability to form hydrogen- and halogen-bonds. *Pa*PAM was productive with a broad range of α-arylalanine analogues including fluoro-, chloro-, bromo-, methyl-, methoxy-, and nitro-substituents on the phenyl ring. Additionally furyl- and thienyl-alanines with heteroaromatic rings were also isomerized to their respective β-arylalanine products (Figure 4.6). Therefore, in contrast to tyrosine aminomutases with a narrow substrate scope,[14] both *Pa*PAM and *Tc*PAM[10] have broader steric and electronic flexibility for its isomerization reaction. Interestingly, *ortho*-chloro, -bromo, and -nitro substituted analogues were non-productive substrates for *Pa*PAM while same substituents at the *meta*- and *para*-positions were productive.

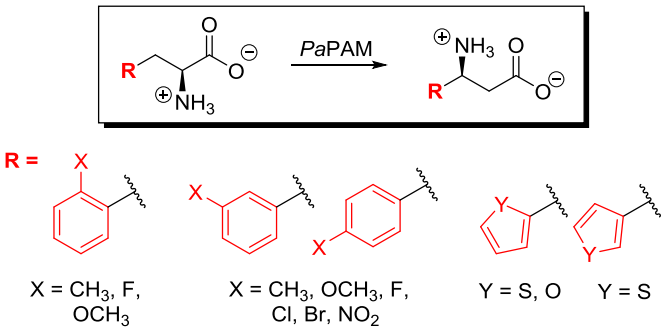

Figure 4.6. Broad substrate scope of *Pa*PAM. Various aryl-substituted and heteroaromatic α-amino acids were productive substrates for *Pa*PAM.

The kinetic constants k_{cat} and K_M of all the productive substrates were calculated from the Hanes-Wolf plots (Figure A.2.20-A.2.38) constructed by measuring the product formation of each substrate at steady state conditions. The kinetic parameters of *Pa*PAM for the natural substrate α-phenylalanine (**1**) were used to compare against the values for each analogue (**2** – **22**). In general, natural substrate **1** had the highest catalytic efficiency (k_{cat}/K_M) of all the substrates tested. The relative catalytic efficiency for each analogue was negatively affected by a decrease in k_{cat} total and/or increase in K_M (Table 4.1). Except the *para*-fluoro substrate **5**, all other *para*-substituted analogues showed a lower catalytic efficiency as a series. *ortho*-Methoxy substrate **19**, the only productive bulkier group at *ortho*-position had the lowest catalytic efficiency due to its exceptionally low catalytic rate (0.003 s^{-1}).

Fluoro-substituted analogue series displayed interesting kinetic parameters. All three *ortho*- (**10**), *meta*- (**3**), and *para*- (**5**) substituted analogues had similar catalytic rates (0.022, 0.031, and 0.023 s^{-1}, respectively) regardless of the substituent position. Furthermore, they bound to *Pa*PAM better than the natural substrate **1** and all the other substrate analogues. Of all the substrates tested, *ortho*-fluoro analogue **10** showed the lowest binding constant of 0.027×10^{-3} M and *para*-fluoro substrate had a comparative binding affinity (0.029×10^{-3} M). Fluorinated molecules are often exploited in medicinal chemistry to enhance the ligand binding to their target proteins.[33,34] It has been suggested that the fluorine substitution leads to an enhancement of binding affinity due a combination of its smaller size (~1.5 Å), higher electronegativity, and increased lipophilicity of the molecule.[33] Thus, fluoro-α-phenylalanines could also bind well to *Pa*PAM likely due to these reasons.

4.3.2. Kinetic Parameters of *ortho*-Substituted Analogues

Of the three productive *ortho*-substrates, the relative catalytic efficiency was highest for *o*-methyl substrate **6** (0.73 compared to 1.93 $s^{-1}{\cdot}M^{-1} \times 10^3$ for **1**). *o*-Methoxy substituent **19** showed the lowest catalytic efficiency of all the substrates (0.02 $s^{-1}{\cdot}M^{-1} \times 10^3$). The K_M values of *Pa*PAM for each of the three productive *ortho*-substrates (**6**, **10**, and **19**) varied only between 1- and 2-fold compared to that of **1**. The *ortho*-substituents, regardless of size, including the bulkier *o*-methoxy of **19**, did not affect the substrate binding. Of the three, *Pa*PAM turned over *o*-methyl substrate (**6**) faster (0.064 s^{-1}) than the *o*-fluoro (**10**, 0.022 s^{-1}) and *o*-methoxy (**19**, 0.003 s^{-1}) compounds (Table 4.1). However, each was isomerized substantially slower (5-, 14-, and 108-fold, respectively) than **1**. The relatively satisfactory binding (i.e., low K_M values) yet poor turnover for **6**, **10**, and **19** suggests that *Pa*PAM binds these substrates in a catalytically ineffective orientation. It should be noted that the *ortho*-substituents on the arylalanine substrates are positioned vicinally to the alanine side chain. The proximity of these groups to the alanyl side chain of the substrates likely creates a steric barrier that skews the aryl ring plane. A canted aryl ring would relax the sterics yet reduce potentially beneficial resonance effects of the substituents on C_β in a charged transition state that could influence substrate turnover. Steric shielding of the β-position of the cinnamate intermediate by *o*-fluoro, -chloro, -bromo and -methyl substituents was also seen during the ammonia addition reactions with *Tc*PAM.[31] *ortho*-substituted cinnamates added NH_2 exclusively at C_α likely due to the unfavorable steric effects caused at C_β from proximal substituents.

Although the *o*-bromo, *o*-chloro, and *o*-nitro substrates **20** – **22** exert similar electronic effects as the corresponding *para*-isomers (Figure 4.7D, J), interestingly, **20** – **22** did not yield

any detectable product in the enzyme reaction. However, their competitive inhibition constants (K_I) of 15.9 (±1.67), 17.7 (±2.11), and 16.9 (±3.35) μM, respectively, indicate that they bind well to *Pa*PAM. The lack of turnover of **20** – **22** by *Pa*PAM was therefore likely caused by poor access of the substrates to a catalytically competent conformation. This may have resulted from the bulkier substituents at the *ortho*-position of the phenyl ring. In contrast to **20** – **22**, *o*-methoxy substrate **19** turned over with *Pa*PAM, yet with the lowest catalytic rate. The productivity of **19** was likely caused by the favorable binding orientation resulted from the H-bonding interactions of *o*-methoxy substituent with active site residue Tyr320 (Figure A.2.39).

4.3.3. Kinetic Parameters of *meta*-Substituted Analogues

The relative catalytic efficiencies were highest for *meta*-halogenated substrates (**2** – **4**) (Table 4.1). The K_M values of *Pa*PAM for *m*-bromo (**2**) and *m*-chloro (**4**) substrates were only negatively affected ~2-fold, and the k_{cat}^{total} values remained essentially unchanged compared to the parameters for **1** (Table 4.1). Interestingly, the relative k_{cat}^{total} for the *m*-fluoro substrate **3** was ~10-fold lower (0.031 s^{-1}) than that for **1**, **2** and **4**, yet the 5-fold lower K_M of *Pa*PAM for **3** made the k_{cat}^{total}/K_M similar to those for **1**, **2** and **4**. The latter suggests that **3** binds tighter than **2** and **4**, which carry halogens (Br and Cl) with larger atomic radii of 185 pm and 175 pm, respectively, compared to the smaller F (147 pm) of **3**. In addition, the fluoro-substituted substrates binds better than the natural substrate containing a smaller H-atom.

Analysis of other *meta*-substituted substrates showed the catalytic efficiencies for *m*-nitro (**9**), *m*-methoxy (**11**), and *m*-methyl (**13**) analogues were 6- to 10-fold lower than that for **1**. The *m*-nitro of **9** only reduced the relative k_{cat}^{total}/K_M of *Pa*PAM by 5.7-fold due to the modest 2.2- and 2.6-fold negative effects on k_{cat}^{total} and K_M, respectively, compared with **1** (Table 4.1). *m*-

Methoxy substrate **11**, showed the second highest K_M (990 μM) of all the substrates while the k_{cat}^{total} was only ~1.6-fold lower than that of **1**. The increased K_M suggested that the sterics of the *m*-methoxy affected substrate binding. In contrast, k_{cat}^{total} of *m*-methyl substrate **13** was ~6-fold lower (compared to **1**) with a K_M negatively affected only by 1.2-fold. Consequently, ~6-fold negative effects of K_M and k_{cat}^{total}, reduced the catalytic efficiency of **11** and **13**, respectively.

4.3.4. Kinetic Parameters of *para*-Substituted Analogues

With the exception of *p*-fluoro substrate **5**, catalytic efficiencies of *para*-substituent analogues (**14** – **18**) were the lowest as a series. Each substrate containing a *para*-substituent (**5**, **14** – **18**), significantly reduced the k_{cat}^{total} of *Pa*PAM by 6 – 25-fold compared to the value for **1** (k_{cat}^{total} = 0.323 s^{-1}). As seen for the trend with the *meta*-substituent series, the *p*-bromo and *p*-chloro substituents were turned over fastest; the chloro substrate was turned over slightly faster. The substrates turned over slowest by *Pa*PAM in this series contained a *p*-nitro, *p*-methyl, or *p*-methoxy substituent (Table 4.1). In general, *para*-substituted analogues bound poorly to *Pa*PAM with *p*-methoxy analogue being the substrate with the lowest affinity (K_M = 1187 μM; a 10-fold increase compared to **1**). However, similar to *ortho*- and *meta*-substituted analogues, *p*-fluoro substrate showed the highest catalytic efficiency of the series due to its unusually low K_M value. In addition to **5**, *p*-methyl substituent also had a lower K_M value (163 μM) compared to other analogues in the series (Table 4.1).

Table 4.1. Kinetic parameters of *Pa*PAM for various substituted aryl and heteroaromatic substrates

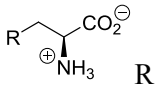	K_M (μM)	k_{cat}^{β} (s^{-1})	k_{cat}^{cin} (s^{-1})	k_{cat}^{total} (s^{-1})	k_{cat}^{total}/K_M (s^{-1}•M^{-1} × 10^3)
1 	168 (± 7)	0.301 92.8%	0.022 7.2%	0.323 (± 0.013)	1.93 (± 0.20)
2 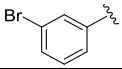	339 (± 15)	0.396 93.9%	0.024 6.1%	0.420 (± 0.014)	1.24 (± 0.12)
3 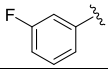	27 (± 5)	0.027 85.2%	0.004 14.8%	0.031 (± 0.002)	1.2 (± 0.4)
4 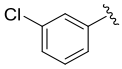	432 (± 26)	0.462 95.2%	0.022 4.8%	0.484 (± 0.02)	1.12 (± 0.14)
5 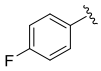	29 (± 1)	0.020 85.7%	0.003 14.3%	0.023 (± 0.001)	0.79 (± 0.06)
6 	88 (± 6)	0.055 83.6%	0.009 16.4%	0.064 (± 0.002)	0.73 (± 0.09)
7 	415 (± 79)	0.143 34.8%	0.093 65.2%	0.236 (± 0.01)	0.588 (± 0.066)
8 	337 (± 27)	0.139 97.2%	0.004 2.8%	0.143 (± 0.004)	0.428 (± 0.063)
9 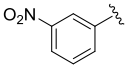	430 (± 15)	0.136 92.6%	0.01 7.4%	0.146 ± 0.003)	0.340 (± 0.025)
10 	73 (± 6)	0.021 95.5%	0.001 4.5%	0.022 (± 0.001)	0.31 (± 0.04)
11 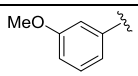	990 (± 124)	0.201 99.0%	0.002 1.0%	0.203 (± 0.012)	0.209 (± 0.050)
12 	132 (± 5)	0.024 90.9%	0.002 9.1%	0.026 (± 0.001)	0.19 (± 0.02)
13 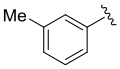	204 (± 4)	0.048 78.3%	0.010 21.7%	0.058 (± 0.001)	0.19 (± 0.01)
14 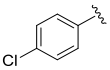	491 (± 82)	0.050 94.1%	0.003 5.9%	0.053 (± 0.003)	0.11 (± 0.03)
15 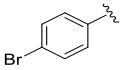	525 (± 44)	0.043 95.6%	0.002 4.4%	0.045 (± 0.001)	0.09 (± 0.01)
16 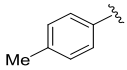	163 (± 9)	0.010 63.6%	0.003 36.4%	0.013 (± 0.001)	0.082 (± 0.010)
17 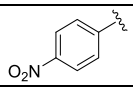	752 (± 39)	0.025 48.0%	0.013 52.0%	0.038 (± <10^{-3})	0.050 (± 0.005)
18 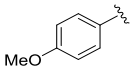	1187 (± 76)	0.022 97.7%	0.0005 2.3%	0.022 (± <10^{-3})	0.019 (± 0.002)
19 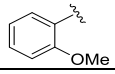	164 (± 7)	0.002 70.0%	0.0007 30.0%	0.003 (± <10^{-3})	0.02 (± <10^{-2})
20 		**21** 		**22** 	

20-22: Non-productive substrates

4.3.5. Substituent Effects on the *Pa*PAM Isomerization Reaction

4.3.5.1. Electronic Considerations on *Pa*PAM Isomerization Reaction

The *Pa*PAM isomerization mechanism is a sequence of two main reaction steps that involves an elimination followed by a hydroamination step (cf. Figure 4.2). In the first reaction sequence, the amino group and the *pro*-(3*S*) benzylic hydrogen from the α-amino acid eliminate to produce the cinnamate intermediate.[18] MIO-dependent aminomutase reactions likely follow an E2 or E1cB elimination mechanism (Figure 4.7A), where both depend on the rate of deprotonation of C_β, as proposed in an earlier work.[35] The electron-withdrawing substituents on the aryl ring of the substrate that stabilize a δ^- charge on C_β should therefore increase the rate of the elimination step (Figure 4.7C, D).

The initial elimination sequence of MIO-containing aminomutases requires the abstraction of a proton from a site of low C-H acidity (p*K*a = 40).[24] The alkylation of the α-amino group from the MIO cofactor, however leads to the acidification of the β-hydrogens and favors the elimination.[23] Although this is sufficient to allow the abstraction of benzylic hydrogens, no MIO-based aminomutases reported to date can isomerize aliphatic amino acids.[10,14] *Pa*PAM was unable to convert (*S*)-2-amino-4-phenylbutyric acid (L-homophenylalanine) and (*S*)-2-amino-5-phenylpentanoic acid to their corresponding β-amino acids. Presumably, additional methylene group/s between the α-amino group and the phenyl ring of these substrates disrupt the potentially beneficial effects of the aromatic ring for proton abstraction. Thus, difficulty of methylene β-hydrogen (p*K*a = 60) abstraction likely resulted the non-productivity of these substrates. (*S*)-styrylalanine was however, a productive substrate of *Pa*PAM although the β-styrylalanine ratio was much lower (10% β-styrylalanine; 90%

styrylacrylate). This suggests that an extended conjugated allyl π-system next to the α-carbon, is required for the α- to β-phenylalanine isomerization.

The final reaction sequence of the MIO-dependent aminomutases involves an α,β-addition reaction, where the NH_2-MIO and a proton (H^+) add across the double bond of the acrylate intermediate (Figure 4.7B). To obtain the β-amino acid in a concerted hydroamination, the polarity of the C_β (δ^+) needs to be opposite of that in the earlier elimination sequence. Here, the nucleophilic NH_2-MIO binds to C_β and the electrophilic H^+ attaches to C_α (Figure 4.7B). Theoretically, a substituent that places negative charge inductively within the ring or mesomerically the on C_{ipso} of the β-arylacrylate intermediate should strengthen the formation of a δ^+ on C_β. Therefore, the electron-donating substituents on the aryl ring of the substrate that stabilize a δ^+ charge on C_β should increase the rate of the hydroamination step (Figure 4.7G, H). To further evaluate the mechanistic basis of the differences in turnover by *Pa*PAM for various *meta*- and *para*-substituted substrates, the dependence of the relative turnover rate on the substituent of the substrate was analyzed using Hammett plots.

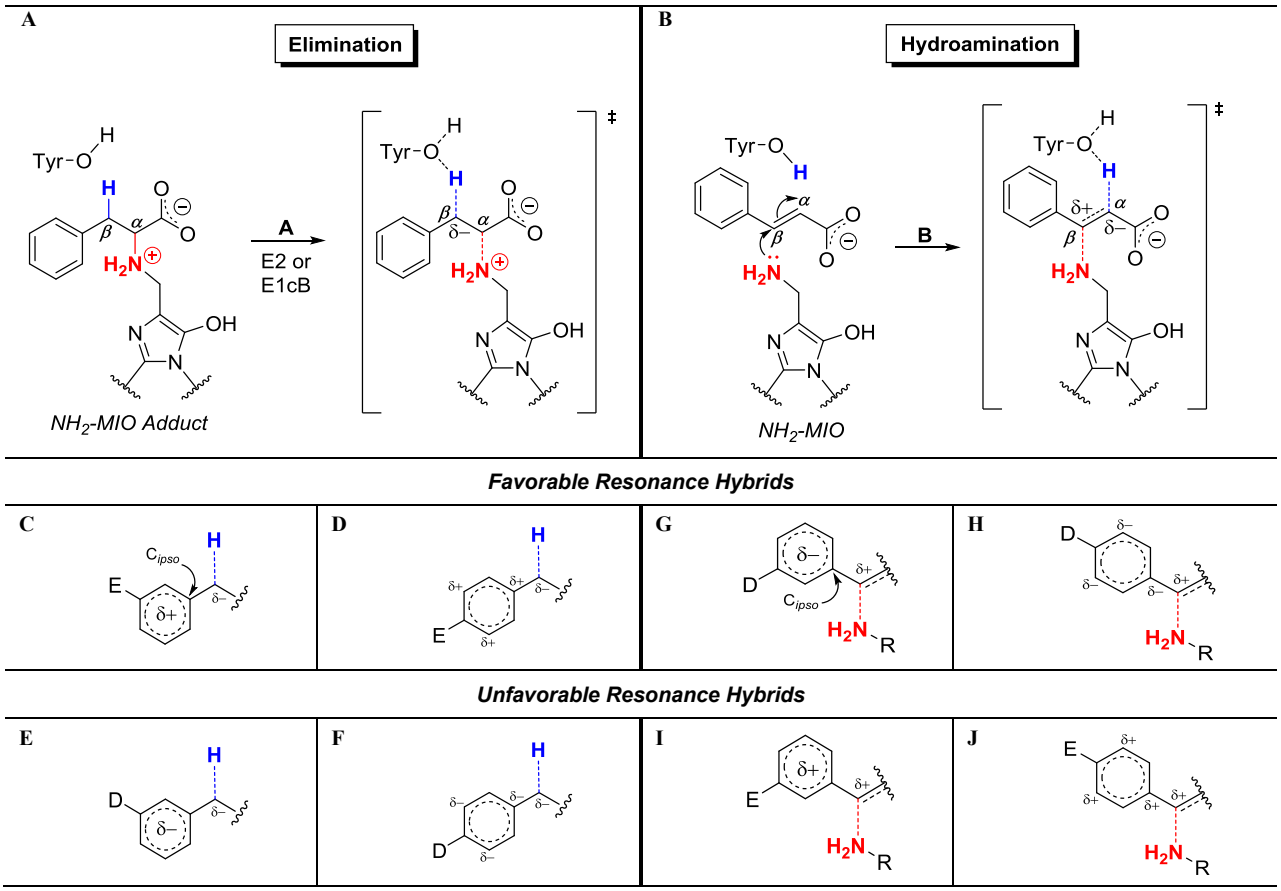

Figure 4.7. Elimination (*A*) and Hydroamination (*B*) reaction sequences of *Pa*PAM isomerization. *C-J*) Resonance hybrids formed from electron-donating (D) or -withdrawing (E) substituents on the phenyl ring. An increase or decrease in electron density, caused by the substituent, within the ring or at C_{ipso} is predicted to support a transient δ^+ or δ^- respectively at C_{β}.

4.3.5.2. Substituent effects on Michaelis Parameters: *meta*-Substituents

The Hammett plot between the calculated $\log(k_{\text{cat}}^{m\text{X}}/k_{\text{cat}}^{\text{H}})$ of *Pa*PAM and substituent constants (σ)[36] for the *meta*-substituted (*m*X) arylalanines (*m*-bromo (**2**), *m*-chloro (**4**), *m*-nitro (**9**), *m*-methoxy (**11**), and *m*-methyl (**13**)) follow a concave-down, parabolic regression curve[37] (Figure 4.8A). The fastest reactions at the apex of the curve occurred with the *m*-bromo and *m*-chloro substrates, and the slowest with *m*-methyl and *m*-nitro, at the extremes. The *m*-methoxy substituent reacted at an intermediate rate. The right side of the correlation plot tends towards a slope (ρ) < 0 and suggested the rate of the *Pa*PAM reaction was slowed by electron-withdrawing substituents. *m*-Bromo (**2**) and *m*–chloro (**4**) substrates however occupy an ambiguous position at the apex of the Hammett plot (Figure 4.8A). Electron-donating substituents appear on the Hammett correlation plot where the slope (ρ) is ≈ +2.9 suggesting that the *Pa*PAM rate was markedly slowed by stronger electron-donating *meta*-substituents.

4.3.5.2.1. Electron-withdrawing Substituents

The $\log(k_{\text{cat}}^{m\text{X}}/k_{\text{cat}}^{\text{H}})$ for *m*-nitro substrate **9** fits on the negative slope ($\rho \approx -1.4$) of the correlation curve (Figure 4.8A). The resonance hybrid of the *m*-nitro places δ^+ in the aromatic ring favoring a buildup of δ^- on C_β (Figure 4.7C). Thus, the strong electron-withdrawing *m*-nitro group is foreseen to accelerate deprotonation of C_β that produces a transient δ^- on the elimination step (Figure 4.7A). In turn, the nitro group was anticipated to negatively affect the β-amination step, which forms a transient δ^+ on C_β (Figure 4.7B, J). The *m*-nitro was therefore expected to slow the amination rate of the *Pa*PAM reaction involving **9** compared to that for **1**. The *m*-nitrocinnamate (7.4%)/*m*-nitro-β-amino acid (92.6%) product apportioned similar to that of analogous products made from **1** (cinnamate (7.2%) and β-amino acid (92.8%)). This result

suggested that the *m*-nitro of **9** likely had a less than imagined affect on the hydroamination of the *m*-nitrocinnamate intermediate.

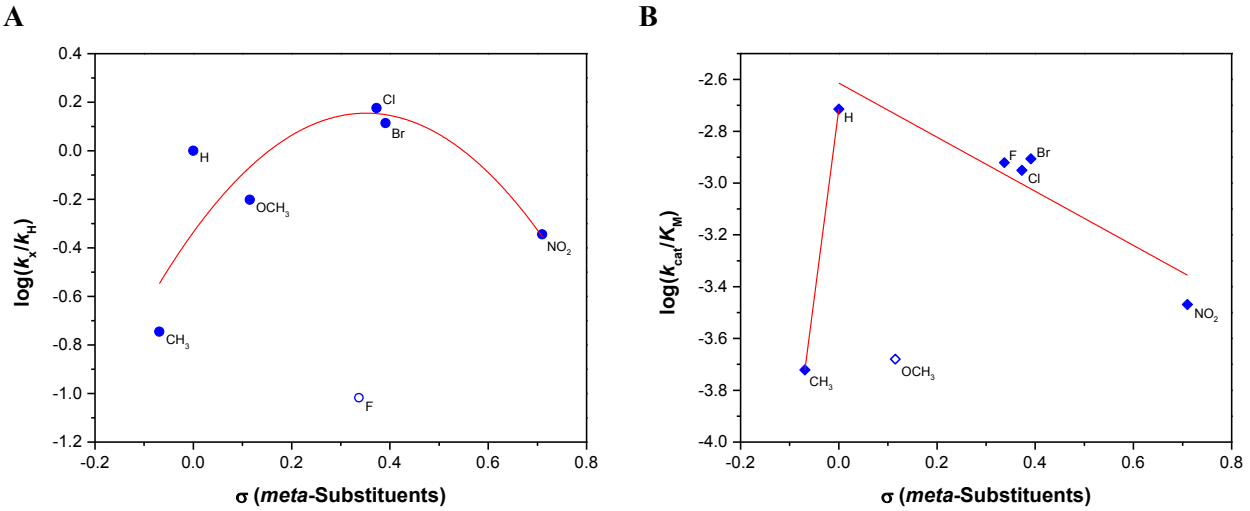

Figure 4.8. Dependence of the observed log(k_{cat}^{mX}/k_{cat}^{H}) [designated as log(k_x/k_H)] (*A*) and log(k_{cat}^{mX}/K_M) [designated as log(k_{cat}/K_M)] (*B*) on the Hammett substituent constant for the *Pa*PAM-catalyzed isomerization of *meta*-substituted α-arylalanines. Here, k_{cat}^{mX} is k_{cat}^{total} for entries **2** – **4**, **9**, **11**, and **13**; k_{cat}^{H} is k_{cat}^{total} for entry **1**. Open circle: outlier *m*-fluoro substrate **3**. Open diamond: outlier *m*-methoxy substrate **11**.

In contrast, *m*-bromo (**2**) and *m*-chloro (**4**) substrates turned over ~3-fold faster than **9** (Table 4.1). Halogens are a group of substituents of the 'push-pull' type. They withdraw electron density by induction and donate electrons by resonance, depending on the type of reaction. The overall effect of the halogens is considered electron-withdrawing as estimated by their Hammett substituent constants. The 'push-pull' effect of **2** and **4** likely tells that electron-release by *m*-bromo and *m*-chloro reduces the electron-withdrawing magnitude that negatively affects the rate, as did the *m*-nitro of **9**. The electron-withdrawing effect of bromo and chloro likely support the transient δ^- on C_β and increases the rate of the elimination step (Figure 4.7C); the electron-donating effect would improve stabilization of a transient δ^+ formed during the hydroamination

across the double bond of the intermediate (Figure 4.7G). These effects likely caused an increase in $k_{\text{cat}}^{\text{total}}$ of substrates **2** (0.420 s^{-1}) and **4** (0.484 s^{-1}) compared to that for natural substrate **1** (0.323 s^{-1}).

It is worth noting, the proportions of *m*-halo-β-amino acid (93.9% *m*-bromo-β-amino acid and 95.2% *m*-chloro-β-amino acid) and *m*-halo-cinnamate (6.1% *m*-bromo-cinnamate and 4.8% *m*-chloro-cinnamate) made by *Pa*PAM from **2** and **4**, respectively, were similar to that of analogous products made from **1** (Table 4.1). Thus, the amination of the *m*-halocinnamate intermediates was not significantly affected by the substituents. This observation supports a mechanism where release of the intermediate as a by-product is slower than hydroamination.

Interestingly, based on Hammett constants, the inductive effects of fluoro (σ = 0.34) on an aryl ring are in principle similar to those of the chloro- (σ = 0.37) and bromo- (σ = 0.39) substituents.[36] Therefore, it was surprising that the *m*-fluoro substrate **3** had a significantly lower $\log(k_{\text{cat}}^{m\text{X}}/k_{\text{cat}}^{\text{H}})$ value and did not fit the Hammett correlation for the *meta*-substituent series (Figure 4.8A). The significant decrease (~10-fold) in $k_{\text{cat}}^{\text{cinn}}$ and k_{cat}^{β} of *Pa*PAM for **3** (compared with the same parameters for **1**) suggested that the *m*-fluoro substituent affected the chemistry at C_{β} during the elimination *and* the hydroamination steps, respectively. The higher proportion of *m*-fluorocinnamate (14.8%) relative to *m*-fluoro β-amino acid (85.2%) made by *Pa*PAM from **3**, (compared with the cinnamate (7.2%) and β-amino acid (92.8%) products made from **1**) suggested that the electronic effects of the *m*-fluoro affected the amination step more than the elimination step.

4.3.5.2.2. Electron-donating Substituents

m-Methoxy and *m*-methyl substrates **11** and **13**, respectively, appear on the Hammett correlation plot where the slope (ρ) is ≈ +2.9 (Figure 4.8A). This suggested that the *Pa*PAM rate was markedly slowed by stronger electron-donating *meta*-substituents.

The electron-donation by *m*-methoxy substituent **11** likely destabilizes the δ^- on C_β upon removal of H_β (Figure 4.7E) and decreases the elimination rate. Reciprocally, the *m*-methoxy substituent would promote the formation of an electrophilic (δ^+) C_β formed during the amination step (Figure 4.8G). Here, the electronic effects of the *m*-methoxy that deterred the elimination rate were likely offset by the rate-enhancing effects on the amination step. The *Pa*PAM-catalyzed product pool from **11** contained the *m*-methoxy-β-amino acid (99.0%) and the *m*-methoxy acrylate at 1.0%. *Pa*PAM converted **1** with less selectivity (β-isomer at 92.8%; cinnamate at 7.2%). This supported that the amination efficiency to make the β-isomer of **11** was most likely facilitated by the substituent. In addition, based on the Hammett constant (+0.12),[36] *m*-methoxy has an electron-withdrawing component that slightly reduces the significant *meta*-substituent effect of its electron-donation into the ring by resonance. *m*-Methoxy substrate **11** showed a moderate $k_{\text{cat}}^{\text{total}}$ with only a 1.6-fold reduction compared to **1**. This supported the balancing effects of electron-donating and -withdrawing ability of the *m*-methoxy substituent on $k_{\text{cat}}^{\text{total}}$.

A methyl-substituent contributes electron density through hyperconjugation (quasi-mesomeric)[38] to the attached aryl ring and exerts resonance effects, to a lesser extent, but similar to those of methoxy.[36] The $\log(k_{\text{cat}}^{m\text{X}}/k_{\text{cat}}^{\text{H}})$ for **13** with an electron-"releasing" *m*-methyl (σ = -0.07) fits on the parabolic Hammett correlation curve (Figure 4.8A). The steep slope in this

region suggested that the rate of the *Pa*PAM reaction is strongly affected by the electron-releasing *meta*-substituent. Despite the smaller *meta*-substituent constant for methyl than for methoxy, the mesomeric *m*-methoxy releases more electron density to the ring than the methyl does through hyperconjugation. Thus, it was postulated that the rate enhancement of the addition step, through a favorable transition state (Figure 4.7G), with **13** was not as significant as with **11**. This likely accounted for the >3.5-fold faster $k_{\text{cat}}^{\text{total}}$ for *m*-methoxy **11** than for *m*-methyl substrate **13**.

The product pool catalyzed by *Pa*PAM from **13** contained more cinnamate analogue (21.7%) compared to that made from other *m*-substituted substrates **2**, **4**, **9**, and **11** that contained between 1.0% and 7.4%. Therefore, the amination of the *m*-methyl aryl acrylate is likely more sensitive to the effects of the substituent. *m*-Fluoro substrate **2** was converted to the cinnamate analogue (14.8%) at a similar proportion as was **13**. Compared with **1**, it is intriguing that substrates **2** and **13**, with opposing electronic and steric properties, similarly affect the k_{cat} of *Pa*PAM and the ratio of the cinnamate:β-amino acid analogues.

4.3.5.2.3. *meta*-Substituent Effects on Catalytic Efficiency

The plot between $\log(k_{\text{cat}}^{m\text{X}}/K_{\text{M}})$ and σ for the *meta*-substituted (*m*X) arylalanines (Figure 4.8B) showed that the substituent effects on the catalytic efficiency ($k_{\text{cat}}^{m\text{X}}/K_{\text{M}}$) mostly paralleled the nonlinear relationship between $\log(k_{\text{cat}}^{m\text{X}}/K_{\text{M}})$ and σ (Figure 4.8A). That is, the catalytic efficiency decreased paradoxically with substituents of higher electron-withdrawing or -donating strength. Thus, the substituent effects on the k_{cat} value of the catalytic efficiency were not masked by the K_{M}. Interestingly, the *m*-fluoro (**2**) substrate, which was an outlier on the parabolic regression plot of $\log(k_{\text{cat}}^{m\text{X}}/K_{\text{M}})$ and σ, fits the linear regression plot between

$\log(k_{\mathrm{cat}}^{m\mathrm{X}}/K_{\mathrm{M}})$ and σ ($\rho = -1.05$). The effects of the electron-withdrawing *m*-fluoro substituent on the catalytic efficiency correlated well with those of *m*-chloro and *m*-bromo (Figure 4.8B). Reciprocally, the *m*-methoxy (**11**) substrate fit the parabolic regression plot between $\log(k_{\mathrm{cat}}^{m\mathrm{X}}/K_{\mathrm{M}})$ and σ (Figure 4.8A), and was an outlier on the $\log(k_{\mathrm{cat}}^{m\mathrm{X}}/K_{\mathrm{M}})$ correlation plot (Figure 4.8B). This result suggested that the catalytic efficiency of *Pa*PAM for substrates **2** and **11** was influenced more by their affinity for *Pa*PAM than by electronic substituent effects. The relatively low K_{M} (27 μM) for **2** likely revealed that the acrylate intermediate and β-amino acid *products* were also released poorly and affected the turnover. Contrastingly, the high K_{M} (990 μM) for **11** showed poor *substrate* binding, which masked the correlation between the electronic effects of the *m*-methoxy and catalytic efficiency.

4.3.5.3. Substituent effects on Michaelis Parameters: *para*-Substituents

The calculated $\log(k_{\mathrm{cat}}^{p\mathrm{X}}/k_{\mathrm{cat}}^{\mathrm{H}})$ of *Pa*PAM and substituent constants (σ) for the *para*-substituted (*p*X) arylalanines (*p*-fluoro (**5**), *p*-chloro (**14**), *p*-bromo (**15**), *p*-methyl (**16**), *p*-nitro (**17**), and *p*-methoxy (**18**)) do not follow a single Hammett plot (Figure 4.9A). Electron-donating substrates **16** and **18**, and the natural substrate **1** follow a positive-slope (ρ = +4.74) linear regression curve with a moderate correlation coefficient (R = 0.87). The linear regression curve between electron-donating substituents **14** and **15**, and **1** showed a negative-slope (ρ = -0.93) with a low correlation coefficient (R = 0.71). The ρ value (+4.74), which is much greater than unity for the electron donating substrates, suggests that catalysis is very dependent on the nature of these substituents. By comparison, the $\rho \approx -1.0$ for substrates **14**, **15**, and **17** suggests a moderate yet significant dependence on the electron-withdrawing strength of the substituent (Figure 4.9A). The intersecting linear regressions of opposite slope (ρ) suggest the substituent

effects transition from affecting the elimination step to affecting the amination step.[37] Unlike the *meta*-substituted substrates with a higher catalytic rate for *m*-chloro and *m*-bromo analogues, all *para*-substituents slowed the isomerization reaction compared to **1**.

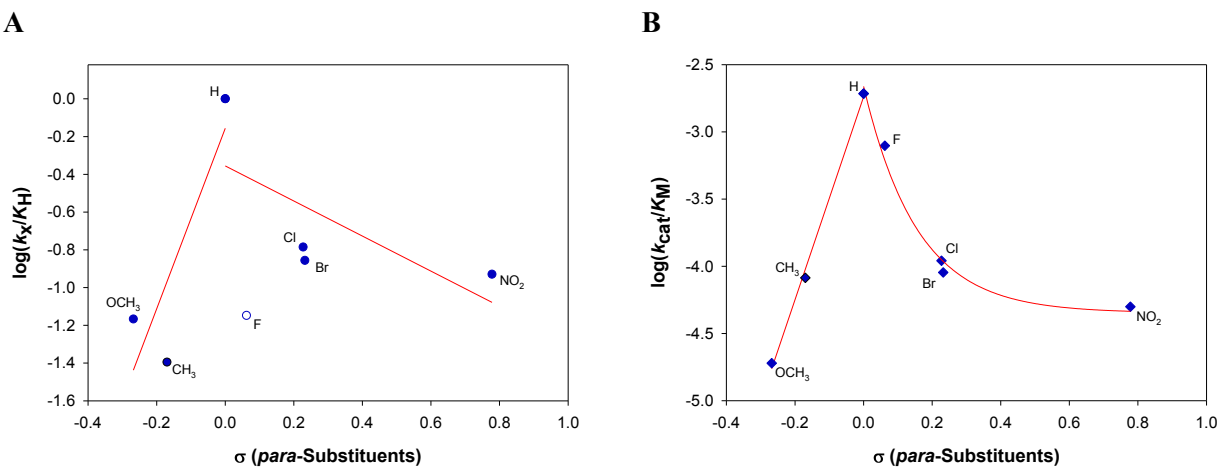

Figure 4.9. Dependence of the observed log(k_{cat}^{pX}/k_{cat}^{H}) [designated as log(k_x/k_H)] (*A*) and log(k_{cat}^{pX}/K_M) [designated as log(k_{cat}/K_M)] (*B*) on the Hammett substituent constant for the *Pa*PAM-catalyzed isomerization of *para*-substituted α-arylalanines. Here, k_{cat}^{pX} is k_{cat}^{total} for entries **14**, **15**, **16**, **17**, and **18**, k_{cat}^{H} is k_{cat}^{total} for entry **1**; k_{cat} is k_{cat}^{total} for entries **5**, **14**, **15**, **16**, **17**, and **18**. Open circle: outlier *p*-fluoro substrate **5**.

4.3.5.3.1. Electron-withdrawing Substituents

The resonance hybrid of the *p*-nitro substrate **17** has a δ^+ directly on C_{ipso} attached to C_β (Figure 4.7D). While this was imagined to strongly increase the elimination rate (i.e., facilitates H_β removal), the 8.5-fold slower k_{cat}^{total} of *Pa*PAM for **17** (0.031 s^{-1}) than for **1** (Table 4.1) likely resulted because the *p*-nitro slowed the hydroamination rate (i.e., deterred nucleophilic attack at C_β) (Figure 4.7J) more than it improved the elimination rate. The higher ratio of *p*-nitrocinnamate (52%) compared to cinnamate (7.2%) made from **1** further supports an affected hydroamination step.

The inductive electron-withdrawing effect of *p*-chloro and *p*-bromo of substrates **14** and **15** on C_{ipso} are lower than thatfor the corresponding *meta*-isomers. The lone-pair electrons of the former however can delocalize by resonance and place a δ^- directly on C_{ipso} attached to C_β in the resonance hybrid. The δ^- will promote the amination step (Figure 4.7H), yet dramatically retard the deprotonation of the elimination step of the *Pa*PAM reaction (Figure 4.7F). Almost similar ratio of *p*-chloro- (5.9%) and -bromocinnamate (4.4%) compared to cinnamate (7.2%) made from the natural substrate suggested that the hydroamination step is not affected from chloro and bromo substituents. Thus, the lower $k_{\text{cat}}^{\text{total}}$ of **14** and **15**, would likely have caused by the unfavorable effects on the elimination step.

The *p*-fluoro substrate **5** was turned over by *Pa*PAM at about the same rate as the *m*-fluoro substrate **3** and *o*-fluoro substrate **10**, but coincidentally at the same rate as the other *para*-substituted substrates. It seems that regardless of regiochemistry, the overarching electronic effect(s) of the fluoro substituent stalls the elimination and hydroamination steps. In addition, based on the β-amino acid:aryl acrylate (85.7:14.3) distribution catalyzed by *Pa*PAM from **5**, it seems that the fluoro affects the efficiency of the β-amination step, compared to the reaction involving **1**. A similar product distribution was also seen for the *m*-fluoro substrate **3**.

4.3.5.3.2. Electron-donating Substituents

The electron-releasing *p*-methyl of **16** and *p*-methoxy of **18** place a δ^- on C_{ipso} of the substrate via hyperconjugation and resonance, respectively. Each theoretically causes the pK_a of H_β to increase and discourages the deprotonation of the presumed rate-limiting elimination step (Figure 4.7F). The Hammett substituent constants predicted the electron-releasing *p*-methyl substituent would affect *Pa*PAM turnover ($k_{\text{cat}}^{\text{total}}$ = 0.013 s^{-1}) more than the methoxy ($k_{\text{cat}}^{\text{total}}$ =

0.022 s^{-1}), as observed (Table 4.1). The electronic effects of **16** and **18** facilitate the hydroamination of the corresponding cinnamate intermediates and the product pool from **18** contained a higher ratio of *p*-methoxy-β-amino acid (97.7%) as expected. Surprisingly, *p*-Methyl substrate had a higher proportion of *p*-methylcinnamate (36.4%) compared to 7.2% cinnamate for **1**.

4.3.5.3.3. *para*-Substituent Effects on Catalytic Efficiency

The relationship between $\log(k_{\mathrm{cat}}^{p\mathrm{X}}/K_{\mathrm{M}})$ and σ for the *para*-substituted (*p*X) arylalanines (Figure 4.9B) showed a similar trend in substituent effects on the catalytic efficiency ($k_{\mathrm{cat}}^{p\mathrm{X}}/K_{\mathrm{M}}$) as seen between $\log(k_{\mathrm{cat}}^{p\mathrm{X}}/K_{\mathrm{M}})$ for *Pa*PAM and Hammett substituent constants (Figure 4.9A). As with the *meta*-substituents, the catalytic efficiency of *Pa*PAM was also sensitive to the *para*-substituents. Electron-releasing substituents (**16** and **18**) fit into a linear regression curve with **1** (correlation coefficient (R) = 1.0; ρ = 7.50) while electron-withdrawing substituents (**5**, **14**, **15**, and **17**) follow a decay curve (R = 0.99). In contrast to the poor correlation between $\log(k_{\mathrm{cat}}^{\mathrm{X}}/k_{\mathrm{cat}}^{\mathrm{H}})$ and σ, *para*-substituents showed a superior correlation in the Hammett plot of catalytic efficiencies. This informed that a reduction in catalytic efficiency was principally dictated by large K_{M} and not the electronic effects of the *para*-substituent that separately affected k_{cat}.

4.3.6. Structure Activity Relationships of *Pa*PAM Substrate Analogues

4.3.6.1. Structural Characteristics of *Pa*PAM Active Site

The overall structure of *Pa*PAM is composed of multiple parallel α-helices that form the catalytically functional tetramer arranged as a dimer of head-to-tail dimers.[18] Each monomer of the tetramer contains an active site which is located at the interfaces between three subunits (Figure 4.10A). Two of the *Pa*PAM active sites revealed β-phenylalanine covalently attached by the amino group to the methylidene carbon atom of MIO (Figure 4.10A), while the other active sites showed an MIO covalent adduct with partial occupancy of both β- and α-phenylalanines.[18] The phenylpropanoid carbon backbone of the substrate resides above the MIO facilitating the α- to β-amino group transfer during the isomerization reaction. The mono-dentate salt bridge interaction between the substrate carboxylate group and highly conserved Arg323 anchors the substrate in the *Pa*PAM active site.[18] In addition, the aromatic binding pocket of *Pa*PAM provides an optimum environment to orient the aromatic ring of arylalanines. The aromatic binding pocket is mostly lined by the side chains of the hydrophobic residues (Leu104, Val108, Leu171, Leu216, Leu421, Met424 and Phe428), which likely contribute to the binding of an aryl ring via van der Waals interactions.

Although the structure of *Pa*PAM bound to the natural substrate/product provides information on key interactions of substrate binding, favorable binding orientations of ring-substituted substrate analogues are not predictable. Additionally, *ortho*- and *meta*-substituted analogues, can orient their substituent groups in two different conformations, where the substituent is *cis* or *trans* to the amino group of the substrate (Figure 4.10B). In "NH_2-*cis*" orientation, the ring substituent is on the same side as the amino group of α-phenylalanine. In the

"*NH_2-trans*" conformation obtained by a 180° rotation of the C_{β}-C_{ipso} bond, the ring substituent is oriented on the opposite side of the amino group. These two substrate binding orientations interact differently with *Pa*PAM due to the differences in the active site residues in either side of the aromatic ring. Therefore, molecular docking of substrate analogues in *Pa*PAM active site was performed to analyze the preferred binding orientations and interactions of substrate analogues.

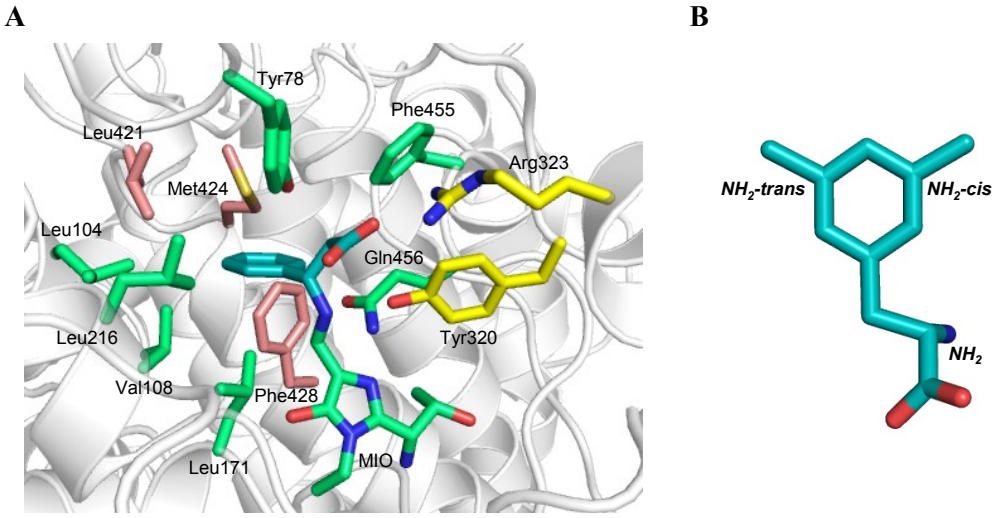

Figure 4.10. Structural characteristics of the *Pa*PAM active site, and *NH_2-cis* and *NH_2-trans* configurations of substrate analogues. *A*) Active site of *Pa*PAM showing side-chains which are in 4 Å distance from the MIO-bound ligand. (ligand atoms are color-coded as: carbon: teal; nitrogen: blue; oxygen: red). The active site residues are color-coded (carbon atoms in green, yellow, and wheat) to differentiate the involvement from each sub unit. *B*) An overlay of the *NH_2-cis* and *NH_2-trans* configurations is illustrated using *meta*-methyl-(*S*)-α-phenylalanine substrate. The methyl group can be positioned on the same side (*NH_2-cis*) or the opposite side (*NH_2-trans*) as the reactive amino group of the chiral substrate.

4.3.6.2. Correlation between Substrate-*Pa*PAM Interaction Energies and K_M

To gain insight into the differences of K_M values of substrate analogues and their preferred binding orientations, all the substrates (**1** – **22**) were docked in *Pa*PAM active site

using SLIDE (Screening for Ligands by Induced-fit Docking, Efficiently) docking tool (version 3.4)[39,40] and Szybki[41-43] 1.7.0 (OpenEye Scientific Software). Bio-active conformation of α-phenylalanine found in the structure of *Pa*PAM was used to generate the substrate conformations employed for molecular docking. The aryl rings of the substrate analogues **2** – **22** were overlaid on to the active conformation of α-phenylalanine structure by using molecular editing in PyMOL 1.5.0.4 (Schrödinger, Inc., New York, NY) and reference coordinates were fixed in OMEGA 2.4.6 (OpenEye Scientific Software, Santa Fe, NM; http://www.eyesopen.com).[44,45]

SLIDE and other docking tools handle cofactors as rigid parts of the protein and therefore, cofactors can have strong constraints on ligand docking.[39,40] In addition, covalently bound ligands are generally interpreted as unfavorable van der Waals collisions during docking processes. Methylidene carbon of the MIO cofactor, which lies in bonding distance from the amino group of the substrate caused unfavorable steric collisions and forced the substrate to dock in a catalytically incompetent orientation. Thus, the alkene carbon atoms of the MIO were removed to facilitate the ligand docking in *Pa*PAM active site.

For SLIDE docking of substrates **2** – **22**, a ligand-based template was created using known hydrophobic and hydrogen-bonding interactions of α-phenylalanine (**1**) with the active site residues. This template was used as a basis for docking other substrates in *Pa*PAM active site. Interactions of the substrate carboxylate- and amino-groups were used as key points to anchor the substrates in both SLIDE and Szybki docking.

The sum of protein-ligand interaction energy [$E_{(p\text{-}l)}$] and ligand internal energy [$E_{(l)}$] values for docked ligand candidates were calculated using Szybki.[41-43] The $E_{(p\text{-}l)}$ term was consisted of electrostatic Coulombic [$E_{C(p\text{-}l)}$] and steric van der Waals interaction energy [$E_{V(p\text{-}l)}$]

terms for each docked conformer. Two approaches were employed to calculate the aforementioned energy terms of the ligand-*Pa*PAM complexes of **1** – **22**. In the first model (static model), the *Pa*PAM binding site was kept in its crystallographic orientation and the energy terms were calculated without any energy minimization. The second model, which is a flexible model, however, allowed the rotation of protein side chains within 4 Å and ligand aryl ring to relieve unfavorable van der Waals interactions.

The correlation coefficient between each energy term and experimental K_M was calculated to understand the energy terms that dictate the substrate binding in *Pa*PAM. For the static ligand modeling, the linear correlation coefficient between [$E_{(p\text{-}l)}$ + $E_{(l)}$] and K_M was 0.48. $E_{V(p\text{-}l)}$ and $E_{C(p\text{-}l)}$ which are components of $E_{(p\text{-}l)}$, had correlation coefficients of 0.54 and 0.33, respectively. The lower correlation between the Coulombic energy and K_M compared to that of van der Waals interaction energy, reflects that the steric effects in the protein-ligand complex and within the ligand are dominant over electrostatic interactions upon substrate binding. Interestingly, energy minimization lowered the correlation coefficient between [$E_{(p\text{-}l)}$ + $E_{(l)}$] and K_M to 0.35. This suggests that the crystallographic orientation of *Pa*PAM active site and the substrates provide the most favorable conformation for the analogues used in this study. The energy minimization protocol likely cause side chain rotations that may reflect catalytically unproductive conformations. For example, nitro substituent was rotated out-of-plane relative to the phenyl ring during energy minimization. However, the analysis of 200 nitrophenyl groups in small-molecule crystal structures in the Cambridge Structural Database 1.1.1 (http://webcsd.ccdc.cam.ac.uk) indicated that 87.5% of the nitrophenyl groups are entirely co-planar, regardless of other features in the structure.[46]

4.3.6.2.1. Preferred Conformations of Ring-substituted Substrates

To identify the preferred binding orientations of *ortho*- and *meta*-substituents, the sum of protein-ligand interaction energy [$E_{(p\text{-}l)}$] and ligand internal energy [$E_{(l)}$] values were calculated for docked *NH_2-cis* and *NH_2-trans* conformers. Van der Waals interaction energy [$E_{V(p\text{-}l)}$] of preferred orientations were also extracted for each docked substrate. If the difference in total energy [$E_{(p\text{-}l)}$ + $E_{(l)}$] between two conformations was ≤25 kcal/mol, the substrates were considered to have no preference for *NH_2-cis* or *NH_2-trans* orientation.

Several active site residues caused unfavorable van der Waals overlaps with the ring substituted substrates binding to *Pa*PAM active site (Figure 4.11A). Compared to *NH_2-cis* conformers, *NH_2-trans* conformers of *ortho*-substituted substrates have less steric barriers created from Leu104 and Leu216. *NH_2-cis* conformers were sterically hindered from Tyr320, Phe428 and Gln456 (Figure 4.11B). Consequently, *o*-methyl (**6**), *o*-bromo (**20**), *o*-chloro (**21**), and *o*-nitro (**22**) energetically favored the *NH_2-trans* orientation (Table A.2.1). However, *o*-fluoro (**10**) substituent with a smaller van der Waals radius had no preference for binding in either orientation. Interestingly, bulkier *o*-methoxy (**19**) substituent showed a lower [$E_{(p\text{-}l)}$ + $E_{(l)}$] energy for the *NH_2-cis* conformer likely due to the favorable hydrogen-bonding interactions of the methoxy group with active site Tyr320 (Figure A.2.39).

For *meta*-substituted substrates, *NH_2-cis* conformers encounter lower steric barriers from Gly85, Tyr320, Phe428 and Gln456, while *NH_2-trans* conformers have higher steric overlaps from Leu104, Val108, and Leu421 (Figure 4.11C). Thus, *m*-bromo (**2**), *m*-chloro (**4**), *m*-nitro (**9**), and *m*-methyl (**13**) preferred to bind in *NH_2-cis* orientation (Table A.2.1). Similar to *ortho*-

substituted analogue, *m*-fluoro (**3**) showed no significant preference for *NH_2-cis* or *NH_2-trans* conformation.

Except *p*-methoxy substituent (**18**), *para*-substrates with a symmetrical aromatic ring showed no significant preference for *NH2-cis* or *NH_2-trans* orientation. However, *para*-substituents encounter van der Waals overlaps with active site residues Val108, Leu421 and Phe428 (Figure 4.11D). Bulkier *t*Bu group was not productive at *para*-position likely due to the unfavorable steric constrains for binding. However, bulky, methoxy substituent of **18** avoids steric repulsion due to its rotational flexibility and preferred to orient towards the NH_2 group in the active site.

The binding affinity order for all substrates approximately corresponded to the van der Waals (vdW) radii of the substituents. *Pa*PAM bound substrates with a fluoro group (~1.5 Å) the best, followed by methyl (~1.9 Å), then bromo and chloro groups (~1.8 Å). All three fluoro substituted substrates (**3**, **5**, and **10**) bound to *Pa*PAM better than the natural substrate. The least favorable substrate binding to *Pa*PAM contained the bulkiest substituents: nitro (~3.1 Å; from the vdW radii of the C_{ar}–N bond length and the terminal O–N=O) and methoxy (~3.4 Å; from the vdW radii of the C_{ar}–O bond and the methyl C–H bonds of the methoxy).[47,48] *p*-Methoxy substrate **18** showed the least favorable binding with the highest K_M of all the substrates. Surprisingly, *o*-methoxy (**11**) (K_M = 164 μM) group bound *Pa*PAM better than expected from its calculated $E_{V(p\text{-}l)}$ (108 kcal/mol).

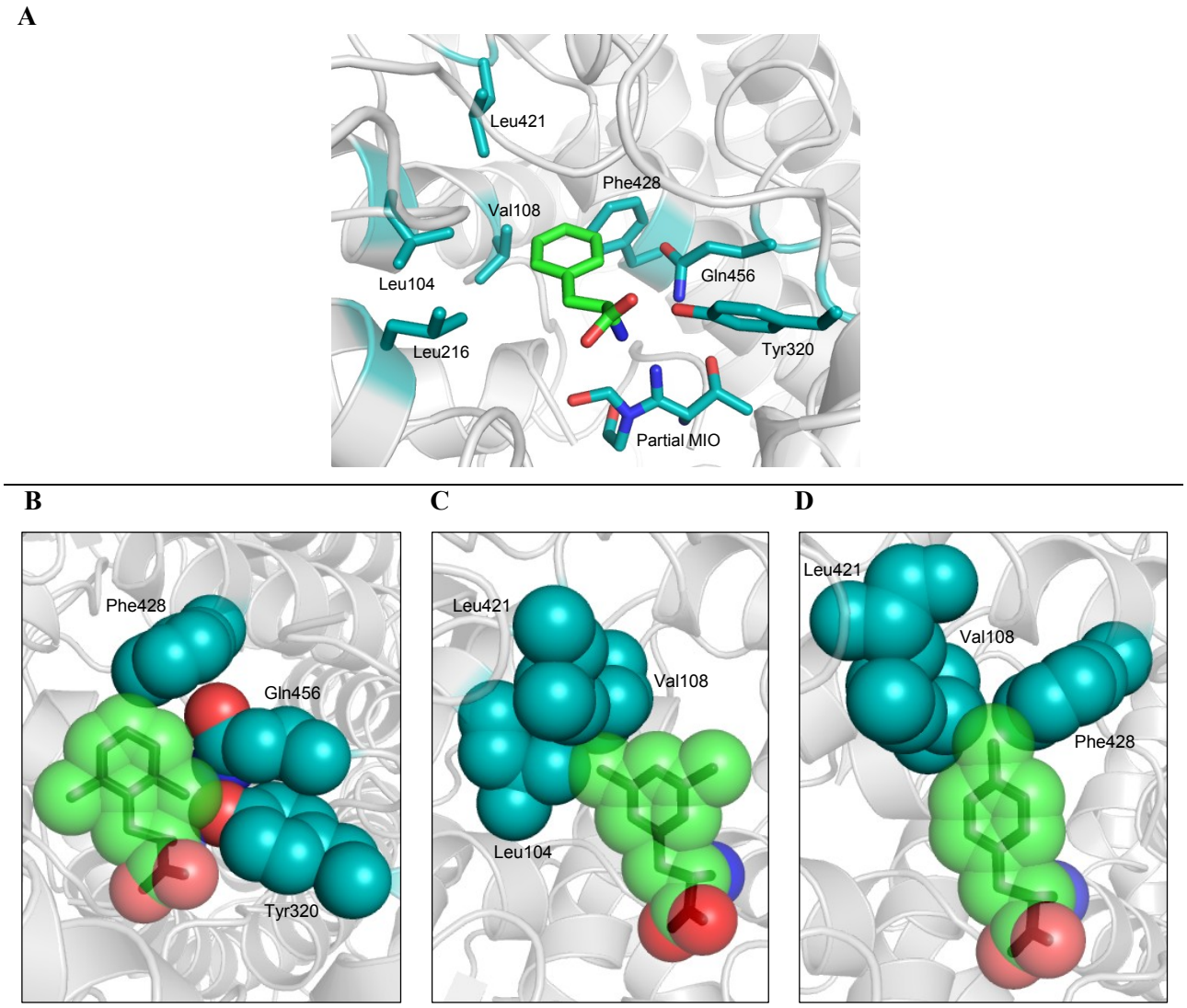

Figure 4.11. *Pa*PAM active site residues that cause van der Waals overlap with the ring-substituted substrates (*A*) and, the active site residues that sterically hinder the *ortho*- (*B*), *meta*- (*C*), and *para*- (*C*) substituted substrates. Partial MIO group is shown. Atoms are color-coded as: carbon: teal (active site residues)/green (ligand); nitrogen: blue; oxygen: red.

4.3.7. Kinetic Parameters and Interaction Energies of Heteroaromatic Substrates

Of the three heteroaromatic substrates, 2-furylalanine (**7**), showed the highest $k_{\text{cat}}^{\text{total}}$ (0.236 s^{-1}) and the catalytic efficiency. 3-Thienylalanine (**8**) turned over with a 1.7-fold slower rate compared to **7**. The 1.2-fold reduction in K_M, however increased the catalytic efficiency of 3-thienylalanine analogue **8**. In contrast to **7** and **8**, K_M of 2-thienylalanine (**12**, 132 μM) was almost similar to the natural substrate **1**. However, **12** was among the substrates with a lower $k_{\text{cat}}^{\text{total}}$ (0.026 s^{-1}) for the isomerization reaction. $k_{\text{cat}}^{\text{total}}$ values of *Pa*PAM for all heteroaromatic substrates (**7**, **8**, and **12**) are about 1.4- to 12-fold lower than that for **1**.

Evaluation of resonance structures of 3-thienylalanine (**8**) showed that a δ^- charge resides on C_{ipso} of the thienyl ring (Figure 4.12A, resonance path 'a') analogous to δ^- charge on C_{ipso} of substrates **5**, **14** – **18** containing an electron-donating *para*-substituent on the phenyl ring (see Figure 4.7F or H). For substrate **8**, however, two vicinal δ^- charges induce a "δ^+" on the C_{ipso}, which likely reduce the magnitude of the δ^- at C_{ipso} (Figure 4.12A, resonance path 'b'). Thus, the lower magnitude δ^- at C_{ipso} of **8**, compared to the δ^- at C_{ipso} for , **5**, **14** – **18** (0.013 – 0.053 s^{-1}) likely affected the rate-determining deprotonation step lesser, as evidenced by its 3- to 10-fold higher $k_{\text{cat}}^{\text{total}}$ of *Pa*PAM for **8** (0.143 s^{-1}).

Similar to the resonance hybrid of **8**, 2-thienylalanine substrate has a resonance structure with a δ^- charge on C_{ipso} (Figure 4.12B, resonance path 'a'). However, **12** has only one δ^- charge vicinal to C_{ipso} (Figure 4.12B, resonance path 'b'), and therefore the induced charge on C_{ipso} (illustrated as "$f\delta^+$") is less than the induced "δ^+" in **8** flanked by two vicinal δ^- charges (Figure 4.12B, resonance path 'b'). Consequently, C_{ipso} of **12** is more δ^- charged compared to **8**. The greater δ^- charge on C_{ipso} of **12** than on **8** likely conflicts with the δ^- formed on C_β during the

transition state of the deprotonation step. Thus, this effect likely caused the ~6-fold slower *Pa*PAM reaction for **12** compared to **8** (0.026 s^{-1} for **12** and 0.143 s^{-1} for **8**).

It was interesting that the 2-furylalanine (**7**, 0.236 s^{-1}) was turned over by *Pa*PAM ~9 fold faster than the analogous 2-thienylalanine (**12**, 0.026 s^{-1}), particularly, since these two heteroaromatic substrates have similar resonance hybrids (Figure 4.12B). However, more electronegative oxygen compared to sulfur of **12** likely induced a larger δ^+ charge on the vicinal C_{ipso} of **7**. Moreover, more electronegative oxygen of **7** distributes its lone pair electrons less than sulfur, and thus likely reduced the magnitude of the negative charge (δ^-) delocalized on C_{ipso} (Figure 4.12B, resonance path 'a'). As a result, the relative magnitude of δ^+ on C_{ipso} of **7** is larger than that of **12**. Increased magnitude of δ^+ at C_{ipso} promotes the removal of H_β in the *Pa*PAM reaction. The higher proportion of (2-furyl)acrylate (65.2%) from **7** compared to only 9.1% (2-thienyl)acrylate from **12**, suggests that the amination step during the isomerization of **7** is negatively affected by the comparatively larger δ^+ on C_{ipso}.

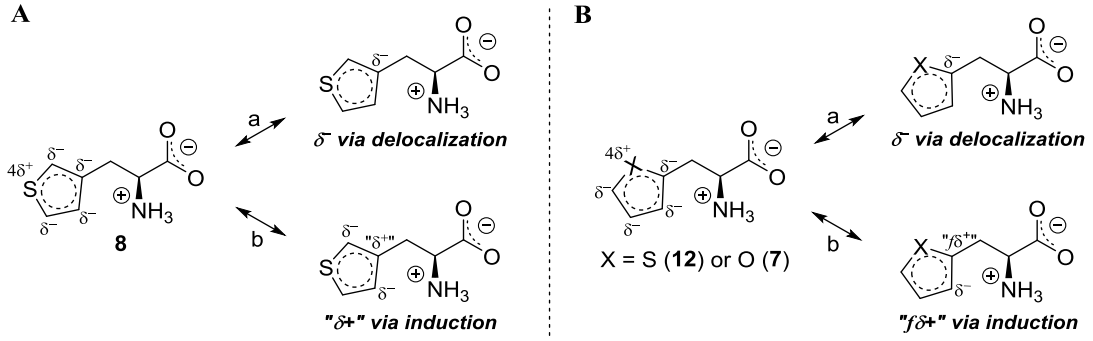

Figure 4.12. Resonance hybrids of 3-thienylalanine (8) (*A*) and, composite resonance hybrids of 2-furylalanine (7) and 2-thienylalanine (12) (*B*). The induced charges on C_{ipso} are designated in quotation marks ("").

Heteroaromatic substrates **7**, **8**, and **12** were also analyzed for their preferred binding orientations in *Pa*PAM active site. Analogous to NH_2-*cis* and -*trans* conformations of aryl substituted substrates, heteroatom of the aryl rings were also oriented in the same- or opposite-side of the substrate amino group. According to energy calculations, both conformations of **7**, **8**, and **12** were equally preferred in *Pa*PAM active site. Calculated van der Waals energy [$E_{V(p\text{-}l)}$] (**7** and **8**: 21 kcal/mol; and **12**: 20 kcal/mol) predicted that all three substrates bind equally well as the natural substrate **1** (19 kcal/mol, 168 μM). However, only 2-thienylalanine (**12**) showed a higher affinity with a lower K_M value (132 μM). Surprisingly, both 2-furylalanine (**7**) and 3-thienylalanine (**8**) bound less tightly to *Pa*PAM (K_M = 415 and 337 μM respectively).

4.4. Conclusion

*Pa*PAM-catalyzed α/β-isomerization reaction has broad substrate scope for 19 arylalanine analogues. α-Arylalanine analogues including fluoro-, chloro-, bromo-, methyl-, methoxy-, and nitro-substituents on the phenyl ring as well as furyl- and thienyl-alanines with heteroaromatic rings were isomerized to their respective β-arylalanine products by *Pa*PAM catalysis. The influence of the substituents on the k_{cat} of *Pa*PAM revealed a concave-down correlations with Hammett substituent constants (σ). The trend of these correlations[37] suggests that the rate-determining step changes from the elimination to the hydroamination step based on the direction and magnitude of the electronic properties of the substituent.

The computational analyses provided a means to predict the docking conformation of substituted 22 arylalanine substrates. The information from computational modeling was useful for designing future targeted amino acid mutagenesis of *Pa*PAM to increase the catalytic efficiency by improving the binding affinity for various other non-natural substrates. The K_M of *Pa*PAM was higher for several substrates with *meta*- and *para*-substituents (except fluoro and methyl) than for **1**. The presumed lower binding affinity was likely due to steric interactions between the substituents and the active site residues of *Pa*PAM. *meta*-Substituted substrates were shown to prefer the *NH_2-cis* configuration to avoid steric clashes with branched hydrophobic residues. Mutation of Leu104, Val108, and Leu421 to alanines may improve the binding of *meta*-substituted substrates by providing flexibility to bind in the *NH_2-cis* or *NH_2-trans* configuration. Furthermore, computational docking predicted that *para*-substituents sterically clash with Phe428, Val108, and Leu421. Therefore, exchange of these residues for alanine may facilitate the binding of *para*-substituted substrates. Surprisingly, the computational

analysis predicted that all *ortho*-substituted α-arylalanines bound well to *Pa*PAM; however, relief of the active site sterics may enable these *ortho*-substituted α-arylalanines to better access a catalytically competent conformation and improve the turnover number for these substrates.

APPENDIX

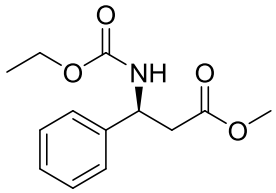

m/*z* = 251

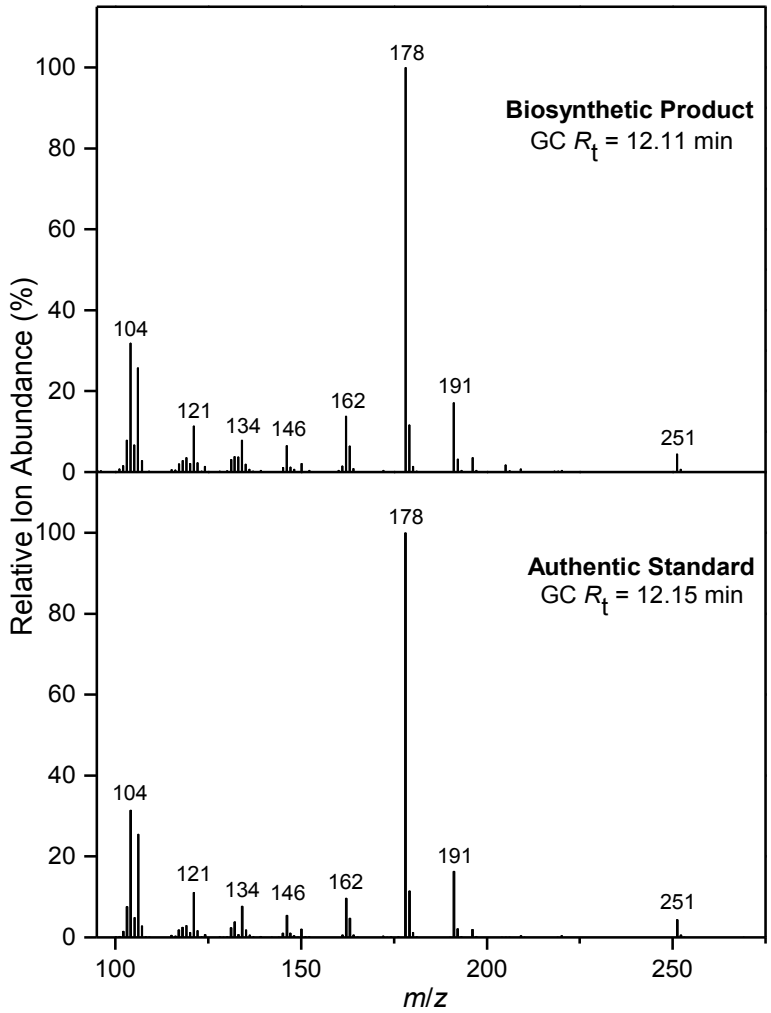

Figure A.2.1. EI-MS spectra of the *N*-(ethoxycarbonyl) methyl ester derivatives of biosynthetic β-phenylalanine made from *Pa*PAM catalysis (top) and authentic β-phenylalanine (bottom). GC retention times (GC R_t) are shown.

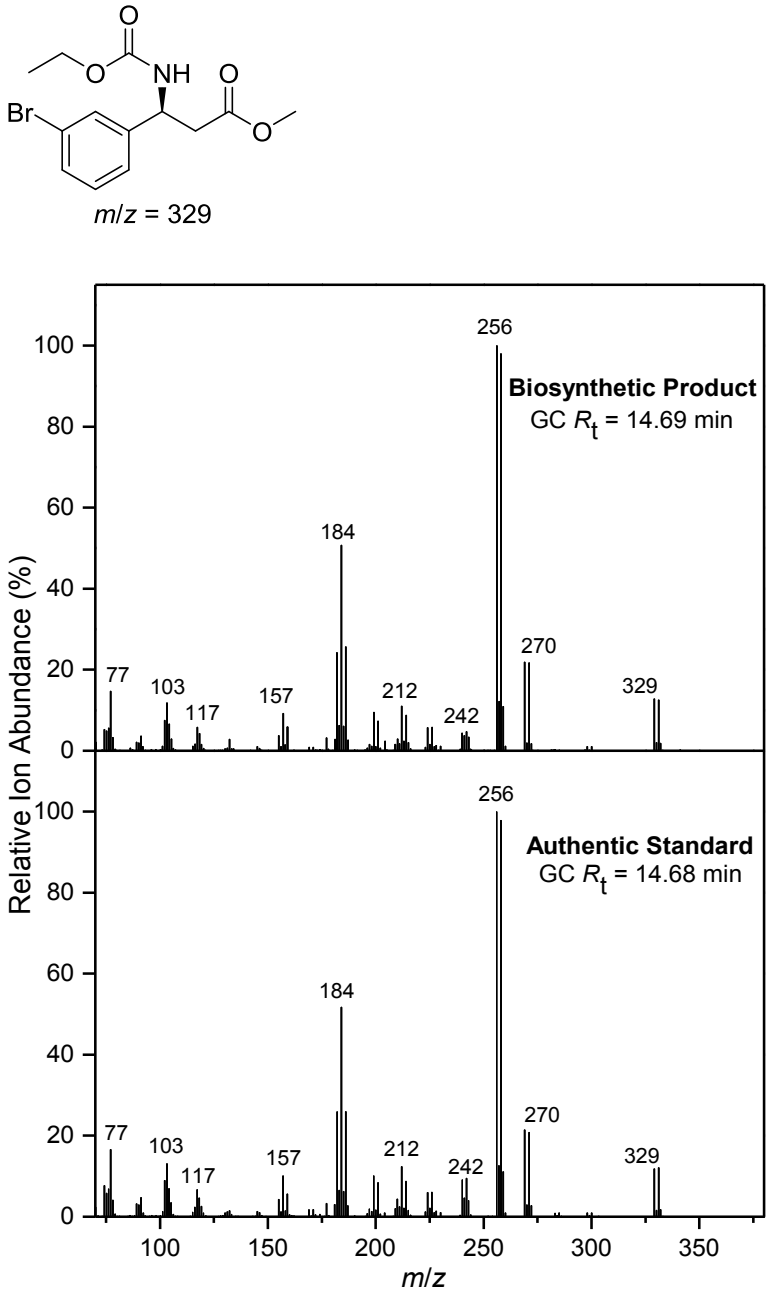

Figure A.2.2. EI-MS spectra of the *N*-(ethoxycarbonyl) methyl ester derivatives of biosynthetic *m*-bromo-β-phenylalanine made from *Pa*PAM catalysis (top) and authentic *m*-bromo-β-phenylalanine (bottom). GC retention times (GC R_t) are shown.

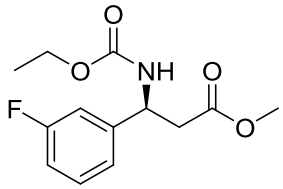

m/z = 269

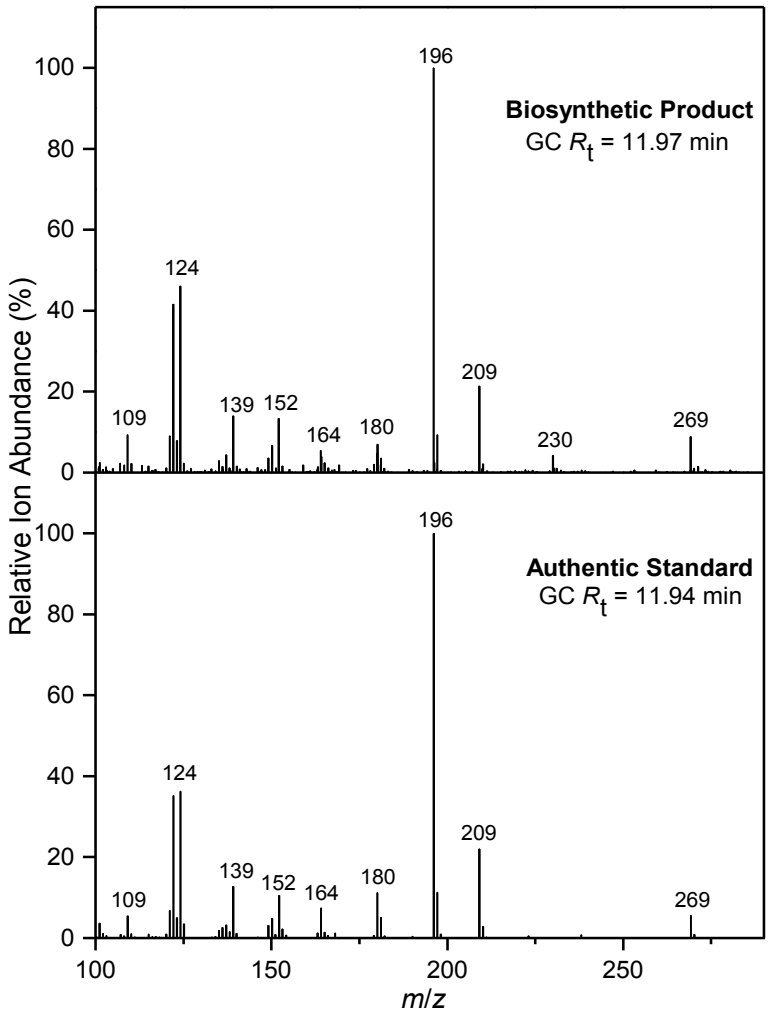

Figure A.2.3. EI-MS spectra of the *N*-(ethoxycarbonyl) methyl ester derivatives of biosynthetic *m*-fluoro-β-phenylalanine made from *Pa*PAM catalysis (top) and authentic *m*-fluoro-β-phenylalanine (bottom). GC retention times (GC R_t) are shown.

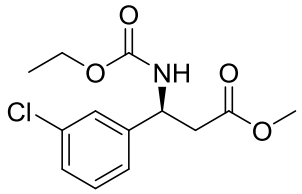

m/z = 285

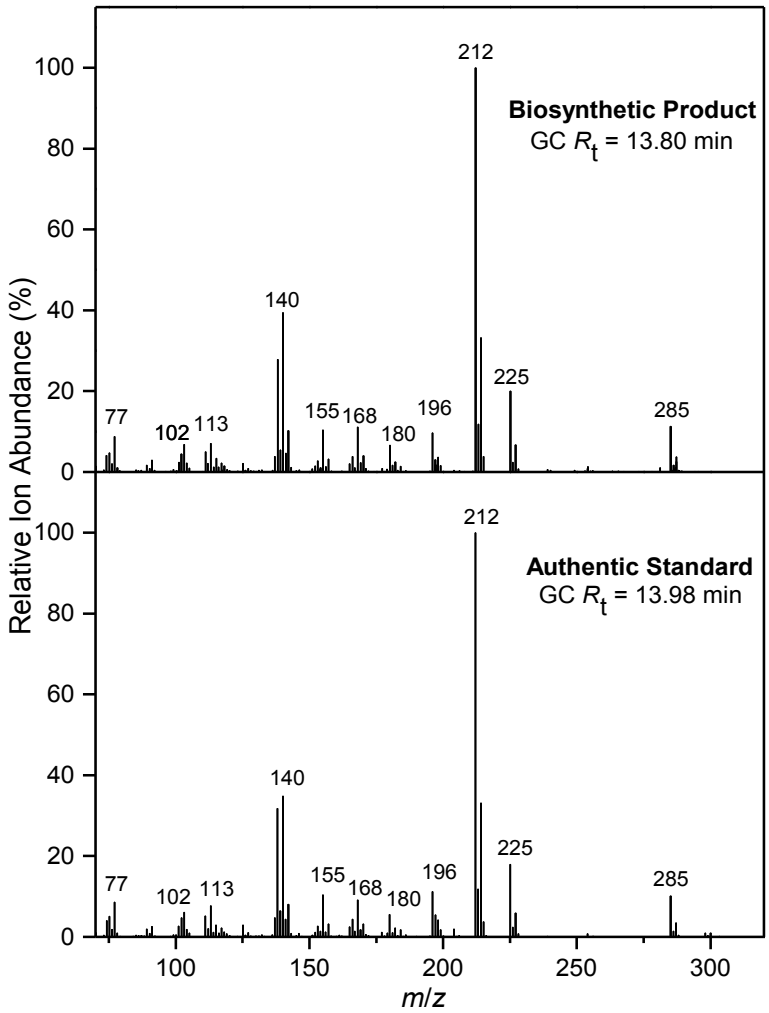

Figure A.2.4. EI-MS spectra of the *N*-(ethoxycarbonyl) methyl ester derivatives of biosynthetic *m*-chloro-β-phenylalanine made from *Pa*PAM catalysis (top) and authentic *m*-chloro-β-phenylalanine (bottom). GC retention times (GC R_t) are shown.

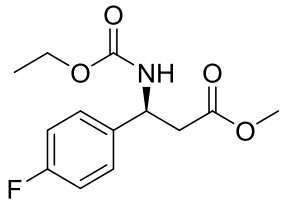

m/*z* = 269

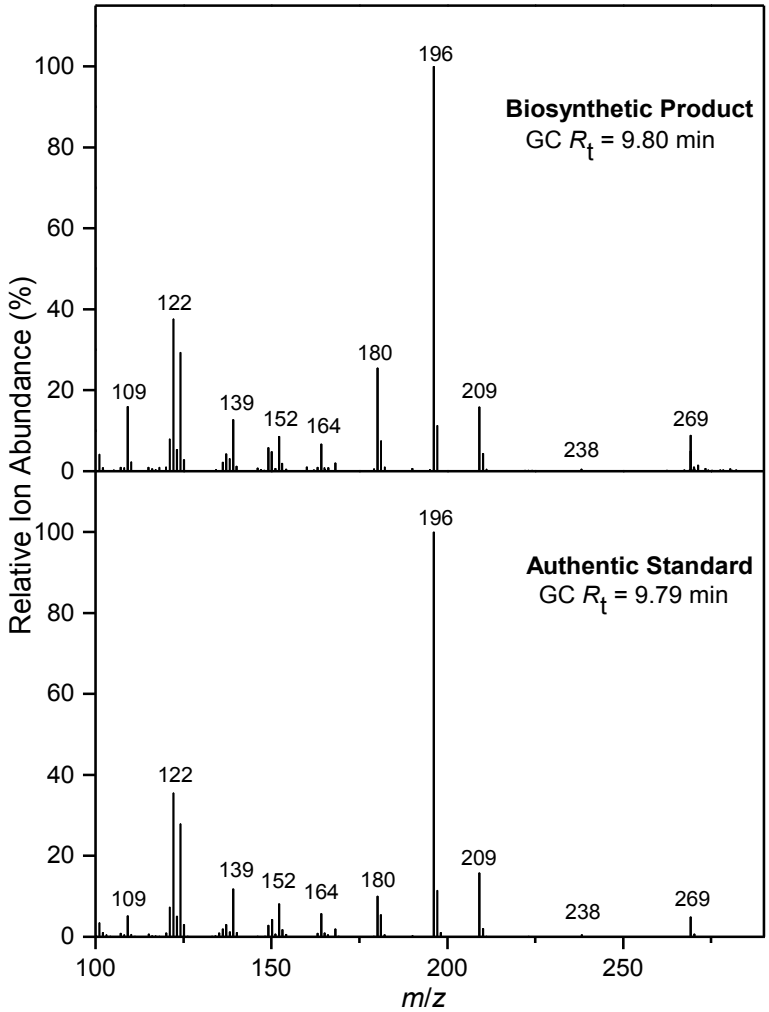

Figure A.2.5. EI-MS spectra of the *N*-(ethoxycarbonyl) methyl ester derivatives of biosynthetic *p*-fluoro-β-phenylalanine made from *Pa*PAM catalysis (top) and authentic *p*-fluoro-β-phenylalanine (bottom). GC retention times (GC R_t) are shown.

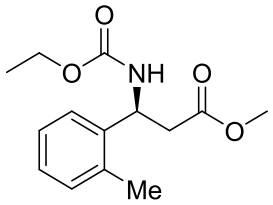

m/*z* = 265

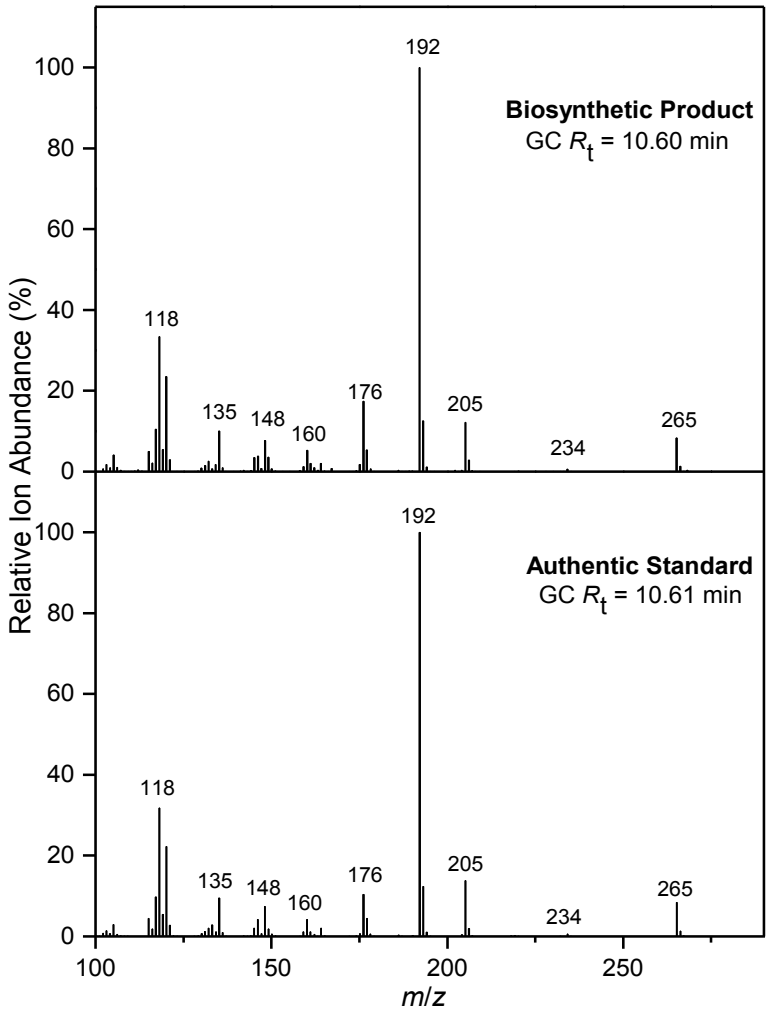

Figure A.2.6. EI-MS spectra of the *N*-(ethoxycarbonyl) methyl ester derivatives of biosynthetic *o*-methyl-β-phenylalanine made from *Pa*PAM catalysis (top) and authentic *o*-methyl-β-phenylalanine (bottom). GC retention times (GC R_t) are shown.

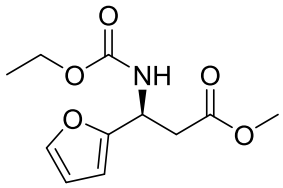

m/z = 241

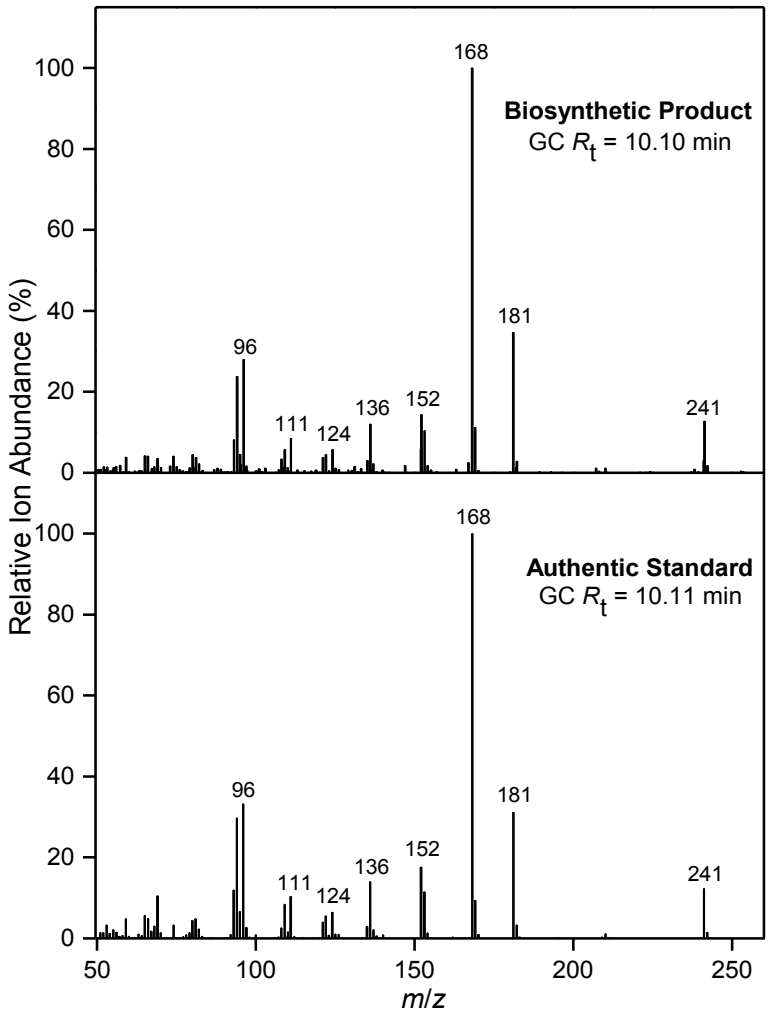

Figure A.2.7. EI-MS spectra of the *N*-(ethoxycarbonyl) methyl ester derivatives of biosynthetic 2-furyl-β-alanine made from *Pa*PAM catalysis (top) and authentic 2-furyl-β-alanine (bottom). GC retention times (GC R_t) are shown.

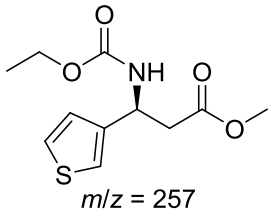

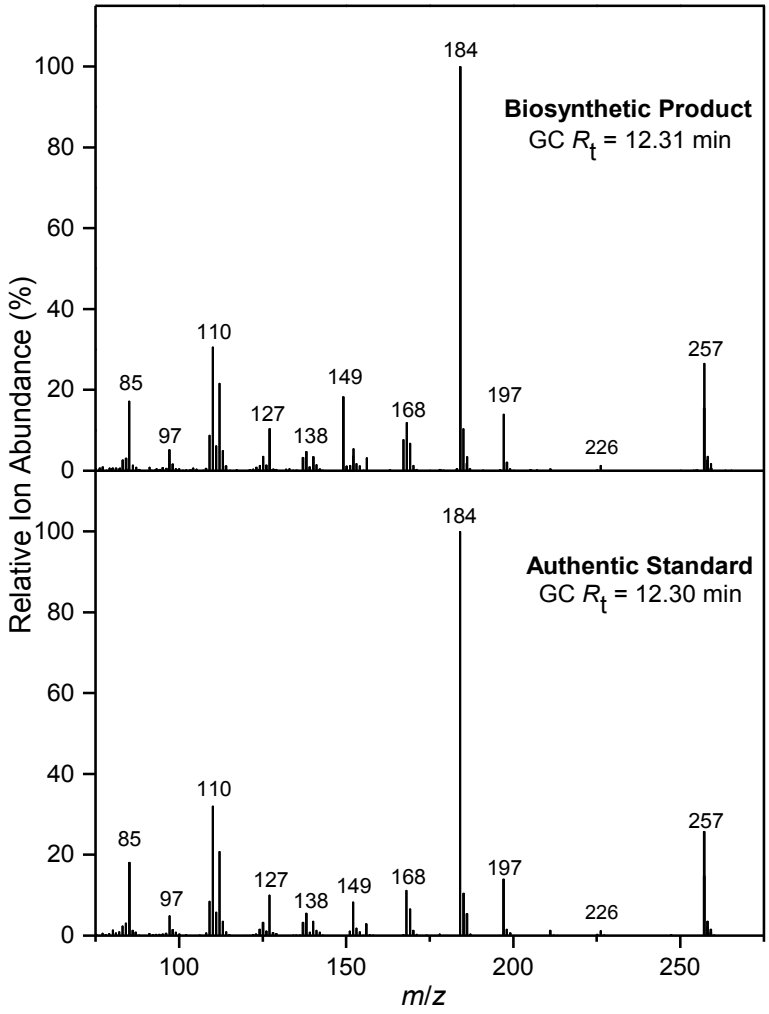

Figure A.2.8. EI-MS spectra of the *N*-(ethoxycarbonyl) methyl ester derivatives of biosynthetic 3-thienyl-β-alanine made from *Pa*PAM catalysis (top) and authentic 3-thienyl-β-alanine (bottom). GC retention times (GC R_t) are shown.

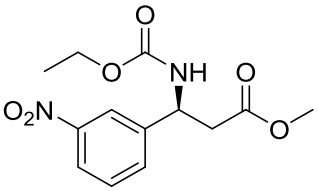

m/z = 296

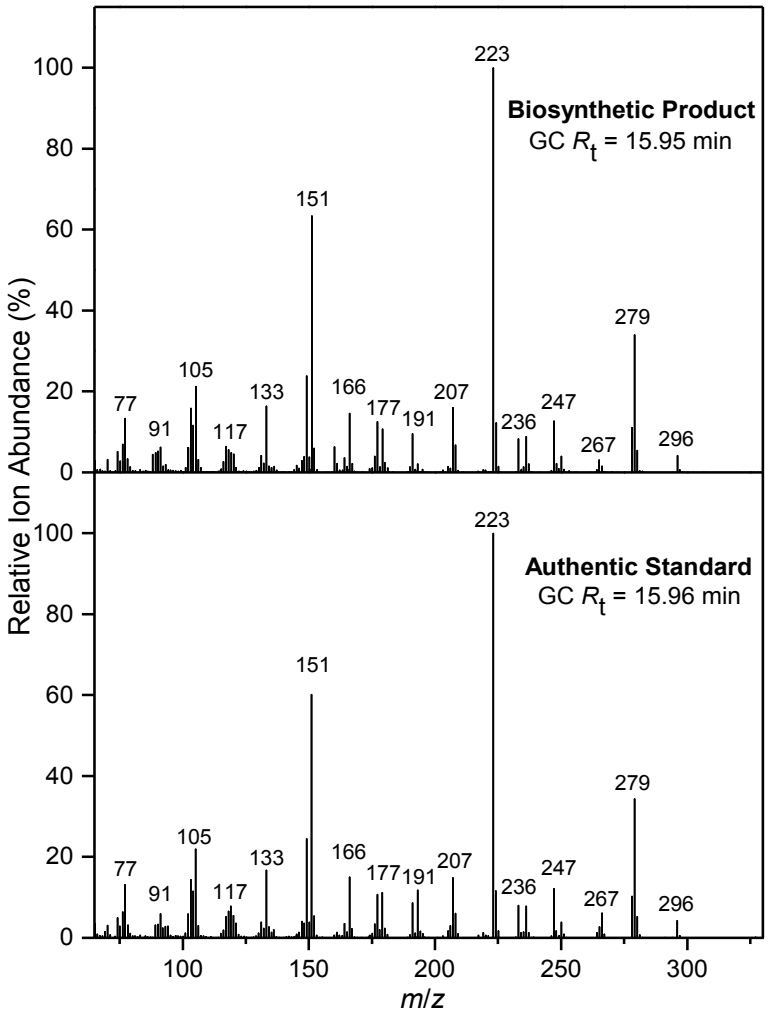

Figure A.2.9. EI-MS spectra of the *N*-(ethoxycarbonyl) methyl ester derivatives of biosynthetic *m*-nitro-β-phenylalanine made from *Pa*PAM catalysis (top) and authentic *m*-nitro-β-phenylalanine (bottom). GC retention times (GC R_t) are shown.

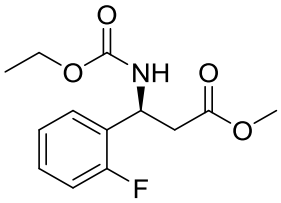

m/z = 269

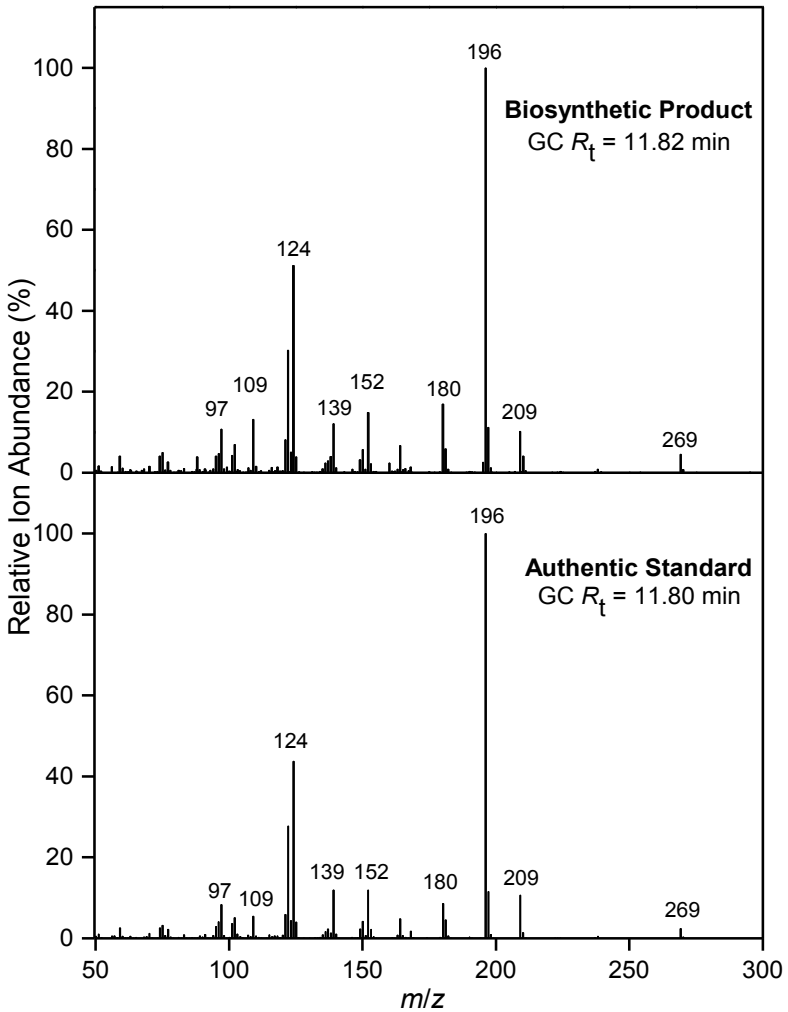

Figure A.2.10. EI-MS spectra of the *N*-(ethoxycarbonyl) methyl ester derivatives of biosynthetic *o*-fluoro-β-phenylalanine made from *Pa*PAM catalysis (top) and authentic *o*-fluoro-β-phenylalanine (bottom). GC retention times (GC R_t) are shown.

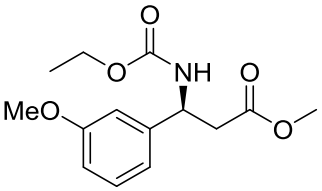

m/z = 281

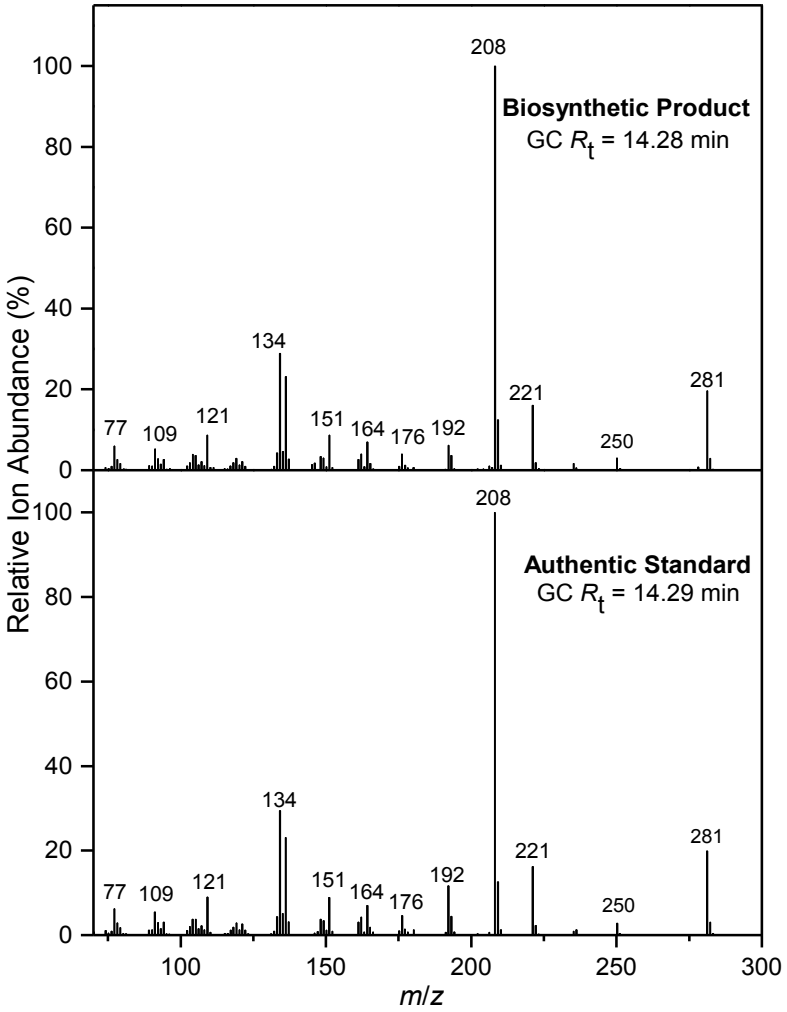

Figure A.2.11. EI-MS spectra of the *N*-(ethoxycarbonyl) methyl ester derivatives of biosynthetic *m*-methoxy-β-phenylalanine made from *Pa*PAM catalysis (top) and authentic *m*-methoxy-β-phenylalanine (bottom). GC retention times (GC R_t) are shown.

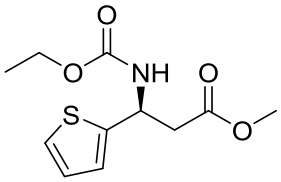

m/*z* = 257

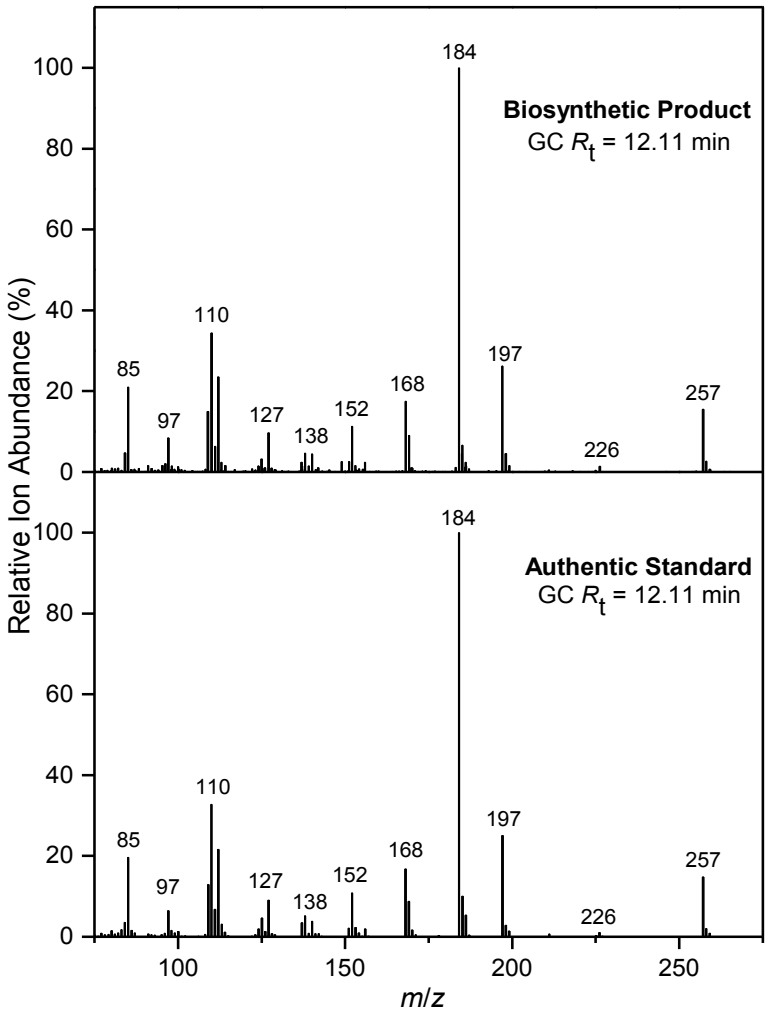

Figure A.2.12. EI-MS spectra of the *N*-(ethoxycarbonyl) methyl ester derivatives of biosynthetic 2-thienyl-β-alanine made from *Pa*PAM catalysis (top) and authentic 2-thienyl-β-alanine (bottom). GC retention times (GC R_t) are shown.

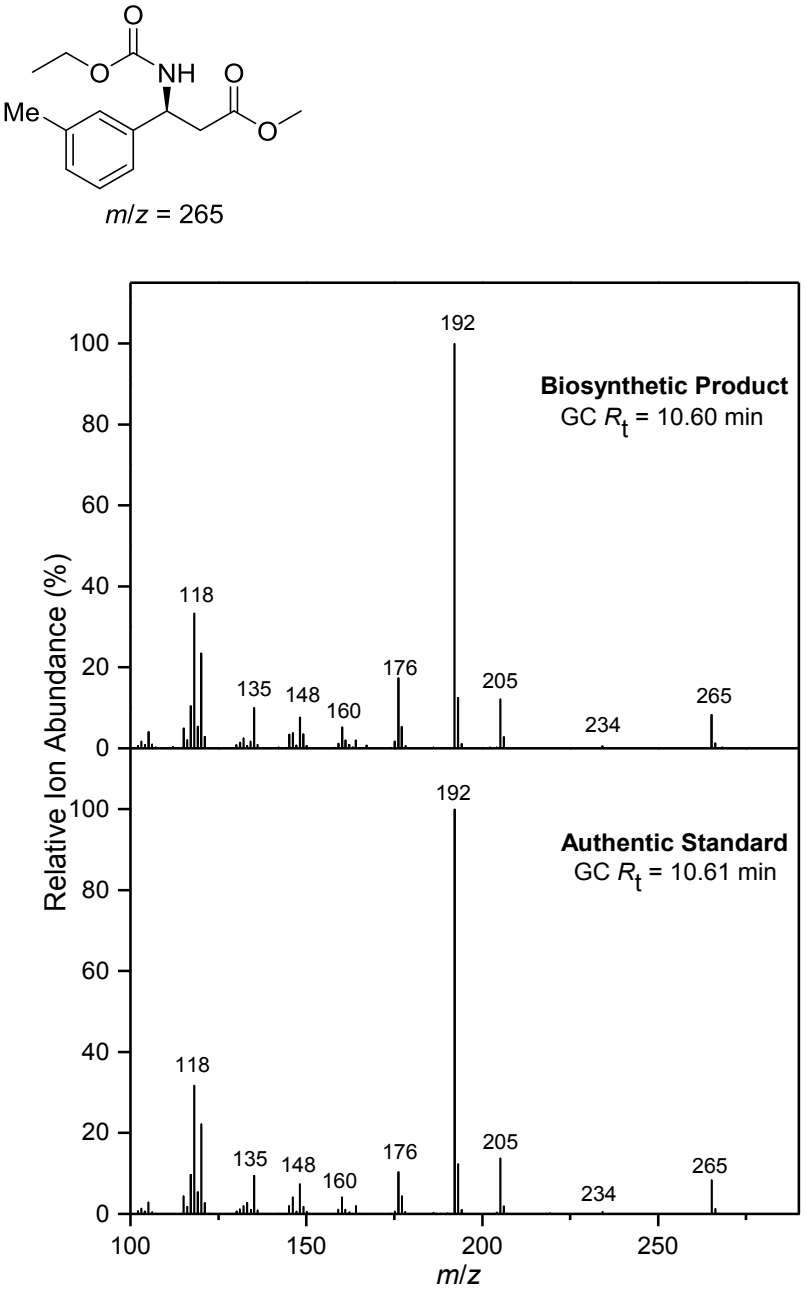

Figure A.2.13. EI-MS spectra of the *N*-(ethoxycarbonyl) methyl ester derivatives of biosynthetic *m*-methyl-β-phenylalanine made from *Pa*PAM catalysis (top) and authentic *m*-methyl-β-phenylalanine (bottom). GC retention times (GC R_t) are shown.

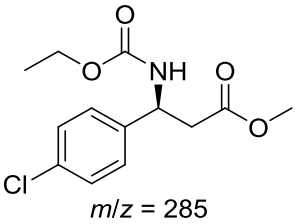

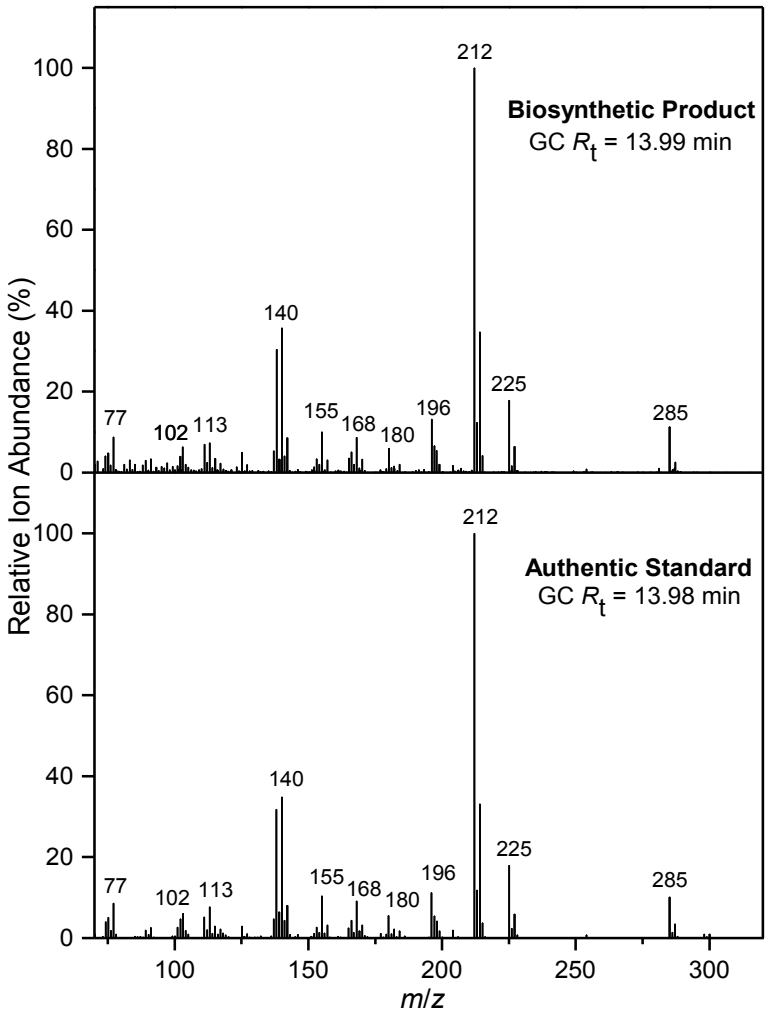

Figure A.2.14. EI-MS spectra of the *N*-(ethoxycarbonyl) methyl ester derivatives of biosynthetic *p*-chloro-β-phenylalanine made from *Pa*PAM catalysis (top) and authentic *p*-chloro-β-phenylalanine (bottom). GC retention times (GC R_t) are shown.

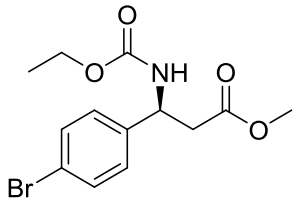

m/z = 329

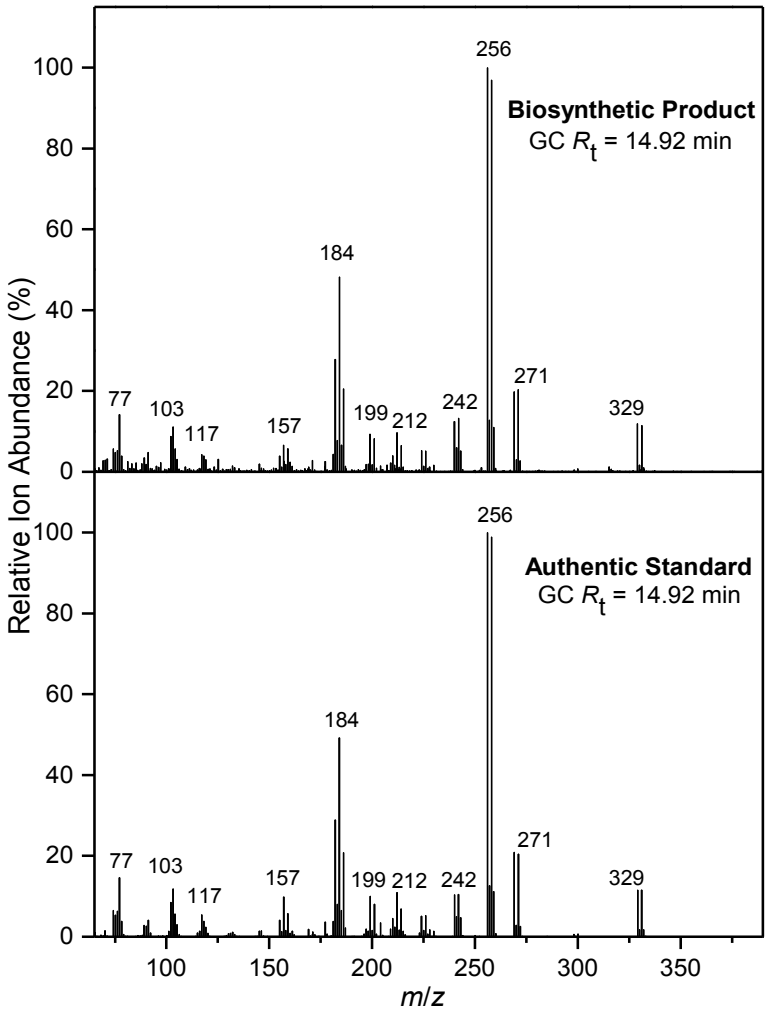

Figure A.2.15. EI-MS spectra of the *N*-(ethoxycarbonyl) methyl ester derivatives of biosynthetic *p*-bromo-β-phenylalanine made from *Pa*PAM catalysis (top) and authentic *p*-bromo-β-phenylalanine (bottom). GC retention times (GC R_t) are shown.

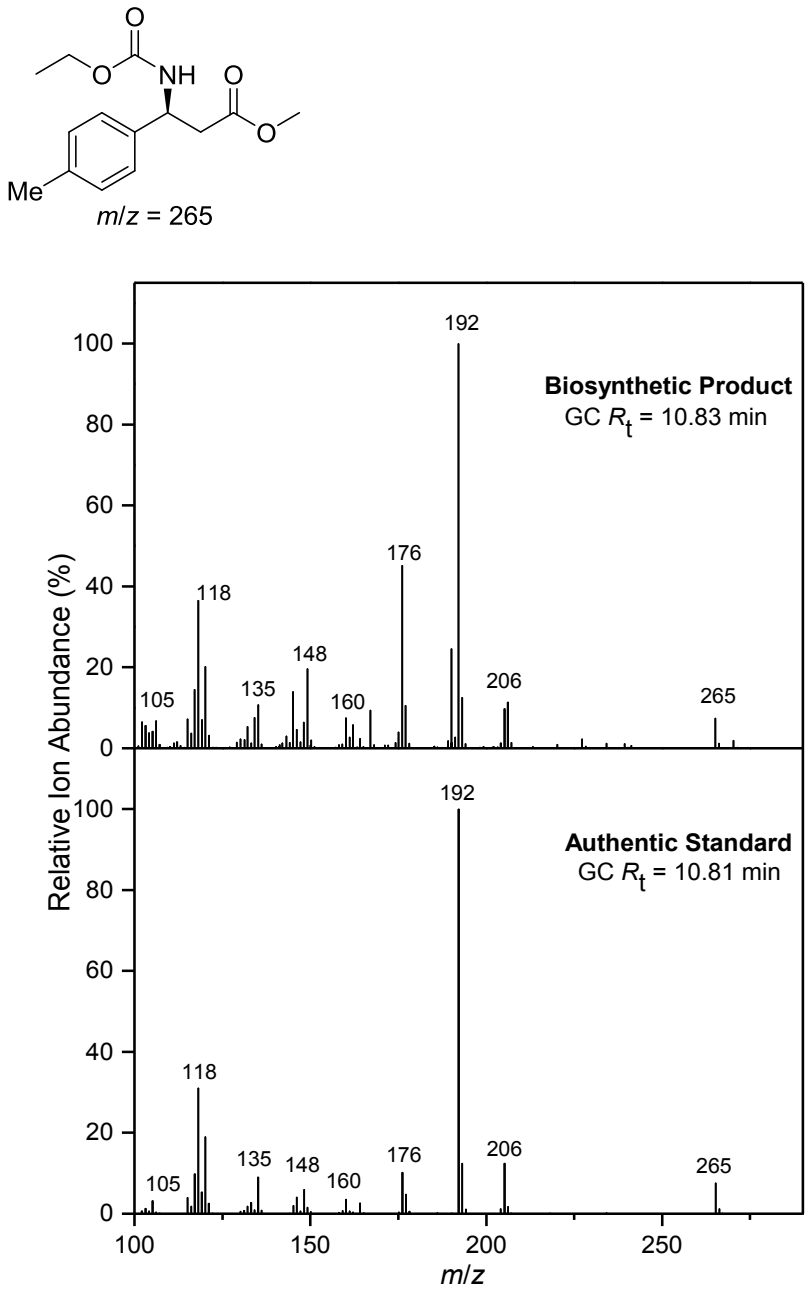

Figure A.2.16. EI-MS spectra of the *N*-(ethoxycarbonyl) methyl ester derivatives of biosynthetic *p*-methyl-β-phenylalanine made from *Pa*PAM catalysis (top) and authentic *p*-methyl-β-phenylalanine (bottom). GC retention times (GC R_t) are shown.

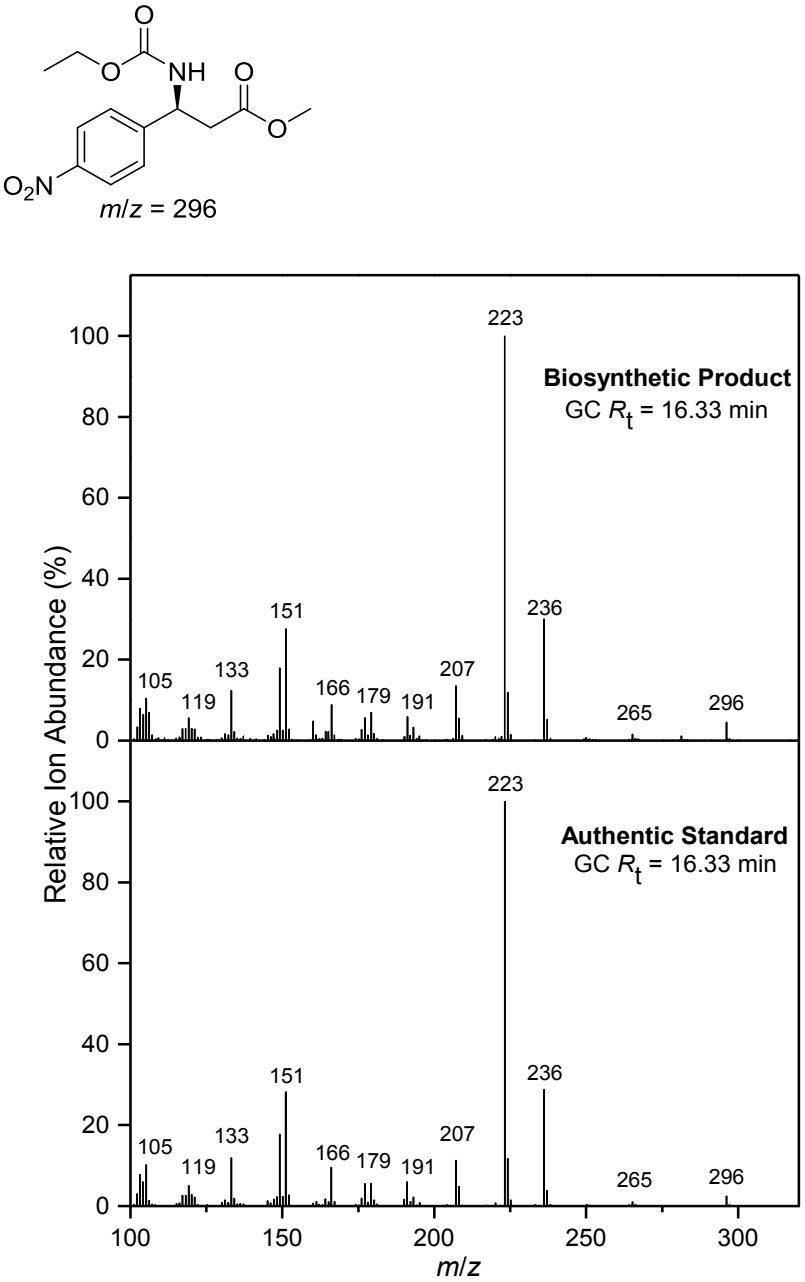

Figure A.2.17. EI-MS spectra of the *N*-(ethoxycarbonyl) methyl ester derivatives of biosynthetic *p*-nitro-β-phenylalanine made from *Pa*PAM catalysis (top) and authentic *p*-nitro-β-phenylalanine (bottom). GC retention times (GC R_t) are shown.

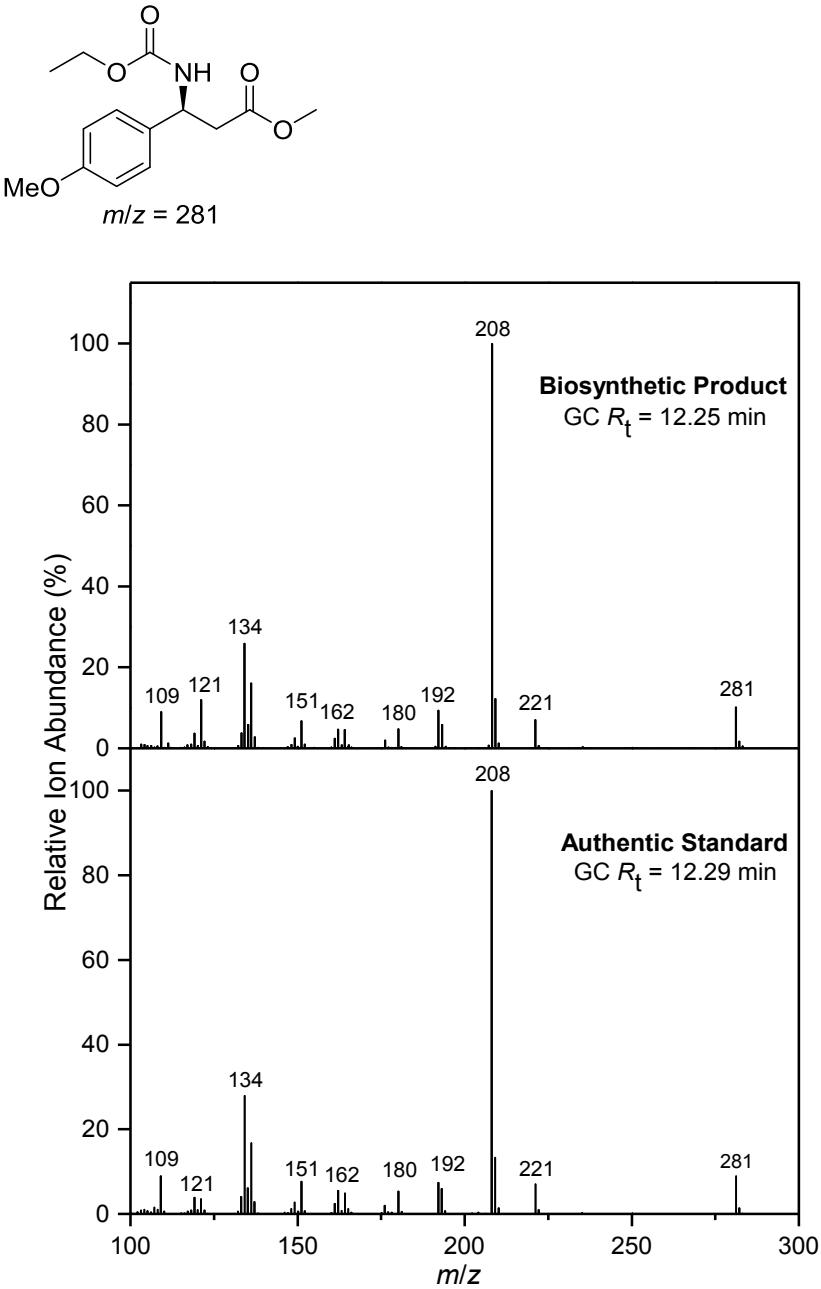

Figure A.2.18. EI-MS spectra of the *N*-(ethoxycarbonyl) methyl ester derivatives of biosynthetic *p*-methoxy-β-phenylalanine made from *Pa*PAM catalysis (top) and authentic *p*-methoxy-β-phenylalanine (bottom). GC retention times (GC R_t) are shown.

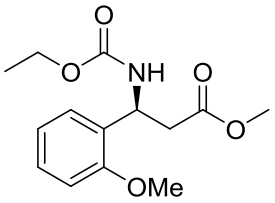

m/z = 281

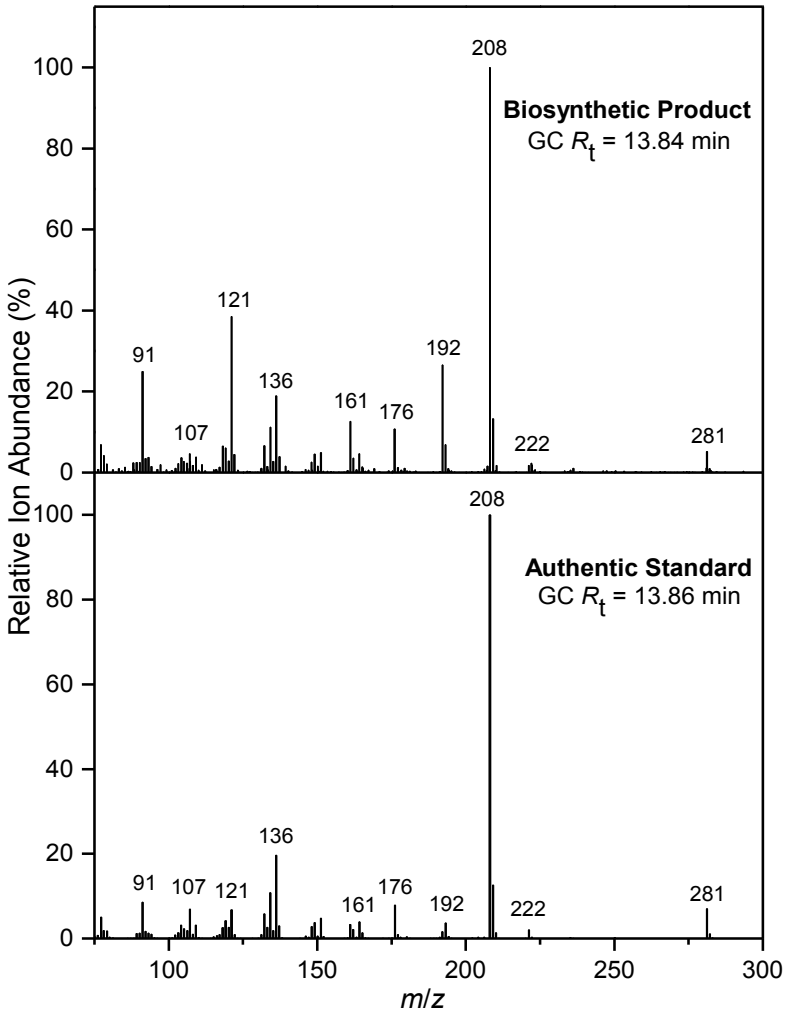

Figure A.2.19. EI-MS spectra of the *N*-(ethoxycarbonyl) methyl ester derivatives of biosynthetic *o*-methoxy-β-phenylalanine made from *Pa*PAM catalysis (top) and authentic *o*-methoxy-β-phenylalanine (bottom). GC retention times (GC R_t) are shown.

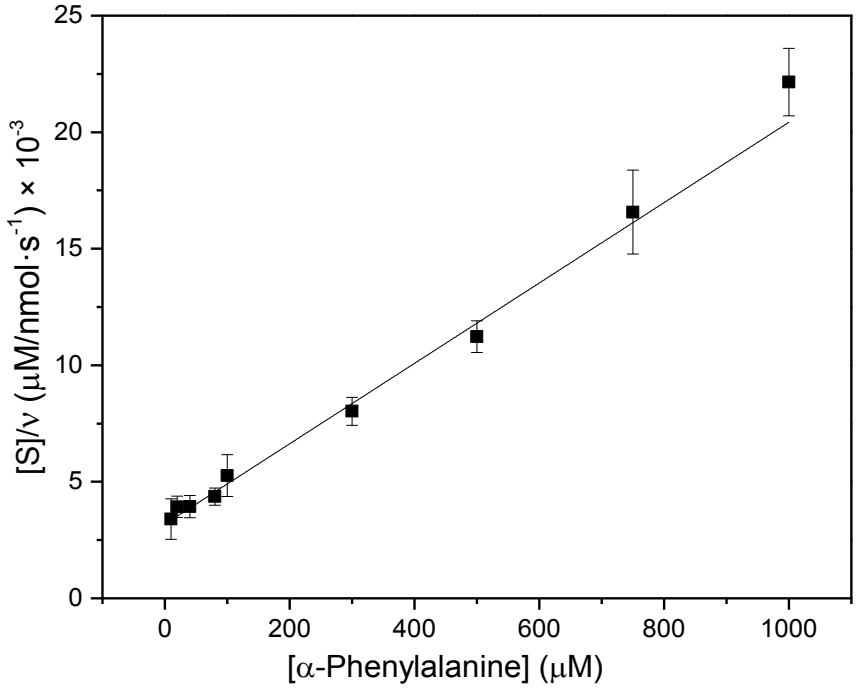

Figure A.2.20. Hanes-Woolf plot of biosynthetic β-phenylalanine (designated as velocity, *v*) catalyzed by *Pa*PAM from α-phenylalanine (S).

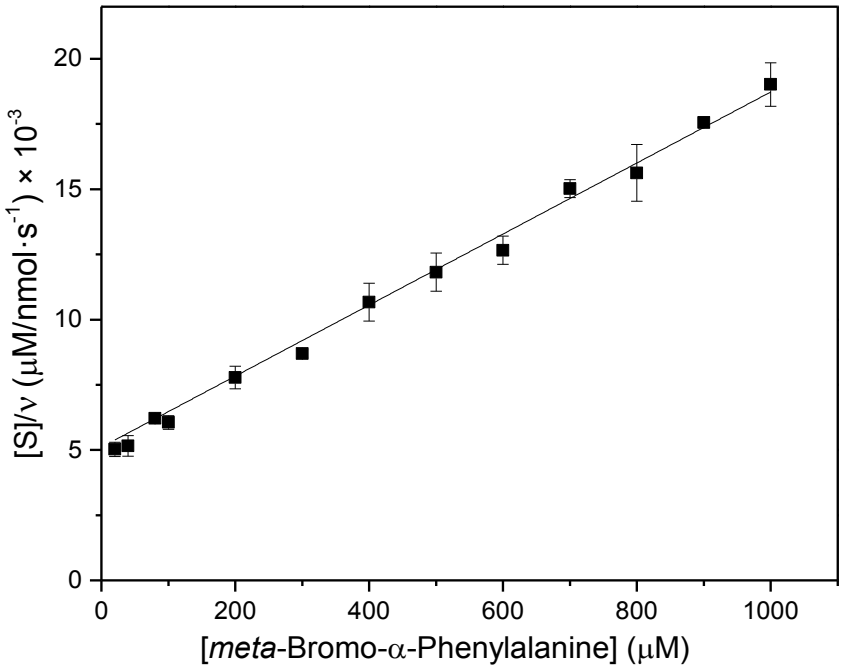

Figure A.2.21. Hanes-Woolf plot of biosynthetic *m*-bromo-β-phenylalanine (designated as velocity, *v*) catalyzed by *Pa*PAM from *m*-bromo-α-phenylalanine (S).

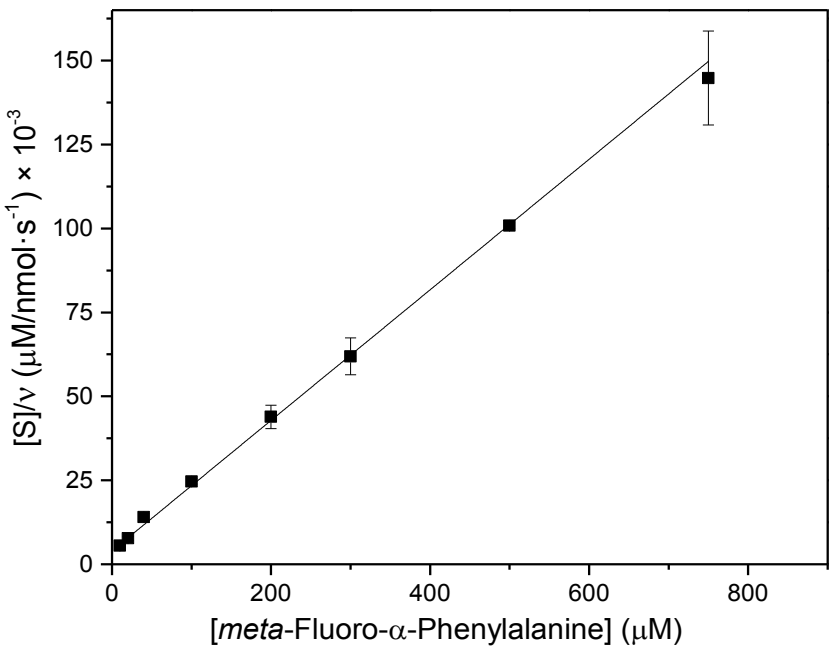

Figure A.2.22. Hanes-Woolf plots of biosynthetic *m*-fluoro-β-phenylalanine (designated as velocity, *v*) catalyzed by *Pa*PAM from *m*-fluoro-α-phenylalanine (S).

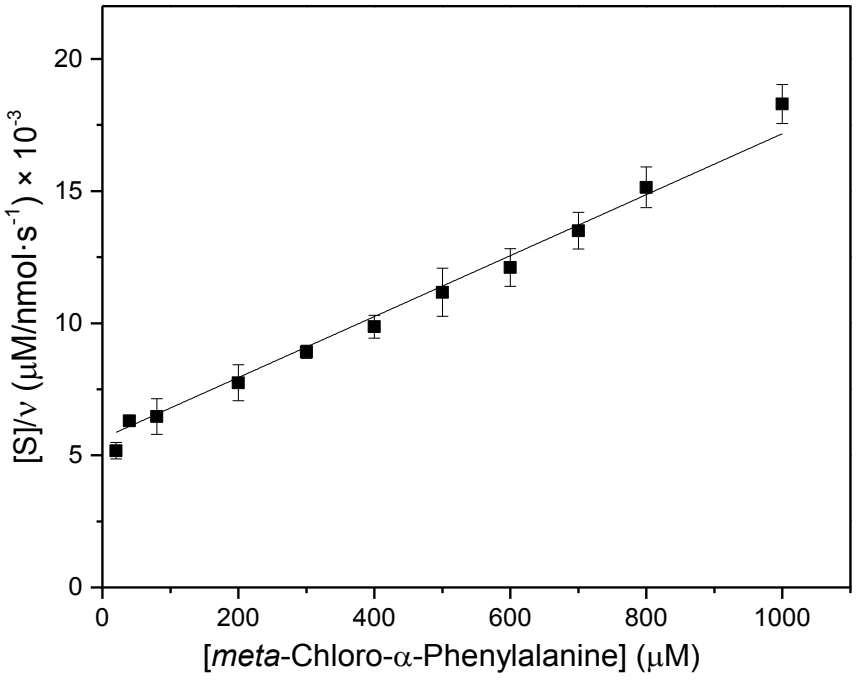

Figure A.2.23. Hanes-Woolf plots of biosynthetic *m*-chloro-β-phenylalanine (designated as velocity, *v*) catalyzed by *Pa*PAM from *m*-chloro-α-phenylalanine (S).

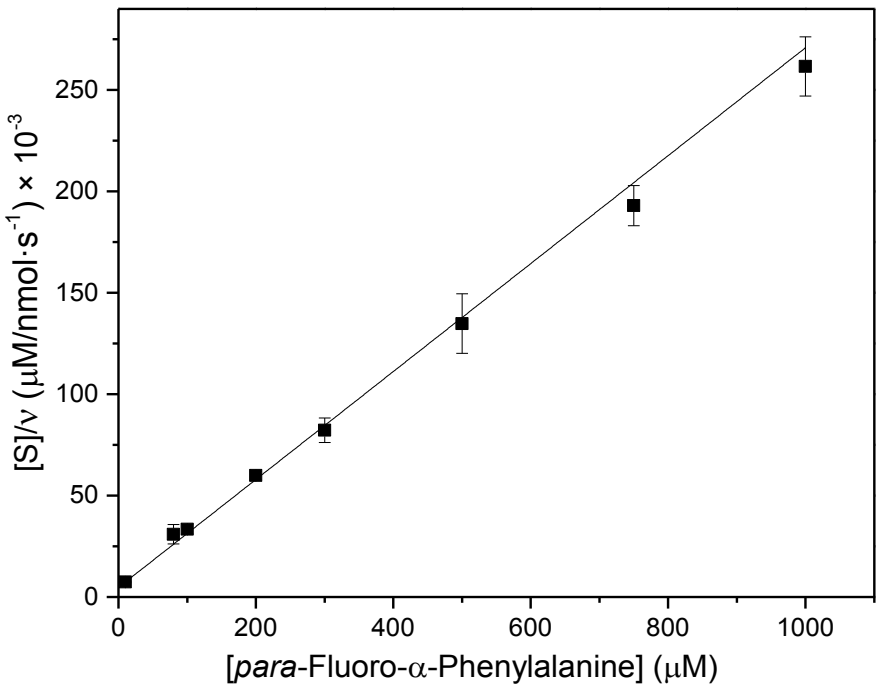

Figure A.2.24. Hanes-Woolf plots of biosynthetic *p*-fluoro-β-phenylalanine (designated as velocity, *v*) catalyzed by *Pa*PAM from *p*-fluoro-α-phenylalanine (S).

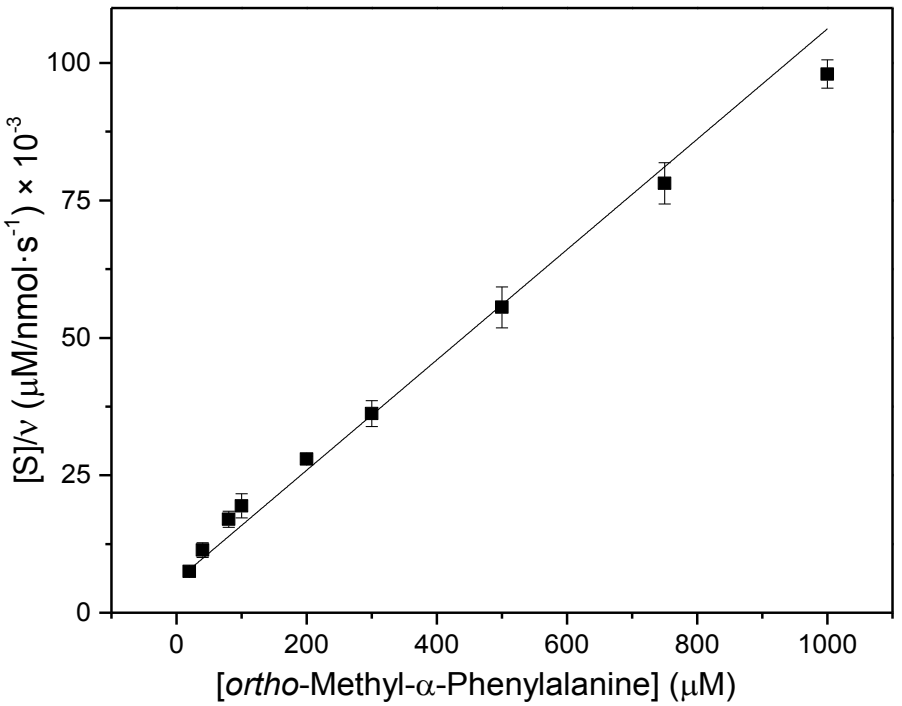

Figure A.2.25. Hanes-Woolf plots of biosynthetic *o*-methyl-β-phenylalanine (designated as velocity, *v*) catalyzed by *Pa*PAM from *o*-methyl-α-phenylalanine (S).

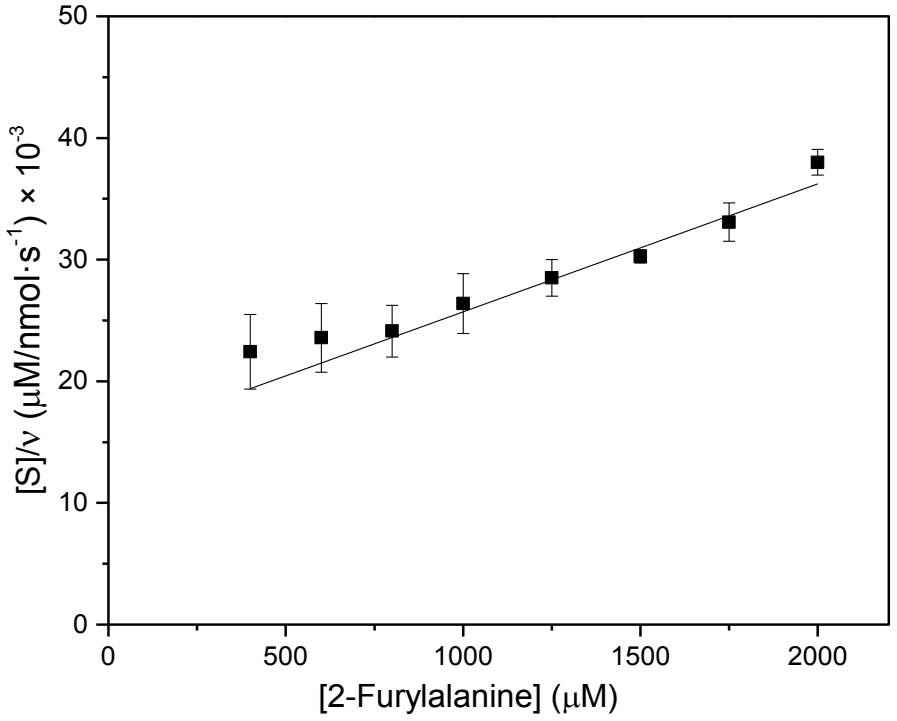

Figure A.2.26. Hanes-Woolf plots of biosynthetic 2-furyl-β-alanine (designated as velocity, *v*) catalyzed by *Pa*PAM from 2-furyl-α-alanine (S).

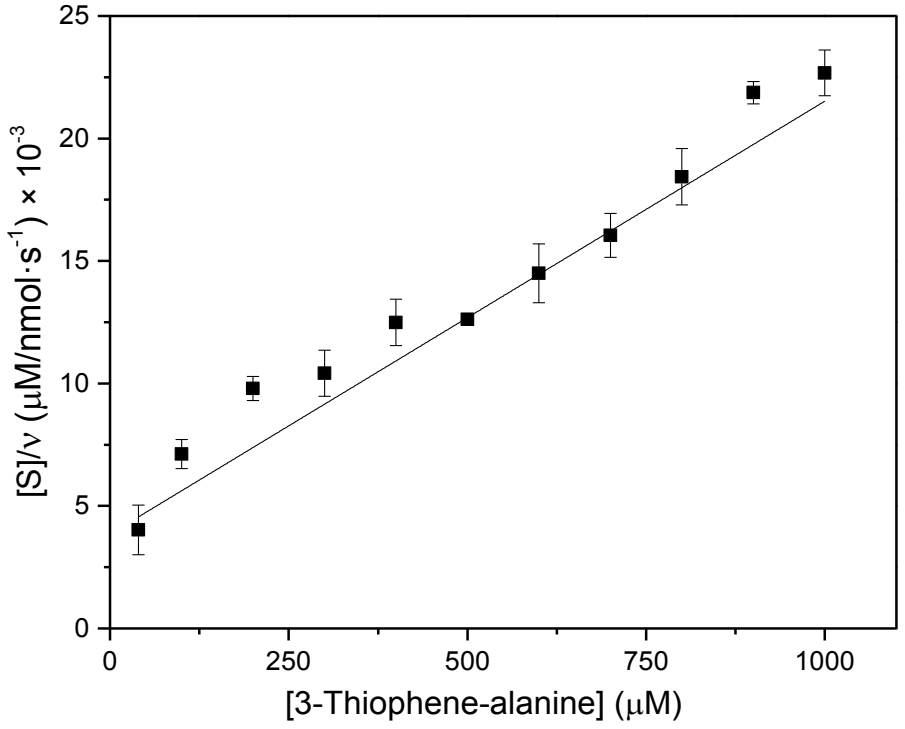

Figure A.2.27. Hanes-Woolf plots of biosynthetic 3-thiophenyl-β-alanine (designated as velocity, *v*) catalyzed by *Pa*PAM from 3-thiophenyl-α-alanine (S).

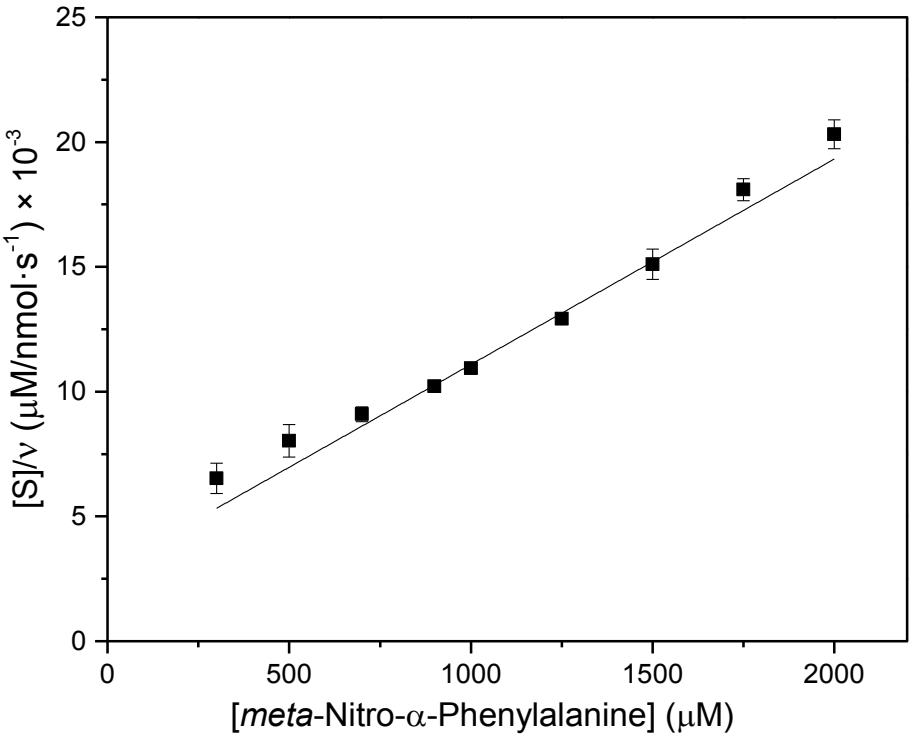

Figure A.2.28. Hanes-Woolf plots of biosynthetic *m*-nitro-β-phenylalanine (designated as velocity, *v*) catalyzed by *Pa*PAM from *m*-nitro-α-phenylalanine (S).

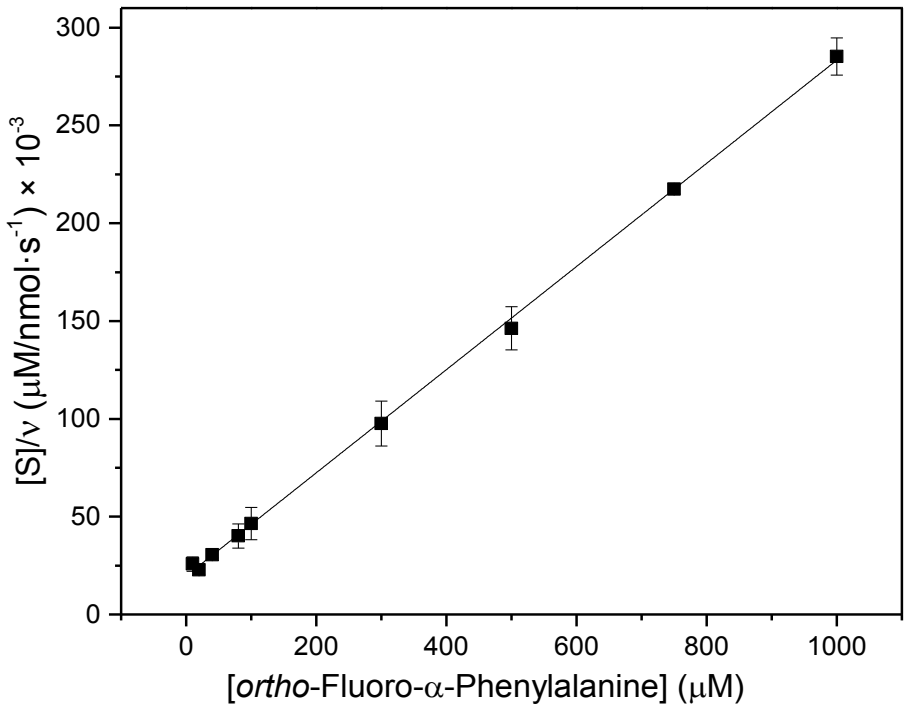

Figure A.2.29. Hanes-Woolf plots of biosynthetic *o*-fluoro-β-phenylalanine (designated as velocity, *v*) catalyzed by *Pa*PAM from *o*-fluoro-α-phenylalanine (S).

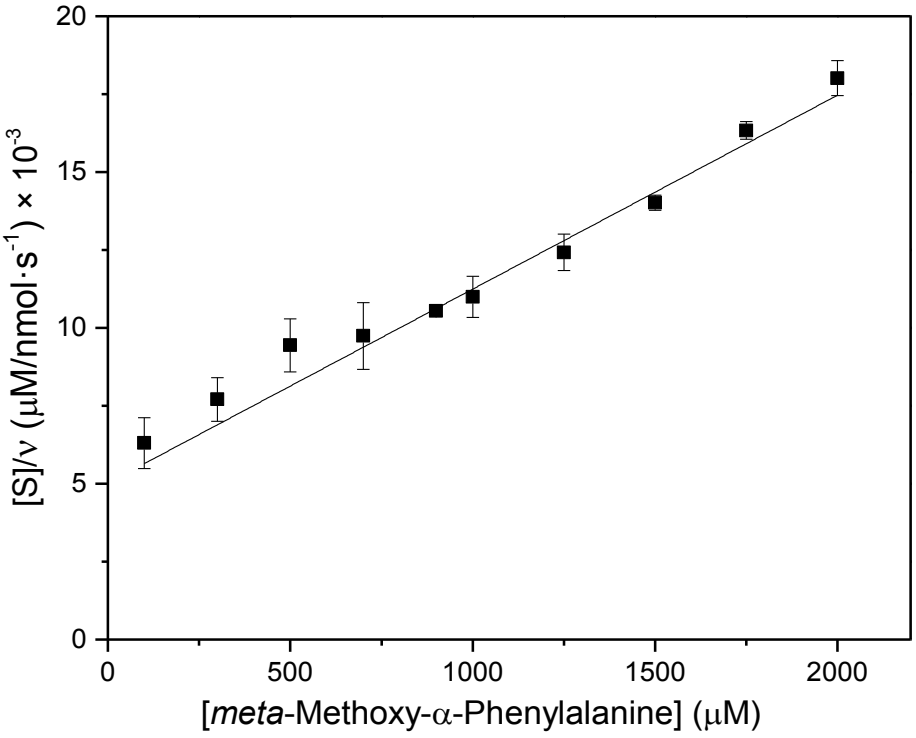

Figure A.2.30. Hanes-Woolf plots of biosynthetic *m*-methoxy-β-phenylalanine (designated as velocity, *v*) catalyzed by *Pa*PAM from *m*-methoxy-α-phenylalanine (S).

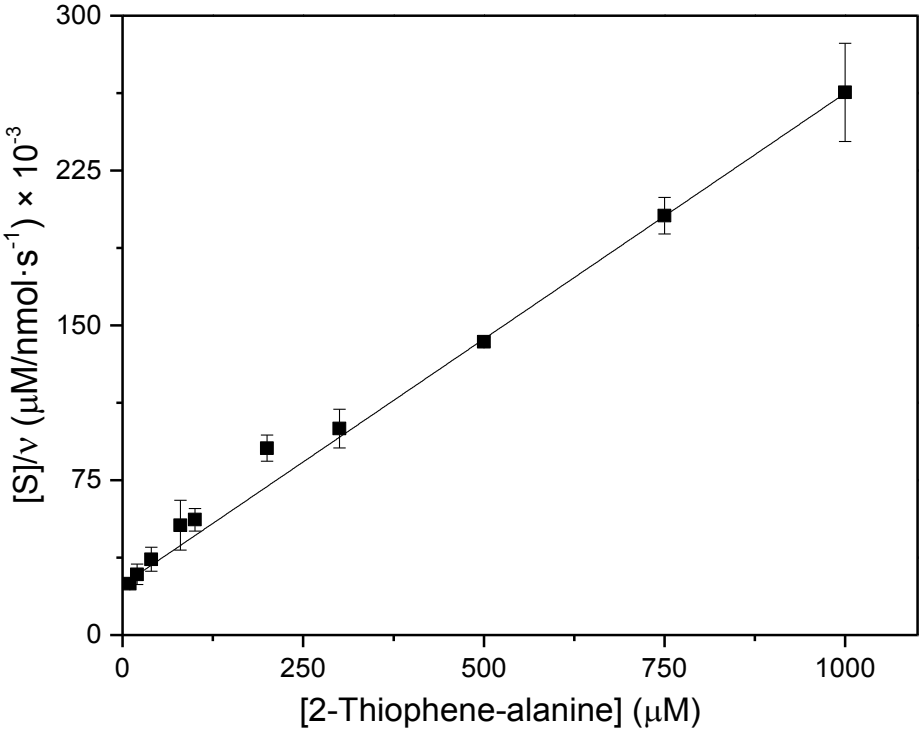

Figure A.2.31. Hanes-Woolf plots of biosynthetic 2-thiophenyl-β-alanine (designated as velocity, *v*) catalyzed by *Pa*PAM from 2-thiophenyl-α-alanine (S).

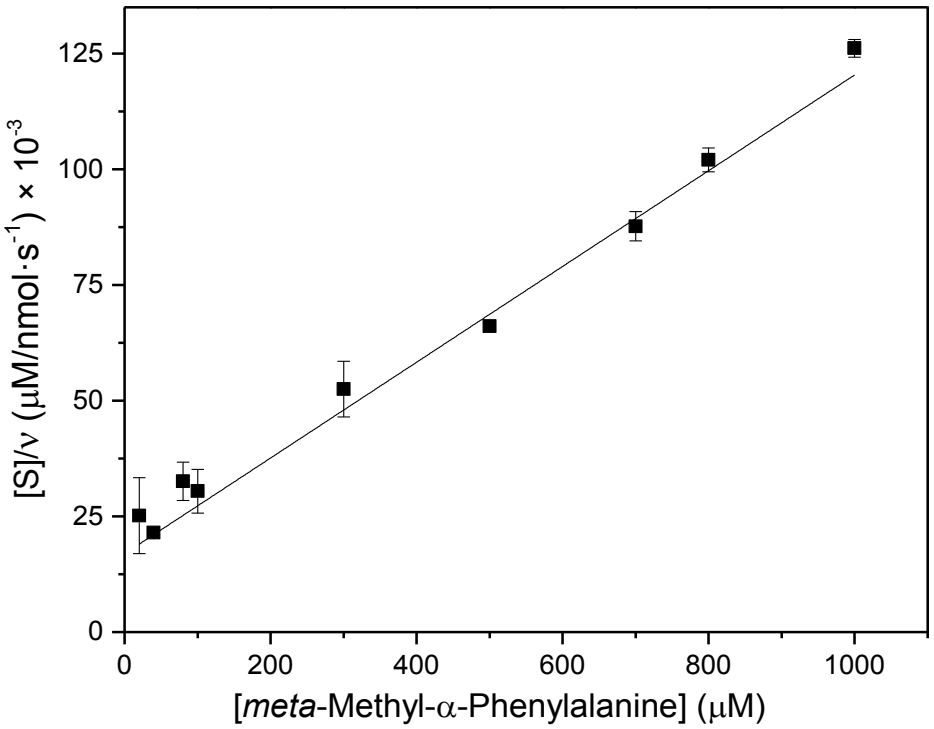

Figure A.2.32. Hanes-Woolf plots of biosynthetic *m*-methyl-β-phenylalanine (designated as velocity, *v*) catalyzed by *Pa*PAM from *m*-methyl-α-phenylalanine (S).

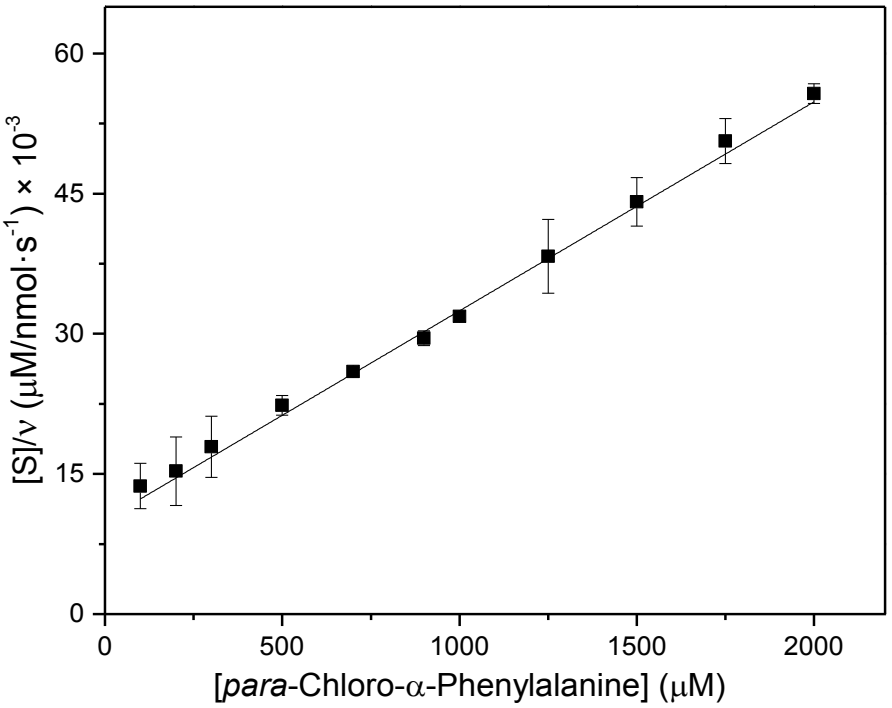

Figure A.2.33. Hanes-Woolf plots of biosynthetic *p*-chloro-β-phenylalanine (designated as velocity, *v*) catalyzed by *Pa*PAM from *p*-chloro-α-phenylalanine (S).

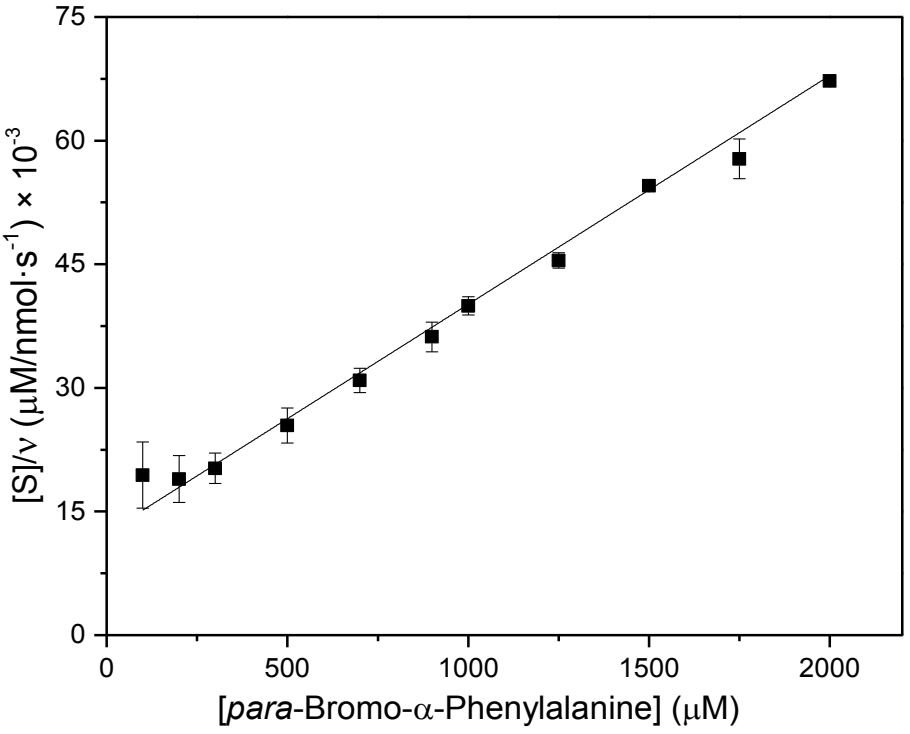

Figure A.2.34. Hanes-Woolf plots of biosynthetic *p*-bromo-β-phenylalanine (designated as velocity, *v*) catalyzed by *Pa*PAM from *p*-bromo-α-phenylalanine (S).

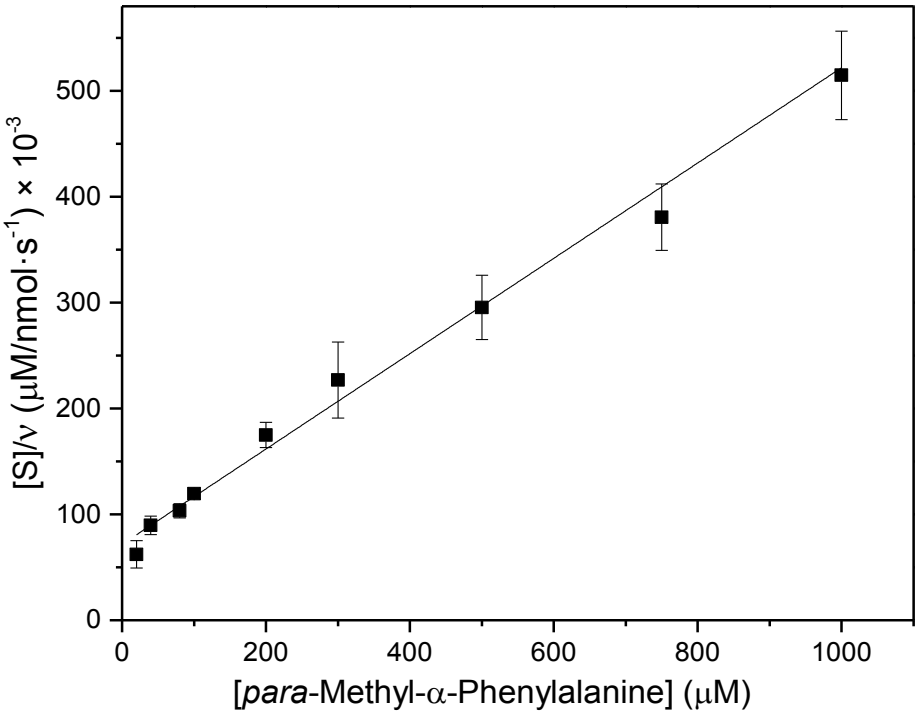

Figure A.2.35. Hanes-Woolf plots of biosynthetic *p*-methyl-β-phenylalanine (designated as velocity, *v*) catalyzed by *Pa*PAM from *p*-methyl-α-phenylalanine (S).

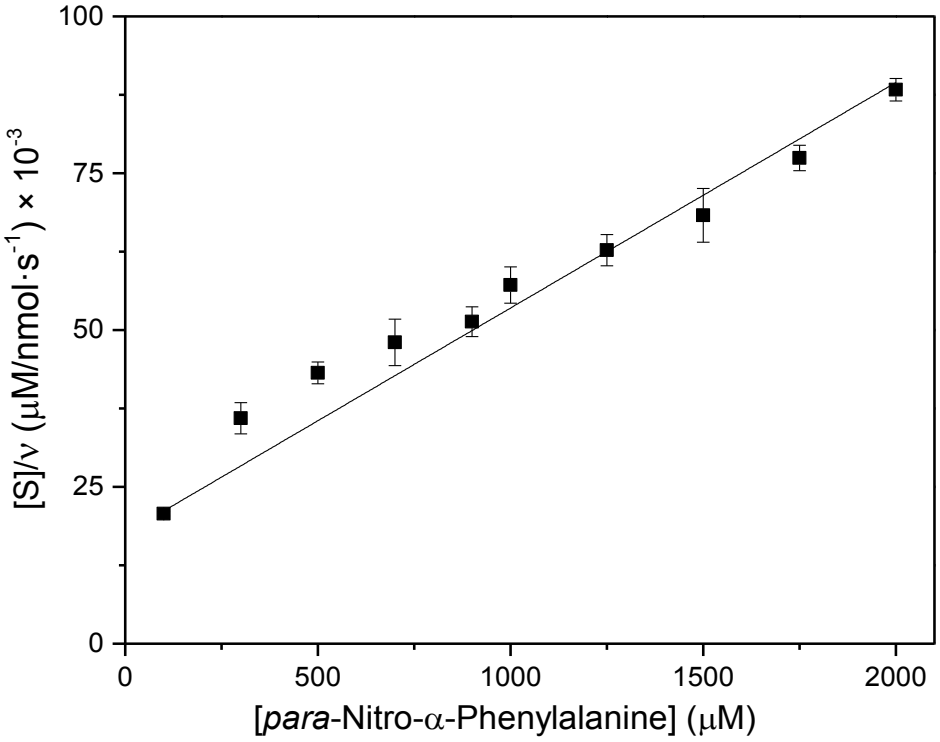

Figure A.2.36. Hanes-Woolf plots of biosynthetic *p*-nitro-β-phenylalanine (designated as velocity, *v*) catalyzed by *Pa*PAM from *p*-nitro-α-phenylalanine (S).

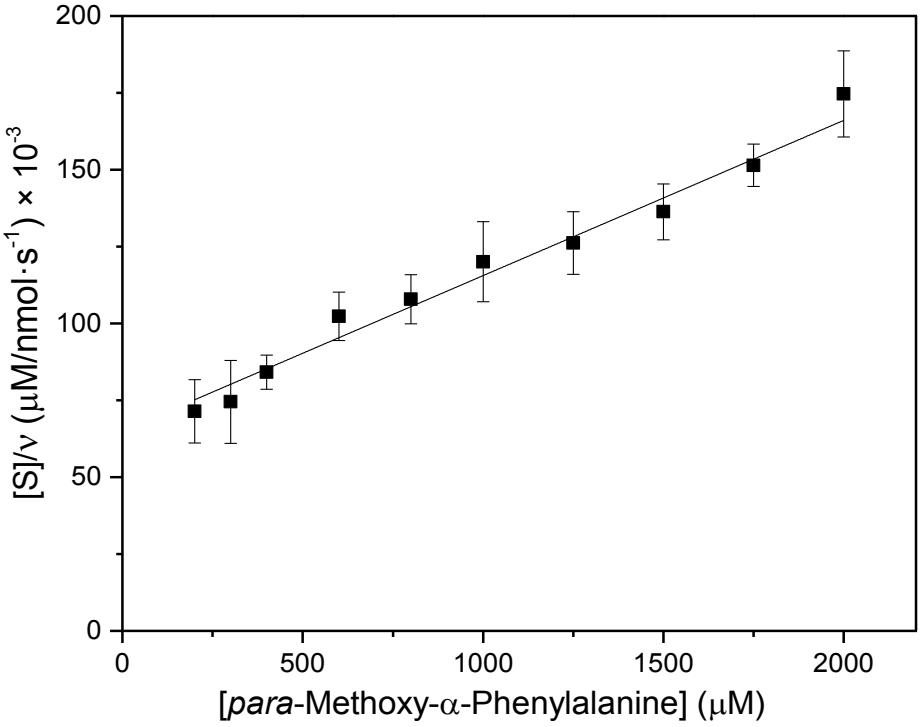

Figure A.2.37. Hanes-Woolf plots of biosynthetic *p*-methoxy-β-phenylalanine (designated as velocity, *v*) catalyzed by *Pa*PAM from *p*-methoxy-α-phenylalanine (S).

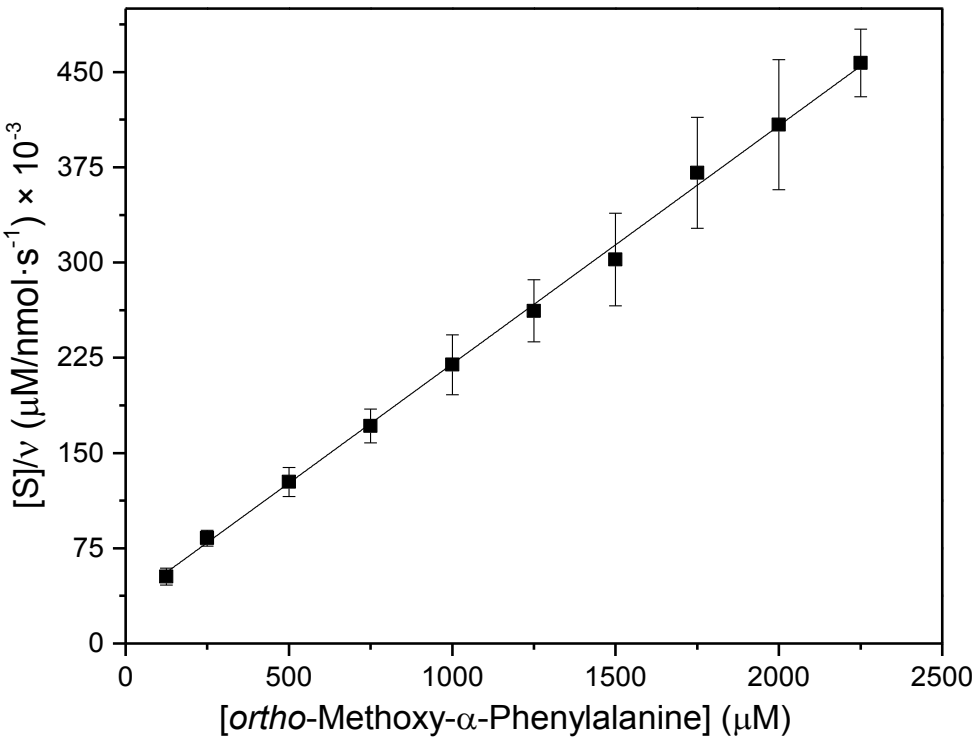

Figure A.2.38. Hanes-Woolf plots of biosynthetic *o*-methoxy-β-phenylalanine (designated as velocity, *v*) catalyzed by *Pa*PAM from *o*-methoxy-α-phenylalanine (S).

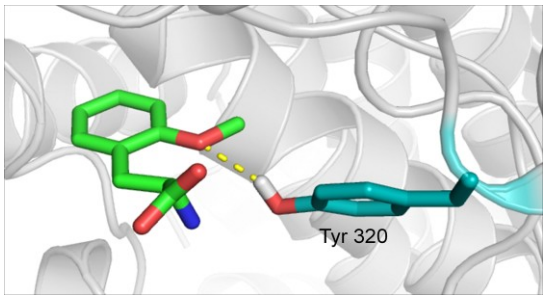

Figure A.2.39. H-bonding interaction of *ortho*-methoxy-α-phenylalanine (19) and active site Tyr320. *ortho*-Methoxy-α-phenylalanine atoms are colored as: carbon: green; nitrogen: blue; oxygen: red and Tyr320 atoms are colored as: carbon: teal; nitrogen: blue; oxygen: red.

Table A.2.1. Calculated $E_{(p\text{-}l)}$ and $E_{(l)}$ values, and preference for *NH_2-cis* versus *-trans* orientation.

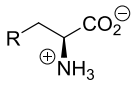 R	($E_{(p\text{-}l)}$ + $E_{(l)}$) (kcal/mol)		$E_{V(p\text{-}l)}$ (kcal/mol)	K_M (μM)	Preferred Orientation
	NH_2-trans	*NH_2-cis*			
1 	149	149	19	168	Symmetrical
2 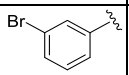	429	188	55	339	*NH_2-cis*
3 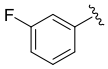	153	148	19	27	NSD[a]
4 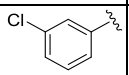	273	166	33	432	*NH_2-cis*
9 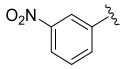	1640	236	48	430	*NH_2-cis*
11 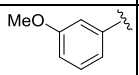	265	240	86	990	NSD
13 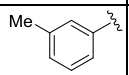	245	174	40	204	*NH_2-cis*
10 	149	165	21	73	NSD
6 	190	489	55	88	*NH_2-trans*
19 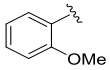	409	292	108	164	*NH_2-cis*
20 	338	525	204	-[b]	*NH_2-trans*
21 	226	401	93	-	*NH_2-trans*
22 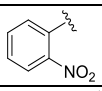	393	2065	205	-	*NH_2-trans*
5 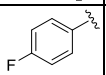	150	150	19	29	Symmetrical
14 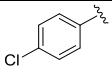	170	170	37	491	Symmetrical
15 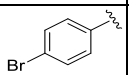	193	193	60	525	Symmetrical
16 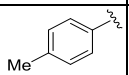	179	179	46	163	Symmetrical
17 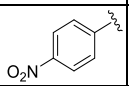	360	360	186	752	Symmetrical
18 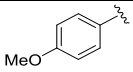	219	947	81	1187	Pseudo *NH_2-trans*

[a]NSD: no significant difference in energy for the *NH_2-cis* or *NH_2-trans* conformation. [b]Non-productive substrates are indicated by hyphens. Note, all energies reported should be considered relative rather than absolute.

REFERENCES

REFERENCES

(1) Grayson, J. I.; Roos, J.; Osswald, S. *Org. Process Res. Dev.* **2011**, *15*, 1201-1206.

(2) Lelais, G.; Seebach, D. *Biopolymers* **2004**, *76*, 206-243.

(3) Yan, S.; Larson, G.; Wu, J. Z.; Appleby, T.; Ding, Y.; Hamatake, R.; Hong, Z.; Yao, N. *Bioorg. Med. Chem. Lett.* **2007**, *17*, 63-67.

(4) Ruf, S.; Buning, C.; Schreuder, H.; Horstick, G.; Linz, W.; Olpp, T.; Pernerstorfer, J.; Hiss, K.; Kroll, K.; Kannt, A.; Kohlmann, M.; Linz, D.; Hubschle, T.; Rutten, H.; Wirth, K.; Schmidt, T.; Sadowski, T. *J. Med. Chem.* **2012**, *55*, 7636-7649.

(5) Ismail, F. M. D. *J. Fluorine Chem.* **2002**, *118*, 27–33.

(6) Wang, J.; Sanchez-Rosello, M.; Acena, J. L.; del Pozo, C.; Sorochinsky, A. E.; Fustero, S.; Soloshonok, V. A.; Liu, H. *Chem. Rev.* **2014**, *114*, 2432-2506.

(7) Zhu, Y.; Wu, G.; Zhu, X.; Ma, Y.; Zhao, X.; Li, Y.; Yuan, Y.; Yang, J.; Yu, S.; Shao, F.; Lei, M. *J. Med. Chem.* **2010**, *53*, 8619-8626.

(8) Huang, X.; O'Brien, E.; Thai, F.; Cooper, G. *Org. Process Res. Dev.* **2010**, *14*, 592-599.

(9) Walker, K. D.; Klettke, K.; Akiyama, T.; Croteau, R. *J. Biol. Chem.* **2004**, *279*, 53947-53954.

(10) Klettke, K. L.; Sanyal, S.; Mutatu, W.; Walker, K. D. *J. Am. Chem. Soc.* **2007**, *129*, 6988-6989.

(11) Magarvey, N. A.; Fortin, P. D.; Thomas, P. M.; Kelleher, N. L.; Walsh, C. T. *ACS Chem. Biol.* **2008**, *3*, 542-554.

(12) Christenson, S. D.; Liu, W.; Toney, M. D.; Shen, B. *J. Am. Chem. Soc.* **2003**, *125*, 6062-6063.

(13) Krug, D.; Muller, R. *Chembiochem* **2009**, *10*, 741-750.

(14) Christenson, S. D.; Wu, W.; Spies, M. A.; Shen, B.; Toney, M. D. *Biochemistry* **2003**, *42*, 12708-12718.

(15) Huang, S. X.; Lohman, J. R.; Huang, T.; Shen, B. *Proc. Natl. Acad. Sci. U. S. A.* **2013**, *110*, 8069-8074.

(16) Schwede, T. F.; Retey, J.; Schulz, G. E. *Biochemistry* **1999**, *38*, 5355-5361.

(17) Christianson, C. V.; Montavon, T. J.; Festin, G. M.; Cooke, H. A.; Shen, B.; Bruner, S. D. *J. Am. Chem. Soc.* **2007**, *129*, 15744-15745.

(18) Strom, S.; Wanninayake, U.; Ratnayake, N. D.; Walker, K. D.; Geiger, J. H. *Angew. Chem. Int. Ed.* **2012**, *51*, 2898-2902.

(19) Kyndt, J. A.; Meyer, T. E.; Cusanovich, M. A.; Van Beeumen, J. J. *FEBS Lett.* **2002**, *512*, 240-244.

(20) Camm, E. L.; Towers, G. H. N. *Phytochemistry* **1973**, *12*, 961-973.

(21) MacDonald, M. J.; D'Cunha, G. B. *Biochem. Cell Biol.* **2007**, *85*, 273-282.

(22) Ratnayake, N. D.; Wanninayake, U.; Geiger, J. H.; Walker, K. D. *J. Am. Chem. Soc.* **2011**, *133*, 8531-8533.

(23) Hermes, J. D.; Weiss, P. M.; Cleland, W. W. *Biochemistry* **1985**, *24*, 2959-2967.

(24) Bordwell, F. G.; Zhao, Y. Y. *J. Org. Chem.* **1995**, *60*, 6348-6352.

(25) Calabrese, J. C.; Jordan, D. B.; Boodhoo, A.; Sariaslani, S.; Vannelli, T. *Biochemistry* **2004**, *43*, 11403-11416.

(26) Mutatu, W.; Klettke, K. L.; Foster, C.; Walker, K. D. *Biochemistry* **2007**, *46*, 9785-9794.

(27) Klee, C. B.; Kirk, K. L.; Cohen, L. A. *Biochem. Biophys. Res. Commun.* **1979**, *87*, 343-348.

(28) Klee, C. B.; Kirk, K. L.; Cohen, L. A.; McPhie, P. *J. Biol. Chem.* **1975**, *250*, 5033-5040.

(29) Schuster, B.; Retey, J. *Proc. Natl. Acad. Sci. U. S. A.* **1995**, *92*, 8433-8437.

(30) Pilbak, S.; Farkas, O.; Poppe, L. *Chem-Eur. J.* **2012**, *18*, 7793-7802.

(31) Szymanski, W.; Wu, B.; Weiner, B.; de Wildeman, S.; Feringa, B. L.; Janssen, D. B. *J. Org. Chem.* **2009**, *74*, 9152-9157.

(32) Wu, B.; Szymanski, W.; Wietzes, P.; de Wildeman, S.; Poelarends, G. J.; Feringa, B. L.; Janssen, D. B. *ChemBioChem* **2009**, *10*, 338-344.

(33) Bohm, H. J.; Banner, D.; Bendels, S.; Kansy, M.; Kuhn, B.; Muller, K.; Obst-Sander, U.; Stahl, M. *Chembiochem* **2004**, *5*, 637-643.

(34) Kim, C. Y.; Chang, J. S.; Doyon, J. B.; Baird, T. T.; Fierke, C. A.; Jain, A.; Christianson, D. W. *J. Am. Chem. Soc.* **2000**, *122*, 12125-12134.

(35) Schuster, B.; Rétey, J. *Proc. Natl. Acad. Sci. U.S.A.* **1995**, *92*, 8433-8437.

(36) Hammett, L. P. *J. Am. Chem. Soc.* **1937**, *59*, 96-103.

(37) Hoffmann, J.; Klicnar, J.; Štěrba, V.; Večeřa, M. *Collect. Czech. Chem. Commun.* **1970**, *35*, 1387-1398.

(38) Fernández, I.; Wu, J. I.; von Ragué Schleyer, P. *Org. Lett.* **2013**, *15*, 2990-2993.

(39) Zavodszky, M. I.; Rohatgi, A.; Van Voorst, J. R.; Yan, H.; Kuhn, L. A. *J. Mol. Recognit.* **2009**, *22*, 280-292.

(40) Zavodszky, M. I.; Sanschagrin, P. C.; Korde, R. S.; Kuhn, L. A. *J. Comput. Aided Mol. Des.* **2002**, *16*, 883-902.

(41) Nicholls, A.; Wlodek, S.; Grant, J. A. *J. Comput. Aided Mol. Des.* **2010**, *24*, 293-306.

(42) Wlodek, S.; Skillman, A. G.; Nicholls, A. *J. Chem. Theory Comput.* **2010**, *6*, 2140-2152.

(43) Halgren, T. A. *J. Comput. Chem.* **1996**, *17*, 490-519.

(44) Hawkins, P. C.; Skillman, A. G.; Warren, G. L.; Ellingson, B. A.; Stahl, M. T. *J. Chem. Inf. Model.* **2010**, *50*, 572-584.

(45) Hawkins, P. C.; Nicholls, A. *J. Chem. Inf. Model.* **2012**, *52*, 2919-2936.

(46) Carpy, A. J. M.; Haasbroek, P. P.; Ouhabi, J.; Oliver, D. W. *J. Mol. Struct.* **2000**, *520*, 191-198.

(47) Batsanov, S. S. *Russ. Chem. Bull.* **1995**, *44*, 18-23.

(48) Li, A. J.; Nussinov, R. *Proteins* **1998**, *32*, 111-127.

Chapter 5: Biocatalytic Production of β-Aryl-β-Amino Acids using *Pa*PAM

5.1. Introduction

5.1.1. Structural diversity and Significance of β-Amino Acids

β-Amino acids are isomers of α-amino acids where the amino group is attached to the β-carbon instead of the α-carbon. In contrast to two side chain substitution positions in α-amino acids, β-amino acids contain four substitution positions (Figure 5.1A). Consequently, β-amino acids with specific side chains can exist as various stereoisomers either at the α- or β-carbon. The flexibility to generate a vast range of regio- and stereo- isomers (Figure 5.1B),[1,2] significantly expands the structural diversity of β-amino acids thereby providing a diverse array of structural elements for molecular design.

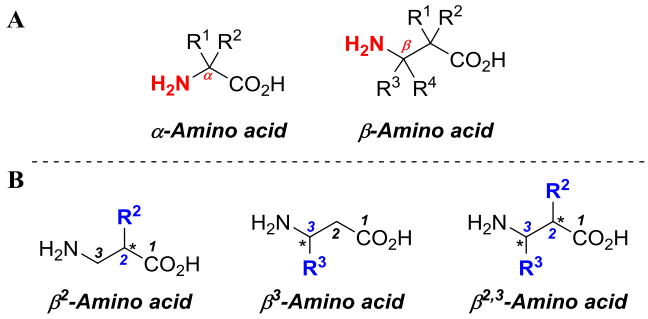

Figure 5.1 Comparison between the substitution patterns of α- and β-amino acids (*A*) and fundamental constitutional-isomers of β-amino acids (*B*). * Indicates a chiral carbon where two stereoisomers are possibly formed increasing the structural diversity of β-amino acids.

Non-proteinogenic β-amino acids are not as abundant in nature as α-amino acids. However, they occur in nature as key components of pharmacologically important natural

products (Table 5.1). Aromatic β-amino acids are found in antibiotic agent andrimid[3] (**1**) from *Pantoea agglomerans*, potent antifungal and insecticidal agent jasplakinolide[4] (**2**) from marine sponges, and potent aminopeptidase inhibitor bestatin,[5] (**3**) from *Streptomyces olivoreticuli*. Furthermore, pharmaceuticals such as sitagliptin[6] (Merck) (**4**) and Taxol[7] (Bristol-Myers Squibb) (**5**) contain moieties derived from β-amino acid precursors. A CCR-5 receptor antagonist maraviroc (Pfizer) (**6**), which is a treatment for HIV infection is built from (*S*)-β-phenylalanine as a synthetic intermediate (Table 5.1).[8]

β-Amino acids have drawn the greatest attention as building blocks for synthetic peptides. Unlike α-peptides, oligomers composed of β-amino acids with proteinogenic side chains are stable against proteolytic, hydrolytic and metabolizing enzymes.[9,10] The stability of β-peptides occur likely due to the lack of substrate recognition by peptidases or proteases and the change of electronic environment of peptide bond upon homologation of α-amino acids. Another important aspect of β-peptide oligomers is their ability to fold into well-defined and stable conformations in solution as well as in the solid state.[11] In contrast to their α-peptidic counterparts, β-peptides with chain lenghts as short as four residues form helical-, turn- and pleated-sheet conformations even in protic solutions (MeOH, H_2O).[11,12] The *in vivo* stability and the diversity of secondary structures enhance the potential application of β-peptides as peptidomimetics in medicinal chemistry. A cyclic-β-tetrapeptide (**7**) was shown to mimic the natural peptide hormone somatostatin (regulator of endocrine and nervous system function), and display biological activity and affinity for human somatostatin receptors.[13] In addition to peptidomimetic ability, poly-β-peptides display other bioactivity properties as well. More recently, a new family of nylon-3 polymers (poly-β-peptides) (**8**) with significant and selective toxicity towards the human fungal pathogen *Candida albicans* was reported (Table 5.1).[14]

Table 5.1 Bioactive natural products, pharmaceuticals, and β-peptides based on β-amino acids

Compound		β-Amino Acid Component	Therapeutic Potential
1	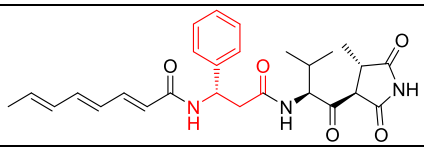	(3*S*)-β-phenylalanine	Antibiotic
2	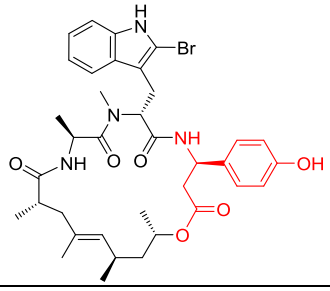	(3*R*)-β-tyrosine	Antifungal and insecticidal
3	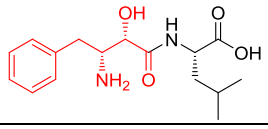	(2*S*,3*R*)-γ-phenyl-β-homoisoserine	Aminopeptidase inhibitor
4	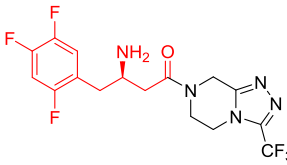	2',4',5'-trifluoro-β-homoalanine	Antidiabetic
5	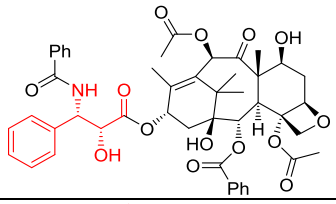	(2*R*,3*S*)-β-phenylserine	Anticancer
6	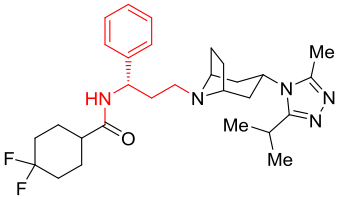	(3*S*)-β-phenylalanine	CCR-5 receptor antagonist
7	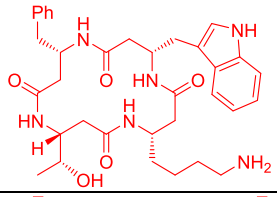	Cyclo-β-tetrapeptide	Human hormone somatostatin mimic
8	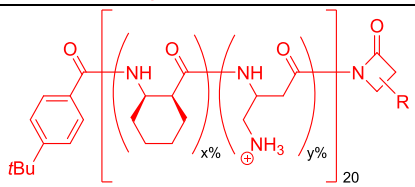	Poly-β-peptide	Antifungal

y = 40, 50, 60, 70, 80 or 90; x + y = 100

5.1.2. Chemical Approaches for Asymmetric Synthesis of β-Amino Acids

Given the importance of β-amino acids as precursors for pharmaceuticals and peptidomimetics, a plethora of methods are known for the stereoselective chemical synthesis of β-amino acids.[15-17] Arndt-Eistert homologation of α-amino acids, diastereoselective and enantioselective conjugate addition reactions, and catalytic asymmetric hydrogenation reactions are highlighted among the various advantageous methods developed.

5.1.2.1. Arndt-Eistert Homologation

Preparation of β-amino acids from α-amino acids via Arndt-Eistert homologation (Figure 5.2) is particularly attractive, since the stereogenic center of α-amino acids is retained during the process without significant racemization. Additionally, the α-amino acids are readily available with low cost and high enantiopurity. Yuan and coworkers have successfully employed the Arndt-Eistert homologation to synthesize the β-homoarginine subunit (58% yield) of TAN-1057-A, and -B dipeptides with antibacterial activity.[18]

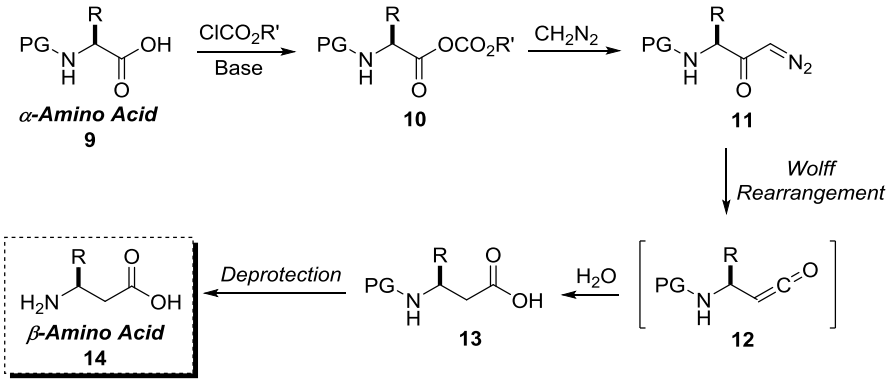

Figure 5.2. Synthesis of β-amino acids from α-amino acids via Arndt-Eistert homologation.

However, costly silver catalyst used in the Wolff rearrangement limits the use of this method for large scale syntheses. In contrast, photochemically induced rearrangement is more suitable for the development of a cost-effective, environmentally friendly process. In the synthesis of the tripeptide Boc-β-HVal-β-HAla-β-HLeu-OMe, the photochemical Wolff rearrangement was demonstrated to be more effective over the silver catalysis.[9]

In addition to the use of silver catalysis, safety concerns and difficult handling associated with carcinogenic, highly volatile, and hazardous diazomethane (CH_2N_2) is a major drawback in Arndt-Eistert homologation method. Nevertheless, in a recent example, risk of handling CH_2N_2 was reduced by generating, extracting, and using diazomethane in a continuous flow system (Figure 5.3).[19] Here in this system, all four successive steps of the Arndt-Eistert homologation synthesis; 1) activation of α-amino acid **9** to the mixed anhydride **10**, 2) synthesis of α-diazoketone **11** by reacting the mixed anhydride with CH_2N_2, 3) photochemical Wolff rearrangement of **11**, and 4) reaction of intermediate ketene **12** with water to form *N*-protected β-amino acid were carried out in a flow system. CH_2N_2 was generated in a microreactor environment and directly extracted from the aqueous feed using a micro-porous gas-permeable membrane. The anhydrous CH_2N_2 extracted was then reacted with the activated α-amino acid. Excess CH_2N_2 was removed from the reaction stream employing a second gas-selective membrane and destroyed in a quench solution thus avoiding the exposure of CH_2N_2. This method was used to synthesize a variety of *N*-protected β-amino acids with modest yields (8 examples, 34-54% yield).

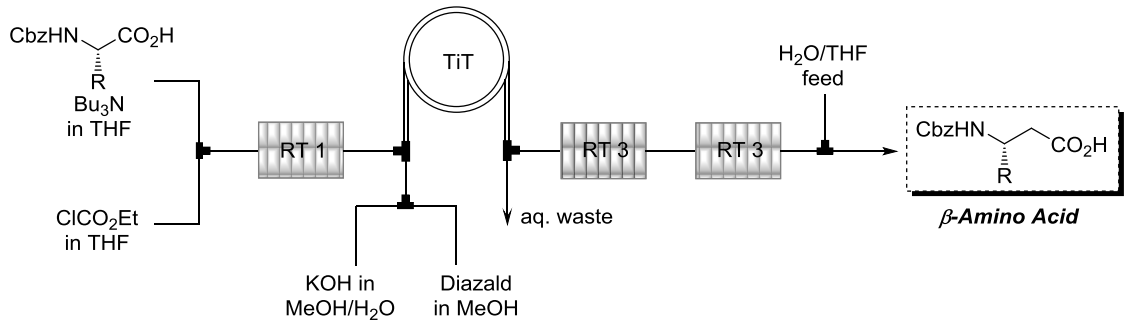

Figure 5.3. Continuous four-step flow system for the production of *N*-protected β-amino acids. RT: residence loops; TiT: tube-in-tube reactor.

5.1.2.2. Conjugate Addition Reactions

Conjugate addition of nitrogen nucleophiles to an α,β-unsaturated carboxylic acid derivatives is among the most important and atom-economic asymmetric synthetic strategies for the synthesis of β-amino acids. Diastereoselective methods are composed of addition of chiral nucleophiles across the double bond (Figure 5.4A) or addition of an achiral nucleophile to a chiral acceptor (Figure 5.4B). Although very challenging, some enantioselective methods (Figure 5.4C) were developed in last few decades.

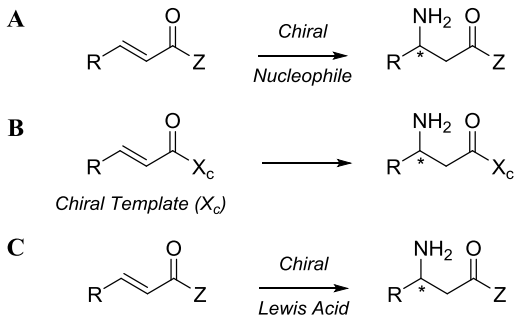

Figure 5.4. Various Conjugate addition approaches for the synthesis of β-amino acids. *A* and *B*) Diastereoselective methods involving a chiral nucleophile and a chiral template. *C*) Enantioselective approaches.

5.1.2.2.1. Diastereoselective Methods

Several chiral amines readily available in both enantiomeric forms are used as synthetic ammonia equivalents in diastereoselective Michael addition reactions.[20] Davies and co-workers demonstrated the highly diastereoselective (>99% *de*) addition of lithium *R*-*N*-benzyl-phenylethylamide to *E*-crotonate esters and methyl *p*-benzyloxycinnamate (Figure 5.5).[21] Subsequent debenzylation with $Pd(OH)_2$ and acid hydrolysis produced *R*-β-amino butanoic acid and *S*-β-tyrosine in excellent enantioselectivity. More recently this diastereoselective strategy was employed in the asymmetric synthesis of α-deuterio-β^3-phenylalanine derivatives.[22]

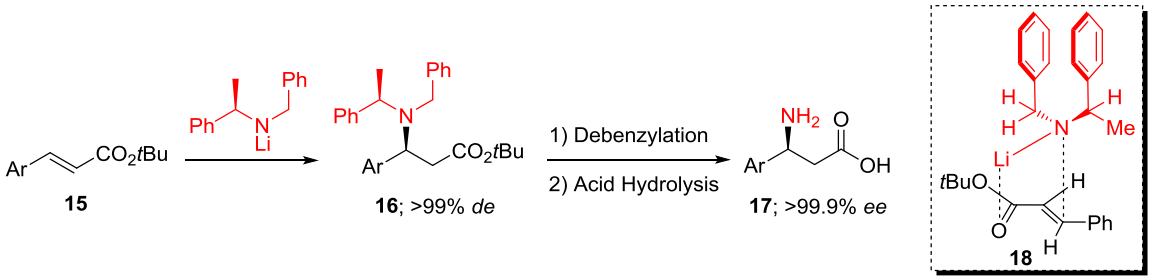

Figure 5.5. Synthesis of chiral β-amino acids using diastereoselective Michael addition of a chiral amine.

Based on computational modeling analyses, a model has been proposed for the origin of highly stereoselective conjugate addition.[23] According to theoretical calculations, dibenzylamide nucleophile adopted a stable conformation where the phenyl rings are parallel to each other. In the lowest energy transition state (**18**), the α,β-unsaturated acceptor reacts from its *s-cis* conformation, lithium is chelated between the carbonyl oxygen and the nitrogen lone pair, and the (*R*)-amide favors the 3-*si* face of the unsaturated ester (Figure 5.5).

In addition to the strategies involving the chiral nucleophiles, diastereoselective α,β-additions are carried out using chiral acceptors and achiral nucleophiles as well. For example chiral chrotonates[24] and chiral *p*-tolylsulfinyl cinnamates[25] were successfully used as the chiral templates for stereoselective conjugate addition reactions.

5.1.2.2.2. Enantioselective Methods

In contrast to the diastereoselective methods, enantioselective conjugate amine addition reactions are generally more challenging. The first enantioselective conjugate addition reaction was developed by Jørgensen and coworkers in 1996 using a BINOL catalyst with only 42% enantioselectivity.[26] Following this initial report, various Lewis acid catalyzed amine additions with good isolated yields and excellent levels of enantioselectivity were reported. Although a variety of alkyl substituents were successfully used in chiral Lewis acid methodologies, β-aryl groups are considerably less reactive than the corresponding β-alkyl substrates. Sibi and coworkers reported the first example of highly enantioselective conjugate addition to cinnamates using catalytic amounts of a chiral Lewis acid.[27] Various β-aryl-β-amino acid derivatives were synthesized with moderate to excellent *ee* using the addition of a highly reactive nitrogen nucleophile *N*-benzylhydroxylamine to the pyrrolidinone-derived enoate **19** (Figure 5.6).

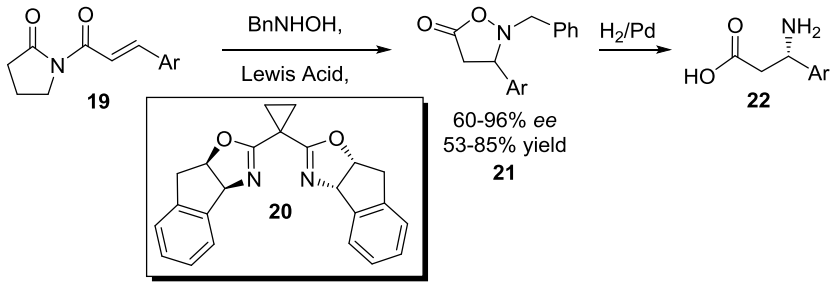

Figure 5.6. Enantioselective addition of *N*-benzylhydroxylamine to pyrrolidinone-derived enoates in presence of a chiral Lewis acid.

5.1.2.3. Catalytic Asymmetric Hydrogenation Reactions

Asymmetric hydrogenation of acrylic acid or nitrile derivatives is one of the most promising chemical approaches for the large-scale synthesis of β-amino acids. Since the initial report of asymmetric hydrogenation of *N*-acyl-β-(amino)acrylates by Noyori,[28] Ru- and Rh-catalyzed homogeneous hydrogenations using chiral phosphorous ligands became a well established procedure. However, both (*E*)- and (*Z*)-isomers of β-acylamido acrylates are produced simultaneously in common synthetic protocols, and their individual hydrogenation requires prior separation. When racemic β-(amino)acrylates are employed, (*E*)-isomers generally lead to higher enantioselectivities, and (*Z*)-isomers frequently react faster, with low enantioselectivity.[29] Nonetheless, a collaborative effort of Börner et. al. and Evonik Degussa GmbH R&D discovered the chiral bisphospholane ligand MalPHOS (marketed as catASium, Solvias AG, Switzerland) bearing a maleic anhydride backbone for the Rh(I)-catalyzed enantioselective hydrogenation of isomeric β-acylamido acrylates (Figure 5.7).[30] With this new catalyst, comparable selectivities were obtained for both (*E*)- and (*Z*)-isomers and the enantioselectivity was higher particularly for the (*Z*)-configured substrates bearing bulkier substituents at the β-position (Et, *i*-Pr, Ph).

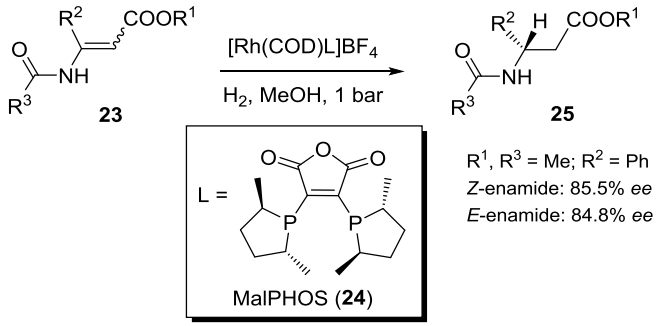

Figure 5.7. Hydrogenation of enamides using chiral bisphospholane ligand MalPHOS.

The enantioselectivity of asymmetric hydrogenation was further improved using a series of diphosphine ligands based on camphor.[31] The hydrogenation of methyl-3-acetylamino-but-2-enoates proceeded with >99% and 94% *ee*, respectively, for the *E*- and *Z*-isomers.

Although ligand design and tuning have improved the enantioselectivity (>95%) of the catalytic asymmetric hydrogenation of unsaturated double bonds, this route is still complex for a large-scale production partly due to the more stages and reaction steps. The need for the large-scale manufacture of the required complex ligands and starting materials will produce more waste and impede the development of a commercial process for the production of β-amino acids.[32] Consequently, more applicable biocatalytic methods have been developed for the synthesis of β-amino acids and their analogues.

5.1.3. Biochemical Approaches for Synthesis of β-Amino Acids

Biocatalysis, use of enzymes as catalysts in synthetic organic chemistry offer some unique advantages over conventional enantioselective chemical catalysis.[33,34] The most important advantage of a biocatalyst is the excellent stereo-, regio- and chemo-selectivity. Additionally, no protection/deprotection steps are required, and therefore, the reactions are generally atom- and reaction-step economical. Other advantages, such as mild operational conditions and reduced hazardous waste generation are also very attractive in commercial applications.[34]

Narrow substrate scope, substrate or product inhibition, lower stability and difficulty of enzyme production in large enough quantities for practical applications were often considered as the most serious drawbacks of biocatalysts.[34] Nonetheless, advent of recombinant DNA technology, developments in protein design tools such as rational design and directed evolution,

and advances in understanding protein structure–function relationships are enabling scientists to rapidly tailor the properties of biocatalysts for particular chemical processes.[33] Substrate specificity, stability, activity, selectivity, and large scale production of enzymes are routinely engineered in the laboratory. Presently, several biocatalytic processes are implemented in pharmaceutical, chemical, agricultural, and food industries.[35]

Three main biocatalysts 1) lipases,[32,36] 2) transaminases,[37] and 3) aminomutases[38,39] are explored for the synthesis of β-amino acids. Compared to the enantioselective syntheses using isomerases and transaminases, enzymatic resolution of lipases is widely investigated in the context of industrial scale synthesis of β-amino acids.[32]

5.1.3.1. Enzymatic Resolution of β-amino acids

One of the earliest, most efficient method for enzymatic resolution of β-amino acids is the use of penicillin G acylase from *E. coli*. Soloshonok and co-workers prepared (*R*)-β-aryl-β-amino acids in good yield and high enantiomeric purity (>95% *ee*) via penicillin G acylase catalyzed hydrolysis of corresponding *N*-phenylacetyl derivatives.[40] Synthesis of the (*S*)-isomer requires separation of the unreacted amide and subsequent acid hydrolysis (Figure 5.8). In addition to the complex procedure of (*S*)-isomer production, the need to separate the products from corresponding aryl acetic acids, and lower atom economy arose from the high mass of phenylacetyl protecting group makes this process less attractive for an industrial scale manufacture of β-amino acids.

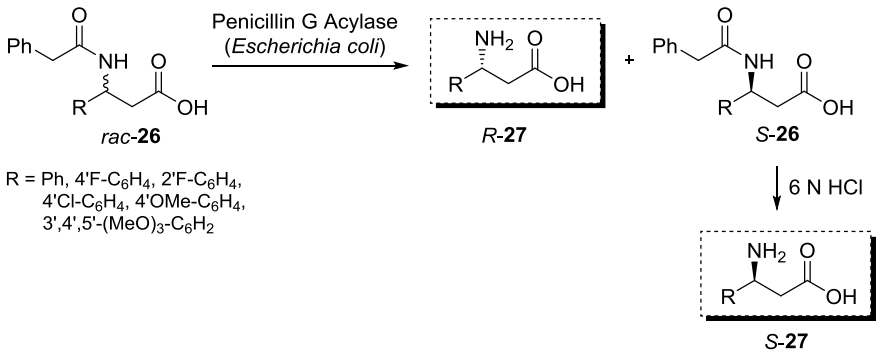

Figure 5.8. Penicillin G acylase route to β-aryl-β-amino acids

Recently, a lipase catalyzed commercial manufacturing route for β-aryl-β-amino acids was developed by modifying the initial conditions reported by Faulconbridge et.al.[36] With the modified conditions, the commercially available Amano lipase PS was capable of hydrolyzing a range of aromatic and heteroaromatic propyl esters with excellent enantioselectivity (98-99% *ee*) and low to high yields (16-50%) (Figure 5.9).[32]

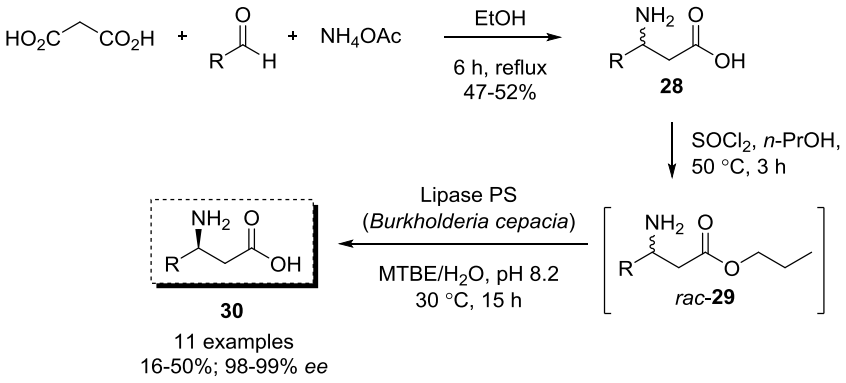

Figure 5.9. Amano lipase PS catalyzed production of β-aryl-β-amino acids.

Enantioselective production of (*S*)-β-phenylalanine using this lipase route was carried out by Evonik Degussa GmbH (Germany) at variuos scales: kilo-lab (3.7-7.4 kg), pilot plant (100

kg), and commercial plant scale (430 kg) without affecting the yield of the reaction (41-43%). The chemical purity of the isolated (*S*)-β-phenylalanine was 98.5-99.5% and the optical purity was >99.5% in each case. The reaction was carried out in a two phase liquid mixture where the lipase and the racemic-propyl ester is dissolved in water and MTBE, respectively. After the reaction, (*S*)-acid crystallizes out from the two phase liquid mixture, and thus the process eliminates additional purification steps.

Although the lipase route was developed for the commercial production of β-aryl-β-amino acids, the enzymatic resolution strategies are limited to a maximum 50% yield. Additionally, corrosive reagents such as $SOCl_2$ is involved in the synthesis of the racemic propyl esters. Furthermore, distillation and extraction steps added before the two-phase lipase resolution reaction. The Amano lipase PS, which contributes most to the process cost, was partially inactivated after the first cycle. A fresh enzyme supplement was required for the recycling of the lipase solution for further catalytic cycles.[32]

Use of aminomutases and transaminases[37] are promising over the enzymatic resolution efforts since the former reactions can lead theoretically to a 100% conversion of the substrate. Furthermore, implementing a whole-cell biocatalytic route instead of *in vitro* enzymes would likely enhance catalyst stability and promote sustainability. For multiple rounds of catalysis, this approach would contrast the Amano lipase PS route where *in vitro* biocatalytic activity was reduced over time.

5.1.3.2. Aminomutases for the Production of β-Amino Acids

In nature, aminomutases are involved in the catabolism of amino acids and biosynthesis of various biologically active natural products.[38] These enzymes catalyze the vicinal exchange of a proton and an amine group present in the substrate. Members of this family, lysine 2,3-, glutamate 2,3-, phenylalanine- and tyrosine-aminomutases are capable of isomerizing α-amino acids into β-amino acids that are part of pharmaceuticals and bioactive natural products.[3,38,41-44] However, lysine- and glutamate-2,3-aminomutases belong to the SAM-dependent family, and anaerobic conditions are required to purify these enzymes.[42,45] In addition, multiple expensive cofactors are needed if these enzymes are used in an *in vitro* biocatalytic processes of lysine- and glutamate-2,3-aminomutases. By contrast, MIO-dependent phenylalanine- and tyrosine-aminomutases function under aerobic conditions and are not dependent on external cofactors.[46,47]

Phenylalanine aminomutases (PAM) are the most extensively studied enzymes of this class of aminomutases. In *Taxus* plants, *Tc*PAM/*Tch*PAM catalyzes the conversion of (2*S*)-α-phenylalanine to (3*R*)-β-phenylalanine, which is the proposed biosynthetic precursor of the phenylisoserine side chain of Taxol (Figure 5.10).[38] A homologous enzyme from *Pantoea agglomerans* (*Pa*PAM) produces the enantiomeric (3*S*)-β-phenylalanine in the biosynthetic pathway to antibiotic andrimid (Figure 5.10).[39] Accessibility to the both enantiomeric forms of β-phenylalanines using homologous enzymes significantly improve the synthetic value of PAM as a biocatalyst.

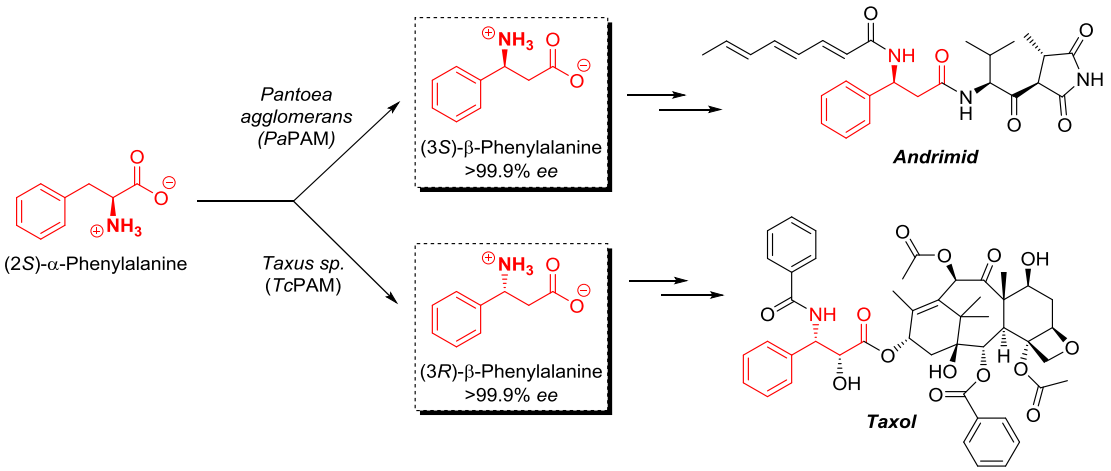

Figure 5.10. Reactions catalyzed by phenylalanine aminomutases *Pa*PAM and *Tc*PAM in their corresponding biosynthetic routes for andrimid and Taxol.

The enzymatic conversion catalyzed by PAMs proceed with excellent enantioselectivity (>99.9%) and these enzymes have a broad substrate scope. A range of α-phenylalanine analogues consisting of various substituents at the phenyl ring (fluoro, chloro, bromo, methyl, methoxy and nitro) as well as other heteroaromatic analogues were successfully converted to corresponding β-amino acids by both PAMs.[48,49]

Recently, various other routes toward enantiomerically pure β-amino acids have been investigated with MIO-dependent aminomutase catalysis. *Tch*PAM from *Taxus chinensis* catalyses the highly enantioselective addition of ammonia to *t*-cinnamic acid, which is an intermediate in the isomerization reaction. Addition of ammonia to cinnamic acid produces a 1:1 mixture of (*S*)-α- and (*R*)-β-phenylalanines with >99.9% *ee*.[50] This amino addition reaction has a broad substrate scope and produces variously substituted α- and β-phenylalanines. While enantioselectivity was not affected, the regioselectivity of this process was significantly affected by the substituents at the aromatic ring. For example, *ortho*-substituted cinnamic acids resulted

almost exclusive production of (*S*)-α-phenylalanine analogues with >98:2 ratio.[51] Furthermore, the regioselectivity of amino addition to cinnamic acid by *Tch*PAM was tailored towards the (*R*)-β-phenylalanines by engineering the active site residues.[52]

Additionally, the synthetic utility of PAMs was recently exploited as an aminotransferase.[53] *Tc*PAM from *Taxus canadensis* was employed as an amino acid:arylacrylate transaminase. The amino group from an α-amino acid ((*S*)-styryl-α-alanine and some other non-natural amino acids) was successfully transferred to an arylacrylate to produce a mixture of α- and β-amino acids. Hence, in an organic synthesis context, the isomerization reaction catalyzed by PAMs is a highly enantioselective, atom economical, cost-effective, and a relatively environmentally benign biocatalytic method for the production of various β-aryl-β-amino acids. However, PAMs have not yet evaluated as whole-cell biocatalysts, which could be applicable in large scale production of β-aryl-β-amino acids.

5.1.4. Whole-cell Biocatalysis

Biocatalysis may be carried out using whole cells or isolated enzymes.[33] Compared to purified enzymes, whole-cell biocatalysts or so called 'designer cells' have several advantages that are particularly attractive for large-scale processes. The use of microbial whole-cells eliminates costly, laborious enzyme purification steps.[54] In whole-cells, enzymes enclosed in their typical environments protected by the cell envelopes are more stable than purified enzymes. Thus, whole-cell biocatalytic processes which use inexpensive biomass such as bacteria and yeast are cost-effective, and the risk of denaturing the enzymes is reduced.[54]

Chemical transformations requiring multiple enzymes are quite complicated with isolated enzymes. Optimizing conditions such as temperature, pH, and reaction buffer for multiple enzymes in one process is often challenging.[55] Tailor-made whole cells that contain all the desired enzymes for a specific transformation can overexpress multiple enzymes and perform multi-step transformations under similar conditions. For example, May and co-workers have developed a production route for L-methionine using a tailor-made recombinant whole-cell biocatalyst.[55] *E.coli* cells were designed to express a modified L-hydantoinase and L-*N*-carbamoylase from *Arthrobacter sp.* DSM 9771, and a hydontoin racemase from *Arthrobacter sp.* DSM3747 (Figure 5.11). This three-enzyme system synthesized 91 mM L-methionine from D,L-5-(2-methylthioethyl)hydantoin (D,L-MTEH) in less than 2 h with >90% conversion of the substrate. Furthermore, L-*tert*-leucine can also be synthesized with the hydantoinase–carbamoylase system on a 100-kg scale.[56]

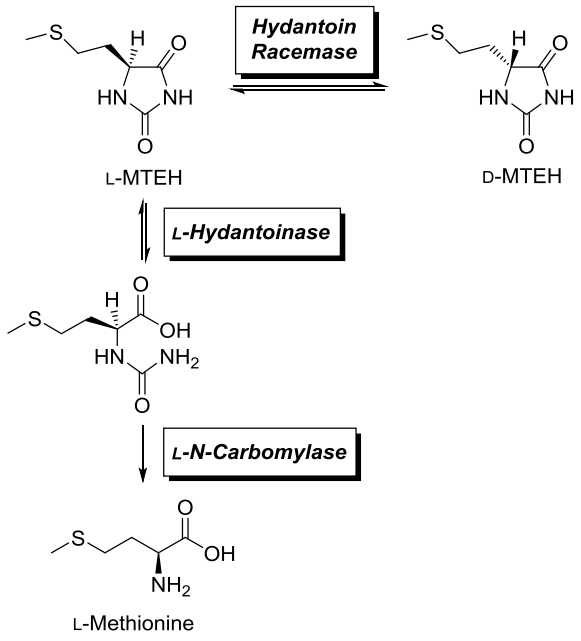

Figure 5.11. Multiple-enzyme catalyzed production of L-methionine from racemic MTEH.

In addition to aforementioned advantages, whole-cell systems allow the use of cofactor pools intrinsic to the cells, and thus, makes cofactor regeneration much easier. Synthesis of chiral alcohols using asymmetric reduction of ketones catalyzed by NAD(P)H-dependent alcohol dehydrogenases is often limited by the higher cost of adding the cofactor exogenously. Therefore an enzyme-coupled cofactor-regeneration system has been developed for the in situ regeneration of NAD(P)H.[57] *R*-Specific alcohol dehydrogenase (ADH) from *Lactobacillus kefir* and *S*-specific ADH from *Rhodococcus erythropolis* were coupled with a cofactor-regenerating enzyme glucose dehydrogenase from *Bacillus subtilis* in a whole-cell biocatalytic system (Figure 5.12). This system operates in aqueous media at substrate concentrations >100 g/L *without* an added external cofactor to produce various functionalized alcohols with >99% *ee* and >90% conversion.

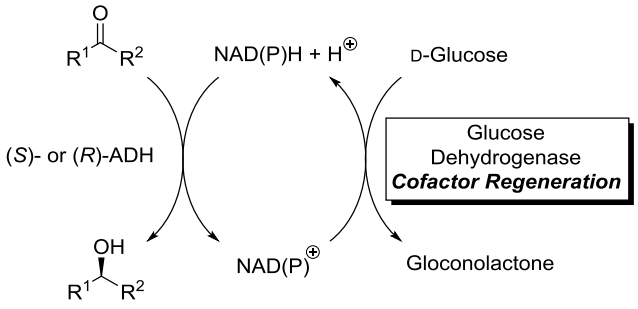

Figure 5.12. Cofactor regeneration strategy using glucose dehydrogenase.

Despite the numerous advantages, reactions catalyzed by whole-cell biocatalytic systems are much slower than those catalyzed by free enzymes.[58] The envelopes of microbial cells often retard the penetration of substrates into the cell and thus prevents the product from being released to the culture medium for an easy recovery.[58,59] Gram negative bacteria is encased by inner and outer cell membranes.[60] The inner cell membrane is a phospholipid bilayer containing various membrane proteins. Hydrophobic molecules can penetrate the lipophilic bilayer faster

than hydrophilic compounds. However, hydrophilic molecules need specific transport proteins to cross the inner cell membrane. The outer membrane contains a densely packed amphiphilic lipopolysaccharide layer and acts as a barrier to both hydrophobic and hydrophilic molecules.[60] Small hydrophilic molecules (<600 Da) are transported into the cells via non-specific transmembrane pores called porins.[61] Nevertheless, passive diffusion through the highly ordered lipopolysaccharide layer is the only method for large synthetic substrates (>600 Da) to cross the outer cell membrane. Consequently, the *E. coli* cell membrane acts as a mass transport barrier between the large, non-natural substrates in the bulk medium and the biocatalyst(s) enclosed in the cell.

Numerous studies have been carried out to alter the cell membrane permeability for chosen substrates. Solvents[62] (ethanol, isopropyl alcohol, toluene, diethyl ether, chloroform), detergents such as Triton X-100,[63] salt stress,[64] freeze-thaw cycles,[65] EDTA, and electropermeabilization[66] are common physical and chemical cell permeabilization methods. In addition, molecular engineering approaches have been exploited to modulate the cell permeability. Mutations in genes that altered the composition of the lipopolysaccharide layer of the outer cell membrane has significantly accelerated the whole-cell biocatalysis reactions by reducing the permeability barrier.[59] Furthermore, cell surface display or displaying enzymes on the microbial cells membranes has circumvented the need for cell permeabilization methods.[67] This method allows an enzyme free access to substrates without the need to cross the cell membrane. In addition, the surface display approach eliminates the undesired side reactions that could possibly occur inside the cell which comprises a broad variety of other enzymes.

Due to the numerous advantages, whole-cell biocatalytic systems are emerging as efficient alternative for conventional catalysis. Currently, various whole-cell biocatalysts are implemented in the manufacture of fine chemicals.[68,69] However, state-of-the-art biocatalytic method for β-arylalanine production is based on purified Amano lipase PS, and there are several limitations associated with this *in vitro* method (see section 5.1.3.1). The investigation described herein involved the development of an efficient and sustainable *Pa*PAM based whole-cell biocatalytic system for producing β-arylalanines.

5.2. Experimental

5.2.1. Substrates, Authentic Standards and Reagents

(*S*)-α-, *p*-methoxy-(*S*)-α-, *p*-nitro-(*S*)-α-, and *p*-chloro-(*R*/*S*)-β-phenylalanine and (trimethylsilyl) diazomethane (2.0 M in diethyl ether) were purchased from Sigma-Aldrich-Fluka (St. Louis, MO). Racemic *p*-nitro-β-phenylalanine was purchased from Oakwood Products, Inc. (West Columbia, SC), and *o*-methoxy-(*S*)-α-, *m*-methoxy-(*S*)-α-, *o*-nitro-(*S*)-α-, *m*-nitro-(*S*)-α-, *o*-methoxy-(*S*)-β-, *m*-methoxy-(*S*)-β-, *o*-nitro-(*S*)-β-, and *m*-nitro-(*S*)-β-phenylalanine were purchased from Chem-Impex International, Inc. (Wood Dale, IL). All other (*S*)-α- and -β-amino acids were purchased from PepTech Corporation (Burlington, MA). All chemicals were used without further purification, unless noted.

5.2.2. Bacterial Strains, Plasmids, and Culture Media

BL21(DE3) *E. coli* bacterial strain transformed with expression vector pET24b(+) was used for the whole-cell biotransformations with *Pa*PAM. *E. coli* cells were grown in M9 minimal medium [$Na_2HPO_4.7H_2O$ (12.8 g·L^{-1}), KH_2PO_4 (3 g·L^{-1}), NaCl (0.5 g·L^{-1}), NH_4Cl (1 g·L^{-1}), $MgSO_4$, (2 mM), $CaCl_2$ (0.1 mM), 100x Basal Medium Eagle vitamins (Sigma-Aldrich, St. Louis, MO; 10 mL·L^{-1}), and glucose (20%), pH 7.4] supplemented with kanamycin (Gold Biotechnology Inc., St. Louis, MO; 50 μg·mL^{-1}). Optical density measurements of cell suspensions were obtained in 1.5 mL polystyrene cuvettes (General Laboratory Supply, Pasadena, TX) using a UV−visible spectrophotometer (Beckmann DU 640, Beckmann Coulter, Brea, CA).

5.2.3. General Instrumentation: GC/EI-MS Analysis

GC-MS analysis was performed on an Agilent 6890N gas chromatograph equipped with a capillary GC column (30 m × 0.25 mm × 0.25 μM; HP-5MS; J&W Scientific) with helium as the carrier gas (flow rate, 1 mL/min). The injector port (at 250 °C) was set to splitless injection mode. A 1-μL aliquot of each sample was injected using an Agilent 7683 auto-sampler (Agilent, Atlanta; GA). The column temperature was increased from 50 – 110 °C at 30 °C/min, then increased by 10 °C/min to 250 °C (total run time of 16 min), and returned to 50 °C over 5 min, with a 5 min hold. The gas chromatograph was coupled to a mass selective detector (Agilent, 5973 *inert*) operated in electron impact mode (70 eV ionization voltage). All spectra were recorded in the mass range of 50 – 400 *m*/*z*.

5.2.4. General Procedure for Whole-Cell Biocatalytic Incubations

BL21(DE3) *E. coli* cells (50 mL, OD_{600} ~1.0) transformed to express the *papam* gene from pET24b(+) were used to inoculate M9 minimal medium (1 L) supplemented with kanamycin (50 μg/mL). The cells were grown at 37 °C until to OD_{600} ~0.6, isopropyl-β-D-thiogalactopyranoside (100 μM) was added to induce the expression of *papam*, and the cultures were incubated for 16 h at 16 °C. The next steps were performed at 4 °C, unless indicated otherwise. The cells were harvested by centrifugation at 3,230*g* (10 min), and the cell pellet was resuspended separately in three different whole-cell feeding media (M9 minimal medium, 50 mM phosphate buffer at pH 7, and 50 mM phosphate buffer at pH 8), each typically adjusted separately to an optical density of 35. For analyses at higher biomass, the optical density was adjusted to 70 and 280 in M9 minimal medium. The α-amino acid substrate (1 mM) was added

to the cell suspension and incubated separately at 16, 25 and 30 °C. In control experiments, transformed *E. coli* cells were incubated without substrate added. Additional control experiments included assays with *E. coli* transformed with an empty pET-24 vector incubated with or without the substrate. All the biotransformation feeding assays were done in triplicate.

The minimum incubation volume for whole-cell biocatalysis was assessed by adding 20 mM of α-phenylalanine to a cell suspension of *E. coli* (OD_{600} ~35) engineered to express *papam* at 16 °C, in 5, 100, or 1000 mL of M9 minimal medium. The cultures were incubated, respectively, in 50-mL screw-cap conical centrifuge tubes (Corning Incorporated Life Sciences, Tewksbury, MA), 250 mL Erlenmeyer flasks, and 2.8 L Fernbach flasks with agitation on a shaker (225 rpm, MaxQ 5000, Thermo Scientific, Waltham, MA) for 6 h. The cells were removed by centrifugation, and the β-phenylalanine in the culture medium of each assay was derivatized and quantified by GC/EI-MS. The yield of β-phenylalanine produced was nominally ~2 $mg{\cdot}L^{-1}$ for bacteria incubated in each volume of culture medium. Thus, a 5-mL volume of culture medium was selected for the bacterial incubations in pilot-scale assays to assess the production levles of the α-arylalanines to their β-isomers *in vivo*.

5.2.5. Derivatization and Quantification of Amino Acids

To terminate the incubation, the reaction medium was separated from the cells by centrifuging at 3,230*g* for 10 min, and the supernatant (1 mL) from each assay was basified to pH 10 (6 M NaOH). Internal standards *m*-fluoro-β-phenylalanine, *p*-methyl-β-phenylalanine, and β-phenylalanine at 20 μM were added, respectively, to quantify three sets of biosynthetic β-amino acids products–Set 1: β-phenylalanine; *o*-, *m*-, and *p*-methyl-; *o*-, *m*-, and *p*-methoxy-; *m*-

and *p*-nitro-; *m*- and *p*-chloro-β-phenylalanine; Set 2: *o*- and *p*-fluoro; *m*-, and *p*-bromo-β-phenylalanine; and (2-thienyl)- and (3-thienyl)-β-alanine; and Set 3: *m*-fluoro-β-phenylalanine. Each solution was treated with ethylchloroformate (50 μL) for 10 min, basified again to pH 10, and reacted with a second batch of ethylchloroformate (50 μL) for 10 min. The solutions were acidified to pH 2-3 (6 M HCl) and extracted with diethyl ether (2 × 2 mL). The organic fraction was removed under vacuum, and to the resulting residue dissolved in ethyl acetate:methanol (3:1, v/v) (200 μL) was added (trimethylsilyl)diazomethane until the yellow color persisted. The derivatized aromatic amino acids were quantified by GC/EI-MS. The peak area was converted to concentration by solving the linear equation obtained from the standard curves constructed with the corresponding authentic standards.

5.2.6. Analysis of Substrate Uptake and Product Release by *E .coli* Cells

To *E. coli* cells expressing *Pa*PAM incubated in M9 minimal medium (45 mL, OD_{600} ~35) was added α-phenylalanine (1 mM) at 16 °C. Aliquots (5 mL) were withdrawn at 1, 2, 4, 6, and 8 h, the cells were harvested by centrifugation (3,230*g*, 5 min), and the culture medium was twice serially basified (6 M NaOH) and treated with ethyl chloroformate. The solution was acidified (pH 2-3, 6 M HCl), extracted with diethyl ether (2 × 2 mL), concentrated in vacuo, and the amino acids were methyl esterified with (trimethylsilyl)diazomethane for quantification by GC/EI-MS analysis. In parallel, the cell pellet was resuspended in 50 mM sodium phosphate buffer (pH 8.0), the cells were lysed by sonication to release the soluble amino acids, and the cellular debris was removed by centrifugation (3,230*g*, 30 min). The supernatant was decanted and the amino acids therein were derivatized by the same reactions used for the culture medium and analyzed by GC/EI-MS.

5.2.7. Effect of Temperature, Time, and Culture Medium Type

After expressing the *papam* gene in *E. coli* for 16 h at 16 °C in M9 minimal medium (12 × 1 L), the cultures were centrifuged, the supernatants were decanted, and the cells from each batch were resuspended separately in M9 minimal medium or 50 mM phosphate buffer (each at pH 7 or 8) to OD_{600} ~35. α-Phenylalanine was added (1 mM) to 45-mL cell suspended in each medium, and the feeding studies were conducted at 16, 25 and 30 °C. Aliquots (5 mL) were withdrawn from each suspension at 0.5, 1, 2, 4, 6, 8, 10, and 12 h. The supernatants were clarified by centrifugation, decanted, and separately treated with derivatizing reagents to form the *N*-(ethoxycarbonyl) α- and β-phenylalanine methyl esters and the cinnamic acid methyl ester, which were quantified by GC/EI-MS.

5.2.8. Effect of Substrate Concentration

To a cell suspension of *E. coli* (OD_{600} ~35), engineered to express *papam* in 5 mL of M9 minimal medium was added separately 1, 5, 10, 15, 20, and 25 mM of α-phenylalanine. The cultures were incubated for 6 h at 16 °C. The cells were removed by centrifugation, and the β-phenylalanine in the culture medium of each assay was quantified after derivatization and analysis by GC/EI-MS.

5.2.9. Effect of the Biocatalyst Amount

The *E. coli* cells harboring *papam* were resuspended in M9 minimal medium to an OD_{600} of 35, 70 or 280. α-Phenylalanine was added to a final concentration of 1, 5, 10, 15, 20, and 25 mM in separate assays at each cell density, and the assays (5 mL) were incubated for 6 h at 16

°C. The culture medium was clarified by centrifugation, and the β-phenylalanine in the supernatant (1 mL aliquot) of each assay was derivatized for and quantified by GC/EI-MS analysis.

5.2.10. Assessing the Substrate Scope of the Biocatalytic System

α-Phenylalanine, its analogues (*ortho*/*meta*/*para*-methyl, -methoxy, -fluoro, -chloro, -bromo, and –nitro), and 2- and 3-thienylalanine were separately incubated in a cell suspension of engineered *E. coli* (OD_{600} ~35) in M9 minimal medium (5 mL) at 16 °C for 6 h. The cells were pelleted by centrifugation, and an aliquot (1 mL) from each supernatant was separately treated with derivatizing reagents to form the *N*-(ethoxycarbonyl) methyl esters of the α-arylalanines and biosynthetic β-arylalanines, and the methyl esters of the biosynthetic arylacrylates for quantification by GC/EI-MS.

5.2.11. Sustainability of the Biocatalytic System

E. coli cells (at OD_{600} ~35) engineered to express *papam* were resuspended in M9 minimal medium (5-mL), and α-phenylalanine at 1 and 5 mM was added separately to different batches of cell suspensions. The cells were incubated for 6 h at 16 °C, the culture medium was clarified by centrifugation at 3,230*g* (10 min). The cell pellets were serially washed (2 × 5 mL) with M9 minimal medium and clarified by centrifugation between each wash to remove residual substrate/product from the cells. The washed cell pellets were resuspended in the culture medium (5 mL), a new batch of α-phenylalanine substrate was added to each suspension, and the biotransformation reactions were incubated for 6 h at 16 °C. The supernatant from each reaction

was twice serially basified (6 M NaOH) and treated with ethyl chloroformate. The solution was acidified (pH 2-3, 6 M HCl), extracted with diethyl ether (2 × 2 mL), concentrated in vacuo, and treated with (trimethylsilyl)diazomethane to methyl esterify the amino acids for quantification by GC/EI-MS. Cell harvesting, cell pellet washing, incubation, and GC/EI-MS quantification of the synthetically derivatized β-phenylalanine from the supernatant were repeated for 4 cycles.

5.2.12. Calculation of Colony-Forming Units (CFU)

An aliquot (50 μL) from each cell suspension was serially diluted between 10-fold and 10^8-fold with the culture medium (in triplicate). The 10^8-fold diluted culture suspension (100 μL) was spread on an agar plate supplemented with kanamycin (50 μg/mL) and incubated for 16 h at 37 °C. The colonies on each plate were counted, and the CFU was calculated.

5.3. Results and Discussion

5.3.1. General Assay Conditions

To construct a whole-cell biocatalyst for the production of β-arylalanines, the *papam* gene from *Pantoea agglomerans* was sub-cloned into the pET24b(+) expression vector. A BL21(DE3) *E. coli* strain transformed with pET24b(+) harboring *papam* was used as the microbial host. LB medium, which is a rich nutrient broth was avoided since it contains α-phenylalanine and would therefore confound *in vivo* biocatalysis results.[70] Thus, *papam* was expressed in host cells grown in M9 minimal medium free of amino acids to avoid background catalysis of α-phenylalanine during gene expression. After overnight expression of *papam*, a 1-L cell culture was pelleted and concentrated 10-fold (OD_{600} ~35) in the culture medium to increase the effective concentration of *Pa*PAM by increasing the cell density towards fermentation conditions.

5.3.2. Assessment of the Whole-cell Biocatalytic Properties of *Pa*PAM

Ideally, the starting materials feed into a whole cell biotransformation system should be transported into the cells with low impedance.[58] Reciprocally, the biosynthesized products should be released into the culture medium for easy recovery without breaking the cells, thus enabling the cells to be used sustainably in additional biocatalytic cycles. Recent investigations found that active transport of phenylalanine and other aromatic amino acids into the *E. coli* cells across the inner membrane is mediated by five distinct transport systems.[71-73] All arylalanines are transported via a general aromatic amino acid permease (AroP),[72] while the permease PheP[74]

specifically transports phenylalanine. A permissive ATP-binding cassette type transporter, LIV-I/LS system, principally conveys branched chain amino acids yet also occasionally transports phenylalanine .[75]

In this study, each productive arylalanine fed to cultures of engineered *E. coli* was biosynthesized to a β-aryl-β-alanine and released into the culture medium for recovery. β-Phenylalanine (benchmark product) was quantified in the medium at 0.5, 1, 2, 4, 6, and 8 h after incubation to evaluate the proportion of β-amino acid remaining in the *E. coli* cells and culture medium. After brief zero-order production of β-phenylalanine (i.e., $\delta[\beta\text{-Phe}]/\delta t$ ~0.46 $mg \cdot h^{-1}$, between 0 and 0.5 h), the change in production rate ($\delta[\beta\text{-Phe}]/\delta t$) approached 0 after 1 h, and β-phenylalanine reached 90 mg in a 1-L culture (OD_{600} ~35) after 8 h. The β-phenylalanine (3.2 mg) obtained from the cells (80 g wet wt) in 1-L of medium accounted for ~3% of the total β-phenylalanine biosynthesized after 8 h (Figure 5.13). These data suggested the substrate crossed the *E. coli* membranes into the cells, while the product released reciprocally into the medium without the need to disrupt the cells.

The colony-forming units (CFU) in the *E. coli* samples at each time point (0.5, 1, 2, 4, 6, and 8 h) remained constant (Figure 5.13), suggesting no time-dependent accumulation of dead cells and cellular protein in the medium at stationary growth phase. Thus, biocatalysis did not occur fortuitously in the culture medium by release of *Pa*PAM from dead cells.

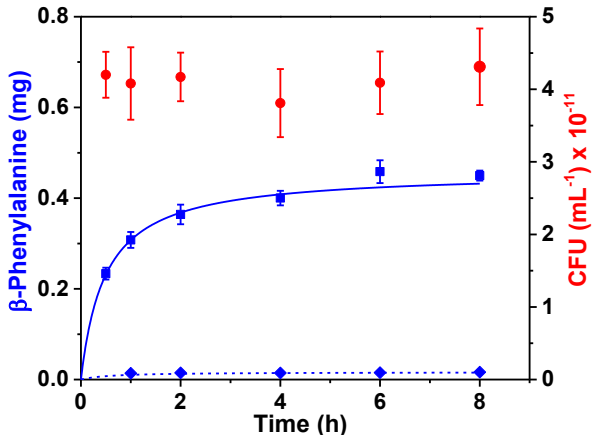

Figure 5.13. Distribution of β-phenylalanine in culture medium and *E. coli* cells. Time course and distribution of β-phenylalanine released to the M9 minimal medium (pH 7.4, 5 mL) (■ *on solid line*) and remaining in the *E. coli* cell pellet (0.4 g) (♦ *on dotted line*) after conversion of α-phenylalanine (1 mM) by *Pa*PAM whole-cell biocatalysis at 16 °C (OD_{600} ~35). CFU values (●) for the bacterial cells at each time point are shown.

5.3.3. Enantiomeric Excess of the Biosynthetic (*S*)-β-Phenylalanine

Driven by the application of chiral building blocks for the synthesis of pharmaceutically active drugs, the development of industrially viable processes for the synthesis of enantiomerically pure compounds continues to accelerate.[76] Hence, optimizing the enantiomeric excess of a catalytic process is an important goal. To analyze the enantioselectivity of the whole-cell biocatalyst used herein, biosynthetic β-phenylalanine was converted to its *N*-(1(*S*)-camphanoyl) methyl ester. The derivatized diastereomeric β-amino acid eluted at a retention time (14.43 min) identical to that of authentic *N*-[(1*S*)-camphanoyl]-(3*S*)-β-phenylalanine (14.43 min) (Figure 5.14) confirming the 3*S*-product stereochemistry. There was no indication of *N*-[(1*S*)-camphanoyl]-(3*R*)-β-phenylalanine (14.41 min) (Figure 5.14) present in the biosynthetic product suggesting >99.9% enantiomeric excess of the biosynthetic (3*S*)-β-amino acid, which was consistent with the product stereochemistry of the *Pa*PAM reaction in earlier *in vitro* assays.[39,77]

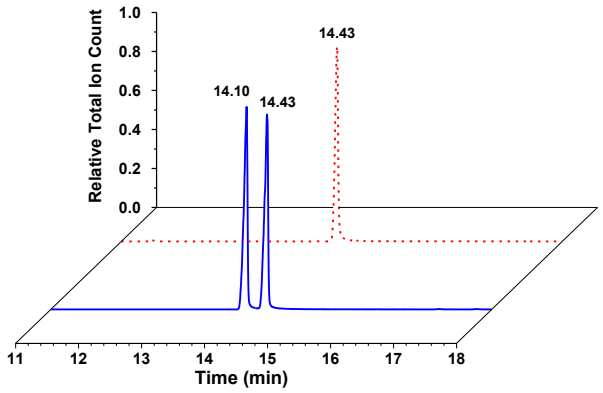

Figure 5.14. Gas chromatogram profiles of the *N*-[(1'*S*)-camphanoyl] methyl esters of authentic racemate 3*R*– (14.10 min) and 3*S*–β–phenylalanine (14.43 min) (*solid line*), and biosynthetic β–phenylalanine (14.43 min) (*dotted line*).

5.3.4. Effect of Temperature on β-Phenylalanine Production

The activity, stability, and selectivity of a whole-cell biocatalyst are important for industrial scale biosynthesis.[78] To examine the thermal stability of the recombinant *E. coli* whole-cell biocatalyst, the cell cultures were incubated at 16, 25 or 30 °C. Aliquots from each thermal sample were withdrawn at 30 min, 1 h, and then every 2 h up to 10 h to measure the β-phenylalanine in the medium (Figure 5.15A). Cultures (OD_{600} ~35) incubated at 16 °C maximally produced β-phenylalanine (0.092 $g \cdot L^{-1}$) at 6 h, yet cultures incubated at 25 and 30 °C nominally produced β-phenylalanine at ~1.5-fold lower maximum (~0.065 $g \cdot L^{-1}$) at 1 h (Figure 5.15A). β-Phenylalanine increased over 6 h at 16 °C and then equilibrated; while at 25 and 30 °C, the production increased over 1 h and then remain constant up to 8 h. The higher reaction temperatures likely affected overall gene expression,[79] enzyme activity, substrate binding, increased the flux of α-phenylalanine towards post-exponential Pex protein synthesis,[80] and/or amplified phenylalanine catabolism[81] in *E. coli* at stationary phase. Therefore, the recombinant *E. coli* biocatalyst expressing *Pa*PAM was incubated at 16 °C to assess the permissivity for

converting other unnatural β-arylalanines. At all three temperatures, the β-phenylalanine decreased markedly after the equilibrium phase beyond 8-h incubation. Analysis of the product distribution at each time point at 16 °C revealed that the concentration of cinnamic acid (a 5% by-product from α-phenylalanine during *Pa*PAM catalysis) increased over time, while the amount of α-phenylalanine rapidly decreased (Figure A.3.1). An increase in cinnamic acid suggested that the occurrence of the reverse reaction catalyzed by *Pa*PAM[82] is converting β-phenylalanine to cinnamate as the β- phenylalanine concentration increased over that of α-phenylalanine in the medium. However, α- phenylalanine did not equilibrate with β-phenylalanine in the reaction medium, likely due to its partitioning to other metabolic pathways.

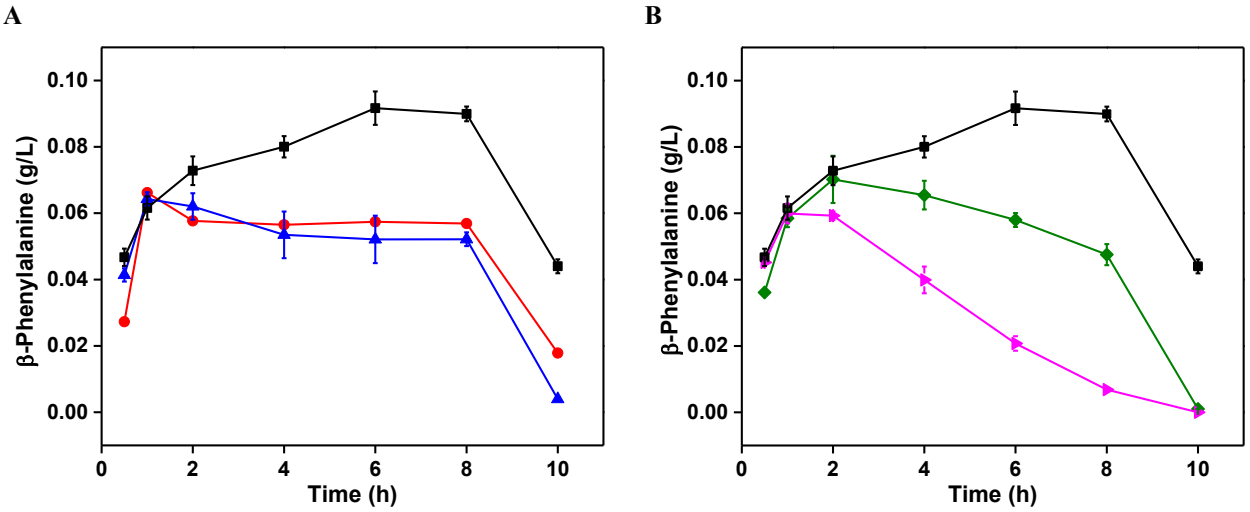

Figure 5.15. Effect of reaction temperature and reaction medium. *A*) The production of β-phenylalanine in *Pa*PAM whole-cell biocatalysis in M9 minimal medium (pH 7.4) containing α-phenylalanine (1 mM) at 16 °C (■), 25 °C (●), and 30 °C (▲). *B*) The production of β-phenylalanine in *Pa*PAM whole-cell biocatalysis in M9 minimal medium (pH 7.4) (■), phosphate buffer at pH 7 (♦), and pH 8 (►), each containing α-phenylalanine (1 mM).

5.3.5. The Effect of Reaction Medium on α- to β-Phenylalanine Isomerization

The influence of pH and buffer type on the stability and activity of the whole-cell biocatalyst was evaluated in phosphate buffer (50 mM, pH 7 and 8) and M9 minimal medium (pH 7.4). The M9 minimal medium contains a supply of nitrogen, phosphorous and sulfur source, mono- and di-valent cations (K^+, Ca^{2+}, Mg^{2+} and Fe^{2+}), BME-vitamins, and a carbon source needed for bacterial cell survival and growth. By comparison, the phosphate buffer lacks a carbon source as well as other nutrients needed for cell growth and viability. In M9 minimal medium, the production rate of β-phenylalanine by the whole-cell biocatalyst (OD_{600} ~35) was ~0.062 $g \cdot L^{-1} \cdot h^{-1}$ between 0.5 – 1 h, and then slowly approached equilibrium at ~0.092 $g \cdot L^{-1}$ β-phenylalanine between 6 – 8 h. β-Phenylalanine was produced in 50 mM phosphate buffer (pH 7 and 8) at an initial rate (~0.059 $g \cdot L^{-1} \cdot h^{-1}$) over 1 h, similar to that made by *E. coli* incubated in M9 minimal medium (cf. Figure 5.15B). By contrast, between 2 – 8 h, β-phenylalanine *decreased* linearly in phosphate buffer at ~0.004 $g \cdot L^{-1} \cdot h^{-1}$ (pH 7) and ~0.006 $g \cdot L^{-1} \cdot h^{-1}$ (pH 8), and slowly *increased* in minimal medium (~0.005 $g \cdot L^{-1} \cdot h^{-1}$). α-Phenylalanine depleted faster in 50 mM phosphate buffer (0.024 $g \cdot L^{-1} \cdot h^{-1}$ and 0.028 $g \cdot L^{-1} \cdot h^{-1}$ at pH 7 and 8, respectively), compared to when the bacteria was incubated in M9 minimal medium (0.012 $g \cdot L^{-1} \cdot h^{-1}$) (Figure A.3.2). We also observed that α-phenylalanine disappeared from the phosphate buffer at a rate greater than β-phenylalanine was exported into the medium over 8 h. This observation suggested that the whole-cell biocatalyst metabolized the exogenous α-phenylalanine (and likely β-phenylalanine) for cell growth and survival in the nutrient-deprived phosphate buffers. Thus, the moderately fortified M9 minimal medium was used for other whole-cell *Pa*PAM biocatalyst assays.

In addition, to assess the cell viability in the different media, CFU·mL^{-1} were calculated for bacteria incubated in M9 minimal medium (pH 7.4) and phosphate buffer (pH 7) containing α-phenylalanine (1 mM). The CFU (4.1×10^{11} mL^{-1}) of *E. coli* incubated for 4 h in minimal medium was ~1.5-fold higher than the CFU (2.9×10^{11} mL^{-1}) of cells incubated in phosphate buffer (pH 7) (Table 5.2). *E. coli* viability in minimal medium did not change when α-phenylalanine was omitted, whereas the CFU reduced 2-fold to 1.6×10^{11} mL^{-1} in phosphate buffer without α-phenylalanine supplementation (Table 5.2). Thus, the exogenous amino acid was likely only slightly mesotrophic for the bacteria in the phosphate medium, causing the cell viability as well as the production rate of β-phenylalanine to decrease (cf. Figure 5.15B).

Table 5.2. Colony Forming Units (CFU) of *E. coli* in different reaction media.

Assay Medium	α-Phenylalanine (mM)	CFU (mL^{-1}) × 10^{-11}
M9 minimal medium	0	4.2±0.33
	1	4.1±0.49
Phosphate buffer (pH 7, 50 mM)	0	1.6±0.17
	1	2.9±0.38

5.3.6. The Effect of α-Phenylalanine Concentration on β-Phenylalanine Production

Theoretically, the production rates of catalytic systems can increase by providing higher substrate concentrations.[83] However, higher concentration of substrates is often deleterious to microbial cells used in whole-cell biocatalytic systems.[83] Thus, α-phenylalanine (1 – 25 mM) was used as the benchmark for all the substrates tested to examine its effect on β-phenylalanine production and *E. coli* whole-cell viability. β-Phenylalanine production in the whole-cells increased 0.09 – 1.2 g·L^{-1} with increasing substrate concentration in 6-h incubations at 16 °C (Figure 5.16A). The highest measured β-phenylalanine production (1.2 g·L^{-1}) was at 25 mM

substrate. However, the percent conversion of α- to β-phenylalanine decreased from 55% at 1 mM substrate to a lower limit of 29% at 25 mM α-phenylalanine (Figure 5.16A). Mass transfer likely reached its limit when the biocatalyst was limiting or the higher concentration of substrate became toxic to the cells.

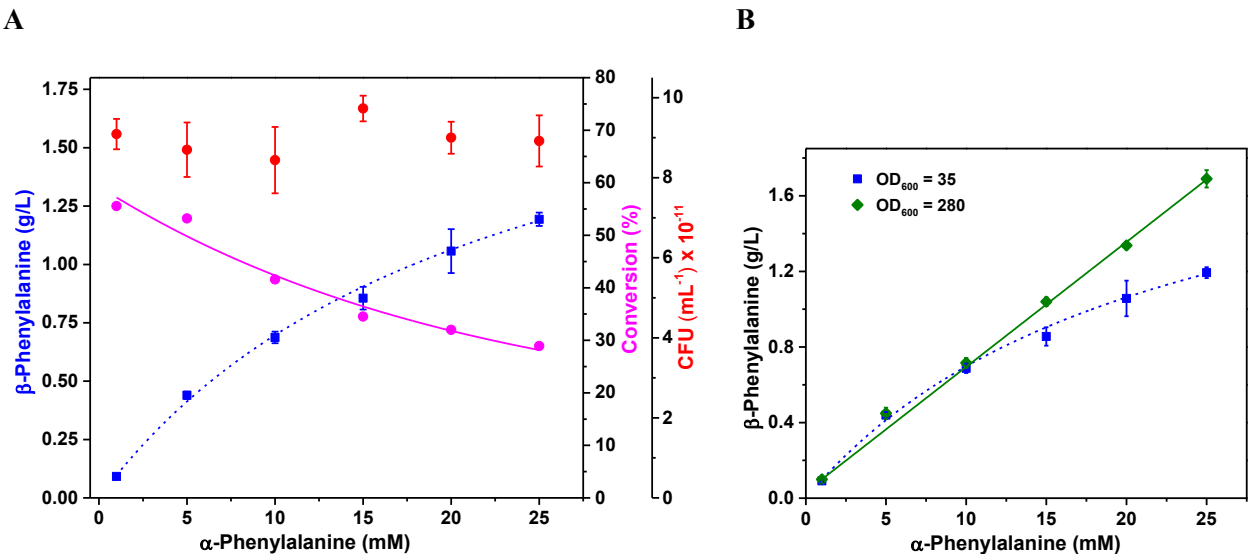

Figure 5.16. Effect of increased substrate concentration and biocatalyst amount. *A*) The production of β-phenylalanine in *Pa*PAM whole-cell biocatalysis in M9 minimal medium (pH 7.4) containing various concentrations of α-phenylalanine (■ *on dashed line*) at 16 °C, percent conversion of α- to β-phenylalanine (● *on solid line*), and CFU (●) at each susbtrate concentration. *B*) Comparison of *Pa*PAM whole-cell biocalyst concentration OD_{600} ~35 (■ *on dashed line*) and 280 (♦ *on soild line*) incubated at various substrate concentrations.

Substrate toxicity was analyzed by incubating *E. coli* cells in increasing substrate concentration. Calculating the CFU of cultures at increasing substrate concentration revealed that the cells remain viable even at 25 mM α-phenylalanine (Figure 5.16A). When the amount *E. coli* cells was increased from OD_{600} ~35 to ~70 and 100, the higher biomasses did not significantly improve the β-phenylalanine production (data not shown). By comparison, at OD_{600} ~280 (an 8-

fold increase in cell biomass over OD_{600} ~35), the β-phenylalanine production increased by 33% when the substrate concentration was between 15 – 25 mM (Figure 5.16B). This suggested moderate scalability of the substrate for the whole-cell *Pa*PAM biocatalyst.

5.3.7. Substrate Scope of the Whole-cell Biocatalytic System

Limited substrate scope is commonly a main disadvantage of enzyme biocatalysis.[84] *Pa*PAM, however, has a broad substrate scope *in vitro*,[49] and thus was anticipated to perform similarly *in vivo*. The *Pa*PAM whole-cell biocatalyst was probed with 21 α-arylalanines, including two heteroaromatic compounds. The productive and inactive substrates were similar to those identified earlier for *Pa*PAM *in vitro*.[49] The biocatalyst did not isomerize *o*-chloro-, *o*-bromo- and *o*-nitro-α-phenylalanine (Table 5.3) *in vivo*; likely, the proximity of the *ortho*-substituent to the alanine side chain caused ineffective substrate binding.[49] Five α-arylalanine substrates (*m*-bromo (96%), *p*-chloro (93%), *p*-bromo (92%), 3-thienyl (92%), and *m*-methyl (90%)) were converted efficiently to their β-amino acids. In general, the whole-cell *Pa*PAM biocatalyst preferentially isomerized *meta*- and *para*-substituted substrates over their *ortho*-substituted isomers; *ortho*-regioisomers (fluoro- (41%), methyl- (27%),and methoxy- (6%)) were converted more poorly.

The rank order between the *in vitro* catalytic rates (k_{cat}) and the production levels of the whole-cell biocatalyst was redistributed for the substrates tested (Table 5.3). For example, the intrinsic k_{cat} values 0.484 and 0.420 s^{-1} of *Pa*PAM *in vitro* for *m*-chloro (**8**) and *m*-bromo (**1**) (ranked 1st and 2nd), respectively, were followed by the natural substrate α-phenylalanine (**11**)

(ranked 3rd) in an earlier study.[49] By comparison, based on the substrate turnover by the whole-cell biocatalyst, *m*-bromo (**1**) ranked 1st (235 mg·L^{-1}), *m*-chloro (**8**) ranked 8th (128 mg·L^{-1}), and the natural substrate (**11**) ranked 11th (96 mg·L^{-1}); interestingly, **11** was isomerized *in vivo* slower than ten other substrates (Table 5.3). Other instances that highlight the differences in turnover by *Pa*PAM in whole cells and *in vitro* are with the *p*-chloro (**3**) and *p*-bromo (**2**) substrates. The k_{cat} values for **3** and **2** (0.053 and 0.045 s^{-1}, respectively) ranked 9th and 10th *in vitro*, while their turnovers unpredictably ranked 3rd and 2nd (186 and 224 mg·L^{-1} for **3** and **2**, respectively) in the whole-cells (Table 5.3). It is interesting that all fluoro-substituted regioisomer substrates (**5**, **9**, and **13**) were isomerized among the slowest *in vitro* (~0.02 s^{-1}), over 10-fold slower than the natural substrate.[49] However, the whole-cell biocatalyst converted the same fluorinated substrates (*ortho*-**13**, 74 mg·L^{-1}; *para*-**5**, 159 mg·L^{-1}; and *meta*-**9**, 113 mg·L^{-1}) at a level similar to several other substrates, including α-phenylalanine (Table 5.3).

In vitro biocatalysts are governed by cofactors (if any), physical conditions (temperature, pH, ionic strength), and the intrinsic properties of the enzymes when reconstituted in buffer. *In vivo* whole-cell biocatalysts are dependent however on factors such as mass transfer across cell membranes, cellular metabolism, protein synthesis, stimulation and inactivation of microbial cell growth, toxicity, and by-product formation.[85] The relative transport rates of molecules across the *E. coli* cell membrane can depend on steric and electronic properties of the substrate.[60] The aromatic amino acid:H^+–symporter permeases (PheP and AroP) in the inner membrane of *E. coli* transport phenylalanine display high affinity (K_M = 2 μM and 0.5 μM, respectively) towards the natural substrate.[86] The AroP permease has similar affinity (K_M = 0.6 μM) for the phenylalanine analogue tyrosine and the bulkier heteroaromatic tryptophan,[87] whereas PheP is more specific for phenylalanine.[88]

Thus, we expect that AroP is the principal transporter for the α-arylalanines used in this whole-cell feeding study. This hypothesis is supported by an earlier inhibition study of the general aromatic amino acid transporter (AroP) by *p*-fluoro-α-phenylalanine and 3-(2-thienyl)-α-alanine,[89] also used as substrates herein. These analogues competitively inhibited the transporter as strongly as natural aromatic amino acids, suggesting that at least these two have equal affinity for AroP.[89] In another study, arylalanines with substituents on the ring (not specified) were also reported as being good substrates for AroP, yet had lower affinity (data not provided) for the permease than the natural substrate.[90] We hypothesize the various arylalanines (1 mM) in the medium, likely bind the permeases with variable affinities and thus transfer through the *E. coli* inner membrane at different maximum velocities. In addition, α-phenylalanine is also a primary metabolite of protein synthesis and likely (including other unnatural arylalanines) is a precursor of catabolic phenylpropanoid degradation. Thus, several combined physiological causes are expected to have affected whole-cell biocatalyst when making each β-arylalanine. As a result, the rank-order correlation was scrambled between the *in vivo* production and the k_{cat} values of *Pa*PAM for the substrates (Table 5.3).

Table 5.3. Production levels and conversions of *Pa*PAM whole-cell biocatalytic system for various α-arylalanine substrates.

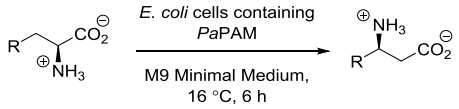

Product	Production ($mg \cdot L^{-1}$)	Yield (%)	Ranking* *In vivo*	Ranking* *In vitro*	Product	Production ($mg \cdot L^{-1}$)	Yield (%)	Ranking* *In vivo*	Ranking* *In vitro*
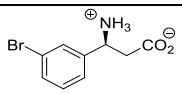	235±3.6	96	**1**	2	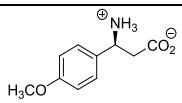	109±9.2	56	**10**	16
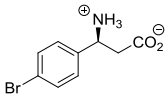	224±5.8	92	**2**	10	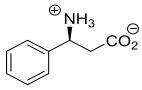	96±2.1	60	**11**	3
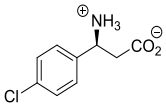	186±4.2	93	**3**	9	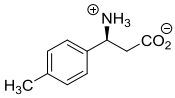	77±2.4	43	**12**	17
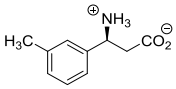	162±7.5	90	**4**	8	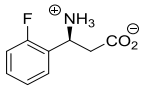	74±3.6	41	**13**	15
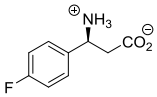	159±0.84	87	**5**	14	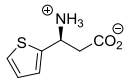	68±2.2	40	**14**	13
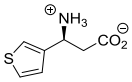	157±4.6	92	**6**	6	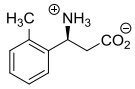	49±3.2	27	**15**	7
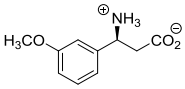	140±4.3	72	**7**	4	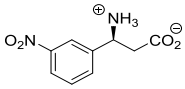	17±1.4	8	**16**	5
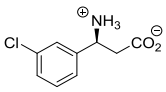	128±6.1	64	**8**	1	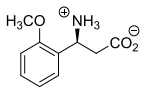	13±0.77	6	**17**	18
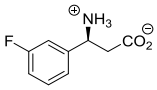	113±1.5	62	**9**	12	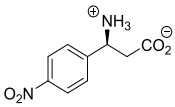	8.5±1.1	4	**18**	11

*Ranking order is based on the β-phenylalanine production of the *in vivo* system and the catalytic rate (k_{cat}) of the *in vitro* system.

5.3.8. Sustainability of the *Pa*PAM Whole-cell Biocatalytic System

Recycling of recombinant cells is an important factor in developing a sustainable industrial process for producing fine chemicals.[78] To test the operational stability of the

recombinant *E. coli* whole-cell biocatalyst towards recycling, a set of consecutive biocatalytic cycles was performed at 16 °C for 30 h using a single sample of the biocatalyst. After each 6-h reaction cycle, the cells were recovered by centrifugation, washed with M9 minimal medium to remove residual substrate and product, and to reduce cell aggregates (at OD_{600} ~35). The cells were recovered by centrifugation and resuspended in M9 minimal medium before the next reaction in the series. β-Phenylalanine production remained almost constant for whole-cell biocatalyst fed α-phenylalanine at 1 mM and 5 mM (0.075 and 0.9 $g \cdot L^{-1}$, respectively) in each of the five batch reaction cycles (Figure 5.17). CFU measurements suggested continued cell viability even after centrifugation and cell resuspension during each cycle (Figure 5.17).

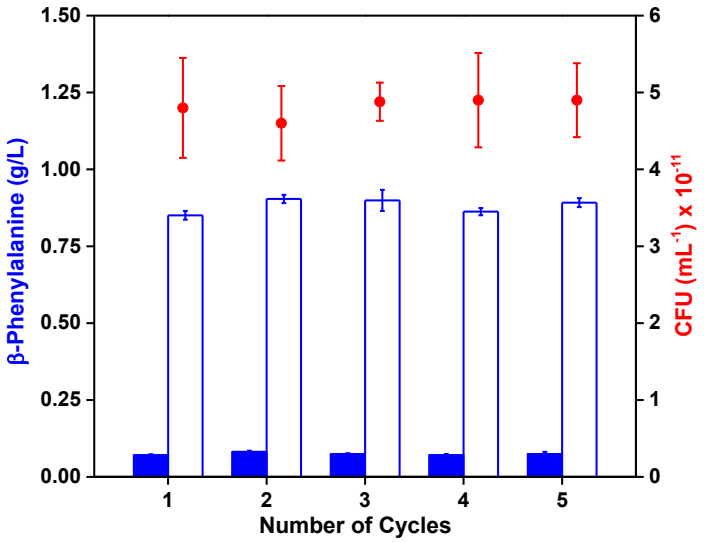

Figure 5.17. Recycling of the *E. coli* whole-cell biocatalyst (OD_{600} ~35) for β-phenylalanine production. The production of β-phenylalanine in *Pa*PAM whole-cell biocatalysis in M9 minimal medium (pH 7.4) incubated with α-phenylalanine (1 mM (*blue bars*) and 5 mM (*white bars*)) at 16 °C for each catalytic cycle. CFU values (●) for the bacterial cells after each reaction cycle in M9 minimal medium (pH 7.4) containing α-phenylalanine (5 mM) at 16 °C are shown.

Using sustainable whole-cell biocatalysts is attractive over biocatalytic routes employing purified enzymes for *in vitro* assays, in part, because of the potential higher risk for enzyme denaturation during purification and incubation with the substrate. For example, a purified Amano lipase PS was used *in vitro* for a commercial (Evonik-Degussa, Hanau-Wolfgang, Germany) biocatalytic process to resolve racemic β-aryl-β-amino acids.[32] The enzyme is inactivated partially after one 15-h batch reaction cycle, yielding a paltry 10-11% conversion in the second batch reaction. To compensate for the loss of activity after each of five biocatalytic cycles, fresh enzyme was added to a fraction of the previous batch reaction.[32] The whole-cell *Pa*PAM biocatalyst, described herein, however, can likely produce several (3*S*)-β-aryl-β-amino acids at a sustainable concentration over multiple, recycled batches of biocatalyst (shown by using β-phenylalanine as the model compound) (Figure 5.17).

5.4. Conclusion

A *Pa*PAM whole-cell biocatalyst was shown to produce several unnatural (3*S*)-β-aryl-β-amino acids at >99.9% *ee*, with the highest turnover rate in M9 minimal medium at 16 °C. The whole-cell biocatalyst biosynthesized 18 β-arylalanines with moderate to excellent converted yield (4-96%) at production levels of 8.5 – 235 $mg \cdot L^{-1}$ over 6 h, respectively. More notably, *E. coli* cells are reusable over *at least* five reaction cycles without a noticeable loss in activity and cell viability. This biocatalyst offers notable advantages over conventional synthetic methods because of its excellent enantioselectivity, broad substrate scope, single-step conversion, and sustainability. In addition, the small-scale production yields of the whole-cell biocatalyst can likely improve by using a bioreactor, increasing the number of bacterial membrane permeases, optimizing the outer membrane permeability,[59] and reducing aromatic amino acid flux through catabolic pathways in engineered *E. coli*.

APPENDIX

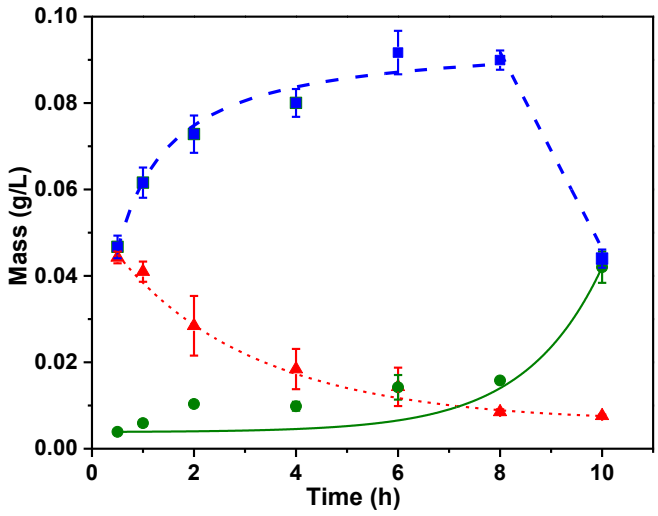

Figure A.3.1. Comparison of product accumulation and substrate depletion over time. β-Phenylalanine (■ *on dashed line*) and cinnamic acid (● *on solid line*) production, and α- phenylalanine (▲ *on short dashed line*) depletion by engineered *E. coli* (OD_{600} ~35) incubated at 16 °C in M9 minimal medium (pH 7.4) containing α- phenylalanine (1 mM).

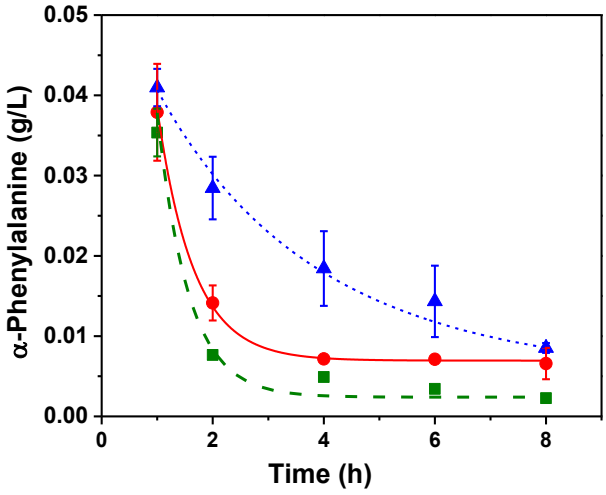

Figure A.3.2. Comparison of substrate depletion in different reaction media. Amount of α-phenylalanine remaining in M9 minimal medium (pH 7.4, ▲ *on short dashed line*), phosphate buffer at pH 7 (● *on solid line*), and pH 8 (■ *on dashed line*) incubated with engineered *E. coli* (OD_{600} ~ 35) at 16 °C. Each medium was supplied with α-phenylalanine (1 mM).

REFERENCES

REFERENCES

(1) Liljeblad, A.; Kanerva, L. T. *Tetrahedron* **2006**, *62*, 5831-5854.

(2) Seebach, D.; Matthews, J. L. *Chem. Commun.* **1997**, 2015-2022.

(3) Jin, M.; Fischbach, M. A.; Clardy, J. *J. Am. Chem. Soc.* **2006**, *128*, 10660-10661.

(4) Crews, P.; Manes, L. V.; Boehler, M. *Tetrahedron Lett.* **1986**, *27*, 2797-2800.

(5) Nishizawa, R.; Saino, T.; Takita, T.; Suda, H.; Aoyagi, T.; Umezawa, H. *J. Med. Chem.* **1977**, *20*, 510-515.

(6) Savile, C. K.; Janey, J. M.; Mundorff, E. C.; Moore, J. C.; Tam, S.; Jarvis, W. R.; Colbeck, J. C.; Krebber, A.; Fleitz, F. J.; Brands, J.; Devine, P. N.; Huisman, G. W.; Hughes, G. J. *Science* **2010**, *329*, 305-309.

(7) Nicolaou, K. C.; Yang, Z.; Liu, J. J.; Ueno, H.; Nantermet, P. G.; Guy, R. K.; Claiborne, C. F.; Renaud, J.; Couladouros, E. A.; Paulvannan, K.; Sorensen, E. J. *Nature* **1994**, *367*, 630-634.

(8) Haycock-Lewandowski, S. J.; Wilder, A.; Ahman, J. *Org. Process Res. Dev.* **2008**, *12*, 1094-1103.

(9) Seebach, D.; Overhand, M.; Kiihnle, F. N. M.; Martinoni, B. *Helv. Chim. Acta* **1996**, *79*, 913-941.

(10) Frackenpohl, J.; Arvidsson, P. I.; Schreiber, J. V.; Seebach, D. *ChemBioChem* **2001**, *2*, 445-455.

(11) Seebach, D.; Abele, S.; Gademann, K.; Bernhard, J. *Angew. Chem. Int. Ed.* **1999**, *38*, 1595-1597.

(12) Seebach, D.; Abele, S.; Gademann, K.; Guichard, G.; Hintermann, T.; Jaun, B.; Matthews, J. L.; Schreiber, J. V. *Helv. Chim. Acta* **1998**, *81*, 932-982.

(13) Gademann, K.; Ernst, M.; Hoyer, D.; Seebach, D. *Angew. Chem. Int. Ed.* **1999**, *38*, 1223-1226.

(14) Liu, R. H.; Chen, X. Y.; Hayouka, Z.; Chakraborty, S.; Falk, S. P.; Weisblum, B.; Masters, K. S.; Gellman, S. H. *J. Am. Chem. Soc.* **2013**, *135*, 5270-5273.

(15) Liu, M.; Sibi, M. P. *Tetrahedron* **2002**, *58*, 7991-8035.

(16) Lelais, G.; Seebach, D. *Biopolymers* **2004**, *76*, 206-243.

(17) Weiner, B.; Szymanski, W.; Janssen, D. B.; Minnaard, A. J.; Feringa, B. L. *Chem. Soc. Rev.* **2010**, *39*, 1656-1691.

(18) Yuan, C. G.; Williams, R. M. *J. Am. Chem. Soc.* **1997**, *119*, 11777-11784.

(19) Pinho, V. D.; Gutmann, B.; Kappe, C. O. *RSC Adv.* **2014**, *4*, 37419-37422.

(20) Sewald, N. *Amino Acids* **1996**, *11*, 397-408.

(21) Davies, S. G.; Ichihara, O. *Tetrahedron-Asymmetr* **1991**, *2*, 183-186.

(22) Davies, S. G.; Foster, E. M.; McIntosh, C. R.; Roberts, P. M.; Rosser, T. E.; Smith, A. D.; Thomson, J. E. *Tetrahedron-Asymmetr* **2011**, *22*, 1035-1050.

(23) Costello, J. F.; Davies, S. G.; Ichihara, O. *Tetrahedron-Asymmetr* **1994**, *5*, 1999-2008.

(24) Dumas, F.; Mezrhab, B.; d'Angelo, J. *J. Org. Chem.* **1996**, *61*, 2293-2304.

(25) Matsuyama, H.; Itoh, N.; Yoshida, M.; Kamigata, N.; Sasaki, S.; Iyoda, M. *Chem. Lett.* **1997**, 375-376.

(26) Falborg, L.; Jorgensen, K. A. *J. Chem. Soc., Perkin Trans. 1* **1996**, 2823-2826.

(27) Sibi, M. P.; Liu, M. *Org. Lett.* **2000**, *2*, 3393-3396.

(28) Lubell, W. D.; Kitamura, M.; Noyori, R. *Tetrahedron-Asymmetr* **1991**, *2*, 543-554.

(29) Zhang, W. C.; Chi, Y. X.; Zhang, X. M. *Acc. Chem. Res.* **2007**, *40*, 1278-1290.

(30) Holz, J.; Monsees, A.; Jiao, H. J.; You, J. S.; Komarov, I. V.; Fischer, C.; Drauz, K.; Borner, A. *J. Org. Chem.* **2003**, *68*, 1701-1707.

(31) Kadyrov, R.; Ilaldinov, I. Z.; Almena, J.; Monsees, A.; Riermeier, T. H. *Tetrahedron Lett.* **2005**, *46*, 7397-7400.

(32) Grayson, J. I.; Roos, J.; Osswald, S. *Org. Process Res. Dev.* **2011**, *15*, 1201-1206.

(33) de Carvalho, C. C. *Biotechnol. Adv.* **2011**, *29*, 75-83.

(34) Arnold, F. H. *Nature* **2001**, *409*, 253-257.

(35) Schmid, A.; Dordick, J. S.; Hauer, B.; Kiener, A.; Wubbolts, M.; Witholt, B. *Nature* **2001**, *409*, 258-268.

(36) Faulconbridge, S. J.; Holt, K. E.; Sevillano, L. G.; Lock, C. J.; Tiffin, P. D.; Tremayne, N.; Winter, S. *Tetrahedron Lett.* **2000**, *41*, 2679-2681.

(37) Rudat, J.; Brucher, B. R.; Syldatk, C. *AMB Express* **2012**, *2*, 11.

(38) Walker, K. D.; Klettke, K.; Akiyama, T.; Croteau, R. *J. Biol. Chem.* **2004**, *279*, 53947-53954.

(39) Magarvey, N. A.; Fortin, P. D.; Thomas, P. M.; Kelleher, N. L.; Walsh, C. T. *ACS Chem. Biol.* **2008**, *3*, 542-554.

(40) Soloshonok, V. A.; Fokina, N. A.; Antonyna V. Rybakova, A. V.; Shishkina, I. P.; Galushko, S. V.; Sorochinsky, A. E.; Kukhar, V. P. *Tetrahedron-Asymmetr* **1995**, *6*, 1601-1610.

(41) Behshad, E.; Ruzicka, F. J.; Mansoorabadi, S. O.; Chen, D.; Reed, G. H.; Frey, P. A. *Biochemistry* **2006**, *45*, 12639-12646.

(42) Ruzicka, F. J.; Frey, P. A. *Biochim. Biophys. Acta* **2007**, *1774*, 286-296.

(43) Rachid, S.; Krug, D.; Weissman, K. J.; Muller, R. *J. Biol. Chem.* **2007**, *282*, 21810-21817.

(44) Christenson, S. D.; Wu, W.; Spies, M. A.; Shen, B.; Toney, M. D. *Biochemistry* **2003**, *42*, 12708-12718.

(45) Chirpich, T. P.; Zappia, V.; Costilow, R. N.; Barker, H. A. *J. Biol. Chem.* **1970**, *245*, 1778-1789.

(46) Walker, K. D.; Klettke, K.; Akiyama, T.; Croteau, R. *J. Biol. Chem.* **2004**, *279*, 53947-53954.

(47) Christenson, S. D.; Liu, W.; Toney, M. D.; Shen, B. *J. Am. Chem. Soc.* **2003**, *125*, 6062-6063.

(48) Klettke, K. L.; Sanyal, S.; Mutatu, W.; Walker, K. D. *J. Am. Chem. Soc.* **2007**, *129*, 6988-6989.

(49) Ratnayake, N. D.; Liu, N.; Kuhn, L. A.; Walker, K. D. *ACS Catal.* **2014**, *4*, 3077-3090.

(50) Wu, B.; Szymanski, W.; Wietzes, P.; de Wildeman, S.; Poelarends, G. J.; Feringa, B. L.; Janssen, D. B. *ChemBioChem* **2009**, *10*, 338-344.

(51) Szymanski, W.; Wu, B.; Weiner, B.; de Wildeman, S.; Feringa, B. L.; Janssen, D. B. *J. Org. Chem.* **2009**, *74*, 9152-9157.

(52) Wu, B.; Szymanski, W.; Wybenga, G. G.; Heberling, M. M.; Bartsch, S.; de Wildeman, S.; Poelarends, G. J.; Feringa, B. L.; Dijkstra, B. W.; Janssen, D. B. *Angew. Chem. Int. Ed.* **2012**, *51*, 482-486.

(53) Wanninayake, U.; DePorre, Y.; Ondari, M.; Walker, K. D. *Biochemistry* **2011**, *50*, 10082-10090.

(54) Nikolova, P.; Ward, O. P. *J. Ind. Microbiol.* **1993**, *12*, 76-86.

(55) May, O.; Nguyen, P. T.; Arnold, F. H. *Nat. Biotechnol.* **2000**, *18*, 317-320.

(56) Breuer, M.; Ditrich, K.; Habicher, T.; Hauer, B.; Kesseler, M.; Sturmer, R.; Zelinski, T. *Angew. Chem. Int. Ed.* **2004**, *43*, 788-824.

(57) Groger, H.; Chamouleau, F.; Orologas, N.; Rollmann, C.; Drauz, K.; Hummel, W.; Weckbecker, A.; May, O. *Angew. Chem. Int. Ed.* **2006**, *45*, 5677-5681.

(58) Chen, R. R. Z. *Appl. Microbiol. Biotechnol.* **2007**, *74*, 730-738.

(59) Ni, Y.; Chen, R. R. *Biotechnol. Bioeng.* **2003**, *87*, 804-811.

(60) Silhavy, T. J.; Kahne, D.; Walker, S. *Cold Spring Harb. Perspect. Biol.* **2010**, *2*, 1-16.

(61) Nikaido, H. *Mol. Microbiol.* **1992**, *6*, 435-442.

(62) Liu, Y.; Hama, H.; Fujita, Y.; Kondo, A.; Inoue, Y.; Kimura, A.; Fukuda, H. *Biotechnol. Bioeng.* **1999**, *64*, 54-60.

(63) Vanderwerf, M. J.; Hartmans, S.; Vandentweel, W. J. J. *Appl. Microbiol. Biotechnol.* **1995**, *43*, 590-594.

(64) Canovas, M.; Torroglosa, T.; Kleber, H. P.; Iborra, J. L. *J. Basic Microbiol.* **2003**, *43*, 259-268.

(65) Matsumoto, T.; Takahashi, S.; Kaieda, M.; Ueda, M.; Tanaka, A.; Fukuda, H.; Kondo, A. *Appl. Microbiol. Biotechnol.* **2001**, *57*, 515-520.

(66) Yang, R. Y.; Bayraktar, O.; Pu, H. T. *J. Biotechnol.* **2003**, *100*, 13-22.

(67) Schuurmann, J.; Quehl, P.; Festel, G.; Jose, J. *Appl. Microbiol. Biotechnol.* **2014**, *98*, 8031-8046.

(68) Becker, U.; Doderer, K.; Osswald, S.; Verseck, S.; Wienand, W. In *Pharm. Technol.* www.pharmtech.com, 2008.

(69) Schwarm, M. In *Application of Whole-Cell Biocatalysis in the Manufacture of Fine Chemicals*; Shioiri, T., Izawa, K., Konoike, T., Eds.; Wiley-VCH Verlag GmbH & Co: Weinheim, 2011, p 183-205.

(70) Strom, S.; Wanninayake, U.; Ratnayake, N. D.; Walker, K. D.; Geiger, J. H. *Angew. Chem. Int. Ed.* **2012**, *51*, 2898-2902.

(71) Piperno, J. R.; Oxender, D. L. *J. Biol. Chem.* **1968**, *243*, 5914-5920.

(72) Chye, M. L.; Guest, J. R.; Pittard, J. *J. Bacteriol.* **1986**, *167*, 749-753.

(73) Whipp, M. J.; Pittard, A. J. *J. Bacteriol.* **1977**, *132*, 453-461.

(74) Pi, J.; Pittard, A. J. *J. Bacteriol.* **1996**, *178*, 2650-2655.

(75) Koyanagi, T.; Katayama, T.; Suzuki, H.; Kumagai, H. *J. Bacteriol.* **2003**, *186*, 343-350.

(76) Petrovic, S. D.; Misic-Vukovic, M. M.; Mijin, D. Z. *Chem. Indust.* **2002**, *1*, 10-16.

(77) Ratnayake, N. D.; Wanninayake, U.; Geiger, J. H.; Walker, K. D. *J. Am. Chem. Soc.* **2011**, *133*, 8531-8533.

(78) Li, Q. S.; Li, G. Q.; Ma, F. Q.; Zhang, Z. M.; Zheng, B. S.; Feng, Y. *Process Biochem.* **2011**, *46*, 477-481.

(79) Gadgil, M.; Kapur, V.; Hu, W. S. *Biotechnol. Progr.* **2005**, *21*, 689-699.

(80) Kolter, R.; Siegele, D. A.; Tormo, A. *Annu. Rev. Microbiol.* **1993**, *47*, 855-874.

(81) Teufel, R.; Mascaraque, V.; Ismail, W.; Voss, M.; Perera, J.; Eisenreich, W.; Haehnel, W.; Fuchs, G. *Proc. Natl. Acad. Sci. USA* **2010**, *107*, 14390-14395.

(82) Fortin, P. D.; Walsh, C. T.; Magarvey, N. A. *Nature* **2007**, *448*, 824-811.

(83) van Bloois, E.; Dudek, H. M.; Duetz, W. A.; Fraaije, M. W. *BMC Biotechnol.* **2012**, *12*.

(84) Reetz, M. T. *J. Am. Chem. Soc.* **2013**, *135*, 12480-12496.

(85) Schrewe, M.; Julsing, M. K.; Buhler, B.; Schmid, A. *Chem. Soc. Rev.* **2013**, *42*, 6346-6377.

(86) Haney, S. A.; Oxender, D. L. *Int. Rev. Cytol.* **1992**, *137*, 37-95.

(87) Brown, K. D. *J. Bacteriol.* **1970**, *104*, 177-188.

(88) Pi, J.; Wookey, P. J.; Pittard, A. J. *J. Bacteriol.* **1991**, *173*, 3622-3629.

(89) Brown, K. D. *J. Bacteriol.* **1971**, *106*, 70-81.

(90) Willshaw, G.; Tristram, H. *Biochem. J.* **1972**, *127*, 71.